Université de Toulouse

THÈSE

En vue de l'obtention du

DOCTORAT DE L'UNIVERSITÉ DE TOULOUSE

Délivré par :

Institut Supérieur de l'Aéronautique et de l'Espace (ISAE)

Présentée et soutenue par :
Dinh Khanh DANG

le jeudi 18 décembre 2014

Titre :

Analyse de performance des technologies sans fil pour les systèmes embarqués avioniques de nouvelle génération

Performance Analysis of Wireless Technologies for New Generation Avionics Embedded Systems

---

École doctorale et discipline ou spécialité :

ED AA :Réseaux, télécom, système et architecture et Systèmes embarqués

Unité de recherche :

Équipe d'accueil ISAE-ONERA MOIS

Directeur(s) de Thèse :

M. Thierry GAYRAUD (directeur de thèse)
Mme Ahlem MIFDAOUI (co-directrice de thèse)

Jury :

M. Thierry GAYRAU, professeur , LAAS-CNRS/Université Paul Sabatier - Directeur de thèse
Mme Ahlem MIFDAOUI, professeur associé, ISAE - Co-directrice de thèse
M. Fabrice VALOIS, professeur, INSA de Lyon- Rapporteur
M. Congduc PHAM, professeur, UPPA - Rapporteur

Abstract

The complexity of avionics communication architecture is increasing inherently due to the growing number of interconnected subsystems and the expansion of exchanged data quantity. To follow this trend, the current architecture of new generation aircraft like the A380, A400M or A350 consists of a high data rate backbone network based on the redundant AFDX (Avionics Full Duplex Switched Ethernet) network to interconnect the critical subsystems. Then, each specific avionics subsystem could be directly connected to its associated sensors/actuators network based on low data rate buses, such as ARINC429 and CAN. Furthermore, to increase the reliability level, a backup network based on Switched Ethernet guarantees a continuous service in case of failure on the redundant AFDX backbone. Although this architecture fulfills the main avionics requirements, it also inherits significant weight and integration costs due to the increasing quantity of wires and connectors. In addition to the cost issue, avionics interconnects are still subject to structural failure and fire hazard, which decreases reliability and ramifies the maintenance. To cope with these arising issues, cable-less avionics implementation will clearly improve the efficiency and reliability of aircraft, while reducing integration, fuel consumption and maintenance costs. Therefore, integrating wireless technologies in avionics context is proposed in this thesis as a main solution to decrease the wiring-related weight and complexity. In this context, our main objective is to design and validate a new Wireless Safety-Critical Avionics Network (WSCAN) to replace the backup network of the AFDX backbone.

To achieve this aim, first, we identify the main challenges when using wireless technologies in avionics to assess the most relevant Commercial Off The Shelf (COTS) technologies versus avionic requirements. Afterwards, we select the High Rate Ultra Wideband (HR-UWB) as the most adequate technology for safety-critical avionics because of its high data rate, contention-free access protocol and high security mechanisms. Then, the design of an alternative backup avionic network based on HR-UWB technology is proposed with the Time Division Multiple Access (TDMA) protocol to guarantee timely communication and various reliability mechanisms, e.g. time and frequency diversity and retransmission with acknowledgment, to guarantee reliability requirements.

Afterwards, to analyze the effects of our proposal on the avionics system's performance,

we introduce the modeling of the proposed architecture when considering time and frequency diversity as reliability mechanisms, using the Network Calculus formalism which defines an arrival curve for each input flow and a service curve for each crossed node. Based on these curves, we conduct timing analysis to compute deterministic upper bounds on end-to-end delays and verify the system's schedulability. Preliminary performance evaluation through a small scale test case shows the ability of our proposal to guarantee system's predictability and reliability.

To reach further enhancements on the system performance and scalability, we investigate different directions to reduce the pessimism of deterministic upper bounds on end-to-end delays. The main proposed solutions are: (i) refining the system modeling using Integer Linear Programming, combined with Network Calculus, to have tighter delay bounds; (ii) exhaustive search of the TDMA configurations, i.e. TDMA cycle duration and slots allocations, to find the optimal one minimizing the delays; (iii) investigating the impact of the reliability mechanism based on retransmission and acknowledgment by introducing stochastic system modeling based on Stochastic Network Calculus. This formalism integrates a small probability of violation on the system's schedulability to compute stochastic upper bounds on end-to-end delays. The preliminary performance evaluation of these introduced solutions has shown significant enhancements in terms of end-to-end delay bounds tightness, and consequently system scalability.

Finally, the validation of our proposal through a realistic avionics case study has been conducted. The obtained results confirm our first conclusions and highlight the ability of the proposed WSCAN to guarantee the system requirements in terms of predictability, reliability and scalability.

Keywords: Avionics, Fly-by-wireless, HR-UWB, TDMA, Network Calculus, Stochastic Network Calculus, Performance analysis, Optimization

List of publications

[**Dang2015**]Dinh-Khanh Dang, Ahlem Mifdaoui. *Stochastic Delay Analysis of a Wireless Safety-Critical Avionics Network*, In: 10th IEEE International Symposium on Industrial Embedded Systems (SIES), 8-10 June 2015, Siegen, Germany. (**submitted**)

[**Dang2014c**] Dinh-Khanh Dang, Ahlem Mifdaoui. *Performance Optimization of a UWB-based Network for Safety-Critical Avionics*, In: 19th IEEE Emerging Technologies and Factory Automation (ETFA), 16-19 September 2014, Barcelona, Spain.

[**Dang2014b**] Dinh-Khanh Dang, Ahlem Mifdaoui. *Timing analysis of TDMA-based Networks using Network Calculus and Integer Linear Programming*, In: 22nd IEEE Modeling Analysis of Computer And Telecomunication Systems (MASCOTS), 9-11 September 2014, Paris, France.

[**Dang2014a**] Dinh-Khanh Dang, Ahlem Mifdaoui and Thierry Gayraud. *Design and Analysis of UWB-based Network for Reliable and Timely Communications in Safety-Critical Avionics*, In: 10th IEEE Workshop on Factory Communication Systems (WFCS), 5-7 May 2014, Toulouse, France.

[**Dang2013**] Dinh-Khanh Dang, Ahlem Mifdaoui and Thierry Gayraud. *Performance analysis of TDMA-based Wireless Network for Safety-critical Avionics.* ACM SIGBED Review 10.2 (2013): 24-24.

[**Dang2012**] Dinh-Khanh Dang, Ahlem Mifdaoui and Thierry Gayraud. *Fly-By-Wireless for next generation aircraft: Challenges and potential solutions.* In: 5th IFIP Wireless Days (WD), 21-23 November 2012, Dublin, Ireland.

Acknowledgments

First of all I would like to thank my supervisor Associate Professor Ahlem Mifdaoui. I appreciate her guidance and support not only of my research but also my life. She is not only a good supervisor, but also a good friend to me. Many thanks to her for all the constructive comments and fruitful discussion. I owe my gratitude to my co-supervisor, Professor Thierry Gayraud, who had gave valuable comments on my research direction. I also wish to thank Prof Emmanuel Lochin and Prof Jerome Lacan for their valuable suggestions for my research direction.

I would like to thank Nicolas Kuhn, Hamdi Ayed, Anh-Dung Nguyen, Tuan Tran Thai, Victor Ramiro and all fellow Ph.D. student of Department of Mathematics, Informatics and Automatics, for their enthusiastic support.

I am grateful to all my friends in France, Vietnam and Japan for the fun and encouragement. Specially thank to Nguyen Le Nam Khuong, an engineer at Airbus, for sharing the knowledge and passion of aircraft.

I owe my loving thanks to my wife Ty Mai for her understanding, continuous support, infinite patience and love. There is no word to express my gratitute to her. I am grateful to my parents and my brother in Vietnam for their unconditional support.

DANG Dinh Khanh

Toulouse, France, March 2015.

Contents

List of Figures

List of Tables

List of acronyms

Acronyms	**Full terminology**
ACK	Acknowledgment
ADCN	Avionics Data and Communication Network
AES	Advanced Encryption Standard
AFDX	Avionics Full Duplex Switch
A-MPDU	Aggregate MAC Protocol Data Unit
A-MSDU	Aggregate MAC Protocol Service Unit
AP	Access Point
ARQ	Automatic Retransmission reQuest
BAG	Bandwidth Allocation Gap
BER	Bit Error Rate
BP	Beacon Period
BPST	Beacon Period Start Time
CAN	Controller Area Network
CAP	Contention Access Period
CCMP	Counter-mode/CBC-MAC Protocol
CFP	Contention-Free Period
CMS	Cabin Management System
COTS	Commercial Off-The-Shelf
CS	Contention Slots
CSMA/CA	Carrier Sense Multiple Access with Collision Avoidance
CTAP	Channel Time Allocation Period
CW	Contention Window
DCF	Distributed Coordination Function
DIFS	DCF Inteframe Space

Acronyms	**Full terminology**
DoS	Denial of Service
EAP	Extensible Authentication Protocol
ECMA-368	Standard of High Rate Ultra Wideband PHY and MAC
EDCA	Enhanced Distributed Channel Access
EMI	ElectroMagnetic Inteference
FDMA	Frequency Division Multiple Access
FEC	Forward Error Coding
FIFO	First In First Out
FP	Fixed Priority
GSC	Ground Control System
GTC	Guarantee Time Slot
GTK	Group Transient Key
HART	Highway Addressable Remote Transducer
HCCA	Hybrid coordination function Controlled Channel Access
HCF	Hybrid Coordination Function
HR-UWB	High Rate Ultra WideBand
IEEE 1588-PBS	IEEE1588-Pairwise Broadcast Synchronization
IFE	In-Flight Entertainment Network
ILP	Integer Linear Programming
IMA	Integrated Modular Architecture
IP	Internet Protocol
ISP	Internet Service Provider
LDPC	Low Density Parity Check
MAC	Medium Access Control
MAS	MAC Access Slot
MIC	Message Integration Code
MIFS	Minimum Interframe Space
MIMO	Multi Input, Multi Ouput
MSDU	MAC Service Data Unit

Acronyms	Full terminology
NACK	Negative ACKnowledgment
NC	Network Calculus
OFDM	Orthogonal Frequency-Division Multiplexing
PCA	Prioritized Contention Access
PCF	Point Coordination Function
PED	Portable Electronic Devices
PEDAMACS	Power Efficient and Delay Aware Medium Access Control
PER	Packet Error Rate
PLCP Preamble	Physical Layer Convergence Protocol
PTK	Pairwise Transient Key
QoS	Quality of Service
RF	Radio Frequency
RI-EDF	Robust Implicit Early Deadline First
RSSI	Received Signal Strength Indication
SAC	Stochastic Arrival Curve
SNC	Stochastic Network Calculus
SNR	Signal-Noise Ratio
SS	Scheduled Slots
SSSC	Stochastic Strict Service Curve
TCP	Transmission Control Protocol
TDMA	Time Division Multiple Access
TKIP	Temporal Key Integrity Protocol
TPSS	Traffic Proportional Slot Sizing
TSMP	Time Synchronized Mesh Protocol
TXOP	Transmission Opportunity
UAV	Unmanned Aerial Vehicule
UDP	User Datagram Protocol
VL	Virtual Link
VLID	Virtual Link Identification
WEP	Wired Equivalent Privacy
WRR	Weighted Round Robin
WSCAN	Wireless Safety-Critical Avionics Network

List of notations

N	Number of traffic classes generated by an arbitrary node
M	Number of end-systems within an arbitrary cluster
$\mathcal{M}$	Number of clusters
$\mathcal{N}$	Maximum number of transmissions
$f_{i,j}^k$	Periodic flow j of traffic class i generated at node k
f_i^k	Aggregate flow of all $f_{i,j}^k$
f^k	Aggregate flow of all f_i^k
$f_{\leq i}^k$	Aggregate flow of all flows that have higher priority than or equal to f_i^k
TC_i	Traffic Class i
T_i	Period of traffic class i
Dl_i	Deadline of traffic class i
L_i	Packet length of a message of traffic class i with No-ACK
L_i^{ETH}	Ethernet packet length of a message of traffic class i
L_i^{UWB}	UWB packet length of a message of traffic class i
L_{max}	Maximum packet length between all packets arriving to the switch
e_i	Transmission time of a message of traffic class i with No-ACK
e_{min}	Minimum transmission time of a packet with No-ACK
e_{max}	Maximum transmission time of a packet with No-ACK
$e_{max}^{1\leq j\leq i}$	Maximum transmission time of a packet with No-ACK between f_j^k $(1 \leq j \leq i)$
$e_{max}^{i<j\leq N}$	Maximum transmission time of a packet with No-ACK between f_j^k $(i+1 \leq j \leq N)$
B	Wireless transmission capacity
s^k	Slot of end system k
$\overline{s^k}$	Lower bound of offered TDMA time slot
$\overline{\overline{s^k}}$	Minimum offered TDMA time slot

WT^k	Maximum waiting time for the first transmission of f^k under FIFO at node k
$WT^k_{\leq i}$	Maximum waiting time for the first transmission of $f^k_{\leq i}$ under FP at node k
w^k_i	Allocated weight for f^k_i under preemptive WRR
$\overline{w^k_i}$	Allocated weight for f^k_i under non-preemptive WRR
$\overline{\overline{w^k_i}}$	Optimal allocated weight for f^k_i under non-preemptive WRR
c	TDMA cycle
c^u	TDMA cycle of cluster u
t_{syn}	Synchronization duration
t_{ACK}	ACK transmission time including SIFS
η_t	Number of packet transmissions on each frequency channel
η_f	Number of frequency channels
p	The crossover probability of the wireless channel
PER_{UWB}	Packet Error Rate induced by the UWB technology
PER_L	Packet Error Rate Level required by avionics
$\alpha^k_{i,j}$	Arrival curve of periodic flow j of traffic class i generated by node k
α^k	The arrival curve of f^k
α^k_i	The arrival curve of f^k_i
$\alpha^{GW_u,in}_{i,j}$	Arrival curve of $f^k_{i,j}$ at the input of the outgoing gateway of cluster u
$\overline{\alpha^{GW_u,in}_{i,j}}$	Scaled arrival curve of $f^k_{i,j}$ at the input of the outgoing gateway of cluster u
$\alpha^{GW_u,out}_{i,j}$	Arrival curve of $f^k_{i,j}$ at the output of the outgoing gateway of cluster u
$\alpha^{SW_v,in}$	Arrival curve of all flows at the input of the switch's outgoing port v
$\alpha^{GW_v,in}$	Arrival curve of all flows at the input of the incoming gateway of cluster v
$\overline{\alpha^{GW_v,in}}$	Scaled arrival curve of all flows at the input of the incoming gateway of cluster v
β_{c,s^k}	Premmptive service curve of node k having a time slot s^k, a cycle c under TDMA
β^k_i	Premmptive service curve of node k offered to flow f^k_i under FP or WRR
$\overline{\beta^k}$	Non-preemptive service curve of node k offered to flow f^k under FIFO
$\overline{\beta^k_i}$	Non-preemptive service curve of node k offered to flow f^k_i under FP or WRR
$\overline{\beta^k_{\leq i}}$	Non-preemptive service curve of node k offered to flow $f^k_{\leq i}$
$\beta^{GW_{out}}$	Total service curve of outgoing gateway
β^{SW}	Total service curve of switch
$\beta^{GW_{in}}$	Total service curve of incoming gateway

$\overline{S}^{GW_{out}}$	Scaling curve of outgoing gateway
$\overline{S}_i^{GW_{out}}$	Scaling curve of outgoing gateway for traffic class i
$\overline{S}^{GW_{in}}$	Scaling curve of incoming gateway
$\overline{S}_i^{GW_{in}}$	Scaling curve of outgoing gateway for traffic class i
$\overline{S_{i,j}^{GW_u,k}}$	Scaling curve of outgoing gateway for $f_{i,j}^k$
$\overline{S_{i,j}^{GW_v,k}}$	Scaling curve of incoming gateway for $f_{i,j}^k$
C	Switch capacity
C^S	Scaled switch capacity
C_i^S	Scaled switch capacity offered to traffic class i
B^S	Scaled wireless transmission capacity
$D_{i,j}^{ES_k}$	Delay bound of $f_{i,j}^k$ at end-system k
$D_{i,j}^{GW_u,k}$	Delay bound of $f_{i,j}^k$ at outgoing gateway of cluster u
D^{GW_u}	Delay bound of all flows at outgoing gateway of cluster u
$D_{i,j}^{SW_v,k}$	Delay bound of $f_{i,j}^k$ at switch's outgoing port v
D^{SW_v}	Delay bound of all flows at switch's outgoing port v
$D_{i,j}^{GW_v,k}$	Delay bound of $f_{i,j}^k$ at incoming gateway of cluster v
D^{GW_v}	Delay bound of all flows at incoming gateway of cluster v
$D_i^{GW_v}$	Delay bound of aggregate flow of TC_i at incoming gateway of cluster v
D_i^{e2e}	End-to-end delay bound of TC_i
$D_i^{e2e,\epsilon_u+\epsilon_v}$	Stochastic end-to-end delay bound of TC_i
D_i^{u,ϵ_u}	Stochastic delay bound of TC_i within cluster u
D_i^{v,ϵ_v}	Stochastic delay bound of TC_i at incoming gateway v
q_c	TDMA cycle sampling
α^ϵ	Stochastic arrival curve
β^ϵ	Stochastic strict service curve
Π^ϵ	Stochastic packet curve
$\overline{\mathcal{P}}$	Cumulative number of packets transmitted including retransmissions
π	Minimum packet curve
Π	Maximum packet curve
$\overline{L_i}$	Packet length of a message of traffic class i with ACK
$\overline{e_i}$	Transmission time of $\overline{L_i}$
ϵ	Probability of violation

Introduction

Context and Motivation

The complexity of avionics communication architecture is increasing inherently due to the growing number of interconnected subsystems and the expansion of exchanged data quantity. To follow this trend, the current architecture of new generation aircraft like the A380, A400M or A350 consists of a high rate backbone network based on a redundant AFDX (Avionics Full Duplex Switched Ethernet) [6] network to interconnect the critical subsystems. Then, each specific avionics subsystem could be directly connected to its associated sensors/actuators network based on low data rate buses like ARINC429 [7] and CAN [8]. Furthermore, to increase the reliability level, a back-up network based on Switched Ethernet guarantees a continuous service in case of failure on the redundant AFDX backbone. Although this architecture fulfills the main avionics requirements, the redundant communication architecture leads to a significant quantity of wires and connectors. For instance, the wiring-related costs during fabrication and installation are estimated at $2000 per kilogram, which leads to a total cost ranging from $14 Million for an aircraft like A320 to $50 Million for one like B787 [9]. The new generation aircraft A380 in particular contains 500 km of cables, which is one of the main reasons for production delays and cost overruns, estimated at $2 billions. In addition to the cost issue, avionics interconnects are still subject to structural failure and fire hazard, which decreases reliability and ramifies the maintenance.

To cope with these arising issues, cable-less avionics implementation will clearly improve the efficiency and reliability of aircraft, while reducing integration, fuel consumption and maintenance costs. Therefore, integrating wireless technologies in avionics context is proposed in this thesis as a main solution to decrease the weight and complexity due to wiring.

Wireless technology has been recently implemented for many real-time applications such as wireless industrial networks [10] and wireless sensor networks [11]. In the specific area of aerospace, the idea of using wireless technologies has been introduced in 1995 in [12] and more recently elaborated with the creation of the *Fly-By-Wireless* workshop [13] in 2007. This workshop brings together leaders from industry such as Airbus and NASA to discuss recent advances in

wireless communications for aerospace applications. Recent solutions based on wireless technologies were proposed for avionics to enhance non-critical functions, e.g., In-Flight Entertainment Network (IFE) [14], in-cabin communication [15] and aircraft health monitoring [5].

Unlike existing approaches in this area, our objective is to design and validate a new Wireless Safety-Critical Avionics Network (WSCAN) to replace the back-up network of the AFDX backbone. Our proposal is based on the ECMA-368 technology [16] (High Rate Ultra Wideband) due to its high data rate (up to 480 Mbps), its collision-free MAC protocol guaranteeing real-time avionics requirements and its high security and reliability mechanisms. However, many interesting challenges still need to be handled due to its sensitivity to interference and jamming attacks, inadequate features for avionics applications. Hence, efficient solutions have to be considered to cope with these limitations and integrate wireless technologies in avionics context.

Original contributions

Our main contributions are as follows:

— **Design of a new WSCAN:** The proposed WSCAN is based on ECMA-368 technology and integrates various features to guarantee the avionics requirements. First, since all end-systems are located in a small area, we propose a hybrid wired/wireless architecture for WSCAN where the end-systems in the same avionics bay can communicate with each other through a single hop communication. This architecture favors timeliness and reliable communication between end-systems at the same avionics bay. Then, we consider the TDMA mechanism as the arbitration protocol with various reliability mechanisms to enhance the system's predictability and reliability. Finally, we introduce some network isolation methods to guarantee security.

— **Timing analysis of WSCAN:** To guarantee the real-time requirements for safety-critical avionics, we introduce an analytical approach based on Network Calculus to evaluate the deterministic upper bounds on end-to-end delays of the proposed WSCAN, which will be compared to time constraints to prove the system schedulability. This timing analysis integrates the impact of the TDMA protocol with different scheduling policies, including First In First Out (FIFO), Fixed Priority (FP) and Weighted Round Robin (WRR); and the considered reliability mechanisms to prove the predictability and reliability of the system.

— **Enhancing WSCAN performances:** To enhance the scalability of avionics applications, we investigate many features of the proposed WSCAN, such as: (i) refining the system model of each end-system by using Integer Linear Programming, combined with

Network Calculus, to reduce the pessimism of delay bounds; (ii) reconfiguring the TDMA cycle and slots allocation for each cluster to obtain the optimal configuration minimizing the delay bounds; (iii) investigating the impact of the reliability mechanism based on retransmissions and acknowledgment, by introducing stochastic system models using the Stochastic Network Calculus [17] (an extension of Network Calculus). The main idea of Stochasitc Network Calculus is to allow a small probability of violation on the system performance evaluation to compute stochastic upper bounds on end-to-end delays, and consequently to reduce the pessimism of the deterministic delay bounds.

— **Validation of WSCAN:** The validation of WSCAN ability to enhance avionics application performances is done through a realistic case study. This case study consists of more than 40 end-systems that send a total of almost 200 different multicast flows. A performance evaluation of the proposed WSCAN is conducted to verify the timeliness and reliability requirements.

Thesis Outline

This thesis consists of five chapters. **Chapter 1** gives an overview of the avionics context and the most relevant work in the area of using wireless technology for real-time applications. First, we present the current safety-critical avionics network based on the AFDX as a backbone and CAN/ARINC429 as sensors/actuators networks. Then, the main benefits and risks of using wireless technology for safety-critical avionics are described. Finally, we present the most relevant work related to using wireless technology for industrial and aerospace applications, by focusing on the main challenges for implementing this technology for safety-critical applications.

In **Chapter 2**, we introduce the proposed WSCAN. First, we investigate the most relevant wireless technologies, which can provide the sufficient data rate and guarantee the major requirements of avionics applications. These technologies are detailed and compared to select the most suitable one. Furthermore, the risk analysis and the corresponding protective measures when using wireless in avionics context are described. Finally, the design of WSCAN is investigated considering the issues of timeliness and reliability.

In **Chapter 3**, we present the performance evaluation of the proposed WSCAN. First, we model the different network components based on the Network Calculus theory to compute deterministic upper bounds on end-to-end delays. Then, schedualability analysis integrating the impact of the considered MAC protocol and reliability mechanisms is provided. Finally, pre-

liminary performance analysis is conducted to estimate the real-time guarantees offered by our proposal.

In **Chapter 4**, we investigate the different directions to enhance the system scalability and reduce the pessimism of the deterministic upper bounds on end-to-end delays. First, we refine the end-systems modeling by using Integer Linear Programming and Network Calculus to obtain tighter delay bounds. Then, we investigate different TDMA configurations by varying the cycle duration and the slots allocation to find the most efficient one in terms of delay bounds. Finally, by considering the reliability mechanisms based on retransmissions with acknowledgment, we introduce a stochastic system modeling using Stochastic Network Calculus, which leads to tighter stochastic delay bounds by allowing a small probability of violation on the system's schedualability.

Chapter 5 presents a realistic case study to validate our network proposal. The end-to-end delay bounds are computed and the comparative analysis between different configurations is conducted. These results show the feasibility of our proposed WSCAN to guarantee the system's requirements, while enhancing its scalability.

Finally, the conclusions and perspectives of this work are presented.

Chapter 1

Background and Related Work

In this chapter, the main characteristics of the current avionic communication architecture and the most relevant work in the area of using wireless technology for real-time applications, including industry and aerospace, are presented. First, the main network technologies used in the current architecture and the avionics requirements are described. Then, the main benefits and risks of using wireless technology for safety-critical avionics are discussed. Finally, existing solutions to guarantee real-time performance while using wireless technologies for real-time applications are reviewed.

1.1 Background: Current Avionics Communication Architecture

1.1.1 Architecture Overview

As shown in Figure 1.1, the current avionics network consists of a redundant backbone network based on the AFDX technology [6] to interconnect the avionics end-systems which are responsible for flight control, cockpit, engines and landing gears. Some specific end-systems admit dedicated sensors/actuators network, based on CAN [8] or ARINC429 [7] buses. Furthermore, to increase the reliability level, a back-up network based on Switched Ethernet guarantees a continuous service in case of failure on the redundant AFDX backbone.

While the sensors and actuators are distributed throughout the aircraft (the head, the wings, the tail,...), the avionics end-systems, interconnected to the backbone network, are geographically concentrated in two avionics bays at the head of the aircraft, the main and the upper, as shown in Figure 1.2. Although this current architecture guarantees the avionics systems performance and reliability, it leads at the same time to inherent weight due to the significant quantity of wires and connectors. The main network standards used in this communication architecture are detailed in the next section.

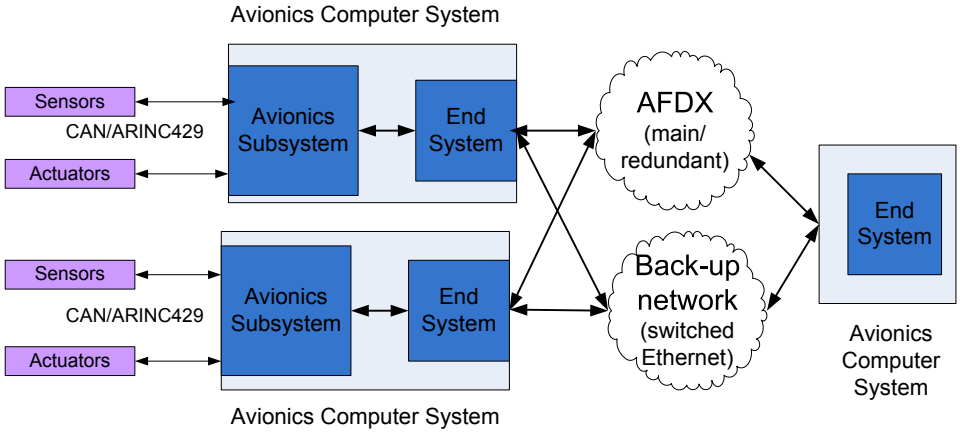

Figure 1.1: Current Avionics Network

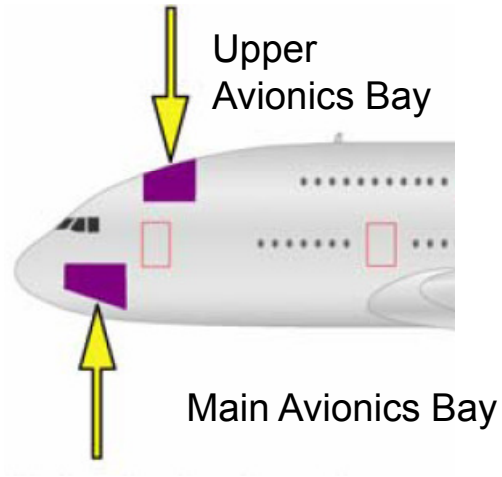

Figure 1.2: Avionics bays

1.1.2 Description of Network Standards

1.1.2.1 ARINC664: Backbone Network

The ARINC664 standard [6] has been introduced to meet the new requirements of Integrated Modular Architecture (IMA) [18]. For instance, AFDX standard based on Full Duplex Switched Ethernet at 100 Mb/s has been introduced in the Airbus A380 as a high-rate backbone. This technology succeeds to support the important amount of exchanged data and guarantee the timing requirements due to its high data rate, its policing mechanisms added in switches and the Virtual Link (VL) concept.

1.1.2.1.1 Virtual Link AFDX virtual link gives a way to reserve a guaranteed bandwidth to each traffic flow. Each VL is assigned an unique VL identification (VLID) of 48 bits. The VL represents a multicast virtual channel, which originates at a single source and sends its messages to a group of destinations. Each VL is characterized by: (i) Bandwidth Allocation Gap (BAG), ranging in powers of 2 from 1 to 128 ms, which represents the minimal inter-arrival time between two consecutive frames; (ii) Maximal Frame Size (MFS), ranging from 64 to 1518 Bytes, which represents the size of the largest frame that can be sent during each BAG. The illustration of Virtual Link Bandwidth control mechanism is shown in Figure 1.3. Using the VL control mechanism, the end-system can transmit several Virtual Links over a single Ethernet physical link.

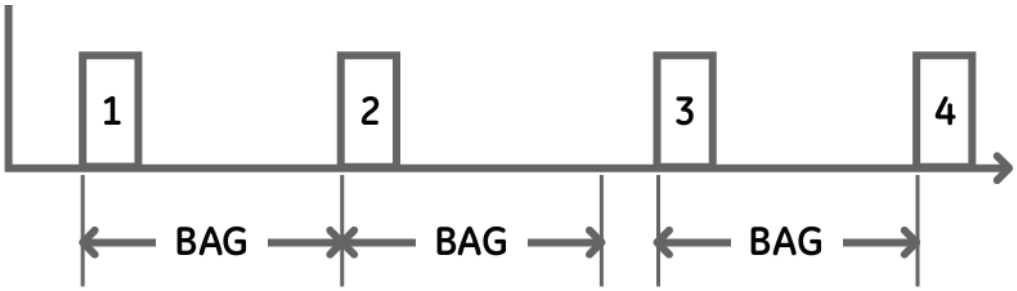

Figure 1.3: Virtual Link Bandwidth control mechanism

1.1.2.1.2 Message flow and Frame Structure The end-to-end communication of a message using AFDX requires the configuration of the source end-system, the AFDX network and the destination end-systems to deliver correctly the message to the corresponding receive ports. Figure 1.4 shows a message M being sent to Port 1 by an avionics subsystem. End-system 1 encapsulates the message in an AFDX frame and sends it to the AFDX network through VL 100, where the destination addresses are specified by VLID 100. The forwarding tables in the network switches are configured to deliver the message to both end-systems 2 and 3. The end-systems are configured to be able to determine the destination ports for the message contained in the frame. In this case, the message is delivered by end-systems 2 and 3 to ports 5 and 6, respectively.

An AFDX frame is based on the Ethernet frame, as shown in Figure 1.5. The Ethernet header identifies the source and destination end-systems. The IP and UDP headers allow each destination end-system to find the corresponding destination ports for the received message with the Ethernet payload. The Ethernet payload includes the IP packet and IP payload that consists of the UDP packet(header and payload). The UDP packet contains the message sent by the avionics applications. Padding is used if UDP payload is less than 18 Bytes, to guarantee the

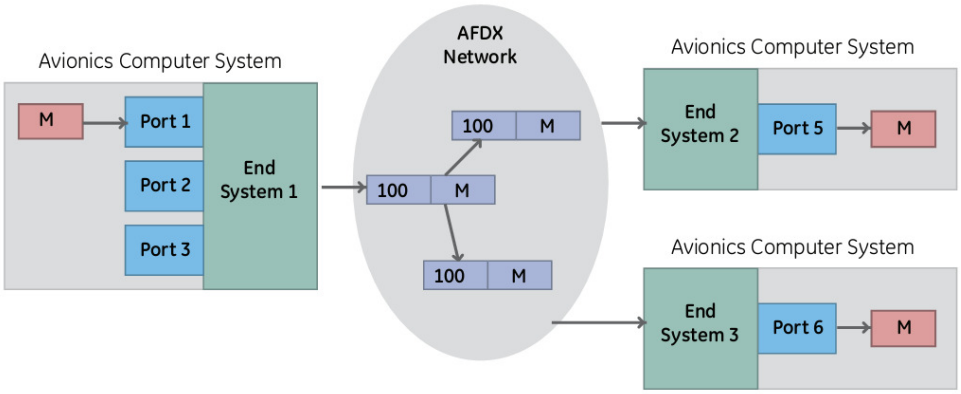

Figure 1.4: Example of application data flow on AFDX

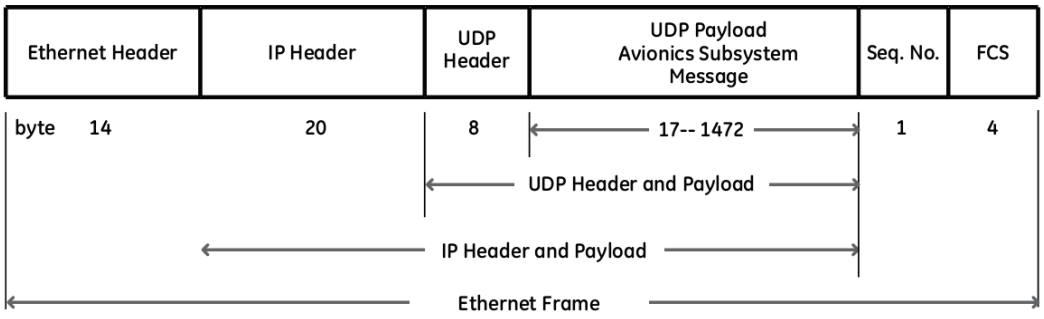

Figure 1.5: Structure of AFDX frame

minimum AFDX frame size of 64 bytes. The maximum frame size is inherited from Ethernet frame of 1518 bytes, without considering the Inter-Frame Gap (IFG) of 12 bytes and the preamble of 8 bytes.

1.1.2.2 Controller Area Network (CAN)

The Controller Area Network (CAN) [8] is a broadcast digital bus designed in 80s by Bosch GmbH for automotive applications, and today it is also used in avionics. CAN is standardized by International Standard Organization (ISO) to provide the data rate 1 Mb/s for cable length of 40 meters and 125 Kb/s for cable lengths up to 500 meters.

For high-speed CAN, there are two versions: the *standard* version with 11-bit identifier and the *extended* version with 29-bit identifier. At PHY layer, CAN uses the Non Return to Zero (NRZ) bit encoding. The two bits are encoded in medium states defined as the ”dominant” bit and ”recessive” bit, usually assigned for 0 and 1, respectively. At MAC layer, controllers con-

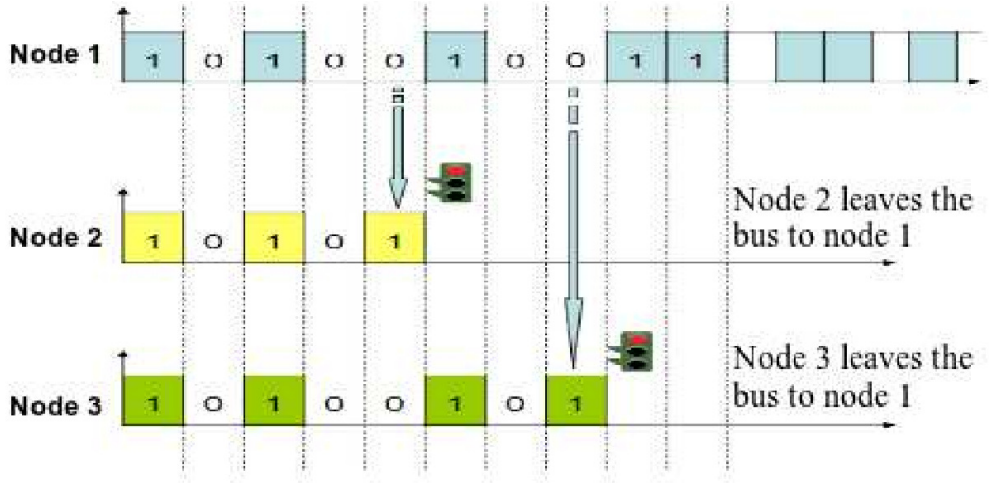

Figure 1.6: Arbitration based on Message Priority: CSMA/CR access mechanism

nected to the CAN bus use Carrier Sense Multiple Access with Collision Resolution (CSMA/CR) for medium access, message transmission and collision resolution. The main idea of CSMA/CR is as following. A CAN controller can transmit a new message only when the bus is idle. However, if two controllers try to transmit at the same time, then a message arbitration protocol is implemented to halt the lower priority message and complete the transmission of the higher priority message (Arbitration based on Message Priority or AMP). The arbitration protocol is performed by using the ADN implementation. The dominant bit state will always win arbitration over a recessive bit state. Therefore, the lower the value in Message Identifier (the field that used in the message arbitration process), the higher the priority of the message. As shown in Figure 1.6, these nodes try to send a message simultaneously. The lowest Message Identifier gains the highest priority to complete its message transmission.

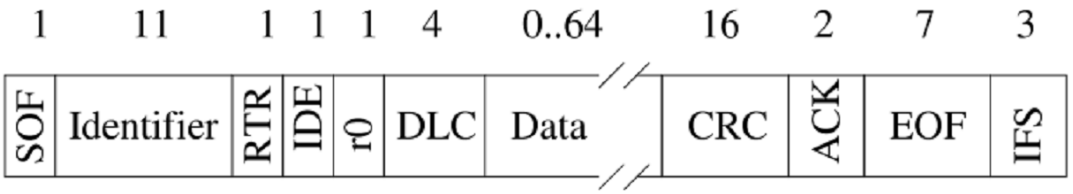

Figure 1.7: CAN 2.0A message format

The message frame format of CAN protocol is shown in Figure 1.7. Each CAN message frame consists of a payload up to 8 Bytes and an overhead of 6 Bytes due to different headers and bit stuffing mechanism. Each CAN frame contains the following bit fields:

— Start Of Frame (SOF) (1 bit): is always a dominant bit marking the beginning of a message transmission;

— Arbitration (13 bits): consists of the 11 bit Identifier, 1 bit of Remote Transmission Request (RTR) for a standard frame (or the Substitute Remote Request - SRR - for an extended frame), and finally the IDentifier Extension (IDE, always recessive bit) to determine if the frame is standard or extended. The arbitration identifies the type of CAN frame and defines the transmission priority on CAN bus;

— Control (5 bits): is composed of r_0 and r_1, reserved bits that are always dominant; and the Data Length Code (DLC) of 4 bits, which specifies the number of Bytes in the Data field;

— Data (1-64 bits): contains the actual information;

— CRC (16 bits): is used to guarantee data integrity;

— ACK (2 bits): allows receivers to acknowledge correct received messages;

— End Of Frame (EOF - 7 bits): indicates the end of the DATA frame;

— Intermission Frame Space (IFS - 3 bits): is the minimum number of bits separating two consecutive messages. During this intermission period, no other communication can start on the CAN bus.

1.1.2.3 ARINC 429

The ARINC standard [7] relies on unidirectional communications with a single transmitter and up to twenty receivers. Hence, it requires two channels or buses for bi-directional transmission. The network topology can be star or bus to interconnect the Line Replaceable Units (LRUs) as shown in Figure 1.8. Each LRU consists of multiple transmitters or receivers communicating in different ARINC429 buses. This simple architecture of the ARINC 429 offers a highly reliable communication with short transmission latencies.

The ARINC 429 is based on 32 bit data word, as described in Figure 1.9. ARINC 429 consists of 5 primary fields:

— Parity (1 bit): ARINC 429 uses odd parity for detecting bit errors to insure accurate data reception;

— Sign/Status Matrix (SSM - 2 bits): This field indicates the sign or direction of words data, reports operating status and depends on the data type;

— Data (19 bits): This field contains the word's data information and has the flexible bit format, e.g Binary (BNR) or Binary Coded Decimal (BCD);

— Source/Destination Identifier (SDI - 2 bits): This field indicates which source is transmitting the data and for which receivers;

— Label (8 bits): is used to identify the word's data type and can contain instructions or data reporting information. Labels may be refined by using 3 bits of the Data field (bit 11-13) to define a source Equipment Identifier (Equipment ID).

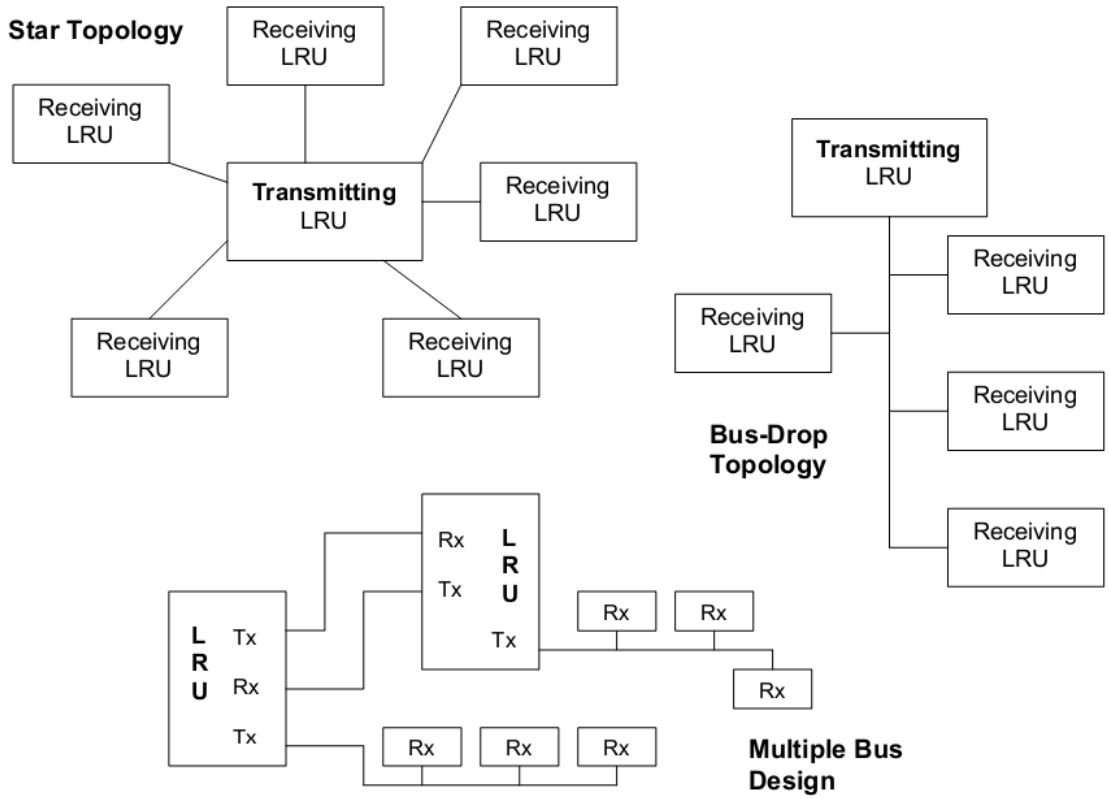

Figure 1.8: ARINC 429 network architectures

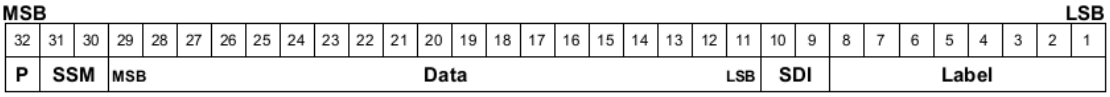

Figure 1.9: ARINC 429 frame format

1.1.3 Avionic Requirements

The Safety-Critical Avionics Network has to fulfill the following set of requirements:

— **Predictability:** the Avionics Network must behave in a predictable manner and the appropriate methods to guarantee its determinism need to be provided by the network

designers. For instance, the communication latencies, the backlog in a network queue or the Packet Error Rate (PER) must be bounded. The required proofs depends on the different avionics applications. For instance, an air pressure sensor has to sense and update the measurement 100 times per second. This information data must be sent periodically to one or many avionic calculators within a duration of 10 ms. To meet the predictability requirement, network designers must check and guarantee the successful delivery of each packet from the source to its all destinations within 10 ms.

— **Reliability:** the avionics network must be fault tolerant, and fulfill the required safety levels. Therefore, AN needs to implement the necessary fault detection and recovery mechanisms to satisfy this condition. One aspect related to the avionics system reliability consists in preventing transmission failure in the network from affecting the normal operations. Several mechanisms can be used to improve the reliability and the robustness of the communication network in avionics context. It is common to use multiple redundant data paths to enhance the network fault tolerance, such a mechanism is supported by the AFDX protocol [6]. Moreover, retransmission mechanisms can be implemented inside network nodes to recover packet losses.

— **Security:** the authors in [19] point out the security requirements which has to guarantee: (i) data confidentiality to ensure the privacy of end-users and keep the information secret by preventing passive eavesdropping from unauthorized users; (ii) data integrity to guarantee that the message from sender is original and not altered in transit by an adversary; (iii) authentication to prevent the unauthorized access to the network.

— **Electromagnetic Compatibility:** the avionics network has to cope with a harsh physical environment with important vibration, temperature variation and humidity. In addition, it must be able to work normally with the presence of intense radio frequency noise and should not cause interference to other aircraft systems.

— **Cost and life cycle:** These requirements are related to the maintainability, manageability and direct costs associated with the avionics system development and maintenance. One important step towards reducing avionics system costs was done with the modular design introduced by the Integrated Modular Avionics (IMA) approach. The flexibility and configurability of avionic systems reduce development cycle duration, and ease incremental design process and maintenance operations. Furthermore, the use of commercial off-the shelf (COTS) technologies and components, which are cheap and largely available,

aims to reduce development and deployment costs of the avionics system. Although the use of COTS technologies in the avionics context required additional development effort due to the strict avionics requirements, this choice offers significant system's cost reduction and it is currently an attractive alternative for aircraft manufacturers.

1.2 Wireless Technology: Candidate for Safety-Critical Avionics

As shown in Section 1.1, the current avionics architecture admits some limitations, mainly related to the significant weight and costs due to cabling.To cope with these arising issues, cable-less avionics implementation will clearly improve the efficiency and reliability of aircraft, while reducing integration, fuel consumption and maintenance costs. Therefore, safety-critical avionics based on wireless connectivity is proposed in this thesis to decrease the weight and complexity of wiring.

Nowadays, wireless technology becomes one of the most cost effective solution due to its ubiquity, simplicity and maturity and it has been recently implemented in many real time applications e.g like wireless sensors network [11] and wireless industrial networks [10]. However, many interesting challenges still need to be handled due to its non deterministic behavior and its sensitivity to interference and jamming. These features could make it inadequate to deliver the hard real time communications required by aerospace applications. In this specific area, there are some recent works for unmanned aerial vehicle (UAV) [20] and some proposed solutions for aircraft that could be classified in accordance with the criticality level and the set of requirements to fulfill.

Hence, wireless technology has progressed and introducing this concept for avionics has become feasible, but also advisable for the following reasons:

— first, a Wireless Safety-Critical Avionics Network (WSCAN) will allow an inherent weight reduction and an increase of system's flexibility and efficiency through less fuel consumption and better flight autonomy;

— second, eliminating the wiring-related problems shall enhance the system scalability and safety due to simpler fault allocation process and less fire hazards;

— third, wireless avionics implementation will inherently reduce the costs not only during design, production and development process but also during maintenance.

Currently, there is a new trend to use commercial off the shelf (COTS) technology rather than designing a dedicated solution to reduce the development costs. However, the problem with COTS is reconciling the different requirements between commercial and safety-critical applications. For wireless technologies, the main concerns are related to the system's susceptibility

against ElectroMagnetic Interferences (EMI). This is mainly due to natural phenomena or man-made events that could be internal or external to the plane, e.g. Portable Electronic Devices (PED), satellite communications or Radio Navigation. This results in both data rate and QoS degradation or a network collapse. Furthermore, there is system security issue due to the access and manipulation of sent information (Man-in-the-Middle) and denial of service (DoS) attacks [13].

As one can notice there is a trade-off to handle between efficiency and dependability when implementing wireless technologies for safety-critical applications. Hence, these issues need to be considered to design a new WSCAN.

1.3 Related work:Wireless Technology and Real-time Applications

Wireless Technologies have been introduced in various industrial applications, such as video surveillance [21], control [22] and vehicle tracking [23], but also for aerospace applications. Most of these applications require a data delivery in timely and reliable fashion where the energy efficiency consumption is no longer the main concern. Hence, we will detail in this section the most relevant work in the domain of using wireless technologies for hard real-time applications. First, we will present the main approaches for industrial applications, and particularly those focusing on the MAC protocol design for the delay-intolerant and loss-intolerant applications with strict requirements in terms of time and reliability, and the worst-case performance analysis of such protocols. Then, we will introduce the most interesting solutions in the aerospace context.

1.3.1 Industrial Applications

1.3.1.1 MAC Protocol Design

Most wireless network proposed for hard real-time applications adopt the Time Division Multiple Access (TDMA) technique for coordination. Using this technique guarantees a collision-free data delivery and predictable data transfer delays. Therefore, building a transmission schedule, which fulfills the end-to-end delay and reliability requirements, becomes feasible. The most notable MAC protocols that can provide such performance bounds for delay-intolerant and loss-intolerant ones are presented next.

1.3.1.1.1 Delay-intolerant Applications This kind of applications can tolerate relatively high loss but data must be received on time. Hence, to fulfill these applications requirements, the data delivery must respect a strict requirement in the time domain, but can be relaxed in

the reliability one. There are four main MAC protocols that have been proposed for this kind of applications and they are detailed as follows.

— **PEDAMACS**[24]: Power Efficient and Delay Aware Medium Access Control protocol for sensor networks (PEDAMACS) is based on centralized scheduling within a high-powered sink. The sink collects information about the traffic and topology during the setup phase. Then, it defines a global scheduling algorithm based on TDMA protocol, that will be broadcasted to the entire network. The protocol assumes that the sink can reach all nodes in a single-hop. The implemented collision-free scheduling algorithm within the sink is based on coloring the corresponding conflict graph of the network. During the setup phase, each node sends information to the sink based on the CSMA/CA protocol. The traffic pattern in this case is convergecast, which is a common communication pattern consisting in sending information from many different source nodes to a single sink. This protocol has been validated through simulations, and the comparative analysis with collision-based protocols shows that PEDAMACS offers a longer lifetime for sensor networks. However, the reliability requirements have not been integrated within the implemented scheduling algorithm, which is considered as a key issue for safety-critical avionics. Furthermore, the need of a high-powered sink, which can directly communicate with all nodes may be unrealistic for some time-critical applications.

— **RT-Link and HYMAC:** RT-Link [25] has been introduced for mobile and multi-hop wireless networks with energy and time constraints. This protocol is based on TDMA mechanism and an accurate synchronization protocol using out-of-band synchronization sources to be convenient for indoor and outdoor deployments. The protocol supports two types of slots: Scheduled Slots (SS) and Contention Slots (CS). Nodes operating in SS obtain exclusive slots to transmit and receive data packets, whereas those transmitting in CS use the slotted Aloha protocol to access to the medium. These contention slots provide new nodes an opportunity to join the network. Based on global topology information, the protocol builds a connectivity graph to define a collision-free slot schedule minimizing the end-to-end delays. RT-Link protocol has been validated through simulation and the comparative analysis with the most used MAC protocols shows its ability to enhance throughput and energy consumption. Hence, this protocol is convenient to support time-critical applications, however the reliability requirement has not been integrated and the use of out-of-band time synchronization sources may limit the application scenarios. Afterwards, the RT-Link has been extended to increase the network performance in terms of end-to-end delays by combining the TDMA and Frequency Division Multiple Access (FDMA) mechanisms in [26], and the extended protocol is called HYMAC. The use of

multiple frequencies has been efficient to avoid interference and allow some close nodes to transmit packets simultaneously. Therefore, with this enhanced scheduling algorithm, HYMAC has reduced significantly the delay bounds, however this protocol implies at the same time a higher hardware complexity to support multiple frequencies.

— **WirelessHART**: WirelessHART [27] is an open standard wireless sensor protocol, developed by the HART communication foundation. This protocol has been specified for industrial process monitoring and control, which requires real-time communication guarantees between devices. WirelessHART is based on a time-synchronized and self-organizing and healing mesh architecture. In this architecture, there are three main elements: the network manager, gateways and field devices (nodes), as illustrated in Figure 1.10.

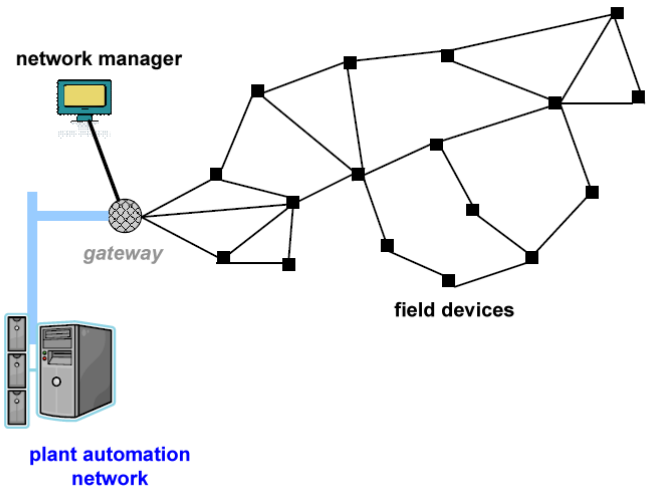

Figure 1.10: WirelessHART architecture

The network manager performs network configuration, communication scheduling between devices and network monitoring. Gateways enable communication between the host applications and the field devices, processing the corresponding equipments. This standard is combining TDMA and FDMA mechanisms and implementing the Time Synchronized Mesh Protocol (TSMP) [28] to guarantee predictability for self-organizing wireless networks.The network manager specifies a time slot and a frequency channel for each communication link between two field devices. This specification enables collision-free and deterministic communication, which guarantees bounded end-to-end delay for each packet delivery. In addition, WirelessHART implements several mechanisms to enhance the network reliability. For instance, the channel hopping and blacklisting techniques and frequency diversity mechanism are used to avoid interference and to guarantee reliability requirement.

Furthermore, the full mesh topology of WirelessHART protocol offers several redundant communication paths, which allow packets to be routed through multiple paths and increase the network reliability. Hence, WirelessHART guarantees the end-to-end delays and improves the reliability levels, which makes it adequate for real-time applications tolerating loss packets. On the other hand, WirelessHART performances depend essentially on the manager ability to schedule the traffic and configure the network, which represents a central point of failure and implementation complexity.

1.3.1.1.2 Delay-intolerant and Loss-intolerant Applications These applications require strict performance in both the time and reliability domains. There are two main solutions that have been introduced to handle these requirements.

— **Burst MAC**: Burst MAC is proposed in [29] to guarantee both timely and reliable communication for WSNs with bursty traffic patterns. The aim of Burst MAC is to reach low overhead with high throughput under high traffic load. This protocol assumes that the network topology is known and its deployment is planned apriori. Before the network deployment, measurement is performed to characterize the quality of the transmission links based on the new metrics B_{max} and B_{min}, which represent the maximum number of lost packets and minimum number of successful transmissions during each window with duration $B_{max} + B_{min}$. Hence, within $B_{max} + 1$ consecutive packet transmissions, there is at least one successful delivery. In addition, Burst MAC implements a scheduling algorithm based on TDMA protocol to avoid interference by allocating the same slot to many no interfering flows, and it overcomes the bursty errors using retransmissions. Hence, Burst MAC guarantees both bounded end-to-end delays and reliability requirements, while offering low overhead and high throughput. However, the need of knowing apriori the reliability metrics B_{max} and B_{min} may limit the use case scenarios.

— **GinMAC**: GinMAC is proposed for WSN with tree topology to guarantee both the timeliness and reliability requirements and its concepts are very similar to Burst MAC protocol. In fact, it is based on an off-line network configuration and implements a TDMA schedule to guarantee predictability, and delay conform reliability control to handle reliability requirements. First, during the off-line configuration process, the network topology, application traffics and communication links characteristics are defined. Pre-deployment is carried out to compute the metric B_{max} for each transmission link similar to the Burst MAC protocol. Then, an adequate TDMA slot is assigned to each node to transmit its data and the duration of the TDMA cycle is fixed. Unlike Burst MAC, the slots are exclusive and cannot be assigned to many nodes at the same time. Afterwards, based on the metric B_{max}, TDMA slots used for retransmissions are added to guarantee reliabil-

ity, while respecting the time constraints. GinMAC has the same limitations than Burst MAC where a pre-deployment phase is necessary to characterize the link characteristics. However, it implies at the same time more overhead than Burst MAC because of using exclusive TDMA slots and it is only adequate for networks with tree topology.

The most relevant features of the detailed MAC protocols are summarized in Table 1.1.

Table 1.1: MAC Protocols for Industrial Applications

Protocol	MAC layer	Delay	Reliability	Topology	Traffic
PEDAMACS	TDMA	Bounded	Medium	tree	Convergecast
RT-Link and HYMAC	TDMA	Bounded	Medium	tree	Convergecast
WirelessHART	TDMA	Bounded	Medium	Mesh	Any
Burst MAC	TDMA	Bounded	high	flat	Any
GinMAC	TDMA	Bounded	high	tree	Convergecast

1.3.1.2 Worst-Case Performance Analysis Approaches

For hard real-time applications with time and reliability requirements, it is important to be able to know before the deployment of the wireless network whether the applications needs can be fulfilled. Nevertheless, most of the MAC protocols detailed in this section have been validated through simulation, which is not enough to prove the worst-case behavior of the system. Analytical models must be introduced to determine end-to-end performance bounds under the worst-case scenario. In this domain, there are two main analytical approaches: Scheduling theory and Network Calculus [30]. The most relevant approaches are detailed next.

1.3.1.2.1 Scheduling Theory The authors in [31] propose a real-time asynchronous MAC protocol for hard real time applications using wireless technologies, called Robust Implicit Early Deadline First (RI-EDF). This protocol is based on Early Deadline First scheduling for the networks with fully connected topology. The main idea of this protocol is to provide efficient transmission of variable-sized packets avoiding bandwidth waste, unlike TDMA-based protocol. This fact consists in giving the opportunity to one node to reclaim the unused bandwidth of another node. The performance analysis of this protocol has been conducted based on the scheduling theory concepts to show its ability to handle the time requirements. However, this analysis considers the assumption of error-free environment and should be extended to the error-prone one.

Another interesting analytical approach based on scheduling theory has been proposed in [22]. The authors introduce an adequate solution for the railway alert system based on a wireless

infrastructure to send alerts to a remote worksite. This solution is based on TDMA protocol to guarantee predictability and frequency diversity to enhance the reliability level. The deployment of this solution requires to know the traffic characteristics (length and priority) and the required packet error rate level a priori. The performance analysis of such a solution has been conducted considering the assumption of preemptive communications and integrating the impact of retransmissions on the delay bounds.

1.3.1.2.2 Network Calculus Authors in [32] and [33] provide an analytical framework based on Network Calculus [30] to compute the guaranteed end-to-end delay bounds with TDMA-based protocols for wireless networks. This framework has been used efficiently to validate wireless sensor network deployment which requires hard guarantees on data delivery. However, the authors consider some restricted assumptions, which are not verified in the general case, such as preemptive communication and error-free environment.

Another interesting approach based on Network Calculus has been introduced in [34]. The main objective of this work is to compute a feasible routing including a set of paths and link activations which guarantee the schedulability constraints of each transmitted packet on Wireless Mesh Networks, based on TDMA protocol. Furthermore, the Delay-Aware Routing and Scheduling problem has been formulated using mixed-integer non-linear programming and solved based on heuristics. This approach has shown its ability to define an admissible routing algorithm respecting the time constraints. However, this work does not consider the impact of packet loss on the end-to-end delay bounds.

1.3.2 Aerospace Applications

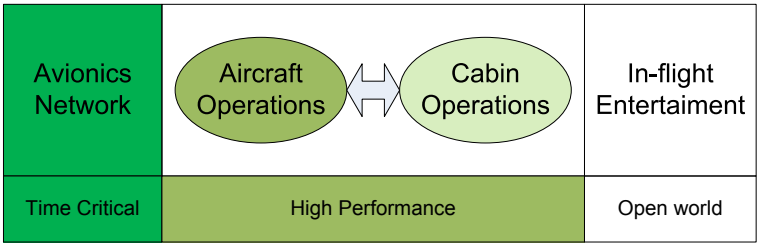

Figure 1.11: Avionics Data and Communication Network

Due to its maturity and reduced costs, wireless technology has been recently implemented in various aerospace applications, such as Unmanned Aerial Vehicle (UAV) and commercial aircrafts. We detail in this section the most relevant work in this domain. As shown in Figure 1.11, the Avionics Data and Communication Network (ADCN) consists of mainly three types of systems where time critical is the highest criticality level, while high performance and open

world correspond to the medium and lowest levels, respectively. For open world applications, one of the main constraint is to increase the bandwidth utilization, whereas the predictability and reliability are not the primary requirements. The high performance applications can be considered as soft real-time applications where most of packets must be delivered on time, thus these applications are considered as delay-tolerant and loss tolerant. Finally, time-critical applications are considered as delay-intolerant and loss-intolerant applications where the predictability and reliability requirements have to be guaranteed.

1.3.2.1 Unmanned Aerial Vehicle (UAV)

AIVA [1] is one of the main UAV frameworks, which is aiming to implement the fly-by-wireless paradigm for a fixed-wing UAV based on Bluetooth technology [35]. The considered UAV has a relatively small size with a height of 1.25m, a wing span of 4.80m and a fuselage of 2.90m. Due to these characteristics, the flight control system is designed based on a star-topology and formed a piconet. The master module can communicate and control sensor and actuator modules, concentrated in the wings and tails of the UAV. The master module consists of one processing unit for the Bluetooth piconet Master, one flight controller unit, one earth link and one embedded vision system. The sensors include GPS, inertial units and servo potentiometers. The actuators are the servo devices, driving the control surfaces, such as ailerons, flaps, elevator and rudder, but also the electric propulsion motors. Figure 1.12 represents this architecture. Using the Bluetooth piconet mode, the master module can communicate with 6 slave nodes through a Time Division Duplex mechanism, which guarantees deterministic communication. Furthermore, Bluetooth can provide a data rate of 1 to 3 Mb/s, which is sufficient for sensors/actuators communication. The first experiments of this fly-by-wireless system have shown its ability to guarantee the predictability and reliability requirements.

Another interesting work in [2] has focused on implementing a fly-by-wireless control for an autonomous quadrotor helicopter, using Zigbee technology [36]. The control loop is performed through a Ground Control System (GCS). Figure 1.13 illustrates the proposed architecture. The platform consists of two main blocks: the on-board electronics and the GCS. Both blocks uses XBee devices to support Zigbee protocol. To guarantee the temporal constraints, a TDMA-based MAC protocol, called Guarantee Time Slot (GTS) and supported by Zigbee standard, is used for communication between the drone and GCS. The determinism of the control-loop system has been proved through simulation and experiments.

1.3.2.2 Open-World Avionics Applications

To further improve the quality of service for passengers, the next generation aircraft aim to provide a wireless-based In-Flight Entertainment (IFE) network, which allows passengers to

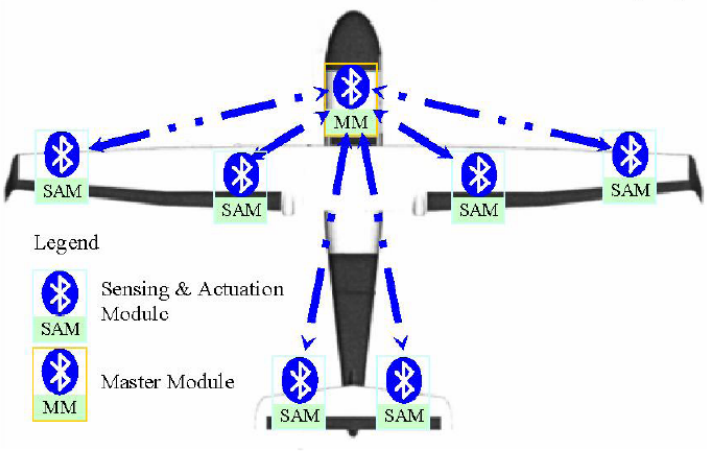

Figure 1.12: AIVA fly-by-wireless framework [1]

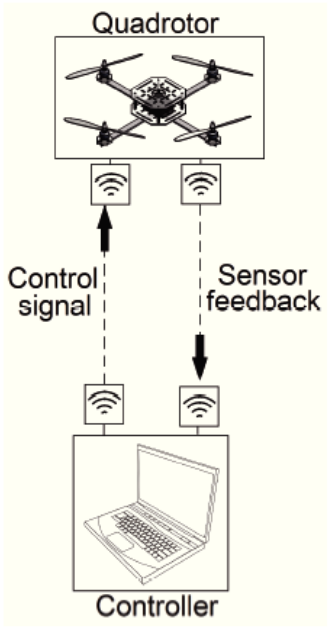

Figure 1.13: Quadrotor helicopter fly-by-wireless framework [2]

connect to Internet or entertainment program through their personal devices, such as phones, tablets and laptops. The IFE system consists of three type of links:

— Ground to aircraft link: it provides the connection between the aircraft and the Internet Service Provider (ISP). It can be implemented using satellite links or a direct ground RF

link;

— On-board Network: the current IFE system commonly uses shielded twisted pair cables inside the aircraft;

— User link: the connection link between a passenger's device and an access point.

To reduce the weight of cables and increase the flexibility, there are some noticeable works on IFE. In [37], the authors propose to use wireless optical communication to allow a reading lamp to work as an access point. To reduce the quantity of cables used for the network distribution, [3] has investigated several wireless technologies to build a light network inside an aircraft cabin. This work proposes to use PowerLine Communication [38] to interconnect the Seat Electronic Box (SEB) and the Data Server. The wireless link is used to connect passengers's devices to SEBs as shown in Figure 1.14. The authors have experimented and simulated different wireless technologies, such as HR-UWB [16], WLAN [39] and Bluetooth [35] to evaluate the network performances and select the most suitable technology for this application.

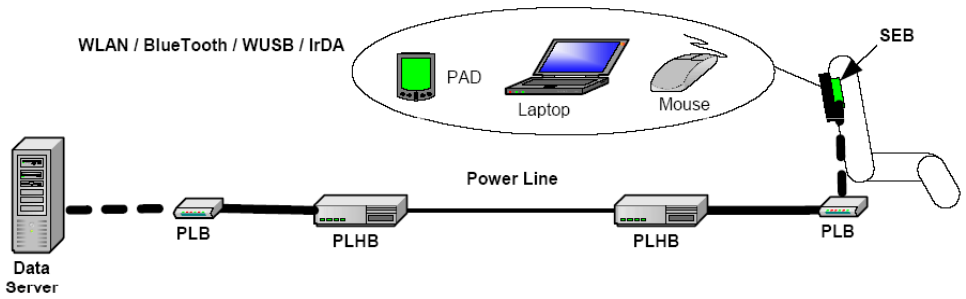

Figure 1.14: Heterogeneous network architecture of IFE [3]

1.3.2.3 High Performance Avionics Applications

High performance avionics applications consists of two main parts: non-critical aircraft monitoring applications and cabin operation. We present herein the related work on high performance avionics network.

— **WINDAGATE [4]**: a wireless sensor network is designed to replace the wired sensor network for gas turbine engine monitoring, which includes 12 km of wiring. This network has the following features: (i) severe RF interference; (ii) non light-of-sight communication; (iii) high-density od sensors (thousands of sensors); (iv) high data-rate and soft real-time transmission requirement with accurate synchronisation; (v) periodic traffic load.

The authors propose to use hybrid wired/wireless architecture with linear cluster topology. The proposed network includes three kinds of devices: Sensor Nodes (SNs), Cluster Heads

(CHs), and Wired Sinks (WSs). These nodes are hierarchically organized into clusters where the SNs communicate with a CH in a single hop, and then the CHs communicate with the Sink through multi-hop. Finally, the sinks are connected to the control computer using wires. Figure 1.15 illustrates the WINDAGATE topology. WINDAGATE investigates different deterministic MAC protocol, such as polling and TDMA-based mechanisms. Furthermore, the authors proposed the optimization of sensors localization and validated this framework through an engining testing.

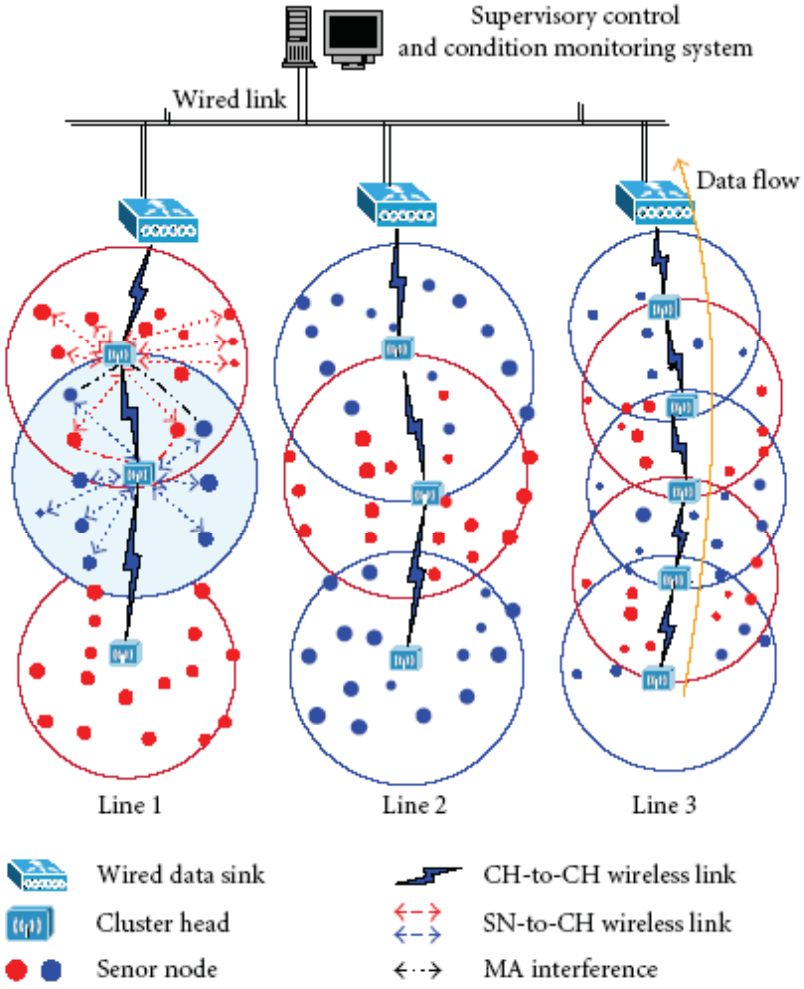

Figure 1.15: WINDAGATE Topology [4]

— **WSN for monitoring aircraft cabin environment** : In [40], the authors present an application of wireless sensor network for monitoring the aircraft environment, such as temperature, humidity and concentrations of $C0_2$ and 0_2. This proposed wireless network

which consists of hundreds of sensors organized in several cells with two redundant access points (sinks), has been deployed on board the Airbus A330-300. Each node is assigned to the closest Access Point (AP). The access to the medium is based on the TDMA protocol to guarantee predictability, and redundant APs have been used to guarantee the reliability requirement. The measurement shows that with two redundant APs, the packet error rate (PER) decreases four times, with reference to using a single AP. Figure 1.16 shows the setup of access points and wireless sensor nodes in the aircraft's cabin.

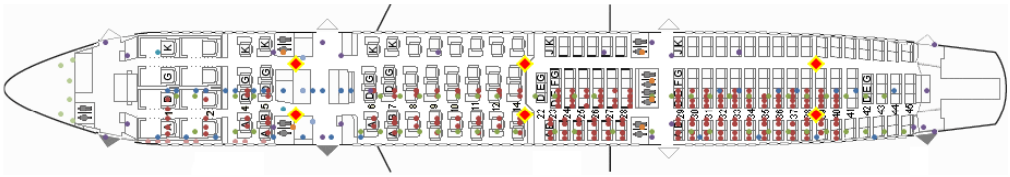

Figure 1.16: Setup of WSN for monitoring the aircraft's cabin [40]

— **Wireless cabin communication network [41]**: This work has focused on replacing the wired network for Cabin Management System (CMS) with the wireless UWB technology. The normal operation of CMS includes mainly illumination cabin, passenger service supply and cabin surveillance. The CMS consists of hundreds to thousands of nodes, which need to handle different traffic types with soft real-time requirements to guarantee various cabin operations. The proposed network topology is based on hybrid wired/wireless network where the end-nodes are clusterized and connected only to an AP via UWB links. Then, the APs are connected with each others via a wired network. Using a TDMA-based MAC protocol and organizing the network topology as a multi-cell network allow the implementation of the spatial re-use. This latter gives the opportunity to two nodes in different cells to transmit packets at the same time, which reduces the communication overheads and end-to-end delays. To optimize the radio resource planning, the authors in [41] have formulated an optimization problem to minimize the number of APs and to reduce the distance between end-nodes and their associated APs, while respecting the time and reliability constraints.

1.3.2.4 Safety-critical applications

In [5], the authors investigate the use of wireless technologies for aircraft control, such as distributed aircraft engine control and flight management control. The architecture of the proposed network for flight control is illustrated in Figure 1.17, where the flight control computer collects the information from sensors and commands the actuators using wireless communication. Furthermore, the authors in [42] [43] have conducted some experimentation to measure

the channel characteristics of the main COTS wireless technologies, including Zigbee [36] and 802.11a/b/g/n. Preliminary results have been presented concerning the BER/PER, the Signal-Noise Ratio (SNR) or the Received Signal Strength Indication (RSSI). These works still are at the first steps of investigation.

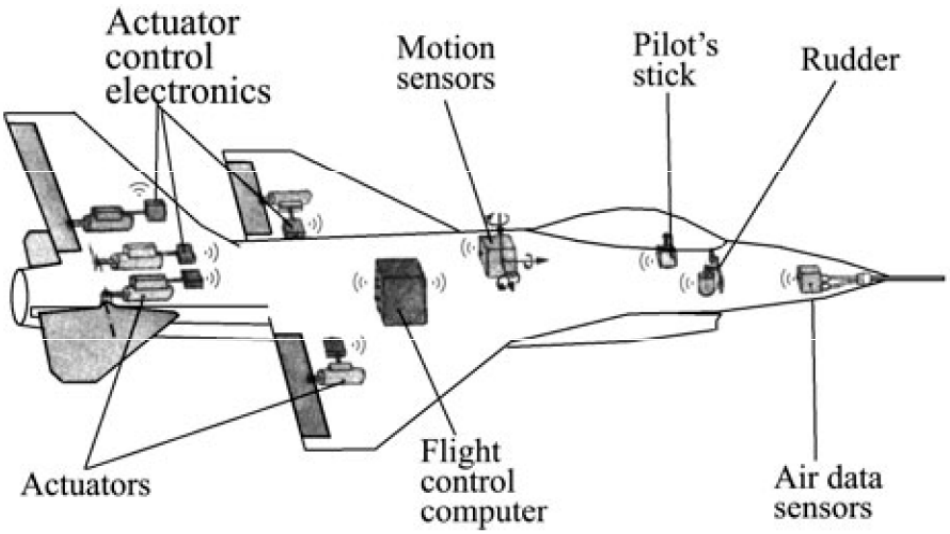

Figure 1.17: Wireless Fight Control System [5]

1.4 Conclusion

The current avionics communication architecture characteristics and its major limitations, mainly related to the wiring weight and costs, have been detailed. To cope with this emerging problem, implementing a cable-less avionics network based on wireless connectivity has been proposed as an interesting solution to improve the efficiency and reliability of aircraft, while reducing integration and fuel consumption costs.

Wireless technologies have been recently implemented for many real-time applications, including industry and aerospace. The main related work in this area has been reviewed in this chapter, and an efficient wireless network design for safety-critical avionics has not yet been addressed. Hence, there is a clear need for this kind of solution to decrease the wiring-related costs and complexity of next generation aircraft.

In the next chapter, we will detail the design of our proposed Wireless Safety-Critical Avionics Network (WSCAN), which guarantees the main system requirements in terms of predictability and reliability.

Chapter 2

Design of Wireless Network for Safety-Critical Avionics

The objective of this chapter is to design a WSCAN for new generation aircraft. First, we detail the main specifications of the WSCAN based on the characteristics of the current backbone network. Then, we assess the most common wireless technologies to satisfy these specifications. Afterwards, we analyze the risks and the introduced protective methods when using wireless technology in the avionics context. Finally, we detail the design of the proposed WSCAN, including the network architecture, the MAC protocol and the reliability mechanisms.

2.1 Specifications of Wireless Communication Network

In this section, the main specifications for WSCAN are detailed. This will allow the assessment of the most common wireless technologies that satisfy these identified specifications.

To replace the back-up part of the current safety-critical avionics network with a wireless technology, the requirements described in Section 1.1.3 of Chapter 1 have to be guaranteed and the specific conditions of avionics context should be integrated. The main identified specifications are the following:

— The offered data rate by the current backbone network is about 100 Mbps. The new technology must provide at least this capacity to meet the scalability requirement during an aircraft's lifetime (20-30 years);

— The range for each avionics bay is short (4-6 meters), and the distance between 2 different avionics bays is 6 meters but can be extendable. Hence, the considered wireless technology should cover at least this range;

— Currently, there are 40 to 80 end-systems connected to the backbone network. Hence, the selected technology for this kind of communication should be able to connect at least this

number of nodes;

— The current avionics end-systems are considered as complex equipments implementing many avionics functions that have to be powered all the time and their positions are fixed. Hence, the issues related to energy consumption and mobility are not applicable in the avionics context;

— The AFDX traffic is transmitted within Virtual Links, which represent multicast communication pattern originated at a single source and delivered to a fixed set of destinations. Hence, the communication pattern should be any and multicast for the WSCAN with peer-to-peer topology;

— The avionics data is time-constrained and has a high safety level. Hence, the determinism and particularly the predictability of end-to-end delays and the reliability of communication are of the utmost importance. These requirements imply contention free access methods with accurate reliability mechanisms.

The main identified characteristics of physical and MAC layers for WSCAN are summarized in Table 2.1.

Table 2.1: Physical and MAC layers Characteristics

		Backbone network
PHY Layer	Per link data rate	$\geq$ 100Mbps
	Network size	$40 - 80$ nodes
	Range (meters)	$4 - 6$ for each avionic bay & ≥ 6 for 2 avionic bays
	Topology	peer-to-peer
	Network pattern	any, multicast
MAC Layer	Mechanism	Contention free access
	Delay	End-to-end delay guarantee
	Reliability	End-to-end reliability guarantee
	Energy	No specific limitations on power consumption

2.2 Assessment of COTS Wireless Technologies vs Avionics Requirements

In this section, the most common wireless technologies that satisfy at least the required data rate for WSCAN are described.

2.2.1 802.11

Among several variants of IEEE 802.11, only the standard IEEE 802.11n [39] can provide the sufficient data rate to replace the current avionics backbone network. Therefore, we present here the overview of IEEE 802.11n standard.

2.2.1.1 PHY layer

To keep compatibility with the old standards (e.g 802.11a/g/b), the IEEE 802.11n operates at 2.4 and 5 GHz bands. At PHY layer, the standard uses three modifications to enhance the network performance, including:

— *Multiple Input, Multiple Out (MIMO)*: The sender and receiver can transmit and receive through two or more spatial channels simultaneously. MIMO-enabled senders and receivers use spatial multiplexing to transmit and receive data over separate antennas, providing high data throughput and allowing more reliable wireless communication.

— *Channel bonding*: The old standards of 802.11 are limited to transmitting over one of several 20-MHz channels. The 802.11n networks employ a channel bonding technique, which consists in combining two adjacent 20-MHz channels into a single 40-MHz channel to double the network capacity.

— *Advanced coding (Low Density Parity Check-LDPC)*: LDPC code is a linear block code specified by a sparse parity check matrix. The IEEE 802.11n LDPC codes are based on block-structured LDPC codes with circular block matrices [44]. Using LDPC for 802.11n brings significant improvement in terms of network reliability and throughput with reference to the old standards based on convolutional codes.

By applying these modifications above, IEEE 802.11n can achieve a maximum data rate of 600 Mbps in a range of 30 meters for indoor environment.

2.2.1.2 MAC layer

IEEE 802.11n implements the enhanced MAC protocol of IEEE 802.11, which is based on carrier-sense multiple access with collision avoidance (CSMA/CA) mechanism. Legacy 802.11 MAC protocol provides two access mechanisms: contention-based Distributed Coordination Function (DCF) and contention-free Point Coordination Function (PCF). The DCF mechanism is as follows: as soon as the sender has a packet to transmit, if the channel is idle, then the sender waits for a duration of DCF Inteframe Space (DIFS) before transmitting the data. If the channel is busy, then the node runs a random number generator of Contention Window (CW) to set up a *back off* clock. It waits until the channel becomes idle, then defers for extra DIFS and starts the backoff process. Figure 2.1 illustrates the IEEE 802.11 DCF channel access.

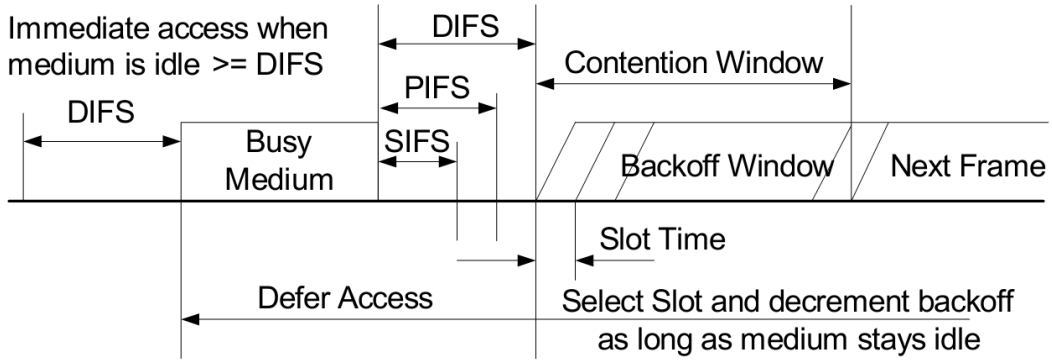

Figure 2.1: IEEE 802.11 DCF channel access

The IEEE 802.11n can also implement the improved mechanism of DCF called Enhanced Distributed Channel Access (EDCA). The EDCA is also a contention-based access mechanism that can provide differentiated QoS for different access categories (e.g video, voice, best effort...) by assigning different values of Interframe Space and Contention Window. Furthermore, EDCA allows the sender to transmit multiple packets in a period of Transmission Opportunity (TXOP) without entering backoff procedure, which reduces the overhead and increases the network utilization. In addition to TXOP, the block acknowledgment (block-ACK) mechanism can be used for further enhancement of the channel utilization efficiency. Figure 2.2 represents the IEEE 802.11n TXOP and block-ACK.

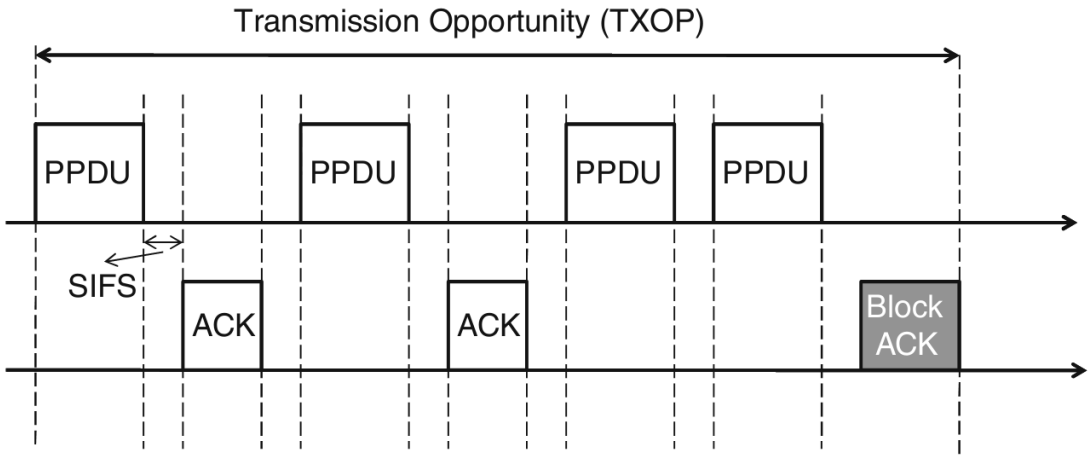

Figure 2.2: IEEE 802.11n TXOP and block-ACK

Furthermore, IEEE 802.11n introduces the aggregation mechanism at two levels: aggregate MAC protocol service unit (A-MSDU) and aggregate MAC protocol data unit (A-MPDU) to reduce the overhead and improve the network efficiency. The aggregation mechanism can work

with A-MPDU, A-MSDU or use both of them to form two-level aggregation.

In infrastructure mode integrating Access Point (AP), IEEE 802.11n supports the contention-free mechanism Point Coordination Function (PCF). The AP, considered as the coordinator, sends beacon frames to all other nodes at regular intervals; and between these beacon frames, the PCF defines two periods: the Contention-Free Period (CFP) and the Contention Period (CP). During the CFP, any node can transmit its data when it is polled by the AP; whereas during CP, the contention-based mechanism DCF is used.

Another enhanced version of PCF supported by IEEE 802.11n is called a Hybrid coordination function Controlled Channel Access (HCCA). With the HCCA, EDCA is used instead of DCF mechanisms during CP and the AP can initiate the CFP almost at anytime. Moreover, during TXOP, a node may send multiple packets in a row.

2.2.1.3 Security mechanisms

For security concerns, the IEEE 802.11n adopts the same mechanisms than IEEE 802.11i based on three data confidentiality protocols: Wired Equivalent Privacy (WEP), Temporal Key Integrity Protocol (TKIP), and Counter-mode/CBC-MAC Protocol (CCMP). The former uses weak Rivest Cipher 4 (RC4) stream cipher, while the two others use Advanced Encryption Standard (AES) algorithm which is more secure against exhaustive search (brute-force) attacks. Furthermore, TKIP and CCMP protocols provide Message Integration Code (MIC), and the authentication is enhanced due to Extensible Authentication Protocol (EAP).

2.2.1.4 Summary

While IEEE 802.11n can provide the sufficient data rate and the required reliability and security mechanisms for avionics applications, there are still less researches focusing on reliable multicast communication using MIMO technique. In addition, with ad-hoc mode, the CSMA/CA protocol cannot provide the required predictability level; whereas in the infrastructure mode, the AP is considered as a single point of failure that can lead to loosing the whole network. These aspects represent real limitations to use the IEEE 802.11n standard for safety-critical avionics where communication pattern is multicast and the predictability is required.

2.2.2 ECMA-368

2.2.2.1 PHY layer

ECMA-368 is a standard for High Rate Ultra WideBand (HR-UWB) technology within a short range operation [16]. This standard operates at large frequency band from 3.1 GHz to 10.6 GHz which is divided into 14 non-overlapping 528 MHz-Bands as illustrated in Figure 2.3. ECMA-368 uses the Multi-Band OFDM for access method that divides each band into

122 sub-carriers: 100 sub-carriers are allocated for data, 12 sub-carriers as pilot for channel estimation, and 10 guard sub-carriers. Furthermore, ECMA-368 can support data rate of 110 Mbps, 200Mbps and 480Mbps in a range of 10m, 6m and 2m, respectively.

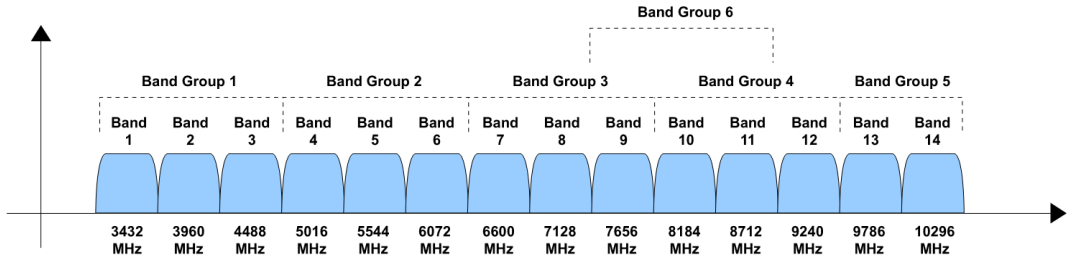

Figure 2.3: ECMA-368 band groups

2.2.2.2 MAC layer

ECMA-368 supports the peer-to-peer topology and two MAC protocols: Prioritized Contention Access (PCA) and Distributed Reservation Protocol (DRP). The former is a contention-based protocol with prioritized Quality of Service (QoS) similar to the EDCA mechanism of IEEE 802.11n; whereas the latter is a distributed TDMA-based protocol which guarantees a contention-free access.

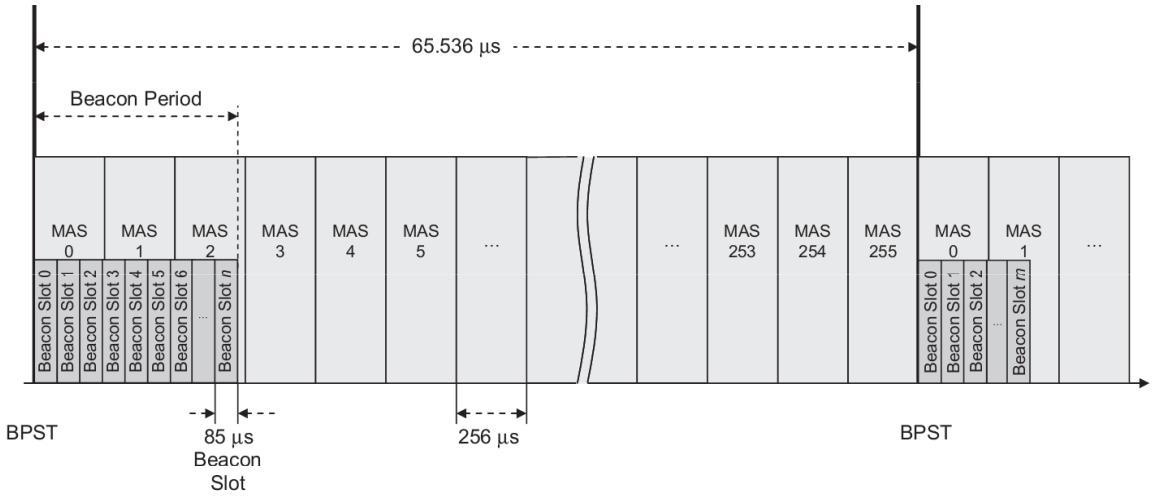

Figure 2.4: ECMA-368 superframe

For TDMA-based protocol, three parameters are defined: Superframe, MAC Access Slot (MAS) and Beacon slot. Superframe is a time duration which always starts with a Beacon Period

Start Time (BPST) and contains MASs. There are exactly 256 MASs in each superframe and each MAS has a duration of 256 μs. This fact induces a superframe duration of exactly 65536 μs. Each beacon slot has 85 μs duration. The Beacon Period (BP) consists of a set of beacon slots and it is used to synchronize, coordinate and reserve the MASs for each node. Figure 2.4 illustrates the time slots configuration in a superframe structure.

In terms of reliability, ECMA-368 supports Forward Error Coding (FEC) convolutional code with different coding rates at PHY layer and retransmission mechanisms with Immediate Acknowledgement (Imm-ACK) and Block Acknowledgement (B-ACK) at MAC layer.

2.2.2.3 Security mechanisms

This standard integrates strong security mechanisms. For data encryption, it uses Advanced Encryption Standard (AES) algorithm with Pairwise Transient Key (PTK) for unicast communications, and Group Transient Key (GTK) for multicast and broadcast communications. Furthermore, like IEEE 802.11n, integrity is guaranteed with Message Integration Code (MIC) and the authentication is based on 4-way handshake.

2.2.2.4 Summary

Due to its high data rate, security mechanisms and deterministic MAC protocol with peer-to-peer topology, ECMA-368 represents a good candidate to replace the current avionics backup network. In addition, its low energy and low range emission make this technology more secured than 802.11n for "man-in-the-middle" attack, which requires of the attackers to be very close to the end-systems.

2.2.3 IEEE 802.15.3c

2.2.3.1 PHY layer

IEEE 802.15.3c is a recent wireless technology, which operates at 60GHz frequency band and can provide data rate up to 5 Gb/s [45]. IEEE 802.15.3c is designed for 5 Usage Models (UM):

1. Uncompressed video streaming
2. Uncompressed multivideo streaming
3. Office desktop
4. Conference ad hoc
5. Kiosk file downloading

Due to conflicting requirements of the different UMs, three different PHY modes are developed:

— Single Carrier PHY mode (SC PHY) that is suitable for UM3 and UM5. SC PHY supports three classes of modulation and coding schemes focusing on different wireless connectivity applications. The data rates provided by these three classes vary from 1.5 Gb/s to 3Gb/s. The modulation schemes can be Binary Phase Shift Keying (BPSK), Quadrature Phase Shift Keying (QPSK), 8-PSK, 16-Quadrature Amplitude Modulation (16-QAM), On-Off Keying (OOK) and Dual Alternate Mark Inversion (DAMI). There are two main FEC schemes specified in this standard: Reed-Solomon (RS) block codes and Low-Density Parity Check (LDPC).

— High-Speed Interface PHY mode (HSI PHY) is suitable for the bidirectional, low-latency communication of the conference ad hoc model (UM4). HSI PHY uses OFDM with three modulation schemes: QPSK, 16-QAM and 64-QAM. The data rates of HSI PHY are ranging from 1.5 to 5.7 Gb/s. In HSI PHY, only the LDPC is used to enhance the reliability, which offers better coding gains than RS coding.

— Audio/visual PHY mode (AV PHY) is used for UM1 and UM2. Since the devices of this mode are designed only as data source (e.g, DVD player) or data sink (e.g, HDTV), the AV PHY is designed for highly asymmetric data transmission. AV PHY mode has two different OFDM-based sub-PHY modes: High-Rate PHY (HRP) for video transmission and Low-Rate PHY (LRP) for the control signal. The HRP can provide data rates of 0.95, 1.9 and 3.8 Gb/s. AV PHY uses only two modulation schemes QPSK and 16-QAM with RS code.

Hence, the HSI PHY is the most suitable PHY mode for critical avionics applications. However, IEEE 802.15.3c is based on directional antennas with Light-of-Sight (LoS) condition, which is not suitable for multicast or broadcast communication patterns.

2.2.3.2 MAC layer

The MAC protocol for IEEE 802.15.3c is under development and TDMA-based MAC protocol is the most promising candidate. For ad-hoc architecture, among a group of devices, one will act as the network coordinator, and the time is divided into sequential superframes. Each superframe has three segments: a beacon period (BP), a contention access period (CAP) and a channel time allocation period (CTAP). In BP, the coordinator sends one or multiple beacons. In CAP, the nodes are based on the CSMA/CA protocol to transmit their messages to the coordinator and other nodes. In CTAP, each node is granted an exclusive slot to transmit its data according to TDMA protocol.

To improve the network utilization efficiency, IEEE 802.15.3c introduces the Block-ACK and the MAC Service Data Unit (MSDU) aggregation with two modes: standard and low-latency. In the standard mode, MSDU are fragmented if they exceed the predefined threshold. In low-

latency mode, the MSDUs from the upper layer are directly mapped into subframes without fragmentation and transmitted as soon as possible.

The security mechanisms of IEEE 802.15.3c are under development.

2.2.3.3 Summary

Because of its LoS requirements and its immaturity, this technology is considered as inadequate to replace the current safety-critical avionics backup network.

2.2.4 Comparative analysis and selected wireless technology

Table 2.2: Wireless Technologies Parameters

Standard	802.11n	HR-UWB	60 GHz
Max Range (m)	30	10	10
Frequency bands	2.4, 5 GHz	3.1-10.6 GHz	60GHz
Bandwidth	20/40Mhz	500MHz-7.5GHz	5-7GHz
Non-overlap channels	3	14	1
LoS requirement	No	No	Yes
Max data rate (Mbps)	600	110 (10m)/ 200(6m)/480(2m)	3000
Encryption	RC4, AES	AES	NA
Topology	ad-hoc, infrastructure	peer-to-peer	ad-hoc
MAC protocol	DCF, PCF, EDCA, HCF	PCA or DRP	TDMA

Table 2.3: Wireless technologies vs avionics requirements

	802.11n	ECMA-368	IEEE 802.15.3c
Determinism	PCF (Yes), DCF (No)	DRP (Yes), PCA (No)	TDMA (Yes)
Reliability	Medium	Medium	Medium
Security	High	High	N.A
EMI Susceptibility	High	Low	Low

The main characteristics of the described wireless technologies are summarized in Table 2.2. The comparison of these three technologies in terms of avionics requirements is shown in Table 2.3. In terms of predictability, only ECMA-368 and IEEE 802.15.3c support deterministic MAC in ad-hoc mode by using TDMA-based protocol. However, in terms of reliability, the three technologies use the Automatic Retransmission reQuest (ARQ) with acknowledgment and FEC code. Concerning security, while 802.11n and ECMA-368 implement advanced mechanisms to

protect the wireless network from security threats, the IEEE 802.15.3c security mechanisms are still under development.

From this analysis, ECMA-368 is considered as the most accurate one to replace the avionics backup network due to its high data rate, deterministic MAC protocol and high security mechanism. Hence, this technology is selected to design our proposed WSCAN. However, there still are some challenging issues to integrate this technology for avionics applications. The risk analysis and the protective measures are detailed in the next section.

2.3 Risk Analysis and protective measures

2.3.1 Risks and transmission failures

Table 2.4: Basic wireless communication risks and their consequences

Basic risks	Consequences
The transmission signal fades because of obstacles	Signal level is low. Bit error rate (BER) increases. Data is corrupted or lost.
Transmission signal fades because of environment conditions	Signal level is low. Bit error rate (BER) increases. Data is corrupted or lost.
Two or more signals interfere with each other and cause improper signal for receiver	BER is high. Data is corrupted or lost.
The signals are reflected from surfaces resulting in echoes and interference.	Signal level is low. Bit error rate (BER) increases. Data is corrupted or lost. Inserted new packets.
Poor capability of a relaying station.	The signal can be delayed due to large amount of traffic or extra signal processing at relaying node.
Nearby wireless network is using similar communication protocol.	One node is substituted intentionally or unintentionally with another node.
Intentional penetration to wireless network.	New packets may be inserted.

Using wireless technology for WSCAN induces several risks having consequences on the communication quality. In the context of WSCAN, the end-systems are static and have no constraints on energy consumption, which avoids the risks caused by node mobility and sleeping nodes. However, there still are several risks that cause the degradation of the communication

quality. Table 2.4 details the basic wireless communication risks and their consequences [46]. For instance, the signal fades due to obstacles or environment conditions can lead to a low signal level, which will increase BER and induce the data corruption or loss. Furthermore, the capability of a relaying node can be degraded under bursty traffic, which will increase the communication delays. Finally, the sensitivity of wireless technologies in open environment increases the risks of intentional penetration, and consequently the insertion of new packets.

These risks will cause the main following transmission failures.

— Duplication: the same packet is sent in duplicate, which may prevent the transmissions of useful packets.

— Corruption: data are changed in the packet. The corruption can be caused by electromagnetic interference, which changes the value of some bits of the packets.

— Deletion: the transmission media is not able to function or there is disturbance so that sometimes the packet cannot be received. Usually detected corruption in a packet leads to deletion (the receiver discards the packet).

— Insertion: the packet is received unintentionally when a receiver gets an additional packet, which is interpreted to have correct address.

— Incorrect sequence: the packet are received in an incorrect order.

— Delay: the data is received correctly but too late. Delay can be caused by interference or bursty traffic.

— Erroneous addressing (masquerade): the packet is not what it pretends to be. Masquerade is caused by an unauthorized packet(e.g. a malicious packet).

Table 2.5 shows the associations between the basic risks and the transmission failures. As shown in Table 2.5, the duplication transmission can be caused by signal reflexion or intentional penetration. Furthermore, the low signal level caused by interference and fading may lead to data corruption or deletion, which reduce the capacity of relaying nodes and increase communication delay. The security related risks, such as intentional penetration or similar protocol of nearby network, provoke the masquerade, incorrect sequence, message insertion or duplication. These transmission failures need to be mitigated to satisfy the requirements of WSCAN.

2.3.2 Protective measures

The general methods to cope with transmission failures for wireless technologies are presented in Table 2.6 [46].

In particular, the ECMA-368 technology implements various defensive methods to cope with the main transmission failures. For instance, the basic methods such as frame sequence number,

Table 2.5: Associations between basic risks and transmission failures

Basic risks	Transmission failures						
	Duplication	Corruption	Deletion	Insertion	Sequence	Delay	Masquerade
The signal fades because of obstacles.		x	x			x	
The signal fades because of environment conditions.		x	x			x	
The signals are reflected from surfaces resulting in echoes and interference.	x		x			x	
Two or more singals interfere with each other and cause improper signal for receivers.		x	x			x	
Poor capability of a relaying station.						x	
Nearby wireless network is using similar communication protocol.				x			x
Intentional penetration to wireless network.	x			x	x		x

Table 2.6: Transmission failures and Protective methods

	Defensive methods													
	In ECMA-368										Not in ECMA-368			
Threat	Sequence number	Time stamp	Time out	Error detecting code	Feedback packet	Authentication control	Identifier for sender and receiver	Collision-free protocol (e.g Time triggered architecture)	Cryptographic codes	Forward Error Code	Diversity (Time & Frequency)	Optimized scheduling	Non overlapping frequency	Network Isolation
Duplication	x	x						x						
Corruption				x	x					x	o		x	x
Deletion	x	x			x			x		x	o		x	x
Insertion	x				x			x			o		x	x
Incorrect Sequence	x	x			o			x	o		o			
Delay			x		x						x	x		
Masquerade	o			x	x	x	x		x	o				x

x: Effective method against the risk

o: Some effect against the risk

time stamp, error detecting codes, feedback and time out are already standardized. Furthermore, ECMA-368 supports the collision-free TDMA-based MAC protocol and convolutional coding for error forward coding that will improve the network predictability and reliability. Furthermore, the security mechanisms of ECMA-368 integrate network authentication, message cryptography and node identification. However, these defensive methods are not sufficient to handle hard real-time communication. Hence, ECMA-368 needs additional mechanisms to be adapted to guarantee the requirements of safety-critical avionics applications.

We will detail in the next section the following modifications of ECMA-368 to design the WSCAN :

— The integration of an optimized TDMA scheduler under different scheduling policies to enhance timing performances;

— The introduction of diversity techniques and enhanced feedback mechanism to offer higher reliability level;

— The network isolation to improve the electromagnetic compatibility and the security of the system.

2.4 Design of WSCAN

In this section, we first present the considered architecture of the proposed Wireless Safety-Critical Avionics Network. Then, we detail the selected MAC protocol to enhance the communication predictability and determinism. Finally, the selected reliability mechanisms to fulfill the avionics requirements are described.

2.4.1 Hybrid Architecture ECMA-368/ Switched Ethernet

As described in Table 2.1, the current backbone network consists of maximum 80 end-systems. They are concentrated in two avionics bays at the head of the aircraft, as shown in Figure 1.2. Furthermore, the area of each avionics bay is less than the area of a 6m-diameter circle. The end-systems in each avionics bay are regrouped into a cluster. Each cluster has a peer-to-peer topology which guarantees single hop intra-cluster communications with a data rate of 200 Mbps in a range of 6 meters.

The inter-cluster communication is handled by specific gateways and the communication patterns between gateways could be unicast, multicast or broadcast. Since the distance between the main and upper avionic bays is about 6 meters (see Figure 1.2), two main solutions could be considered for the gateways interconnection: wireless or wired interconnection.

With wireless interconnections between the gateways, the end-to-end delays can inherently increase due to the required contention-free access mechanism and half-duplex communication.

Moreover, this architecture should be more sensitive to interference and reduce system scalability. In fact, the addition of new avionics bays in the middle or in the back of the aircraft will require many relaying nodes between the gateways. The offered rate in this case is about 200Mbps between two consecutive relaying nodes, but much lower between the gateways. Hence, this solution is considered as inadequate for the inter-cluster communications within the avionics network.

To cope with the limitations of a full-wireless architecture, a hybrid architecture based on a Full Duplex Switched Ethernet [47] at 1Gbps to interconnect the two clusters is considered as an interesting solution. As shown in Figure 2.5, a central switch is used to connect the two gateways. Unlike the wireless interconnection where the gateways have to transmit their packets only during their exclusive slots, with the Full Duplex Switched Ethernet, each gateway can transmit immediately its packets to the switch, to be then relayed to the final destination(s).

Hence, this characteristic allows high rate, deterministic and reliable communications. Furthermore, this hybrid architecture is more scalable since additional avionics bays can be easily interconnected in the middle or in the back of the plane. Given all these advantages, we consider the hybrid architecture to design the Wireless Avionics Network.

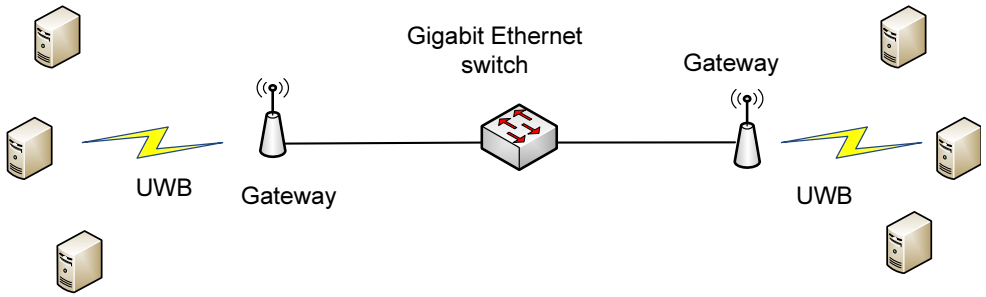

Figure 2.5: Proposed Avionics Network with hybrid architecture

The gateways and the switch in this hybrid architecture have key functions. Each gateway has to convert the received ECMA-368 frames from any end-system in its associated cluster to Ethernet frames that will be transmitted to the Ethernet switch. Hence, to keep the end-to-end communication transparency, each gateway proceeds as follows: each received ECMA-368 packet from an end-system in the associated cluster is encapsulated in an Ethernet frame (which respects the minimal and maximal sizes) and then transmitted to the Ethernet switch; and each received Ethernet frame from the Gigabit Ethernet switch is decapsulated to extract the ECMA-368 packet to be then transmitted to the final destination. ECMA-368 and Gigabit Ethernet frames are described in Figures 2.6 and 2.7.

The Ethernet Switch is an active device that identifies the destination port of an incoming

packet and relays it to the specific port. If multiple packets have the same destination port, then buffers are used to solve the problem of collisions. Ethernet switches can be identified by their switching technique and their scheduling policy. First, two types of switching techniques are currently implemented in Ethernet switches: *Cut Through* and *Store and Forward*. With the first, only the header of each packet is decoded to determine its destination port and the rest is forwarded without any error checking mechanism. With the latter, the switch waits until the complete reception of the packet and forwards it to the destination port if it is successfully verified. In our case, we choose the "store and forward" switching technique for safety reasons since no corrupted packet will be forwarded. Then, the scheduling policy is used to forward packets at the switch output port. We consider the widely implemented policy, First In First Out (FIFO), where packets are served in their arrival order without taking into account their temporal characteristics.

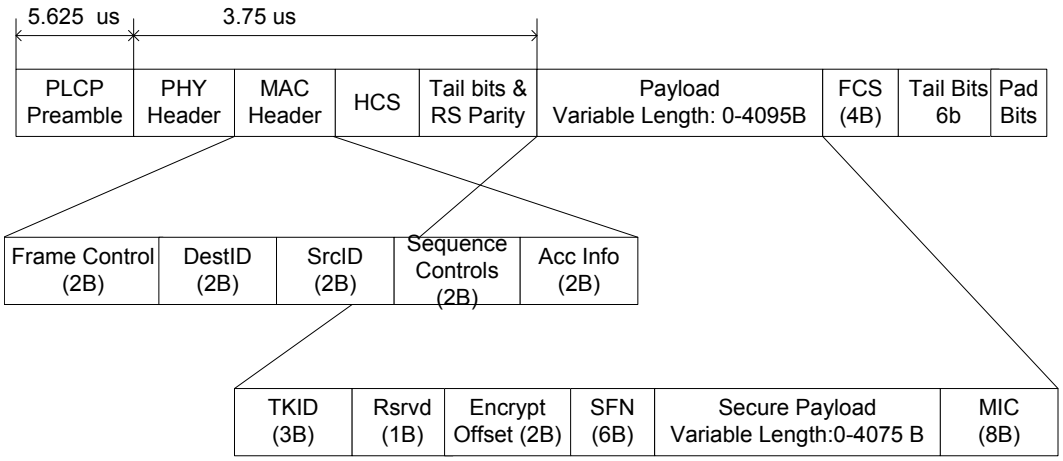

Figure 2.6: ECMA-368 Frame Structure

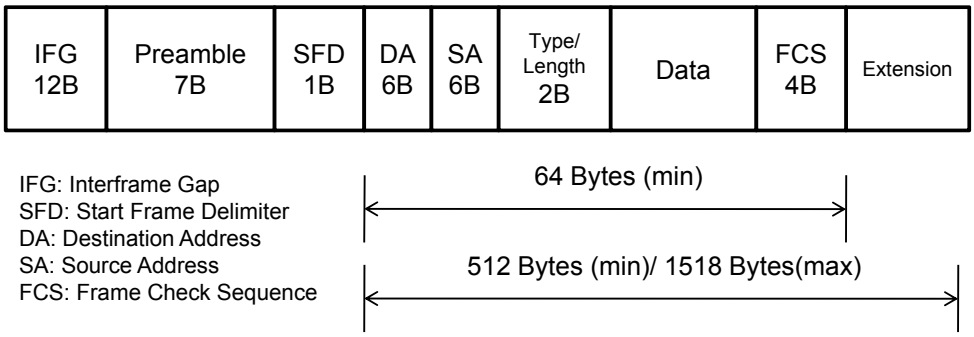

Figure 2.7: Ethernet frame structure

Furthermore, the use of hybrid wired/wireless architecture allows the isolation of each cluster by using electromagnetic shielding methods which will be presented in Section 2.4.4. The isolation allows the reuse of the same frequencies in each cluster and avoid interference and jamming attacks.

2.4.2 MAC Protocol

As described in section 2.2.2, ECMA-368 supports two MAC protocols: PCA and DRP. The former is a contention-based protocol with prioritized Quality of Service (QoS), whereas the latter is a TDMA-based protocol to guarantee a contention-free access.

Since for avionics applications, it is essential to guarantee predictable behavior under hard real time constraints, the DRP protocol seems more accurate than the PCA one for this context. However, the slots allocation and the cycle duration must be carefully configured to handle efficiently different types of traffic and guarantee different temporal constraints.

The following assumptions are considered for our proposal:

— **Off-line configuration**: since all generated packets are known a priori, the slots allocation mechanism is configured off-line and it will be followed in a static manner by all the end-systems during the network deployment;

— **Slots and cycles durations**: under DRP protocol, the classic superframe format may imply a long synchronization phase and long transmissions delays which are unsuitable for avionic applications with short deadlines ranging from 2 to 128 ms. Hence, we modify this classic superframe as shown in Figure 2.8. During each minor cycle, the allocated time slot for each end-system is fixed and has a defined duration that depends on its generated traffic. Hence, the time slots are not equally allocated to the different end-systems and the cycle duration could differ from one cluster to another. The classic beacon mechanism illustrated in Figure 2.4 to guarantee synchronization is disabled and replaced with an enhanced synchronization protocol that is detailed in the next paragraph, to reduce the synchronization phase duration.

— **Synchronization protocol**: to implement an accurate TDMA protocol for time-critical avionics network, the precision's degree of the used synchronization protocol is of the utmost importance. For wired networks, many synchronization protocols were successfully implemented with a precision degree about few nanoseconds, and the most known one is the IEEE1588 protocol [48]. However, for wireless networks, achieving this tight precision's degree seems more complicated due to many variable factors during communication. A recent work [49] investigated the IEEE1558 performances for wireless sensor networks and the obtained precision is less than 200 nanoseconds. However, the proposed protocol in [49] cannot be applied directly to our context due to the large number of exchanged packets for

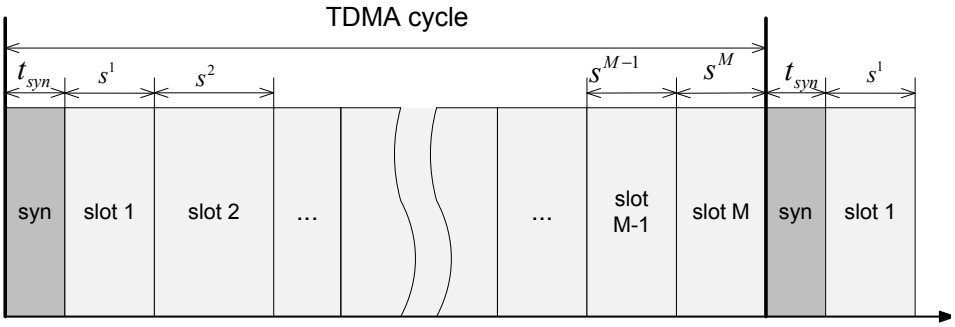

Figure 2.8: Modified UWB Superframe

synchronization. The authors in [50] proposed an enhanced version for broadcast, single hop communications, named IEEE 1588-PBS (Pairwise Broadcast Synchronization). The main objective of this protocol consists in reducing the synchronization phase overhead and minimizing the energy consumption, while achieving a precision degree about 200 nanoseconds.

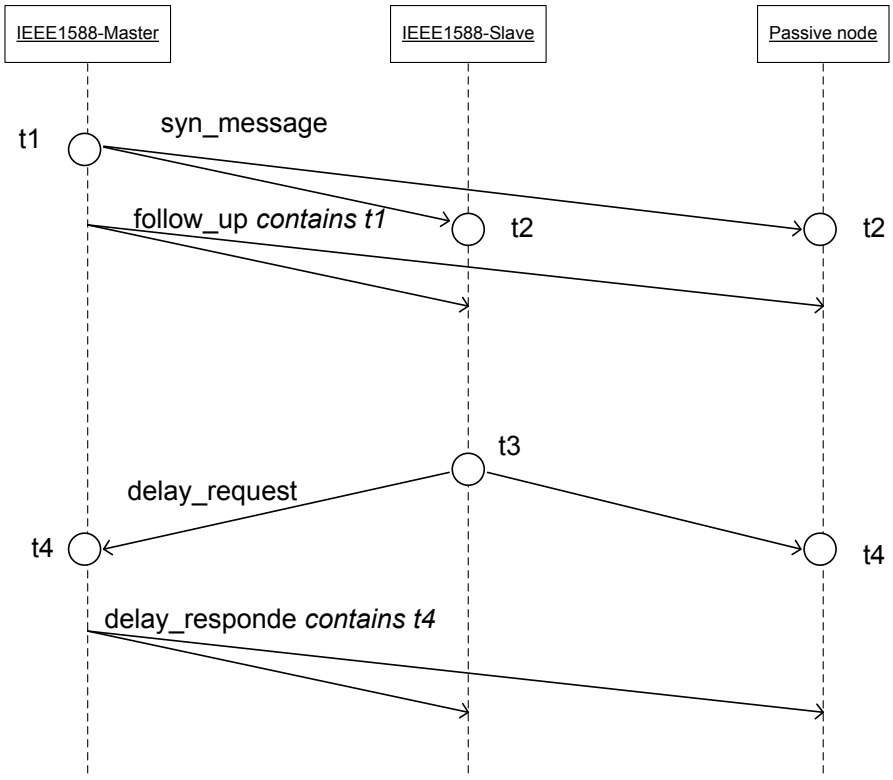

Figure 2.9: IEEE-PBS synchronization

IEEE 1588-PBS is illustrated in Figure 2.9 and it is based on one time master to perform

the synchronization mechanism; and one active slave to receive the synchronization packet and to send the request to the master. The other nodes are passive nodes, which listen to the exchanged data between the master and the active slave to estimate the current time. It is worth noting the high availability of this mechanism, since if the active node fails one of the passive nodes can be elected to perform synchronization. Hence, because of its high precision, good availability and reduced overhead, the IEEE1588-PBS is considered as an interesting candidate for time-critical avionics applications to guarantee the accuracy of TDMA implementation.

2.4.3 Reliability Mechanisms

In this section, we present two principle methods to guarantee the reliability requirement of safety-critical avionics applications.

2.4.3.1 Disabling the acknowledgment mechanism

The first method consists in disabling the acknowledgment and using frequency and time diversity mechanisms. For frequency diversity, each packet is transmitted through different non-overlapping frequencies at the same time, which increases the possibility of having a successful delivery. For time diversity, each packet is transmitted several times on the same frequency. Figure 2.10 illustrates an example of the frequency and time diversities with two frequencies and two transmissions per packet. These mechanisms are adequate because of the low fade margins of UWB technology.

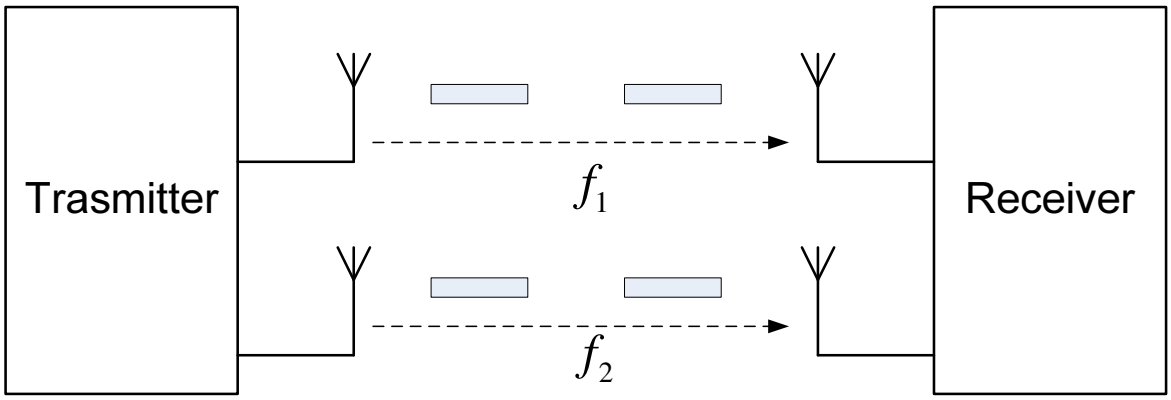

Figure 2.10: Frequency and Time Diversity

The use of No-ACK allows the activation of the burst mode, which induces less overhead compared to the normal mode, where the frame structure shown in Figure 2.6 has shorter

preamble $PLCP_Preamble = 5.625\mu$s for each transmission, and two packets can be transmitted consecutively with MIFS =1.875 μs. Figure 2.11 shows the packet transmission in burst mode.

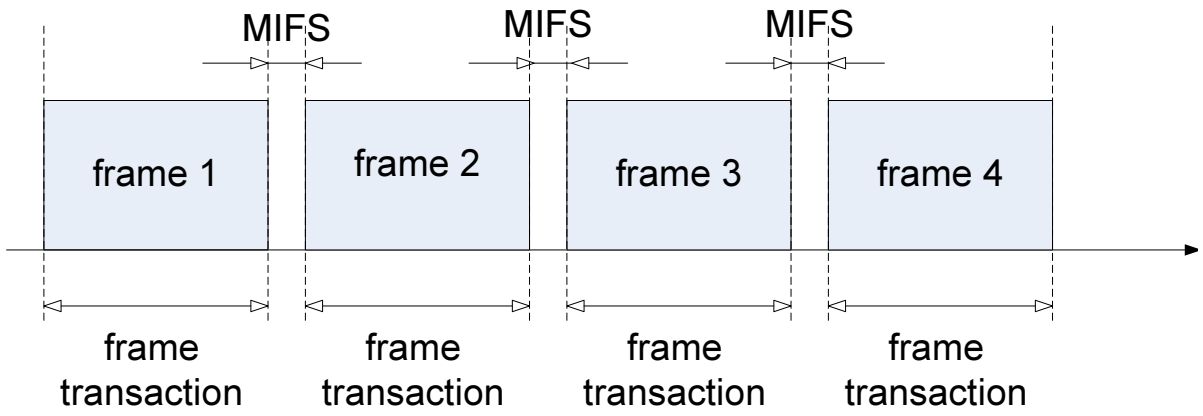

Figure 2.11: Burst mode with No-ACK

2.4.3.2 Retransmissions with ACK

While disabling the acknowledgment mechanism reduces the communication overhead due to the burst transmission mode, it may induce at the same time a poor network utilization since each packet is retransmitted a fixed number of times even if it is successfully received. Hence, activating the acknowledgement combined with frequency diversity mechanism is considered as a second alternative. The ACK mechanism is activated to inform the sender to retransmit the same packet or transmit a new one. However, the communication pattern for avionics applications is multicast and the acknowledgement mechanism is not trivial. Indeed, we need an enhanced mechanism to avoid the collisions among the acknowledgments sent by different receivers and to reduce the overhead.

To handle this problem, we choose to use the acknowledgment mechanism proposed by [51] for multicast communications. This approach consists in selecting one of the receivers as a "leader" to send a feedback to the sender. If the packet is correctly received, then the leader will send a positive acknowledgement (ACK) to the sender, else there is no feedback from the leader. However, in case of erroneous transmission for the other receivers, they will reply with Negative ACKs. Consequently, these NACKs will collide with the ACK packet sent by the leader, which will prompt the retransmission from the sender. Finally, when the sender receives NACK or the time out occurs, the packet is immediately retransmitted to all the receivers. This approach is illustrated in Figure 2.12.

When activating the ACK mechanism, we still can use the burst mode transmission where $PLCP_Preamble = 5.625\mu$s. However, the overhead is increasing because the receiver needs to

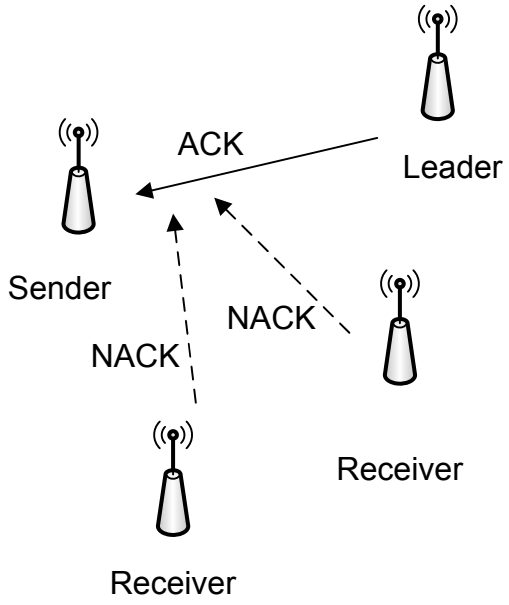

Figure 2.12: A multicast reliable transmission

send the ACK message while respecting the Short Interframe Space (SIFS). Figure 2.13 illustrates the transmission of frames with the enhanced ACK mechanism where two consecutive messages can be transmitted after the duration of two SIFS and one (N)ACK.

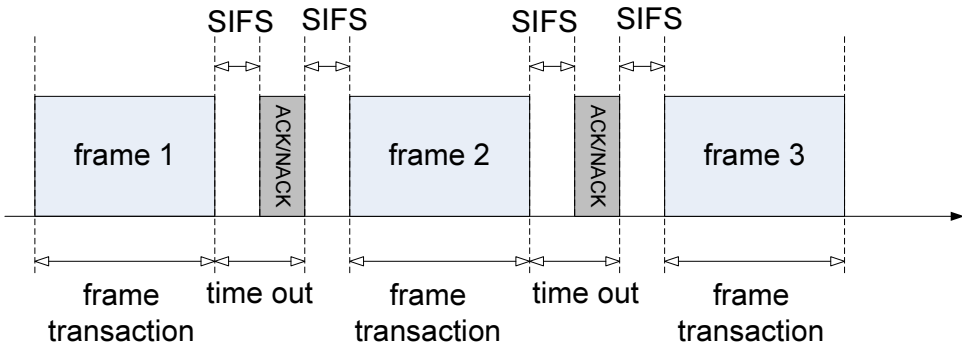

Figure 2.13: Standard transmission mode with ACK/NACK/Time out

2.4.4 Electromagnetic Compatibility and Security

To protect the WSCAN from external interference and jamming attacks, we introduce some network isolation methods, based on the shielding solutions. The geographical concentration of end-systems in a short range of 6 meters facilitates the isolation of the backup network by using various methods described in [52], e.g., special painting and lightweight anechoic chamber. These methods can block the radio signal with frequency range from 100 KHz to 10 GHz or

even 100 GHz. Therefore, the attackers from outside cannot access, modify or interfere with the WSCAN. In addition, the In-Flight Entertainment network consisting of passengers devices could not interfere with the different clusters of WSCAN.

2.5 Conclusion

In this chapter, we have assessed the main wireless technologies that can provide the sufficient data rate for WSCAN to replace the backup part of the current safety-critical avionics network. Among these candidates, the ECMA-368 is selected as the most suitable one due to its high data rate, collision-free MAC protocol, low susceptibility to electromagnetic interference and high security mechanisms. Furthermore, to satisfy the strict requirements of safety-critical avionics applications, we have analyzed the general risks and transmission failures, and proposed the basic protective methods. Afterwards, we have detailed the WSCAN design, based on hybrid architecture and enhanced MAC protocol and reliability mechanisms.

Although our proposed WSCAN integrates various features to enhance the system predictability and reliability, the use of wireless technology may increase the communication latencies due to transmission errors. Hence, system constraints have to be verified under error-prone environment. This issue will be handled in the next chapter.

Chapter 3

System Modeling and Timing Analysis of Wireless Network for Safety-critical Avionics

In this chapter, to verify the WSCAN predictability, we first detail the system and the traffic models. Afterwards, a timing analysis based on Network Calculus [30] is conducted under different scheduling policies, such as First In First Out (FIFO), Fixed Priority (FP), and Weighted Round Robin (WRR), and various reliability mechanisms. Finally, preliminary performance evaluation through a small scale network is provided under error-free and error-prone environments.

3.1 System Model and Metric

3.1.1 Metric: end-to-end delay

To evaluate the timing performance of the proposed network, we consider as a metric the worst-case end-to-end delay of each message that will be compared to its temporal deadline. Using Network Calculus [30], we can compute the upper bound of end-to-end delay for each transmitted message m, which is denoted as D_m^{e2e}. This schedulability test results in a sufficient but not necessary condition due to the pessimism introduced by the upper bounds. Nevertheless, we can still infer the traffic schedulability as follows:
$\forall m \in messages$,

$$D_m^{e2e} \leq Dl_m \Longrightarrow \text{The } messages \text{ set is schedulable}$$

where Dl_m is the respective deadline.

Figure 3.1 presents the inter-cluster end-to-end delay which includes the delays at the end-system, the outgoing gateway, the central switch and the incoming gateway.

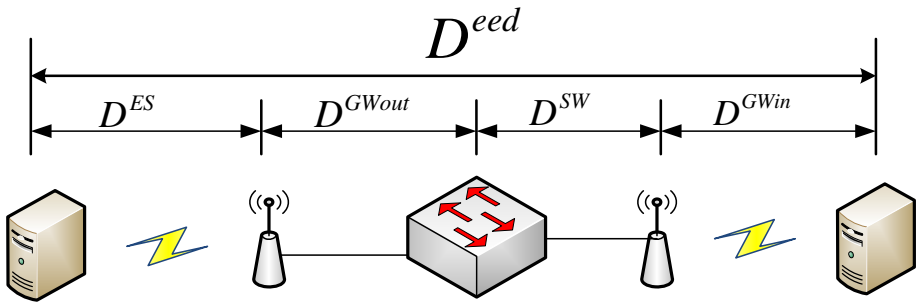

Figure 3.1: End-to-end delay of Inter-Cluster Traffic

To compute upper bounds on end-to-end delays of transmitted messages using Network Calculus, we need to model each message flow to obtain its maximum arrival curve, and the behavior of each node along its path to compute the minimum service curve. Then, the maximum horizontal distance between these two curves corresponds to an upper bound on the intermediate delay of the associated message flow. Afterwards, the sum of these bounds represents an upper bound on end-to-end delay. These models are detailed in the next sections and the basic concepts of Network Calculus are detailed in Appendix A.

3.1.2 Traffic Model

The proposed UWB-based network, as an alternative backup network for the AFDX backbone network, has to integrate the specifics of AFDX network and consequently Virtual Links. As described in Section 1.1.2.1 of Chapter 1, Virtual Links are characterized by minimal inter-arrival time (BAG), Maximal Frame Size (MFS), a source and a set of destinations.

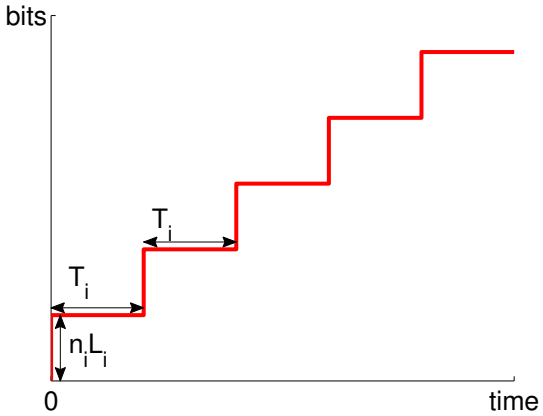

Figure 3.2: Traffic Arrival Curve

To replace the current avionics backup network with the proposed UWB-based network, each data generated by an avionic application is encapsulated in an UWB frame, which defines the source and destination addresses. Afterwards, we consider that any aggregate traffic flow f_i^k generated by an end-system k consists of n_i periodic (or sporadic) subflows $f_{i,j}^k$, where $1 \leq j \leq n_i$, and belongs to a traffic class TC_i. TC_i is characterized by a tuple (T_i, Dl_i, L_i, e_i) for period (or minimum inter-arrival time for sporadic flow), deadline (equal to T_i unless otherwise explicitly specified), frame size integrating the protocol overhead and delivery time (i.e., $e_i = L_i/B$ where B is the medium transmission capacity), respectively. The arrival curve of the aggregate traffic flow f_i^k, based on a packetized model, is given as follows and illustrated in Figure 3.1:

$$\alpha_i^k(t) = \sum_{j=1}^{n_i} \alpha_{i,j}^k(t) = n_i L_i \lceil \frac{t}{T_i} \rceil \tag{3.1}$$

3.1.3 End-Systems and Shared Network Models

Avionic end-systems transmit their generated message flows according to a TDMA arbitration protocol under different scheduling policies, i.e FIFO, FP and WRR. The end-systems follow a static TDMA schedule to transmit their message flows, which is defined as a sequence of time slots repeated each cycle with a fixed duration, called c. During each cycle, end-system k can only transmit during its predetermined time interval, called TDMA time slot s^k. In avionics context, the time slots associated to end-systems have not necessarily equal durations and the message transmission is non-preemptive. Consequently, if the remaining time during a slot is insufficient for a complete message transmission, then the message has to wait for the next slot. Hence, the cycle duration is as follows:

$$c = \sum_{k=1}^{M} s^k + t_{sync} \tag{3.2}$$

where M is the number of end-systems and t_{sync} the duration of the synchronization phase described in Section 2.4.2 of Chapter 2.

The classic timing analysis of TDMA arbitration protocol for a fluid model [53], [54], [55] is based on the following key idea: a computing unit with a time slot s^k may not have access to the shared network during at maximum $c - s^k$. After this maximum duration, the computing unit has exclusive access to the medium during its time slot s^k to transmit its messages with the medium transmission capacity, B.

Hence, the classic service curve when FIFO policy is implemented in the computing unit has the following analytical expression:

$$\beta_{c,s^k}(t) = B \max(\lfloor \frac{t}{c} \rfloor s^k, t - \lceil \frac{t}{c} \rceil (c - s^k)), \forall t \geq 0 \tag{3.3}$$

When considering a FP policy, each message flow will be transmitted before all lower priority flows and after all higher priority flows. Consider N message flows $f_1^k, .., f_N^k$ where f_i^k has higher priority than f_j^k if $i < j$. The residual service curve offered to message flow f_i^k using Theorem 8 of Appendix A has the following analytical expression:

$$\beta_i^k(t) = (\beta_{c,s^k}(t) - \sum_{1 \leq j \leq i-1} \alpha_j^k(t))_\uparrow \tag{3.4}$$

These models are extended in next sections to integrate the impact of non-preemptive message transmission with FIFO and FP policies. However, for WRR combined with TDMA, to the best of our knowledge, this model has not been treated in literature. Hence, we will introduce the models in this case for preemptive and non-preemptive message transmissions .

3.1.3.1 FIFO Policy

The maximum waiting time to access to the medium and the lower bound of offered TDMA time slot have to be adjusted in case of non-preemptive message transmission, and then used to extend the service curve guarantee.

Consider an end-system with a TDMA time slot s^k during each TDMA cycle c. This end-system generates N traffic flows $f_i^k, i = 1, 2, .., N$ with associated maximum and minimum delivery times e_{max} and e_{min}, respectively. Based on the worst-case scenario illustrated in Figure 3.3, the corresponding parameters are as following.

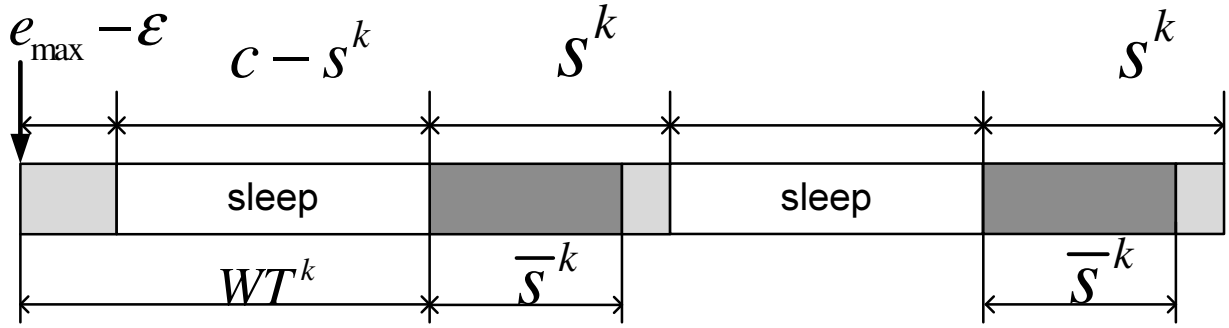

Figure 3.3: Worst-case scenario with FIFO policy

— The *maximum waiting time* WT^k occurs when the first message of a backlogged period has a maximum delivery time e_{max} and arrives just at the instant when the remaining time during the current slot is slightly less then the required delivery time, i.e., $e_{max} - \epsilon (0 < \epsilon << 1)$. In this case, the message has to be delayed until the next slot and the *maximum waiting time* is then $WT^k = e_{max} + c - s^k$ instead of $c - s^k$ in the classic model described in Equation 3.3.

— The *lower bound of offered TDMA time slot* $\overline{s^k}$ depends on traffic flows characteristics. If the generated messages are homogeneous, i.e., all the messages have the same delivery time e, then the end-system can send at maximum $\lfloor \frac{s^k}{e} \rfloor$ messages during its respective time slot s^k; else, the idle time is always less than e_{max} and the *lower bound of offered TDMA time slot* is always greater then e_{min}. Hence, $\overline{s^k}$ is as follows:

$$\overline{s^k} = \begin{cases} \lfloor \frac{s^k}{e} \rfloor e & \text{if } e_{max} = e_{min} = e \\ \max\{s^k - e_{max}, e_{min}\} & \text{Otherwise} \end{cases} \tag{3.5}$$

The *maximum waiting time* WT^k may occur only at the beginning of the backlogged period. Then, during the next cycles the node may wait at most $c - \overline{s^k}$ to access to the network and transmit messages. Hence, the strict service curve guaranteed in this case is $\overline{\beta^k}(t) = \beta_{c,\overline{s^k}}(t - (WT^k - (c - \overline{s^k})))$ which represents the curve defined in Equation 3.3 and extended in our model with $\beta_{c,\overline{s^k}}(t) = 0$, $\forall t < 0$ shifted to the right with the positive duration $WT^k - (c - \overline{s^k})$.

This is explicitly defined in the following theorem. The corresponding proof is detailed in Appendix C.

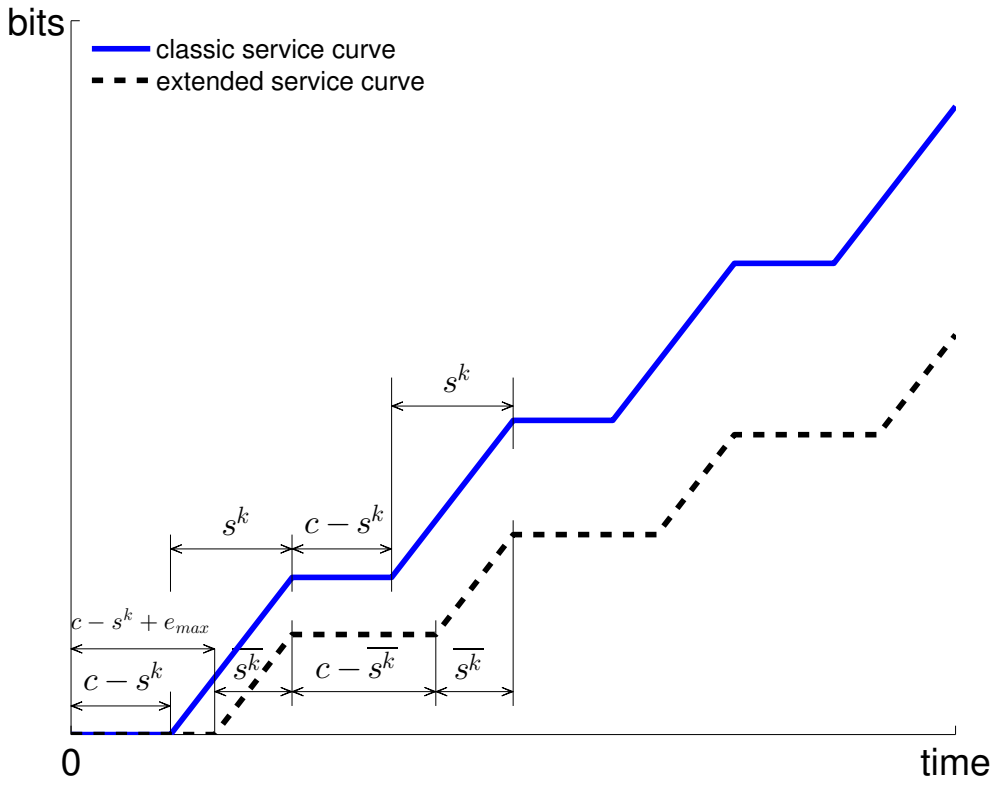

Figure 3.4: Classic vs extended service curves with FIFO policy

Theorem 1. *Consider an end-system having a lower bound of offered time slot $\overline{s^k}$, generating N traffic flows and implementing a FIFO policy, the offered strict service curve when considering non-preemptive message transmission is:*

$$\overline{\beta^k}(t) = \beta_{c,\overline{s^k}}(t - WT + (c - \overline{s^k})), \forall t \geq 0 \tag{3.6}$$

where

$$WT^k = e_{max} + c - s^k$$

and

$$\overline{s^k} = \begin{cases} \lfloor \frac{s^k}{e} \rfloor e & \text{if } e_{max} = e_{min} = e \\ \max\{s^k - e_{max}, e_{min}\} & \text{Otherwise} \end{cases}$$

This extended service curve is illustrated in Figure 3.4. As we can notice, extended service curve is lower than classic one, described in Equation 3.3, which will lead to greater delay bounds mainly due to the non-preemptive message transmission.

3.1.3.2 FP Policy

As for the FIFO policy case, the *maximum waiting time* to access to the medium and the *lower bound of offered TDMA time slot* for transmission have to be adjusted in case of non-preemptive message transmission. First, we compute the offered service curve for the aggregate message flow $f^k_{\leq i}$ including message flows f^k_1,..,f^k_i with priorities higher or equal to i. Then, we deduce the individual service curve for each traffic flow f^k_i applying Theorem 8 of Appendix A. Based on the worst-case scenario illustrated in Figure 3.5, the corresponding parameters are as follows:

— The *maximum waiting time* $WT^k_{\leq i}$ occurs when the first message of the aggregate message flow $f^k_{\leq i}$ arriving at the beginning of a backlogged period and having a maximum delivery time $e^{1\leq j\leq i}_{max}$ is blocked during the transmission time of a message with lower priority and maximum delivery time. This blocking time corresponds to $e^{i<j\leq N}_{max} - \epsilon (0 < \epsilon << 1)$. Furthermore, after that blocking time, the remaining time during the current slot is slightly less then the required delivery time of the considered message and is equal to $e^{1\leq j\leq i}_{max} - \epsilon (0 < \epsilon << 1)$. In this case, this message has to wait until the next slot to be transmitted. The *maximum waiting time* is then bounded by $e^{i<j\leq N}_{max} + e^{1\leq j\leq i}_{max} + c - s^k$. However, if the TDMA time slot s^k is smaller than $e^{i<j\leq N}_{max} + e^{1\leq j\leq i}_{max}$, then the *maximum waiting time* is reduced to one cycle c. Hence, for aggregate flow $f^k_{\leq i}$, the *maximum waiting time* is as follows:

$$WT^k_{\leq i} = \min(e^{i<j\leq N}_{max} + e^{1\leq j\leq i}_{max} + c - s^k, c) \tag{3.7}$$

— The *lower bound of offered TDMA time slot* associated to aggregate flow $f^k_{\leq i}$, called $\overline{s^k_{\leq i}}$, can be deduced from Eq. 3.5 by considering only aggregate flow $f^k_{\leq i}$ instead of all the generated flows. Hence, $\overline{s^k_{\leq i}}$ associated to aggregate flow $f^k_{\leq i}$ is as follows:

$$\overline{s^k_{\leq i}} = \begin{cases} \lfloor \frac{s^k}{e} \rfloor e & \text{if } e^{1\leq j\leq i}_{max} = e^{1\leq j\leq i}_{min} = e \\ \max(e^{1\leq j\leq i}_{min}, s^k - e^{1\leq j\leq i}_{max}) & \text{Otherwise} \end{cases} \tag{3.8}$$

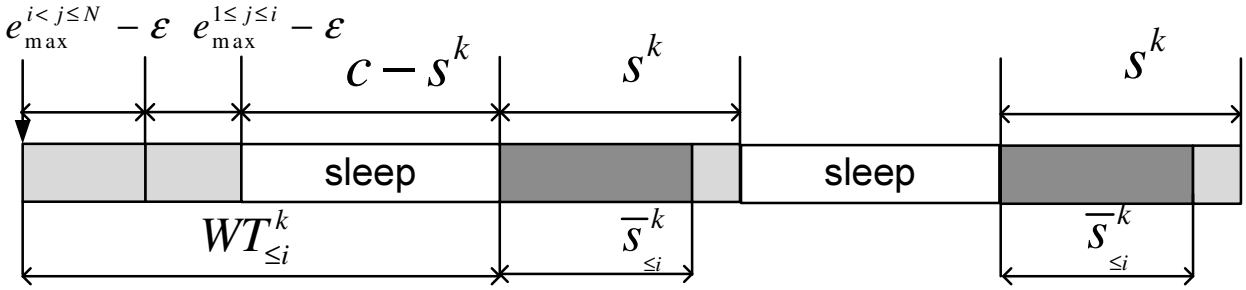

Figure 3.5: Worst-case scenario with FP policy

The extended service curve with FP policy is defined in the following theorem and the mathematical proof is detailed in Appendix C.

Theorem 2. *Consider aggregate flow $f^k_{\leq i}$ having a lower bound of offered TDMA time slot $\overline{s^k_{\leq i}}$, transmitted by an end-system implementing FP policy, the strict service curve guaranteed to $f^k_{\leq i}$ when considering non-preemption feature is:*

$$\overline{\beta^k_{\leq i}}(t) = \beta_{c,\overline{s^k_{\leq i}}}(t - WT^k_{\leq i} + (c - \overline{s^k_{\leq i}})), \forall t \geq 0 \tag{3.9}$$

where

$$WT^k_{\leq i} = \min(e^{i<j\leq N}_{max} + e^{1\leq j\leq i}_{max} + c - s^k, c),$$

and

$$\overline{s^k_{\leq i}} = \begin{cases} \lfloor \frac{s^k}{e} \rfloor e & \textit{if } e^{1\leq j\leq i}_{max} = e^{1\leq j\leq i}_{min} = e \\ \max(e^{1\leq j\leq i}_{min}, s^k - e^{1\leq j\leq i}_{max}) & \textit{Otherwise} \end{cases}$$

Hence, using Theorems 2 and 8 of Appendix A, the residual service curve offered to message flow f^k_i is as follows:

$$\overline{\beta_i}^k(t) = (\overline{\beta^k_{\leq i}}(t) - \sum_{j=1}^{i-1} \alpha^k_j(t))_{\uparrow} \tag{3.10}$$

This extended service curve is illustrated in Figure 3.6. Extended service curve is lower than the classic one, which leads to greater delay bounds due to the non-preemptive message transmission.

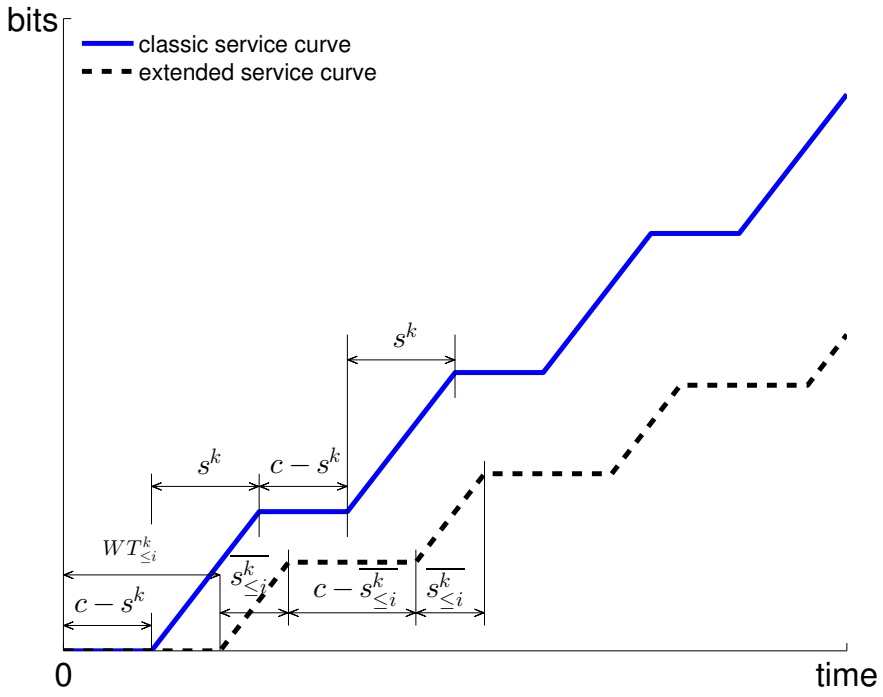

Figure 3.6: Classic vs extended service curves with FP policy

3.1.3.3 WRR policy

In this part, we introduce the non-preemptive WRR policy combined with TDMA protocol. First, we detail a service curve model for preemptive-WRR policy combined with TDMA protocol for a fluid flow model, which to the best of our knowledge has not been investigated in literature. Then, we extend this model to the packet flow model to integrate the impact of non-preemptive message transmission.

As illustrated in Figure 3.7, for each flow f_i^k in an end-system, we consider a respective access time to the medium, called w_i^k during each WRR round, where $\sum_{i=1}^{N} w_i^k = s^k$. During a backlogged period of a flow f_i^k, the *maximum waiting time* occurs when it is blocked by all other flows having simultaneously their backlogged period. Hence, the *maximum waiting time* is bounded by $\sum_{j=1,j\neq i}^{N} w_j^k + c - s^k = c - w_i^k$. Then, flow f_i^k receives the right to send during its respective access time w_i^k. This behavior is repeated according to the WRR scheduling and the analytical expression is given in Theorem 3.

Theorem 3. *The minimum service curve for flow f_i^k transmitted by a node implementing a preemptive WRR combined with TDMA system, with a respective access time to the medium w_i^k such that $\sum_{i=1}^{N} w_i^k = s^k$ is*

$$\beta_i^k(t) = \beta_{c,w_i^k}(t) \tag{3.11}$$

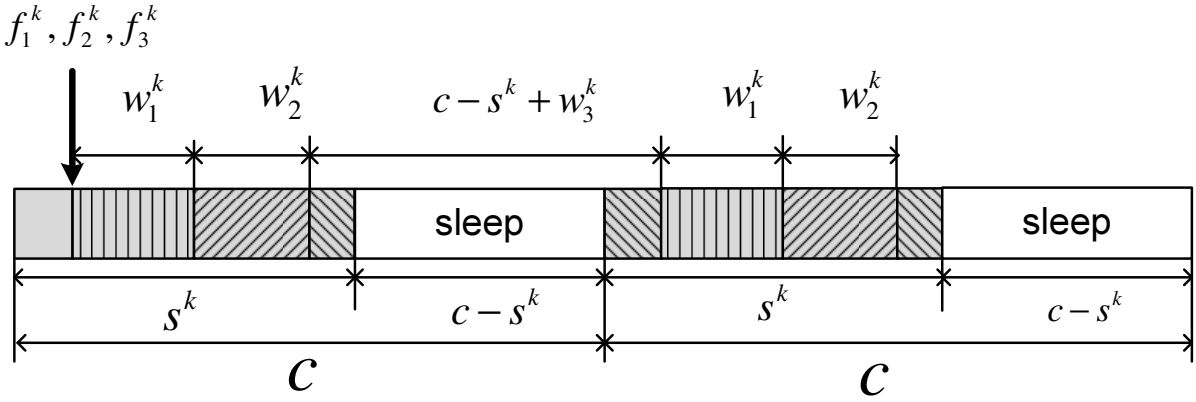

Figure 3.7: Access-time distribution with preemptive WRR combined with TDMA

Proof. During any duration c, flow f_i^k can access and transmit messages during at least w_i^k. Hence, the minimum service curve of f_i is given by $\beta_i^k(t) = \beta_{c,w_i^k}(t)$. □

Then, we extend this first model to integrate the non-preemption. This condition impacts the *maximum waiting time* and the respective access time to the medium w_i^k for each flow f_i. As shown in Figure 3.8,

— The respective access time to the medium of flow f_i^k corresponds to the amount of time to transmit completely $\lfloor \frac{w_i^k}{e_i} \rfloor$ messages within a slot duration that is equal to $\overline{w_i^k} = \lfloor \frac{w_i^k}{e_i} \rfloor * e_i$.

— The *maximum waiting time* occurs when flow f_i^k starts its backlogged period and it is blocked by all the other backlogged flows during the slot. The *maximum waiting time* has also to integrate the remaining idle time between two slots due to flow f_l^k as shown in Figure 3.8, which is slightly less than e_{max}. Consequently, the flow has to be delayed to the next slot. Hence, the *maximum waiting time* is bounded by $e_{max} + c - s^k + \sum_{j=1, j\neq i}^{N} \overline{w_j^k}$. It is worth noting that during any period $\overline{c} = e_{max} + c - s^k + \sum_{1 \leq j \leq N} \overline{w_j^k}$, the backlogged flow f_i^k can transmit at least $\lfloor \frac{w_i^k}{e_i} \rfloor$ messages.

The analytic expression of this offered service curve in this case is given in Theorem 4 and the proof is detailed in Appendix C.

Theorem 4. *The strict service curve for flow f_i^k, transmitted by a node implementing a non-preemptive WRR combined with TDMA system is*

$$\overline{\beta_i^k}(t) = \beta_{\overline{c},\overline{w_i^k}}(t) \tag{3.12}$$

where $\overline{w_i^k} = \lfloor \frac{w_i^k}{e_i} \rfloor * e_i$, *and* $\overline{c} = e_{max} + (c - s^k) + \sum_{j=1}^{N} \overline{w_j^k}$.

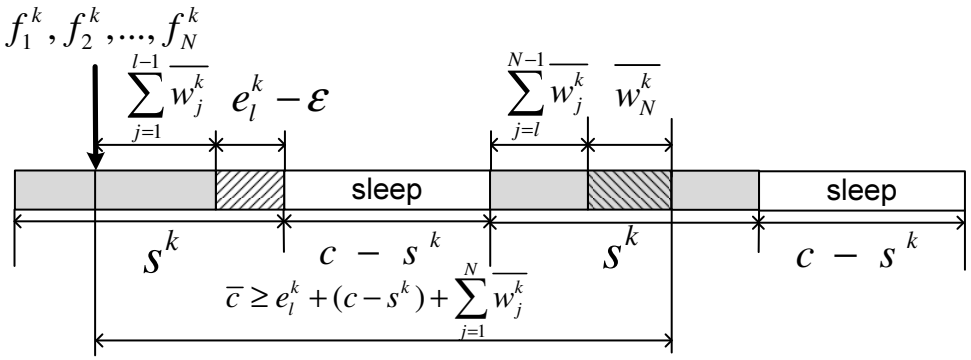

Figure 3.8: Worst-case scenario with WRR policy

3.1.4 Gateway Model

In this section, we introduce the outgoing and incoming Gateway models, based on maximum scaling function proposed in [56].

3.1.4.1 Outgoing Gateway Model

The outgoing gateway performs two tasks: (i) encapsulate the UWB frame into the Gigabit Ethernet frame, (ii) perform the FIFO scheduling for the encapsulated Ethernet frames and forward them to the Gigabit switch. Therefore, the outgoing gateway is modeled by two components: the scaling function and the wired interface as shown in Figure 3.9.

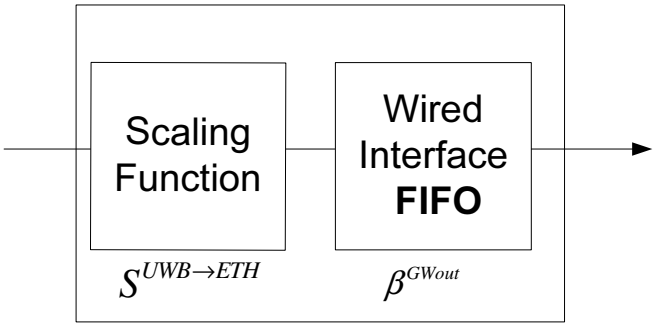

Figure 3.9: Model of an Outgoing Gateway

The scaling function models the encapsulation process of the UWB frame in an Ethernet frame. This function denoted as S, is a wide-sense increasing function that maps any amount of data a to $S(a)$ and it was proposed in [56]. Consequently, the arrival curve of input traffic is scaled and then transmitted to the wired interface. To model the upper bound of this function, we use the concept of an upper scaling curve, defined in Definition 7 of Appendix A. Hence, for

any flow f_i^k,

$$\overline{S_i}^{GW_{out}}(a) = \frac{L_i^{ETH}}{L_i^{UWB}} a \tag{3.13}$$

Consequently, the scaling curve of the aggregate flow f^k is given by:

$$\overline{S}^{GW_{out}}(a) = \max_{\forall i} \frac{L_i^{ETH}}{L_i^{UWB}} a \tag{3.14}$$

where L_i^{ETH} and L_i^{UWB} represent the Ethernet and UWB frame lengths, respectively.

For the wired interface, based on Theorem 9 of Appendix A, the service curve of the outgoing gateway is given by:

$$\beta^{GW_{out}}(t) = \left[Ct - \max_{\forall i} L_i^{ETH}\right]^+ \tag{3.15}$$

where C is the switch capacity and $[x]^+ = \max(0, x)$.

3.1.4.2 Incoming Gateway Model

The incoming gateway performs two tasks: (i) decapsulate the Ethernet frame into the UWB frame, (ii) perform the FIFO/FP/WRR scheduling for the original UWB frames and forward them to the end-systems according to the TDMA protocol. Therefore, the incoming gateway is modeled by two components: the scaling function and the wireless interface as shown in Figure 3.10.

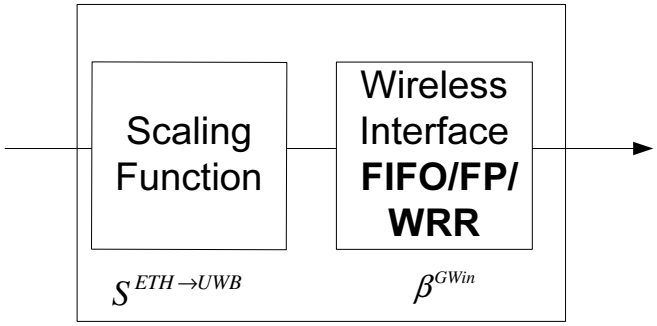

Figure 3.10: Model of an Incoming Gateway

The first component models the decapsulation process of the Ethernet frames in a UWB frame. As the outgoing gateway, the amount of input traffic is scaled and then transmitted to the wireless interface of the incoming gateway. Hence, the scaling curve of any flow f_i^k is given by:

$$\overline{S_i}^{GW_{in}}(a) = \frac{L_i^{UWB}}{L_i^{ETH}} a \tag{3.16}$$

Consequently, the scaling curve of the aggregate flow f^k is given by:

$$\overline{S}^{GW_{in}}(a) = \max_{\forall i} \frac{L_i^{UWB}}{L_i^{ETH}} a \tag{3.17}$$

The wireless interfrace of the incoming gateway is modeled as one of the end-systems implementing FIFO, FP or WRR policies under TDMA protocol. The corresponding service curve is detailed in Section 3.1.3 and called $\beta^{GW_{in}}$.

3.1.5 Switch Model

The Gigabit Switch will forward incoming packets from different outgoing gateways to the corresponding incoming gateways according to FIFO policy. As the switch capacity is C, from Theorem 9 of Appendix A, the service curve of the output port of the switch is given by:

$$\beta^{SW}(t) = [Ct - L_{max}]^{+} \tag{3.18}$$

where L_{max} is the maximum packet length among the packets arriving to the switch's output port and $[x]^{+} = \max\{x, 0\}$.

3.2 Timing Analysis

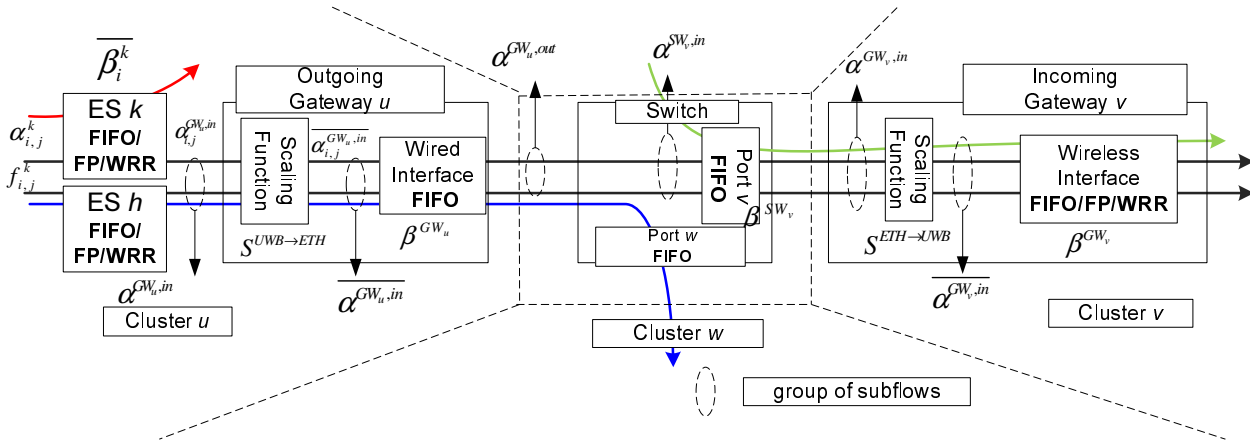

Figure 3.11: Flow Paths

In this section, we evaluate the upper bounds on end-to-end delays for intra-cluster and inter-cluster traffic by integrating the effect of each crossed node, e.g. end-system, outgoing and incoming gateways and switch. Figure 3.11 shows the path of a flow generated by the end-system k in cluster u and has its destinations (end-systems) in cluster v. First, we detail the obtained bounds for error-free environment. Then, we explain the extension of this analysis to the error-prone environment when taking into account the reliability mechanisms.

3.2.1 Error-Free Environment

3.2.1.1 Delay Bound in End-Systems

The delay bounds imposed by the end-system k to each subflow $f_{i,j}^k$ belonging to the aggregate traffic flow f_i^k, can be computed as the maximum horizontal distance between the associated arrival curve and the minimum service curve guaranteed by each end-system under FIFO, FP or WRR, and they are defined as following:

— with FIFO policy, using Equations 3.1 and 3.6, $\forall f_{i,j}^k$

$$D_{i,j}^{ES_k} = h(\alpha^k, \overline{\beta^k}) \text{ where } \alpha^k(t) = \sum_{i=1}^{N} \alpha_i^k(t) \tag{3.19}$$

— with FP/WRR policies, using Equations 3.1, 3.10 and 3.12, $\forall f_{i,j}^k$

$$D_{i,j}^{ES_k} = h(\alpha_i^k, \overline{\beta_i^k}) \tag{3.20}$$

3.2.1.2 Delay Bound in the Outgoing Gateway

First, the arrival curve at the input of the outgoing gateway is the sum of input arrival curves of subflows in S_{GW_u}, which is the set of all subflows generated by any end-system k in cluster u and transmitted to the outgoing gateway GW_u and it is as follows:

$$\begin{aligned} \alpha^{GW_u,in}(t) &= \min\{ \sum_{f_{i,j}^k \in S_{GW_u}} \alpha_{i,j}^{GW_u,in}(t), Bt\} \\ &= \min\{ \sum_{f_{i,j}^k \in S_{GW_u}} \alpha_{i,j}^{ES_k,out}(t), Bt\} \end{aligned} \tag{3.21}$$

where B is the maximum transmission capacity of the wireless link, and $\alpha_{i,j}^{ES_k,out}$ is the arrival curve of the subflow $f_{i,j}^k$ at the output of the end-system k. This latter is defined as $\alpha_{i,j}^{ES_k,out}(t) = \alpha_{i,j}^k(t + D_{i,j}^{ES_k})$ using Equations 3.1, 3.19 and 3.20.

Then, each received UWB packet from cluster u at the outgoing gateway GW_u is encapsulated in an Ethernet frame. Hence, the input arrival curve at the wired interface of the outgoing gateway GW_u, after the scaling process and using Equations 3.21 and 3.14, is the following:

$$\begin{aligned} \overline{\alpha^{GW_u,in}}(t) &= \min\{ \sum_{f_{i,j}^k \in S_{GW_u}} \overline{\alpha_{i,j}^{GW_u,in}}(t)), B^S t\} \\ &= \min\{ \sum_{f_{i,j}^k \in S_{GW_u}} \overline{S_{i,j}^{GW_u,k}}(\alpha_{i,j}^{ES_k,out}(t)), B^S t\} \end{aligned} \tag{3.22}$$

where $B^S = \max_i \frac{L_i^{ETH}}{L_i^{UWB}} B$ is the scaling transmission capacity of the wireless link.

Hence, the delay bound imposed by the outgoing gateway GW_u to any subflow $f_{i,j}^k \in S_{GW_u}$, based on Equations 3.15 and 3.22, is:

$$D_{i,j}^{GW_u,k} = D^{GW_u} = h(\overline{\alpha^{GW_u,in}}, \beta^{GW_u}) \tag{3.23}$$

3.2.1.3 Delay Bound in the Switch

The Gigabit Ethernet switch will forward incoming packets from the different outgoing gateways to the corresponding output port of the switch according to FIFO. The input arrival curve of the output port of the switch, associated with the incoming gateway GW_v of cluster v, is the sum of output arrival curves of subflows in S_{SW_v}, which is the set of all subflows transmitted by any outgoing gateway GW_u to the output port of the switch associated with incoming gateway GW_v of cluster v, and it is as follows:

$$\alpha^{SW_v,in}(t) = \sum_{f_{i,j}^k \in S_{SW_v}} \alpha_{i,j}^{GW_u,out}(t) \tag{3.24}$$

where $\alpha_{i,j}^{GW_u,out}(t) = \overline{\alpha_{i,j}^{GW_u,in}}(t + D_{i,j}^{GW_u,k})$ using Equations 3.22 and 3.23.

Hence, the delay bound imposed by the output port SW_v of the switch to any subflow $f_{i,j}^k \in S_{SW_v}$, using Equations. 3.24 and 3.18, is as follows:

$$D_{i,j}^{SW_v,k} = D^{SW_v} = h(\alpha^{SW_v,in}, \beta^{SW_v}) \tag{3.25}$$

3.2.1.4 Delay Bound in the Incoming Gateway

The input arrival curve at GW_v is the sum of output arrival curves of subflows in S_{SW_v}, and it is as follows using Equations 3.24 and 3.25:

$$\begin{aligned} \alpha^{GW_v,in}(t) &= \min\{\sum_{f_{i,j}^k \in S_{SW_v}} \alpha_{i,j}^{SW_v,out}(t), Ct\} \\ &= \min\{\alpha^{SW_v,out}(t), Ct\} \\ &= \min\{\alpha^{SW_v,in}(t + D^{SW_v}), Ct\} \end{aligned} \tag{3.26}$$

As the outgoing gateway, the amount of input traffic is scaled and then transmitted to the wireless interface of GW_v. Hence, the input arrival curve at the wireless interface of the incoming gateway GW_v after the scaling process, using Equations 3.26 and 3.17, is:

$$\begin{aligned} \overline{\alpha^{GW_v,in}}(t) &= \min\{\sum_{f_{i,j}^k \in S_{SW_v}} \overline{\alpha_{i,j}^{GW_v,in}}(t), C^S t\} \\ &= \min\{\sum_{f_{i,j}^k \in S_{SW_v}} \overline{S_{i,j}^{GW_v,k}}(\alpha_{i,j}^{SW_v,out}(t)), C^S t\} \end{aligned} \tag{3.27}$$

where $C^S = \max_i \frac{L_i^{UWB}}{L_i^{ETH}} C$ is the scaling switch capacity.

Similarly, the input arrival curve of traffic class TC_i at the wireless interface of the incoming gateway GW_v after the scaling process is given by:

$$\overline{\alpha_i^{GW_v,in}}(t) = \min\{ \sum_{f_{i,j}^k \in S_{SW_u,i}} \overline{S_{i,j}^{GW_v,k}}(\alpha_{i,j}^{SW_v,out}(t)), C_i^S t\} \tag{3.28}$$

where $C_i^S = \frac{L_i^{UWB}}{L_i^{ETH}} C$ and $S_{SW_u,i}$ is the set of all subflows in S_{SW_u} and belonging to TC_i.

Therefore, the delay bound imposed by the incoming gateway GW_v to any subflow $f_{i,j}^k \in S_{SW_v}$ is as follows:

— Under FIFO, using Equations 3.6 and 3.27,

$$D_{i,j}^{GW_v,k} = D^{GW_v} = h(\overline{\alpha^{GW_v,in}}, \overline{\beta^{GW_v}}) \tag{3.29}$$

— Under FP and WRR, using Equations 3.10, 3.12 and 3.28,

$$D_{i,j}^{GW_v,k} = D_i^{GW_v} = h(\overline{\alpha_i^{GW_v,in}}, \overline{\beta_i^{GW_v}}) \tag{3.30}$$

3.2.1.5 End-to-End Delay Bounds

The end-to-end delay bounds for intra-cluster and inter-cluster traffic are as follows:

— for intra-cluster traffic, for any aggregate flow f_i^k in cluster u:

$$D_i^{e2e} = D_i^u = \max_{\forall f_{i,j}^k} D_{i,j}^{ES_k} \tag{3.31}$$

— for inter-cluster traffic, for any aggregate flow f_i^k transmitted from cluster u to cluster v:

$$D_i^{e2e} = \max_{\forall (u,v)} D_i^{u \to v} = D_i^u + D^{GW_u} + D^{SW_v} + D_i^{GW_v} \tag{3.32}$$

3.2.2 Error-Prone Environment

In this section, we first model the considered reliability mechanism. Then, we extend the end-to-end delay bounds for error-prone environment.

3.2.2.1 Reliability Mechanisms Modeling

As described in Section 2.4.3.1 of Chapter 2, to guarantee the required PER level of avionic applications, PER_L, there are two reliability mechanisms. We consider in this chapter time and frequency diversity mechanisms to enhance the offered PER of UWB technology, PER_{UWB}. To

conduct timing analysis of such a network, we need to integrate the impact of these reliability mechanisms, which certainly will increase the offered reliability level but at the same time increase the end-to-end delay bounds.

We consider η_f the number of frequency channels due to frequency diversity mechanism, and η_t the number of packet transmissions on each frequency channel due to time diversity mechanism. Consequently, if the two diversity mechanisms are combined, then each message is transmitted $\eta_f \times \eta_t$ times. Hence, the offered PER of such a network is equal to $PER_{UWB}^{\eta_f \times \eta_t}$, and the avionic reliability requirement is guaranteed if the following condition is verified:

$$PER_{UWB}^{\eta_f \times \eta_t} \leq PER_L \tag{3.33}$$

Hence, the following conditions has to be verified:

$$\eta_t \geq \lceil \frac{log_{PER_{UWB}}(PER_L)}{\eta_f} \rceil \tag{3.34}$$

Increasing the number of transmissions of the same message leads to increasing the quantity of traffic generated by each end-system and consequently the associated maximum arrival curve. The decorrelated η_f frequency channels can be modeled as η_f redundant wireless links, and on each considered wireless link there are η_t copies of the same generated message by any end-system. Hence, we need to update the traffic arrival curves to integrate these features.

3.2.2.2 End-to-End Delay Bounds

To integrate the impact of reliability mechanisms, the delay bounds imposed by the end-system k, computed in Equations 3.19 and 3.20, are updated as following.

— under FIFO policy, $\forall f_{i,j}^k$

$$D_{i,j}^{ES_k} = h(\eta_t.\alpha^k, \overline{\beta^k}) \tag{3.35}$$

— under FP and WRR policies, $\forall f_{i,j}^k$

$$D_{i,j}^{ES_k} = h(\eta_t.\alpha_i^k, \overline{\beta_i^k}) \tag{3.36}$$

Similarly, the delay bounds in incoming gateway v in Equations 3.29, 3.30 have to be updated by considering η_t copies of each forwarded packet. The delay bounds in outgoing gateway and switch are not effected by the diversity techniques since only one correct copy of each packet will be forwarded. Hence, Equations 3.31 and 3.32 are updated based on Equations 3.35 and 3.36.

3.3 Preliminary Performance Analysis

In this section, we conduct the detailed timing analysis in Section 3.2 through a small scale network to highlight the ability of our proposal to guarantee the system requirements, in terms of predictability and reliability.

3.3.1 Test case

Table 3.1: TDMA cycle and slots allocation for each cluster

	Node type	Number	Slot duration	TDMA cycle
Cluster 1	End-system	7	120	1000
	Gateway	1	160	
Cluster 2	End-system	5	120	1000
	Gateway	1	400	

Table 3.2: Traffic configuration

(a) Traffic classes characteristics

Traffic classes	T(μs)	Dl(μs)	e(μs)
TC_1	8000	8000	40
TC_2	16000	16000	35

(b) Clusters communication

Node type	Traffic classes	Number of subflows
End-system	TC_1	1
	TC_2	2
Incoming gateway 1	TC_1	2
	TC_2	5
Incoming gateway 2	TC_1	3
	TC_2	6

We consider an example of a wireless UWB network with transmission capacity $B = 200Mbps$ and 12 end-systems which are located in two clusters: 7 end-systems in cluster 1, 5 end-systems in cluster 2. The TDMA cycle duration of each cluster is 1 ms. Each end-system has an allocated TDMA time slot duration of 120 μs. Table 3.1 summarizes the TDMA cycles and slots configuration of the two clusters. The traffic configuration and the intra-cluster and inter-cluster communication are presented in Table 3.2.

The end-to-end delay bounds are computed under FIFO , FP and WRR policies in end-systems, and varying the network utilization by increasing the number of subflows in each end-system.

3.3.2 Error-Free environment

Figure 3.12 illustrates the end-to end delay bounds when varying the network utilization under FIFO, FP and WRR policies. As shown from these results, we have:

— First, enhanced system's schedulability under FP and WRR, with reference to FIFO. For instance, the configuration becomes unschedulable under FIFO, FP and WRR when the network utilization is greater than 0.21, 0.4, 0.26, respectively.

— Second, a better system schedulability under FP, with reference to WRR. This fact is mainly due to the impact of non-preemptive message transmission. According to Equations 3.9 and 3.12, the lower bound of offered TDMA slots to TC_1 and TC_2 under FP and WRR are equal to (80,80) and (40,35), respectively. This means that the network utilization could not be greater than 80 % and 75 %, under FP and WRR, respectively.

Hence, the FP is considered as the most efficient policy under error-free environment to enhance system schedulability.

3.3.3 Error-Prone Environment

We consider the same test case in Section 3.3.1 where the PER_L is equal to 10^{-10}, the PER_{UWB} is varying in $[10^{-5}, 1[$, the number of frequency channels $\eta_f \in \{1, 2, 3, 4\}$.

First, the number of packet transmissions η_t is computed when varying the number of frequency channels η_f and the PER_{UWB}, and the obtained results are illustrated in Figure 3.13.

As we can notice for a given PER_{UWB}, η_t decreases when η_f increases. Furthermore, when η_f increases, the PER_{UWB} for which $\eta_t = 1$ increases. For instance, the PER_{UWB} value under $n_f = 1$ is lower than 10^{-5} and the corresponding one under $n_f = 4$ is between $[10^{-3}, 10^{-2}]$. However, for high value of PER_{UWB}, η_t goes to infinite.

Then, the end-to-end delay bounds are calculated under FIFO, FP and WRR policies when varying the number of frequency channels η_f and the PER_{UWB}. The obtained results are illustrated in Figures 3.14, 3.15 and 3.16, respectively. These results show some interesting features:

— First, under FIFO , FP and WRR policies, for a given PER_{UWB}, end-to-end delay bounds decrease when η_f increases. For instance, with $PER_{UWB} = 10^{-3}$ and FIFO scheduling, the end-to-end delay bound is lower than the deadline (8 ms) with $\eta_f = \{2, 3, 4\}$ while it is greater than 16 ms with $\eta_f = 1$.

— Second, the tolerated PER_{UWB} value which respects the system schedulability is better under FP or WRR, with reference to FIFO. For instance, with FIFO policy, with two frequency channels, the tolerated PER_{UWB} is in $[10^{-3}, 10^{-2}]$ interval, while with FP and WRR policies, the tolerated one is in $[10^{-2}, 10^{-1}]$ interval when considering the schedulability of the lowest priority traffic.

— Third, when comparing FP and WRR policies, for the higher priority flow (TC_1) FP outperforms WRR because the whole service curve can be used for its transmission. However, for the lower priority flow TC_2, the performances are quite similar for both policies.

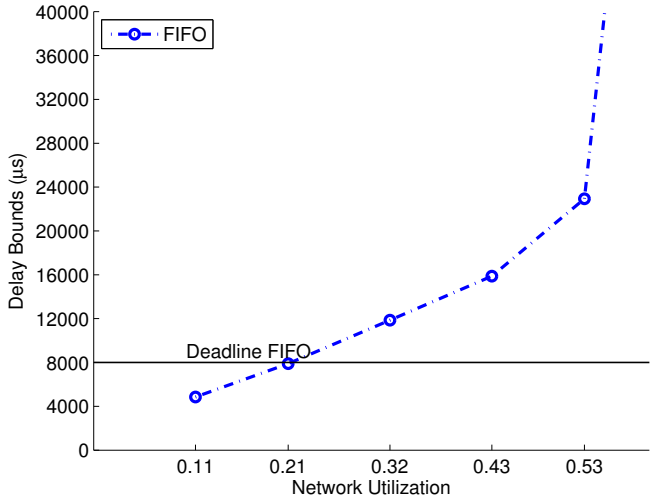

(a) FIFO Scheduling

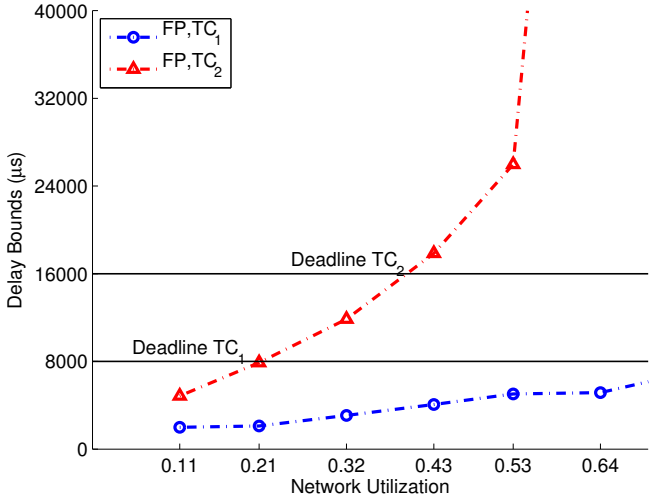

(b) FP scheduling

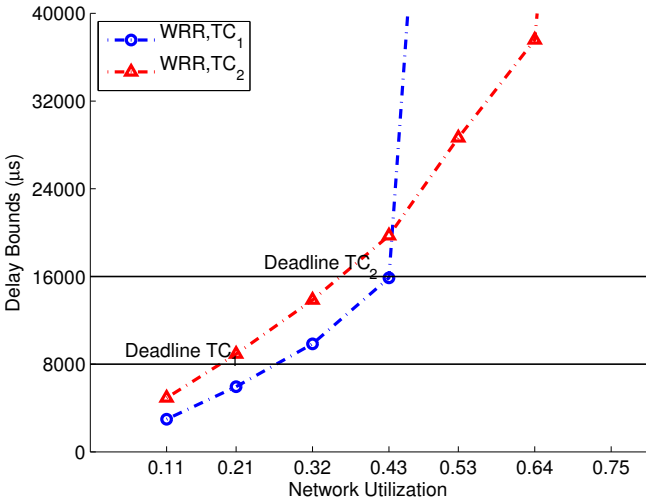

(c) WRR scheduling

Figure 3.12: Delays vs Network Utilization under error-free environment

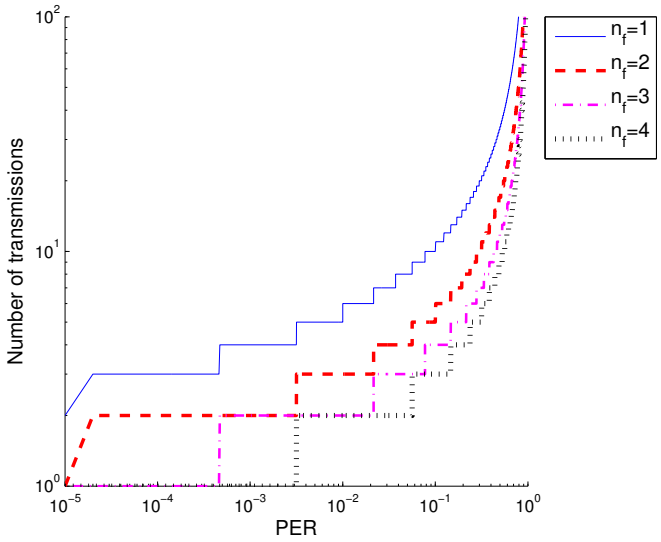

Figure 3.13: Number of transmissions vs PER and frequency number

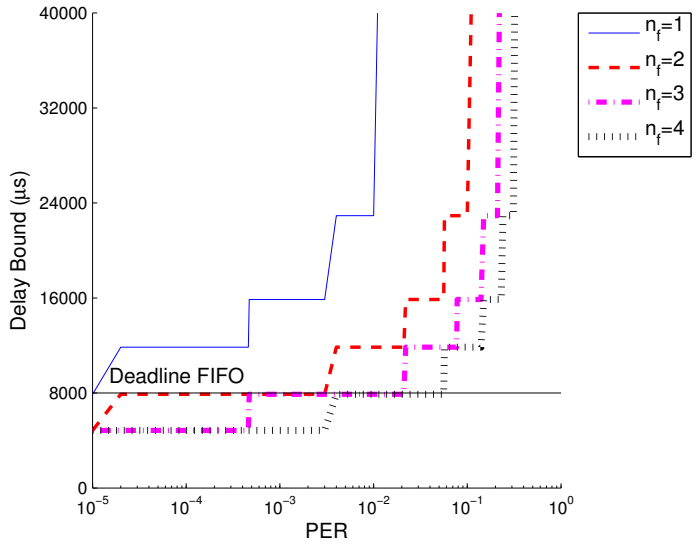

Figure 3.14: Delays vs PER with different frequencies for FIFO

Hence, we can deduce two main conclusions from these results. The first one confirms the results under error-free environment where FP policy is still the most efficient policy with reference to FIFO and WRR. The second concerns the system reliability where we can notice that the frequency diversity enhances the system schedulability. However, this fact may increase at the same time the system complexity. Therefore, there is a trade-off between time and frequency diversity mechanisms to enhance the system schedulability while limiting the system's complexity.

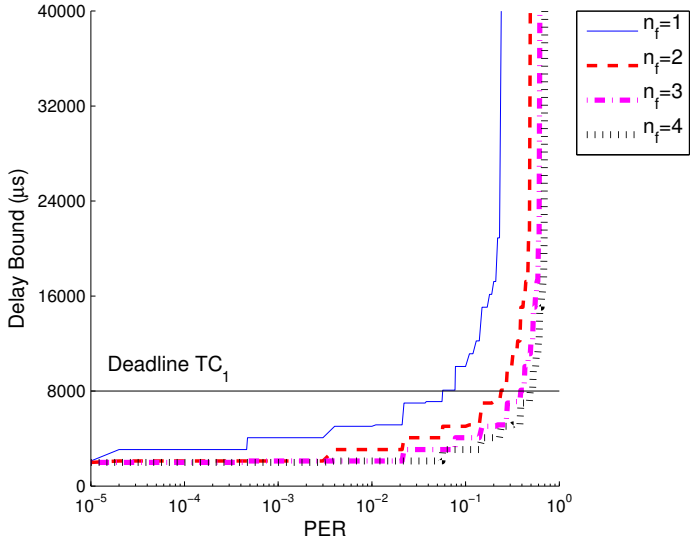

(a) FP scheduling (higer priority)

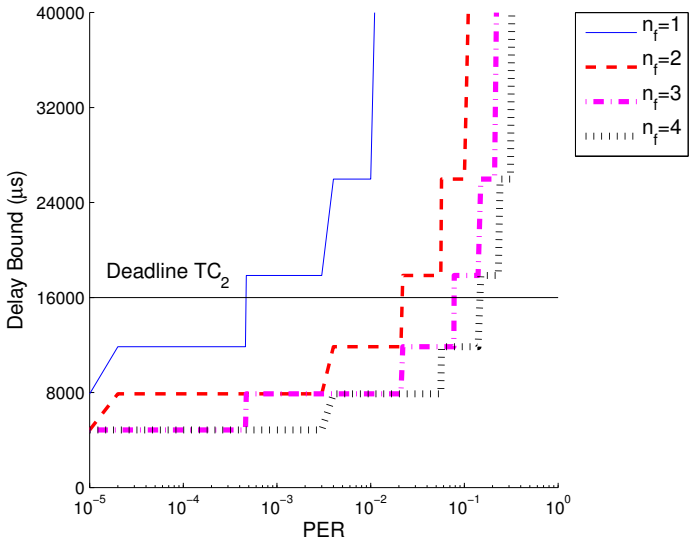

(b) FP scheduling (lower priority)

Figure 3.15: Delays vs PER with different frequencies for FP

Afterwards, the end-to-end delay bounds are computed when considering FIFO, FP and WRR policies, fixing the $PER_{UWB} = 10^{-3}$ and varying the number of frequency channels and network utilization of the network. The results are illustrated in Figure 3.17. As we can notice:

— First, under the different policies, increasing the number of frequencies enhances the system schedulability and scalability. For instance, under FIFO, the network utilization is equal to 0.21 under $\eta_f = 4$, while it is equal to 0.11 under $\eta_f = 2, 3$. Furthermore, the network is unschedulable under $\eta = 1$.

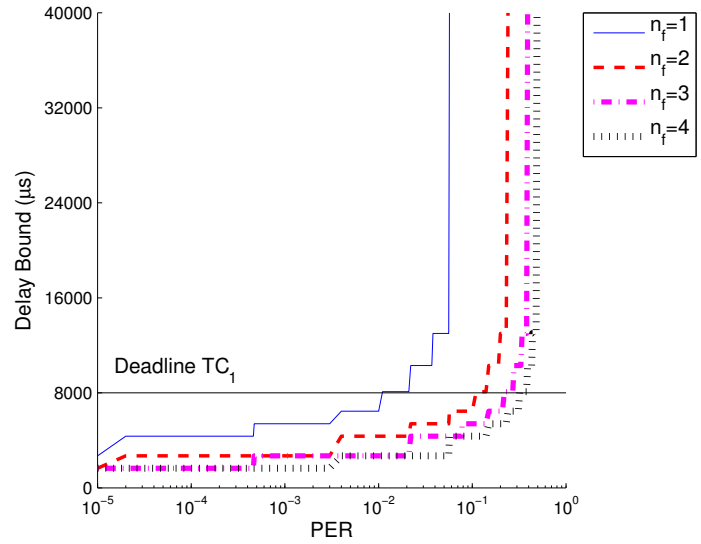

(a) WRR scheduling (TC_1)

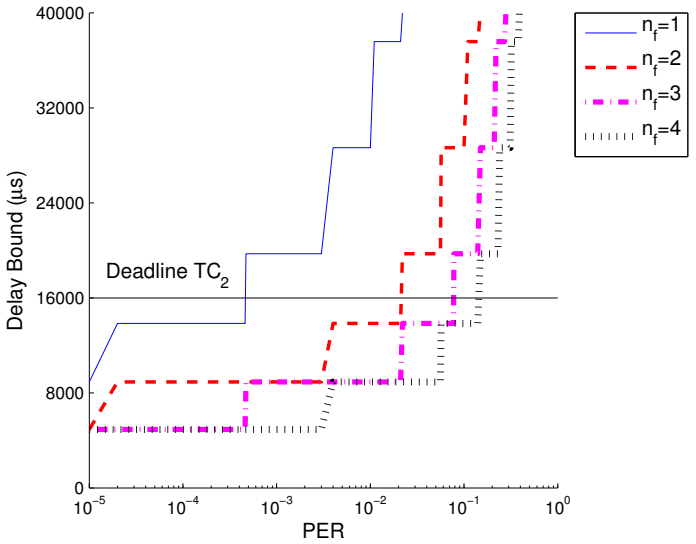

(b) WRR scheduling (TC_2)

Figure 3.16: Delays vs PER with different frequencies for WRR

— Second, FP leads to a better system's schedulability than FIFO and WRR. For instance, under FIFO or WRR and $\eta_f = 2$, the network utilization is equal to 0.11 while it is equal to 0.21 under FP.

Hence, in addition to enhancing the system predictability and reliability, the FP is the most efficient policy in terms of system scalability.

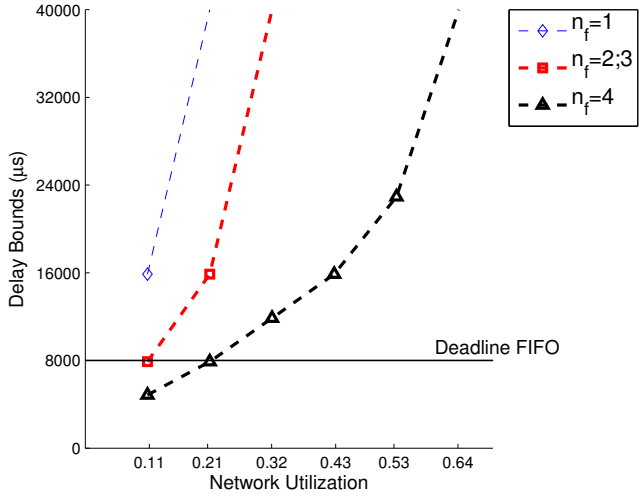

(a) FIFO Scheduling

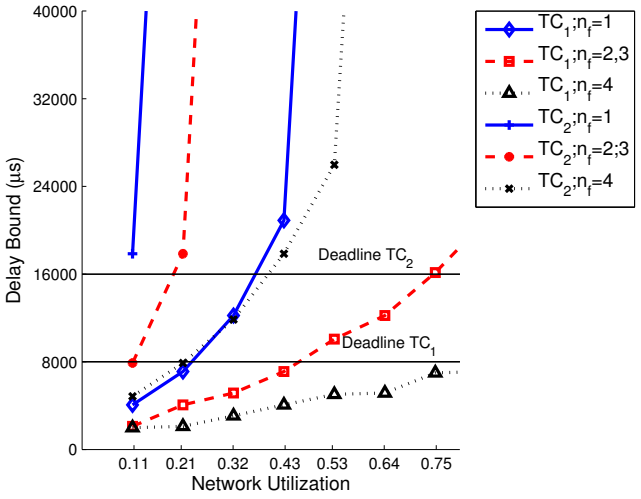

(b) FP scheduling

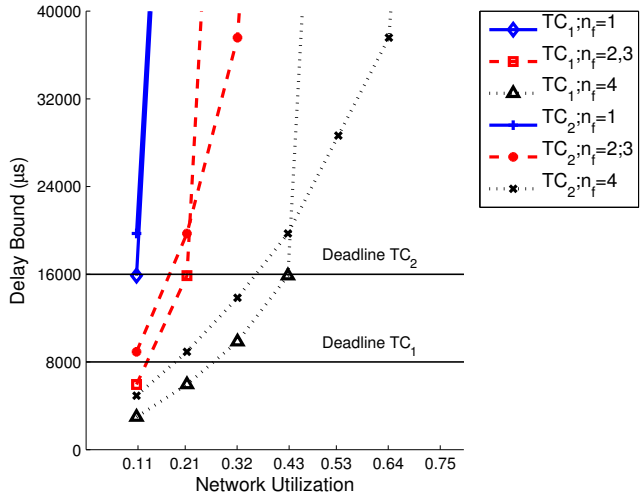

(c) WRR scheduling

Figure 3.17: Delays vs Network Utilization With Different Frequencies

3.4 Conclusion

In this chapter, a timing analysis approach has been introduced to verify the schedulability of our proposed WSCAN. First, we have extended the Network Calculus models to integrate the non-preemptive communication and reliability mechanisms based on time and frequency diversity to evaluate the end-to-end delay bounds of traffic flows under different scheduling policies as FIFO, FP and WRR. Then, the preliminary performance evaluation through a small scale network has been conducted. The obtained results have shown the efficiency of the FP policy combined with the time and frequency diversity to guarantee system predictability and reliability, with reference to FIFO and WRR.

These results have also shown that the system's schedulability is guaranteed only under low network utilization. This fact is mainly due to the pessimism of the delay bounds, which depend on many system parameters, such as the TDMA cycle duration and configuration, but also the selected reliability mechanism. Therefore, a major challenge consists in enhancing the system performances to increase the network utilization while guaranteeing the system's schedulability and reliability. This problem will be addressed in the next chapter where different solutions will be provided.

Chapter 4

Performance Enhancements of Wireless Network for Safety-critical Avionics

In this chapter, some enhancements of the system performance are conducted to obtain tighter delay bounds, and consequently to improve the system scalability and reliability. First, we propose refined system models based on the Network Calculus formalism and Integer Linear Programming approach to minimize the end-to-end delay pessimism. Then, an adequate optimization approach to find the optimal TDMA cycle duration and slots allocation is concluded to maximize the system's scalability. Afterwards, we consider the reliability mechanisms based on the retransmissions and the acknowledgment mechanisms to evaluate their impact on the system's reliability, with reference to disabling the acknowledgment mechanism detailed in the previous chapter. Finally, preliminary performance evaluation integrating these introduced enhancements is conducted through a small scale case study.

4.1 Refining System Models Using Integer Linear Programming

In this section, the refined models of end-systems and TDMA protocol using Network Calculus and Integer Linear Programming (ILP) are detailed to obtain refined service curves. The impact of these new service curves on the delay bounds is then evaluated and discussed.

4.1.1 Refined Model of End-Systems and Shared Network

In this section, we refine the strict service curve of the end-systems detailed in Section 3.1.3 under different policies. Our objective is to find the minimum offered TDMA time slot to obtain

tighter delay bounds.

4.1.1.1 FIFO

To obtain the minimum duration of the *offered TDMA time slot* $\overline{\overline{s}}$, we first formulate the problem under FIFO multiplexing. Then, we extend this formulation under FP and WRR multiplexing.

For each end-system k generating N traffic flows, we consider x_i the number of messages of traffic flow f_i^k that can be transmitted within a time slot s^k. The respective ILP problem is as follows:

minimize

$$\overline{\overline{s^k}} = \sum_{i=1}^{N} x_i * e_i \tag{4.1}$$

subject to:

$$\sum_{i=1}^{N} x_i * e_i \leq s^k \tag{4.2}$$

$$s^k - (\sum_{i=1}^{N} x_i * e_i) < e_{max} \tag{4.3}$$

$$x_i \in \mathbb{N}, 1 \leq i \leq N \tag{4.4}$$

where,

— the objective is to minimize the offered TDMA time slot when transmitting a variable number of messages of the different flows ($1 \leq i \leq N$) to maximize the remaining time and cover the worst-case scenario;

— the first constraint guarantees that the offered TDMA time slot $\overline{\overline{s^k}}$ is lower than the allocated TDMA time slot s^k;

— the second constraint guarantees that the remaining time within the minimum offered TDMA time slot is lower than the maximum message delivery time e_{max};

— the third constraint guarantees that the number of transmitted messages x_i^k of each traffic flow f_i^k is non-negative integer.

The minimum offered TDMA time slot that results from this ILP problem $\overline{\overline{s^k}}$ is integrated in the extended service curve model described in Theorem 1 to obtain the refined service curve model defined in the following corollary. The proof of Corollary 1 is detailed in Appendix C.

Corollary 1. *Consider an end-system having the minimum offered TDMA time slot* $\overline{\overline{s^k}}$*, a refined strict service curve guaranteed on TDMA-based network under FIFO multiplexing is*

$$\overline{\overline{\beta^k}}(t) = \beta_{c,\overline{\overline{s^k}}}(t - WT + (c - \overline{\overline{s^k}})) \tag{4.5}$$

4.1.1.2 FP

The previous ILP formulation can be easily extended under FP policy. To find the minimum *offered TDMA time slot* $\overline{\overline{s^k_{\leq i}}}$ of the aggregate flow $f^k_{\leq i}$, we need to consider only the subset of traffic flows $\{f^k_1, f^k_2, .., f^k_i\}$ instead of all traffic flows N in the ILP problem formulation (4.1). The optimization is presented explicitly as follows.

minimize

$$\overline{\overline{s^k_{\leq i}}} = \sum_{j=1}^{i} x_j * e_j \tag{4.6}$$

subject to:

$$\sum_{j=1}^{i} x_j * e_j \leq s^k_{\leq i} \tag{4.7}$$

$$s^k_{\leq i} - (\sum_{j=1}^{i} x_j * e_j) < e_{max} \tag{4.8}$$

$$x_j \in \mathbb{N}, 1 \leq i \leq i \tag{4.9}$$

The obtained minimum offered slot $\overline{\overline{s^k_{\leq i}}}$ is then integrated in the extended service curve described in Theorem 2 to obtain the refined service curve defined in the following corollary. The proof of Corollary 2 is detailed in Appendix C.

Corollary 2. *Consider aggregate flow $f^k_{\leq i}$ having the minimum offered TDMA time slot $\overline{\overline{s^k_{\leq i}}}$, a refined strict service curve guaranteed on TDMA-based network under FP multiplexing is*

$$\overline{\overline{\beta^k_{\leq i}}}(t) = \beta_{c, \overline{\overline{s^k_{\leq i}}}}(t - WT^k_{\leq i} + (c - \overline{\overline{s^k_{\leq i}}}))$$

Using Theorem 8 of Appendix A and Corollary 2, a refined service curve for flow f^k_i is given by:

$$\overline{\overline{\beta^k_i}}(t) = (\overline{\overline{\beta^k_{\leq i}}}(t) - \sum_{j=1}^{i-1} \alpha^k_j(t))_{\uparrow} \tag{4.10}$$

The optimization problem can be seen as a bin-packing problem which is known to be NP-hard. However, from a practical point of view, if the number of traffic flows is not too large (less than 100), we can solve efficiently this optimization problem in a short time.

4.1.1.3 WRR

Our objective is to find the most accurate access time $\overline{\overline{w_i^k}}$ for each flow f_i^k using ILP. Hence, the ILP formulation for WRR is as follows:

$$\text{minimize} \quad \sum_{i=1}^{N} |w_i^k - x_i * e_i| \tag{4.11}$$

subject to:

$$e_{max} + c - s + \sum_{i=1}^{N} x_i * e_i = \overline{\overline{c}}$$
$$\sum_{i=1}^{N} x_i * e_i \leq s$$
$$\frac{x_i * e_i * B}{\overline{\overline{c}}} \geq r_i, \forall 1 \leq i \leq N$$
$$x_i \in \mathbb{N}^+, \forall 1 \leq i \leq N$$

where,

— the objective function is to minimize the difference between the offered access times in preemptive and non-preemptive cases for all flows;

— the first constraint guarantees the respect of the maximum round robin cycle duration $\overline{\overline{c}}$;

— the second constraint guarantees that the sum of all access times is lower than the initial slot duration;

— the third constraint is needed to guarantee the stability condition of any flow i where the offered service rate has to be greater than the traffic rate r_i.

— the forth constraint guarantees that the number of transmitted messages x_i of each traffic flow f_i^k is a positive integer.

Let $(x_1^*, x_2^*, .., x_N^*)$ be the optimal solution of the optimization problem above. Flow f_i^k is allowed to transmit up to x_i^* messages during each WRR round. Hence, the respective access time is $\overline{\overline{w_i^k}} = x_i^* * e_i$ to obtain the refined service curve defined in the following corollary. The proof of Corollary 3 is detailed in Appendix C.

Corollary 3. *Consider a flow f_i^k, the refined strict service curve guaranteed on TDMA-based network under non-preemptive WRR multiplexing is*

$$\overline{\overline{\beta_i^k}}(t) = \beta_{\overline{\overline{c}}, \overline{\overline{w_i^k}}}(t) \tag{4.12}$$

where $\overline{\overline{w_i^k}} = x_i^* * e_i$ and $\overline{\overline{c}} = e_{max} + c - s + \sum_{j=1}^{N} \overline{\overline{w_j^k}}$

4.1.2 Numerical Results and Discussions

We revisit the test case detailed in Section 3.3.1 of Chapter 3. In this part, we will show the end-to-end delay bounds improvement when using the refined service curves under error-free and error-prone environment with the different scheduling policies.

4.1.2.1 Error-Free environment

— For FIFO scheduling, Figure 4.1 shows the delay bounds with different network utilization under the extended and the refined models. We observe that the delay bounds are tighter under the refined model with reference to the extended model. For instance, under a network utilization of 20 %, both the refined and extended model guarantees the system schedulability; however, the refined one can provide safer margin than the extended one.

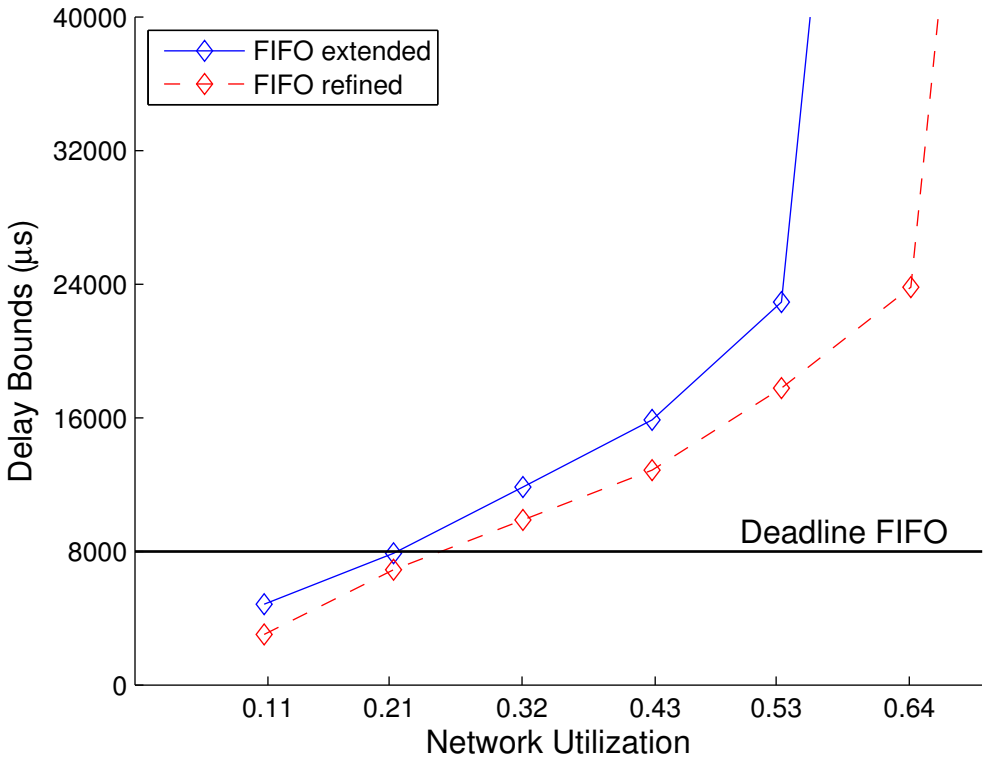

Figure 4.1: FIFO delay bounds under extended and refined models

— For FP scheduling, we also observe the enhancement of the network schedulability under the refined model as shown in Figure 4.2. For instance, for a network utilization of 40 %, the extended model leads to a delay greater than the longest deadline (16 ms) and consequently cannot guarantee the system schedulability unlike the refined model. However, the improvement is only observed for the low priority flow because Equations 3.8 and 4.6

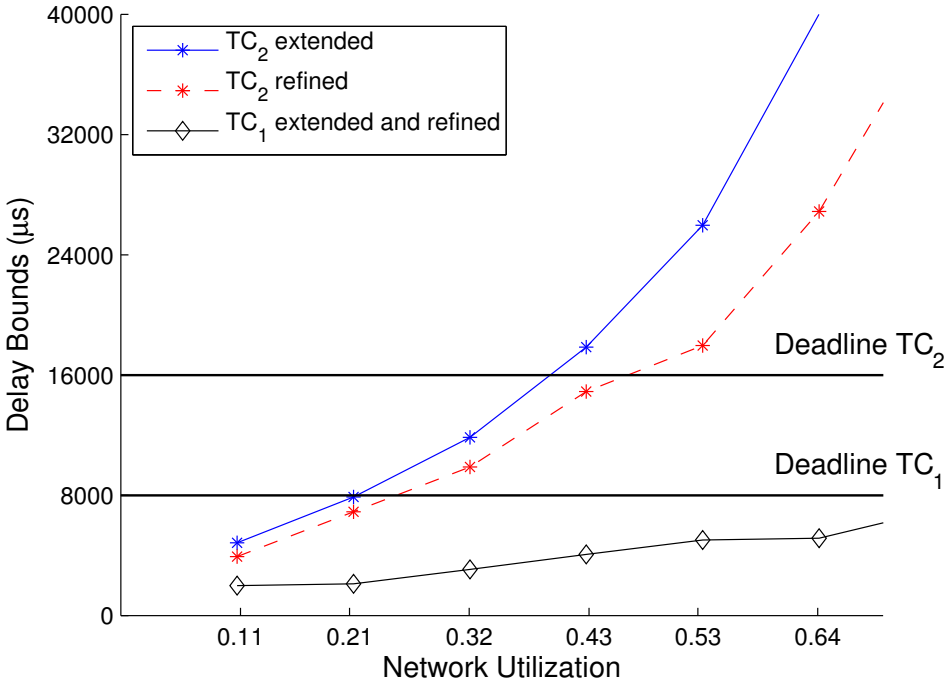

Figure 4.2: FP delay bounds under extended and refined models

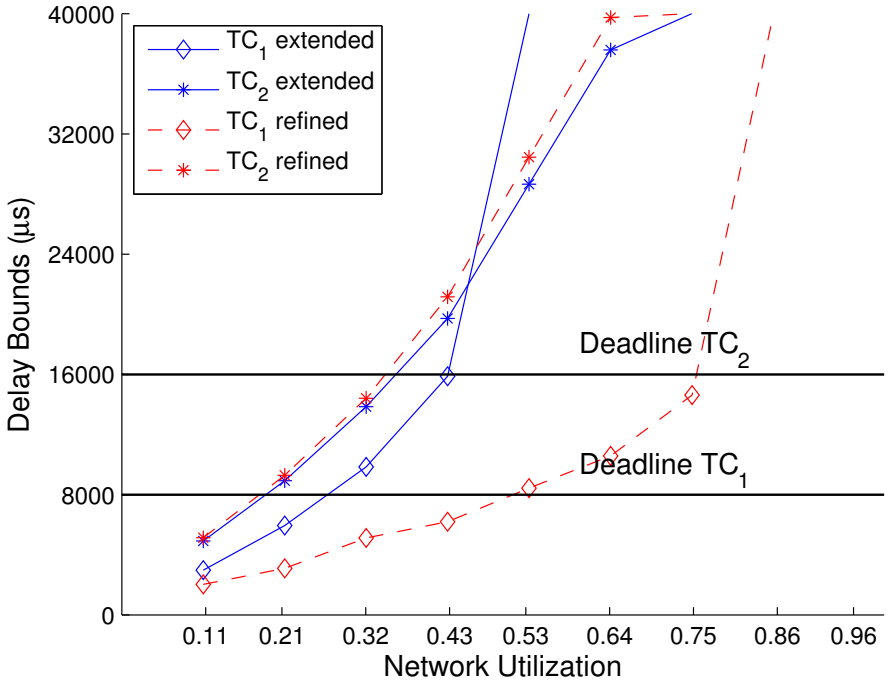

Figure 4.3: WRR delay bounds under extended and refined models

give the same value of the offered TDMA slot for the highest priority flow, $s^1 = 120$ μs. For TC_2, the offered TDMA slots of the extended and refined models are 80 and 105 μs, respectively. This difference explains the tighter delay bounds under the refined model.

— For WRR scheduling, the weight of TC_1 is increased from $\overline{w_1^k} = 40$ to $\overline{\overline{w_1^k}} = 80$ and the weight of TC_2 is unchanged under the refined model. Therefore, as shown in Figure 4.3, the delay bounds are improved for TC_1 under the refined model, while there are almost the same for TC_2, with reference to the extended model.

These results show the importance of the used model to verify the system schedulability, and the beneficial impact of refined model, with reference to the extended one.

4.1.2.2 Error-Prone environment

Under error-prone environment, we consider $PER_{UWB} = 10^{-3}$ and $PER_L = 10^{-10}$. When considering frequency and time diversity as reliability mechanisms, for a number of frequencies $\eta_f = \{1, 2, 3, 4\}$, the necessary number of time diversity is $\eta_t \in \{4, 2, 2, 1\}$, respectively. With $\eta_t = 1$, the results are the same as the ones obtained in error-free environment. Therefore, we only consider $\eta_t \in \{4, 2\}$:

— $\eta_f = 1 \Leftrightarrow \eta_t = 4$. Figure 4.4 shows the delay bounds under different scheduling policies (FIFO, FP and WRR) under the extended and refined models. For FP, the conclusion on the system performance is changed from unschedulable to schedulable when considering the refined model. This fact highlights the importance of refined model in terms of network schedulability enhancement.

— $\eta_f = 2, 3 \Leftrightarrow \eta_t = 2$. Figure 4.5 shows the delays of each flow under different scheduling policies using extended and refined models. Similarly to results of Figure 4.4, the delay bounds are tighter under refined models with the different scheduling policies. Moreover, under FP, we notice a better schedulability when considering refined models. For instance, the system becomes schedulable under a network utilization of 20 %, which was limited to 10 % under the extended models.

These results confirm our first conclusions under error-free environment. Furthermore, we notice that the FP policy outperforms FIFO and WRR, in terms of schedulability and scalability of the system.

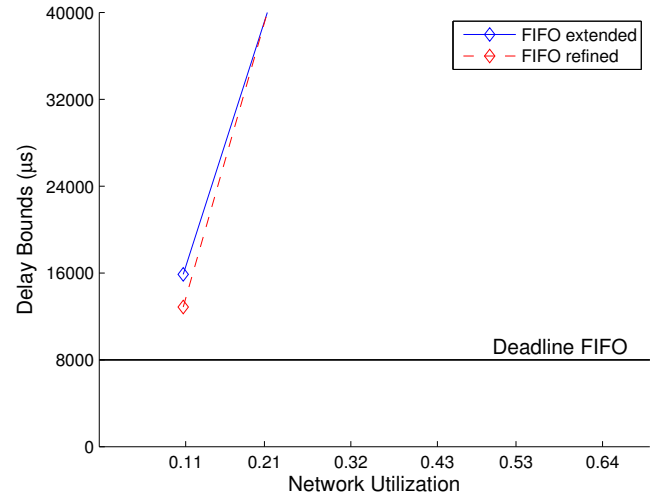

(a) FIFO Delays

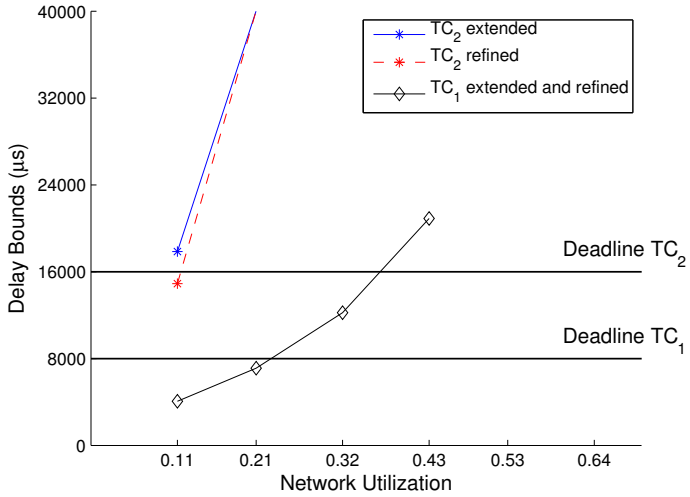

(b) FP Delays

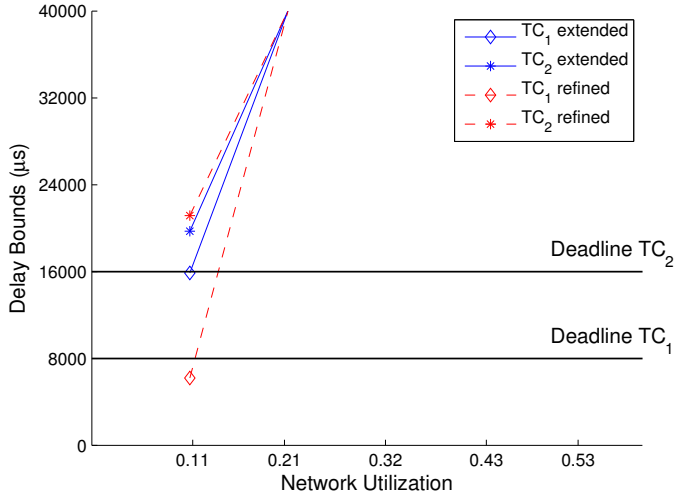

(c) WRR Delays

Figure 4.4: Extended vs refined models with $\eta_f = 1$

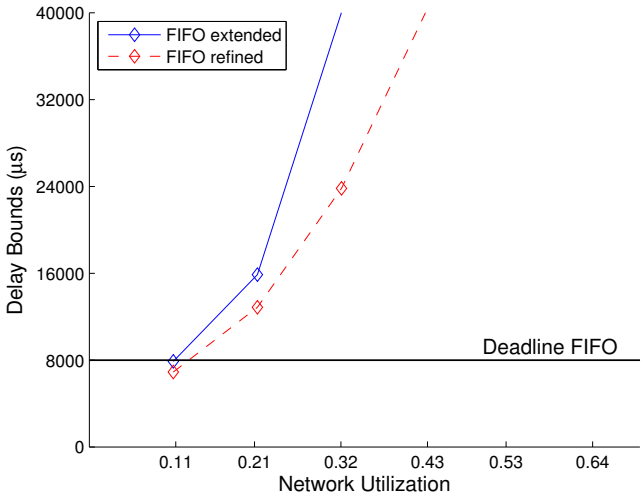

(a) FIFO Delays

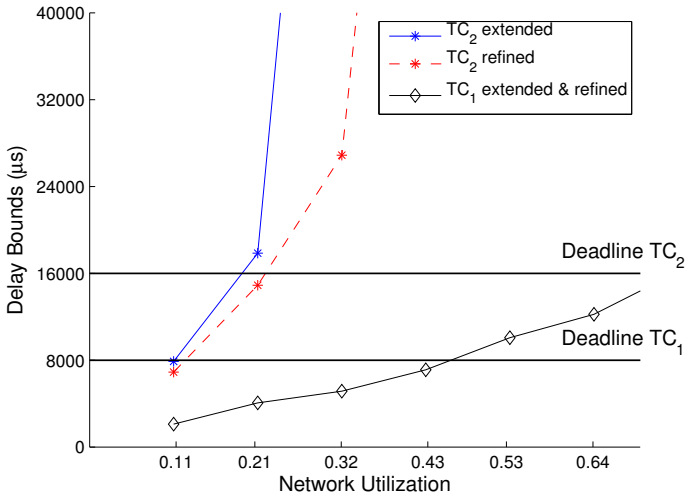

(b) FP Delays

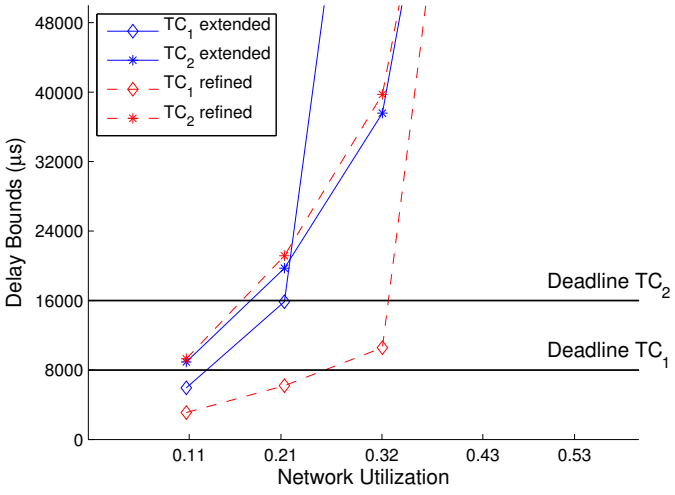

(c) WRR Delays

Figure 4.5: Extended vs refined models with $\eta_f = 2$

4.2 Optimization of TDMA Cycle

In this section, we present the optimization problem to find the optimal TDMA cycle duration, which minimizes the delay bounds. Then, we detail the optimization approach to solve this later. The impact of the optimized TDMA cycle duration on the delay bounds is finally evaluated and discussed.

4.2.1 Problem Formulation

The aim is to find the optimal TDMA cycle duration and slots allocation for the different avionic clusters to guarantee the system schedulability and to minimize delay bounds. We can formulate the optimization problem as follows:

$$\begin{aligned} &\underset{\forall u,(c^u,s^{1,u},s^{2,u},...,s^{M,u})}{\text{minimize}} && D_i^{e2e}, \forall i = 1, 2, ..., N \\ &\text{subject to} && D_i^{e2e} \leq Dl_i,\ i = 1, \ldots, N. \end{aligned} \tag{4.13}$$

This is a non-linear multi-criteria optimization problem which is complex to solve in the general case. Therefore, to simplify this problem, we will transform it to a mono-criteria optimization problem. Under FIFO, we consider as an objective function

$$D^{e2e} = \max_i D_i^{e2e} \tag{4.14}$$

However, under FP and WRR, we allocate a weight u_i to each criteria to have as an objective function:

$$D^{e2e} = \sum_{i=1}^{N} u_i D_i^{e2e} \tag{4.15}$$

where $u_i = \dfrac{1}{Dl_i}$ which guarantees that if $Dl_i < Dl_j$, then $u_i > u_j$.

To solve this problem, we reduce the number of variables by using the *traffic proportional slot sizing* (TPSS) [55] for slots allocation, i.e., to allocate to each end-system a slot proportional to its generated rate. Hence, the only variable to optimize is the cycle duration c^u for each cluster u and the optimization problem is then reformulated as follows:

$$\begin{aligned} &\underset{\forall u,c^u}{\text{minimize}} && D^{e2e} \\ &\text{subject to} && D_i^{e2e} \leq Dl_i, \forall 1 \leq i \leq N \end{aligned} \tag{4.16}$$

4.2.2 Optimization Algorithm

The following algorithm is used to find the optimal cycle duration for each cluster, which minimizes the delay bounds and respects the system's schedulability.

Step 1: For each cluster u, we consider:

$$min\_cycle(u) = t_{syn} + \sum_{\forall k \in clt_u} \max_{f_i^k} e_i \tag{4.17}$$

$$max\_cycle(u) = \min_i Dl_i \tag{4.18}$$

where clt_u is the set of all end-systems in cluster u.

Step 2: For each cluster u, we build the set $\mathcal{C}^u$ of all TDMA cycle durations in $[min\_cycle(u), max\_cycle(u)]$ with q_c corresponding to a sampling step as follows:

for $i := \lceil \frac{min\_cycle(u)}{q_c} \rceil$ **to** $\lfloor \frac{max\_cycle(u)}{q_c} \rfloor$ **do**

$c^u \leftarrow q_c.i$

$\mathcal{C}^u \leftarrow \mathcal{C}^u \cup c^u$

end for

Step 3: Consider $\mathcal{M}$ clusters, for each configuration $\{c^1, c^2, ..., c^{\mathcal{M}}\}$ in $\mathcal{C}^1 \times \mathcal{C}^2 \times ... \times \mathcal{C}^{\mathcal{M}}$, we apply TPSS for slots allocation in each cluster c^u. Then, we compute the end-to-end delay bound D_i^{e2e} for each traffic class TC_i to verify the schedulability constraint.

Step 4: Among all the schedulable configurations, we select the one minimizing the objective function, which is considered as the optimal configuration.

4.2.3 Numerical Results

We revisit the test case in Section 3.3.1 of Chapter 3 to highlight the impact of the cycle duration on system performance. End-to-end delays are computed under two configurations for error-free and error-prone environment. The first one corresponds to a default configuration where the TDMA cycle duration is equal to 1 ms. The second one corresponds to the configuration where the TDMA cycle is computed based on the described algorithm in Section 4.2.2 with a sampling step $q_c = 500$ μs.

4.2.3.1 Error-Free environment

For the error-free environment, Figure 4.6 shows the delay bounds when varying the network utilization under the different scheduling policies (FIFO, FP and WRR) and the two TDMA configurations, i.e., default and optimized. As can be noticed, the delay bounds and system's schedulability are improved under the optimized configuration, with reference to the default configuration. For instance, under FIFO, the system becomes schedulable when considering the optimized configuration for a network utilization of 30 % , which was limited to 20 % under the default one. The same observation holds under FP and WRR where the network utilization that guarantees the system schedulability is increased from 40 % to 60 %, and from 30 % to 50 %, respectively.

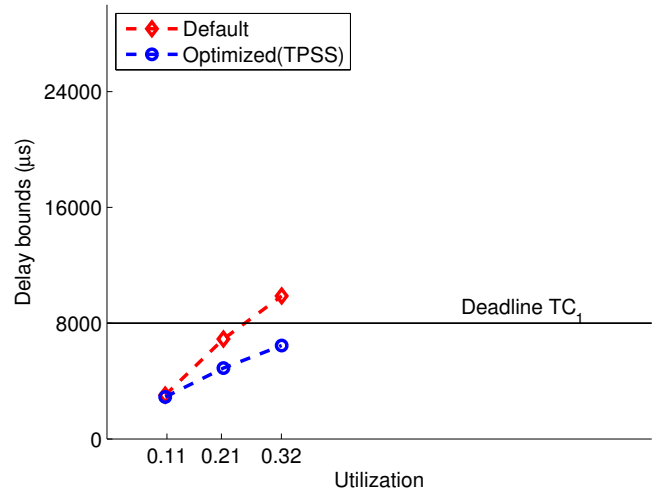

(a) FIFO Delays

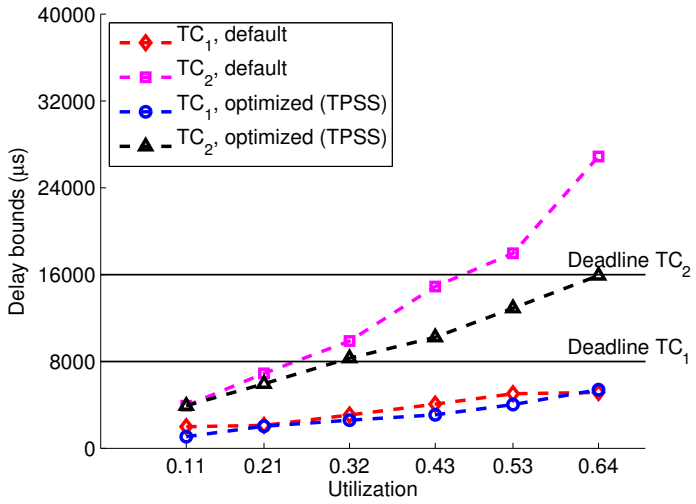

(b) FP Delays

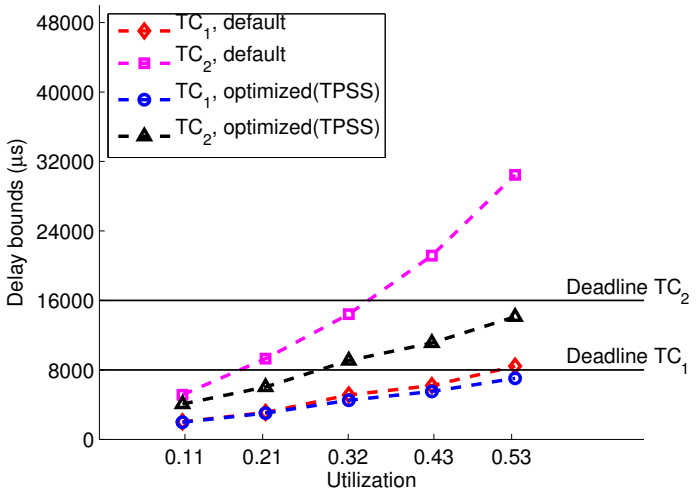

(c) WRR Delays

Figure 4.6: Default vs Optimized configurations under error-free environment

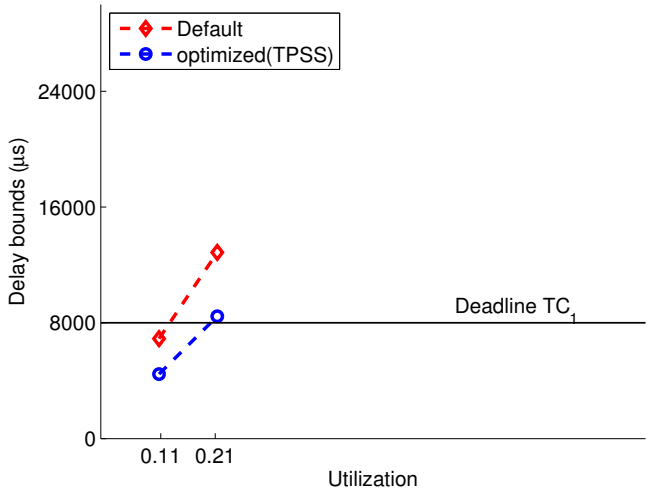

(a) FIFO Delays

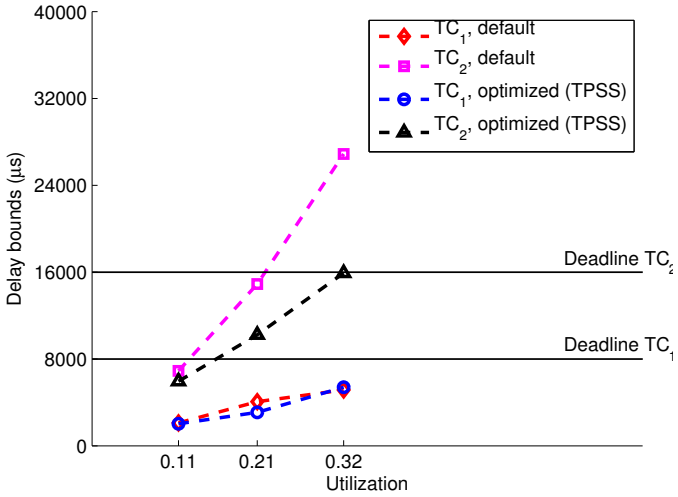

(b) FP Delays

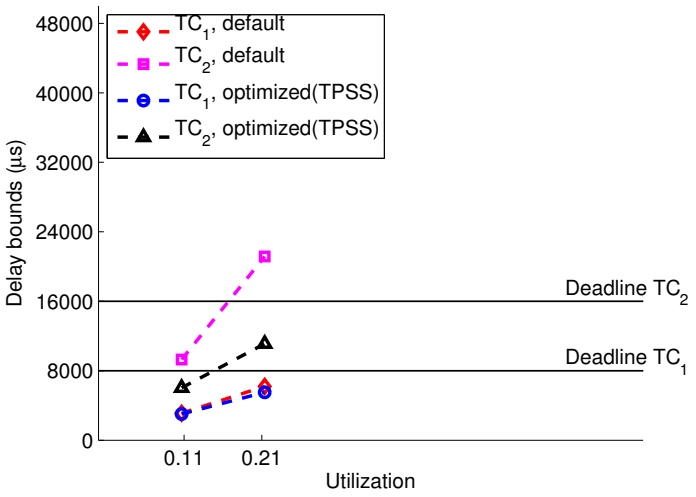

(c) WRR Delays

Figure 4.7: Default vs Optimized configuration (TPSS) with $\eta_f = 2$ under error-prone environment

4.2.3.2 Error-Prone environment

In error-prone environment, for the same reasons detailed in Section 4.1.2.2, we consider the frequency diversity $\eta_f = \{1, 2\}$. With $\eta_f = 1$, under the default configuration and for a network utilization less than 10 %, the network is schedulable only with FP and WRR scheduling policies. For higher network utilization, the network becomes unschedulable for all the considered scheduling policies.

Hence, we present herein the delay bounds under the different scheduling policies with $\eta_f = 2$ when considering the default and optimized TDMA configurations. The results are shown in Figure 4.7. As we can notice, the system schedulability is enhanced under the optimized configuration where the network utilization which guarantees the system schedulability has been increased with reference to the default configuration. For instance, it increases from 10 % to 20 % under FIFO and WRR, and from 10 % to 30 % under FP. Hence, the results confirm our first conclusions under the error-free environment which show the significant impact of the TDMA cycle duration and the scheduling policy choice on the system schedulability.

4.3 Enhancing Reliability Mechanisms

In this section, the impact of the reliability mechanism based on retransmission and acknowledgment on the end-to-end delay bounds is investigated. First, we introduce the stochastic modeling of the system, based on Stochastic Network Calculus [17]. Then, the analysis and the evaluation of the stochastic end-to-end delays are detailed and discussed.

4.3.1 Problem Formulation and General Assumptions

As detailed in Chapter 3, to guarantee the required level PER of avionic applications, PER_L, we considered time and frequency diversity mechanisms while disabling the acknowledgment to enhance the offered PER of UWB technology, PER_{UWB}. The conducted timing analysis based on Network Calculus of such a network shows the impact of these considered reliability mechanisms on the system performance by increasing the offered reliability level, but at the same time the end-to-end delay bounds. In this chapter, to enhance the delay bounds tightness, we activate the retransmission and acknowledgment mechanisms while keeping the frequency diversity. These considered reliability mechanisms will guarantee the required PER_L, but at the same time will complicate the system modeling. Indeed, in this case, the system is based on unreliable links with retransmission where the number of retransmissions of each packet can vary according to the wireless channel behavior. This fact introduces a stochastic dimension to the system model and requires the transfer of the Network Calculus concepts from the deterministic networks domain to the stochastic one.

To achieve this aim, we use the Stochastic Network Calculus [17], detailed in Appendix B which is adequate to compute stochastic upper bounds on delays when considering a tolerated probability on the schedulability violation ϵ. In our case, we consider a very small ϵ to guarantee the required reliability level of avionics applications. There are various interesting approaches in the domain of modeling unreliable links using Stochastic Network Calculus. There are the noticeable works of Wang [57] [58], Lubben [59] and Xie [60], which model the data loss of the unreliable links based on impairment processes. In [59] and [60], the data loss has been explicitly taken into account and integrated as a stochastic process into the service curve to propose the so-called error server model. A different approach is proposed in [57] [58], which models the losses due to unreliable links and the impact of retransmission schemes using a scaling function integrated within the offered service curve. Then, the authors introduce a fixed-point computation to determine the stochastic arrival curve of the traffic. This approach is efficient in the case of small scale network, but it may infer a high complexity when increasing the flows number.

Unlike the approaches in [59] [60] which focus on modeling the unreliable links using stochastic service curves, and similar to the work in [57] [58], we propose in our case a simpler approach based on modeling the stochastic behavior of the input retransmitted traffic using stochastic arrival curve. Then, we deduce the stochastic service curves of intermediate nodes on each traffic flow path by propagating its burstiness constraint. To handle this problem, we introduce within the Stochastic Network Calculus framework, extended theorems applicable in the specific case of strict stochastic service curve [61] and stochastic arrival curve [17] to compute the performance bounds, such as stochastic delay and backlog and stochastic residual service curve. These theorems and the associated proofs are detailed in Appendix B.

To model such a network, we consider the following set of assumptions:

— a simple model of channel behavior where the occurred packet transmission errors are independent and the crossover probability is p. This probability is equivalent to PER_{UWB} offered by the UWB technology;

— if the packet is successfully received, then the receiver will send a positive acknowledgment to the sender, else the packet will be retransmitted after a timer expiration. Hence, the acknowledgment delay is upper bounded and denoted as t_{ACK};

— the maximum number of transmissions of each packet is bounded by $\mathcal{N}$;

— the cumulative function of packets of the input traffic has the maximum and minimum packet curves $\Pi(t)$ and $\pi(t)$ [62], respectively .

4.3.2 Stochastic Arrival Curves for Retransmission Flows

Our objective is to define the stochastic arrival curve $\alpha^{\epsilon}(t)$ of the cumulative retransmission traffic $R(t)$, such that:

$$\forall t \geq s \geq 0, Pr\{R(t) - R(s) > \alpha^{\epsilon}(t-s)\} < \epsilon \tag{4.19}$$

where ϵ is the tolerated violation probability.

First, we will detail this curve in the case of homogeneous traffic, i.e., all the flows have the same frame size (L). Then, we generalize this curve to heterogeneous traffic with variable frame size.

4.3.2.1 Homogeneous Traffic

Since we have a homogeneous traffic with constant frame size L, we can express α^{ϵ} as following:

$$\forall t \geq s \geq 0, \alpha^{\epsilon}(t-s) = \overline{L}\Pi^{\epsilon}(t-s) \tag{4.20}$$

where $\overline{L} = L + B.t_{ACK}$ which integrates the overhead of the acknowledgment mechanism and $\Pi^{\epsilon}(t-s)$ is the stochastic arrival curve of the cumulative number of packets transmitted during the interval $[s,t]$. We also call Π^{ϵ} the stochastic packet curve which is the extended definition of the maximum packet curve $\Pi(t)$ [62]. The formal definition of Π^{ϵ} can be found in Appendix B.

Consider $\overline{\mathcal{P}}(t)$ the cumulative number of packets transmitted at the instant t and including retransmissions due to unreliable links, then Equation 4.19 is equivalent to the following:

$$\forall t \geq s \geq 0, Pr\{\overline{\mathcal{P}}(t) - \overline{\mathcal{P}}(s) > \Pi^{\epsilon}(t-s)\} < \epsilon \tag{4.21}$$

Hence, $\forall [s,t]$, consider $n \in \mathbb{N}^*$ such that $\Pi^{\epsilon}(t-s) = n$ and $Pr\{\overline{\mathcal{P}}(t) - \overline{\mathcal{P}}(s) > n\} < \epsilon$. This latter is equivalent to

$$\sum_{l>n} Pr\{\overline{\mathcal{P}}(t) - \overline{\mathcal{P}}(s) = l\} < \epsilon \tag{4.22}$$

Therefore, if we evaluate $Pr\{\overline{\mathcal{P}}(t) - \overline{\mathcal{P}}(s) = l\}$ for any $[s,t]$, then we can easily evaluate $\Pi^{\epsilon}(t-s)$ and consequently $\alpha^{\epsilon}(t-s)$.

To achieve this aim, we consider $\mathcal{P}(t)$ the cumulative number of packets transmitted at the instant t and assuming a reliable link ($p = 0$). During any $[s,t]$, let $h, k \in \mathbb{N}$ such that $h = \pi(t-s)$ and $k = \Pi(t-s)$. Hence, $h \leq \mathcal{P}(t) - \mathcal{P}(s) \leq k$. Since for any packet the maximum number of transmissions is $\mathcal{N}$, then

$$h \leq \overline{\mathcal{P}}(t) - \overline{\mathcal{P}}(s) \leq \mathcal{N}k \tag{4.23}$$

Based on Equation 4.23, Equation 4.22 is equivalent to the following:

$\forall[s,t]$, $\exists n \in \mathbb{N}^*$ such that

$$\begin{aligned} & Pr\{\overline{\mathcal{P}}(t) - \overline{\mathcal{P}}(s) > \Pi^{\epsilon}(t-s)\} < \epsilon \\ \Leftrightarrow \quad & Pr\{\overline{\mathcal{P}}(t) - \overline{\mathcal{P}}(s) > n\} < \epsilon \\ \Leftrightarrow \quad & \sum_{l \in [n+1, \mathcal{N}k]} Pr\{\overline{\mathcal{P}}(t) - \overline{\mathcal{P}}(s) = l\} < \epsilon \end{aligned} \tag{4.24}$$

Moreover, $\forall[s,t]$,

$$\begin{aligned} & Pr\{\overline{\mathcal{P}}(t) - \overline{\mathcal{P}}(s) = l\} \\ = \quad & \sum_{m=h}^{k} Pr\{\overline{\mathcal{P}}(t) - \overline{\mathcal{P}}(s) = l | \mathcal{P}(t) - \mathcal{P}(s) = m\} Pr\{\mathcal{P}(t) - \mathcal{P}(s) = m\} \\ \leq \quad & \max_{h \leq m \leq k} Pr\{\overline{\mathcal{P}}(t) - \overline{\mathcal{P}}(s) = l | \mathcal{P}(t) - \mathcal{P}(s) = m\} \sum_{m=h}^{k} Pr\{\mathcal{P}(t) - \mathcal{P}(s) = m\} \\ = \quad & \max_{h \leq m \leq k} Pr\{\overline{\mathcal{P}}(t) - \overline{\mathcal{P}}(s) = l | \mathcal{P}(t) - \mathcal{P}(s) = m\} \end{aligned} \tag{4.25}$$

To evaluate $Pr\{\overline{\mathcal{P}}(t) - \overline{\mathcal{P}}(s) = l | \mathcal{P}(t) - \mathcal{P}(s) = m\}$, we consider $(X_1, ..., X_m)$ an independent and identical distribution (i.i.d) random variables (r.v), where for any $i \in [1,m]$ X_i is the number of transmissions on unreliable links with PER p during $[s,t]$ of the i^{th} packet among m packets.

$$\begin{aligned} & Pr\{\overline{\mathcal{P}}(t) - \overline{\mathcal{P}}(s) = l | \mathcal{P}(t) - \mathcal{P}(s) = m\} \\ = \quad & \sum_{\{\forall i \in [1,m]: 1 \leq x_i \leq \mathcal{N}, \sum_{i=1}^{m} x_i = l\}} Pr\{X_1 = x_1, X_2 = x_2, ..., X_m = x_m\} \\ = \quad & \sum_{\{\forall i \in [1,m]: 1 \leq x_i \leq \mathcal{N}, \sum_{i=1}^{m} x_i = l\}} \prod_{i=1}^{m} Pr\{X_i = x_i\} \\ \leq \quad & \Phi(l, m, \mathcal{N}) \max_{\{\forall i \in [1,m]: 1 \leq x_i \leq N, \sum_{i=1}^{m} x_i = l\}} \prod_{i=1}^{m} Pr\{X_i = x_i\} \end{aligned} \tag{4.26}$$

where $\Phi(l, m, \mathcal{N})$ is the number of combinations of $(x_1, ..., x_m)$ such that for any $i \in [1,m]$, $1 \leq x_i \leq \mathcal{N}$ and $\sum_{i=1}^{m} x_i = l$. This function can be computed recursively as follows:

$$\Phi(l, m, N) = \Phi(l-1, m-1, \mathcal{N}) + \Phi(l-2, m-1, \mathcal{N}) + ... + \Phi(l-\mathcal{N}, m-1, \mathcal{N}) \tag{4.27}$$

where,

$$\Phi(l, m, \mathcal{N}) = \begin{cases} 1 & \text{if } l = m, \\ 0 & \text{if } l < m, \end{cases}$$

and

$$\Phi(l, 1, \mathcal{N}) = \begin{cases} 1 & \text{if } 1 \leq l \leq \mathcal{N}, \\ 0 & \text{if } l > \mathcal{N} \end{cases}$$

On the other hand, for any $i \in [1, m]$, $Pr\{X_i = x\}$ is computed as follows:

$$Pr\{X_i = x\} = \begin{cases} 1-p & \text{if } x = 1, \\ (1-p)p & \text{if } x = 2, \\ (1-p)p^2 & \text{if } x = 3, \\ .... & \\ (1-p)p^{N-2} & \text{if } x = \mathcal{N}-1, \\ p^{N-1} & \text{if } x = \mathcal{N} \\ 0 & \text{if } x \geq \mathcal{N}+1. \end{cases} \tag{4.28}$$

As we can notice, for any $i \in [1, m]$, $\sum_x Pr\{X_i = x\} = 1$ and $\forall 1 \leq x \leq \mathcal{N}, Pr\{X_i = x\} \leq p^{x-1}$. Using Equations 4.26 and 4.28, Equation 4.25 can be rewritten as follows:

$$\begin{aligned} & Pr\{\overline{\mathcal{P}}(t) - \overline{\mathcal{P}}(s) = l\} \\ \leq & \max_{h \leq m \leq k} Pr\{\overline{\mathcal{P}}(t) - \overline{\mathcal{P}}(s) = l | \mathcal{P}(t) - \mathcal{P}(s) = m\} \\ \leq & \max_{h \leq m \leq k} \Phi(l, m, \mathcal{N}) \max_{\{\forall i \in [1,m]: 1 \leq x_i \leq \mathcal{N}, \sum_{i=1}^{m} x_i = l\}} \prod_{i=1}^{m} Pr\{X_i = x_i\} \\ \leq & \max_{h \leq m \leq k} \Phi(l, m, \mathcal{N}) p^{l-m} \end{aligned} \tag{4.29}$$

Based on Eqs. 4.24 and 4.29, we have:

$$Pr\{\overline{\mathcal{P}}(t) - \overline{\mathcal{P}}(s) > \Pi^{\epsilon}(t-s)\} \leq \sum_{l \in [n+1, \mathcal{N}k]} \max_{h \leq m \leq k} \Phi(l, m, N) p^{l-m} \tag{4.30}$$

From Eq. 4.30, to identify $\Pi^{\epsilon}(t-s)$, we need to minimize $n \in \mathbb{N}$ such that $\Pi^{\epsilon}(t-s) = n$ and the following holds:

$$\sum_{l \in [n+1, Nk]} \max_{h \leq m \leq k} \Phi(l, m, \mathcal{N}) p^{l-m} < \epsilon \tag{4.31}$$

To achieve this aim, we will compute the smallest value of n, which verifies the condition of 4.31 based on the following algorithm.

Step 1: For each $\Delta \geq 0$, we can find (h, k) such that $\pi(\Delta) = h$ and $\Pi(\Delta) = k$ from the deterministic packet curves.

Step 2: For each Δ, we compute $n \in \mathbb{N}$ such that $\Pi^{\epsilon}(\Delta) = n$ as follows:

$l \leftarrow \mathcal{N}k$

$s \leftarrow 0$ ▷ Sum of probabilities of violation

while $s < \epsilon$ **do**

$s \leftarrow s + \max_{h \leq m \leq k} \Phi(l, m, \mathcal{N}) p^{l-m}$

$l \leftarrow l - 1$

end while

Step 3:

$n \leftarrow l$ ▷ n is the smallest integer that verifies condition 4.31

Based on this algorithm, we can formulate the stochastic packet curve Π^{ϵ}. After defining Π^{ϵ}, the stochastic arrival curve α^{ϵ} is obtained using Equation 4.20.

4.3.2.2 Heterogeneous Traffic

The heterogeneous traffic consists of a set of sub-flows that have constant packet length. Consider f the aggregate flow of m sub-flows having packet lengths $\overline{L_1}, ..., \overline{L_m}$ and packet curves $\Pi_1, .., \Pi_m$ [62]. There are two ways to formulate the t.a.c stochastic arrival curve of f.

In the first approach, we consider that for any $i \in [1, m]$, $\epsilon_i = \dfrac{\epsilon}{m}$. Using Theorem 12 in Appendix B, the stochastic arrival curve $\overline{\alpha^{\epsilon}}$ is given by:

$$\overline{\alpha^{\epsilon}}(t) = \sum_{i=1}^{m} \alpha_i^{\epsilon/m}(t) \tag{4.32}$$

In the second approach, we use directly the stochastic packet curve Π^{ϵ} of the aggregate flow f to formulate the stochastic arrival curve $\overline{\overline{\alpha^{\epsilon}}}$. Without loss of generalization, we assume that $\overline{L_1} > \overline{L_2} > ... > \overline{L_m}$. For any $t \geq 0$, let $n \in \mathbb{N}$ such that $\Pi^{\epsilon}(t) = n$. Consider the number of packets of f_i as $x_i \in [1, \mathcal{N}\Pi_i(t)]$ where $\sum_{i=1}^{m} x_i = n$. Hence, for the stochastic arrival curve $\overline{\overline{\alpha^{\epsilon}}}$, there holds:

$$\overline{\overline{\alpha^{\epsilon}}}(t) \geq \sum_{i=1}^{m} x_i \overline{L_i} \tag{4.33}$$

Therefore, $\overline{\overline{\alpha^{\epsilon}}}(t) = \max_{x_i} \sum_{i}^{m} x_i \overline{L_i}$. For any $i \in [1, m]$, the value of x_i which maximizes $\overline{\overline{\alpha^{\epsilon}}}$ is as follows:

$$x_i = [\min(\mathcal{N}\Pi_i(t), n - \sum_{j=1}^{i-1} \mathcal{N}\Pi_j(t))]^{+} \tag{4.34}$$

where $[x]^{+} = \max\{x, 0\}$.

Therefore,

$$\overline{\overline{\alpha^{\epsilon}}}(t) = \sum_{i=1}^{m} \overline{L_i} [\min(\mathcal{N}\Pi_i(t), n - \sum_{j=1}^{i-1} \mathcal{N}\Pi_j(t))]^{+} \tag{4.35}$$

The final stochastic arrival curve is derived using Equations 4.32 and 4.35 as follows:

$$\alpha^{\epsilon}(t) = \min\{\overline{\alpha^{\epsilon}}(t), \overline{\overline{\alpha^{\epsilon}}}(t)\} \tag{4.36}$$

4.3.3 Stochastic Strict Service Curves for End-systems

We detail in this section the impact of the stochastic arrival curves of retransmission flows on the offered service curve of the end-system. Hence, we extend the detailed service curves in Section 3.1.3 of Chapter 3 to integrate this stochastic dimension. Consider the end-system k which generates N flows f_i^k where each flow has a t.a.c stochastic curve α_i^{k,ϵ_i}. Based on Theorem 12 in Appendix B, the aggregate flow f^k has t.a.c stochastic curve $\alpha^{k,\epsilon}(t) = \sum \alpha_i^{k,\epsilon_i}(t)$ where $\epsilon = \sum_{i=1}^{N} \epsilon_i$.

We denote $\overline{e_i}$ the corresponding transmission time of $\overline{L_i}$. For different scheduling policies, the stochastic strict service curves offered by the end-system k are given as follows:

— Under **FIFO**, the stochastic strict service curve is deduced from Equation 3.6 in Chapter 3 by replacing $\overline{e_i}$ to e_i;

— Under **FP** , based on Theorem 17 and Corollary 6 in Appendix B, the stochastic service curve offered for flow f_i^k is given by β_i^{k,ϵ_i}:

$$\beta_i^{k,\epsilon_i^{\beta}} = \left(\overline{\beta_{\leq i}^k} - \sum_{j<i} \alpha_j^{\epsilon_j} - \max_{k \geq i} \overline{L_i} \right)_{\uparrow} \tag{4.37}$$

where $\epsilon_i^{\beta} = \epsilon_1 + .. + \epsilon_{i-1}$.

— Under **WRR**, the stochastic strict service curve is deduced from Equation 3.12 in Chapter 3 where $\overline{w_i^k} = \lfloor \frac{w_i^k}{\overline{e_i}} \rfloor * \overline{e_i}$.

4.3.4 Scaling Functions for Gateways

We operate in this section in the same way as for end-systems to define the offered service curves of the incoming and outgoing gateways, which integrate the impact of the stochastic arrival curves. Consider $\overline{L_i^{UWB}}$ the UWB packet length when acknowledgment mechanism is activated, and it is as follows:

$$\overline{L_i^{UWB}} = L_i^{UWB} + t_{ACK} * B \tag{4.38}$$

The scaling functions for the incoming and outgoing gateways are obtained, based on Equations 3.13, 3.14, 3.15, 3.16 and 3.17 in Chapter 3 when replacing L_i^{UWB} by $\overline{L_i^{UWB}}$.

4.3.5 Stochastic End-to-End Delay Bounds

To compute the stochastic end-to-end delay bounds for each flow f_i^k under different scheduling policies, we need to compute the stochastic delay in the end-system k and the incoming gateway of the associated cluster. These delay bounds are computed based on Theorem 16 in Appendix B when considering the detailed arrival and service curves in Sections 4.3.2, 4.3.3, and 4.3.4. However, the delay bounds at the outgoing gateway and the switch are still computed based on deterministic curves as shown in Sections 3.2.1.2 and 3.2.1.3 in Chapter 3. We denote the delays at the outgoing gateway u and the switch's outgoing port v as D^{GW_u} and D^{SW_v}, respectively.

Hence, we present herein how to compute the stochastic delays only in end-systems and the incoming gateway. Using Theorem 16 in Appendix B, the stochastic delay bounds in any end-system k in cluster u are given as follows.

— Under **FIFO**:

$$D_u^{k,\epsilon_k} = D_i^{k,\epsilon} = h(\alpha^{k,\epsilon}, \overline{\beta^k}) \tag{4.39}$$

— Under **FP**, based on Equation 4.37:

$$D_u^{k,\epsilon_k} = D_i^{k,\sum_{j=1}^{i}\epsilon_j} = h(\alpha_i^{k,\epsilon_i}, \overline{\beta^{k,\sum_{j=1}^{i-1}\epsilon_j}}) \tag{4.40}$$

— Under **WRR**:

$$D_u^{k,\epsilon_k} = D_i^{k,\epsilon_i} = h(\alpha_i^{k,\epsilon_i}, \overline{\beta_i^k}) \tag{4.41}$$

Hence, the intra-cluster stochastic delay bound for any traffic class TC_i generated by end-system k in cluster u is given by:

$$D_u^{\epsilon_u} = \max_{\forall k}\{D_u^{k,\epsilon_k}\} \tag{4.42}$$

where $\epsilon_u = \max \epsilon_k$.

To compute the stochastic delay of the incoming gateway, we first propagate the arrival curves under error-free environment from the output of the end-system until the input of the incoming gateway. Then, we transform the obtained deterministic arrival curve on a stochastic arrival curve by considering a fixed probability of violation as detailed in Section 4.3.2 to integrate the error-prone environment conditions.

Let D_i^k be the delay upper bound of f_i^k at the end-system k under the error-free environment. Hence, the maximum input packet curve of f_i^k at the outgoing gateway GW_u, based on the f_i^k is as follows:

$$\Pi_i^{GW_u,in,k}(t) = \Pi_i^k(t + D_i^k) \tag{4.43}$$

Since the delay bounds at the outgoing gateway GW_u and the switch's outgoing port v are D^{GW_u} and D^{SW_v}, respectively, then the maximum input packet curve of f_i^k at the incoming

gateway v based on Equation 4.43 is given by:

$$\Pi_i^{GW_v,in,k}(t) = \Pi_i^{GW_u,in,k}(t + D^{GW_u} + D^{SW_v}) = \Pi_i^k(t + D_i^k + D^{GW_u} + D^{SW_v}) \tag{4.44}$$

Hence, the maximum packet curve of the aggregate flow of TC_i at incoming gateway GW_v is given by:

$$\Pi_i^{GW_v,in}(t) = \sum_{f_i^k \in S_{GW_v,i}} \Pi_i^{GW_v,in,k}(t) \tag{4.45}$$

where $S_{GW_v,i}$ is the set of all flows f_i^k belonging to TC_i and arriving to the incoming gateway GW_v.

From Equation 4.45, we can formulate the t.a.c stochastic arrival curve of TC_i and the corresponding stochastic service curves as in Section 4.3.2. The stochastic delay $D_i^{GW_v,\epsilon_v}$ is computed based on Equations 4.39, 4.40 and 4.41.

For inter-cluster traffic, the stochastic end-to-end delay bound for TC_i is given by:

$$D_i^{e2e,\epsilon_u+\epsilon_v} = D_i^{u,\epsilon_u} + D^{GW_u} + D^{SW_v} + D_i^{v,\epsilon_v} \tag{4.46}$$

4.3.6 Numerical Results

In this section, we will show the impact of the retransmission and acknowledgment mechanisms on the packet curves and consequently on the end-to-end delays, with reference to the deterministic delays obtained in Chapter 3.

4.3.6.1 Deterministic vs Stochastic Packet Curves

We revisit the test case shown in Section 3.3.1 of Chapter 3. We will compare herein the impact of the two reliability methods (No-ACK and ACK) on the packet curves under FIFO and FP policies with the number of frequencies $\eta_f = \{1, 2\}$. Since the $PER_L = 10^{-10}$ and the guaranteed PER using time and frequency diversity mechanisms in Chapter 3 is 10^{-12}, we consider as a probability of violation under the retransmission and acknowledgment mechanism, $\epsilon = (10^{-10} - 10^{-12})/2$. Disabling the acknowledgment mechanism is modeled by using deterministic packet curves, whereas activating the retransmission with acknowledgment mechanisms are modeled based on the stochastic packet curves.

Figures 4.8, 4.9 and 4.10 show the stochastic and deterministic curves of the cumulative number of packets under FIFO and FP scheduling, respectively. We can see clearly that the stochastic curves are lower than the deterministic ones for both cases. Furthermore, when the cumulative number of packets increases, the difference between the stochastic and deterministic curves increases. This fact will certainly impact the delay bounds tightness when using stochastic arrival curves to model the retransmssion and acknowledgment mechanisms with reference to time and frequency diversity mechanism.

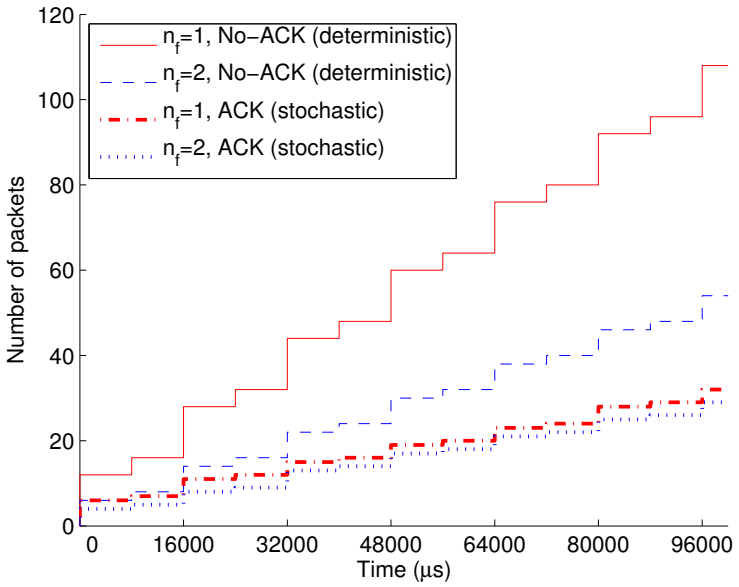

Figure 4.8: Stochastic vs deterministic packet curves under FIFO

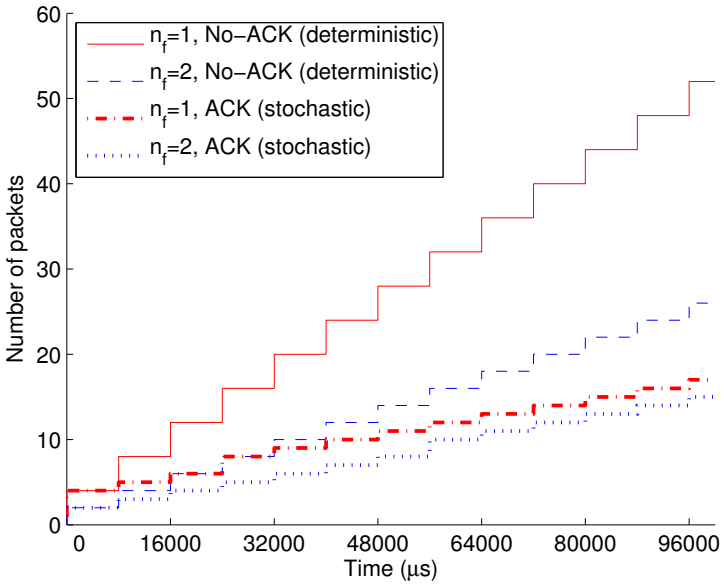

Figure 4.9: Stochastic vs deterministic packet curves for TC_1 under FP

4.3.6.2 Delay Bounds

When the acknowledgment mechanism is activated, then the transmission of a packet of TC_i is computed as:

$$\overline{e_i} = e_i + t_{ACK}$$

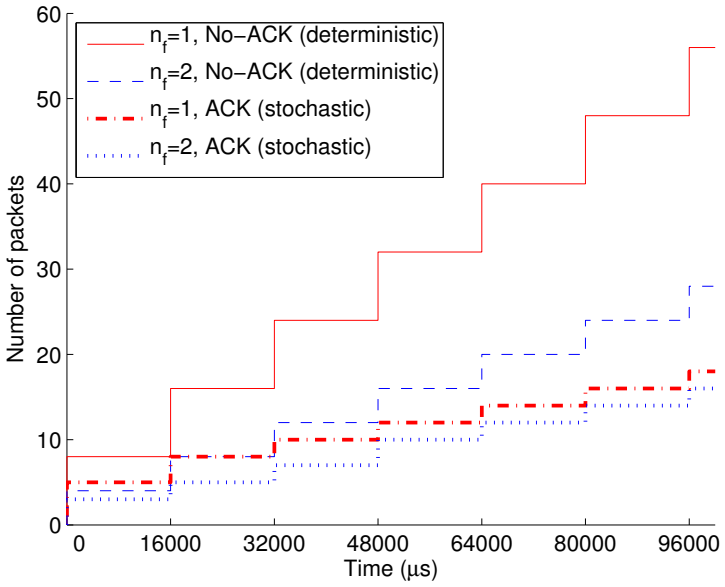

Figure 4.10: Stochastic vs deterministic packet curves for TC_2 under FP

where $t_{ACK} = ACK + 2 * SIFS - MIFS$. MIFS and ACK are the durations of Minimum InterFrame Space and acknowledgement, respectively. SIFS is Short InterFrame Space which is the duration for electronics circuit to switch from transmitting mode to receiving mode. According to ECMA-368 standard, $SIFS = 10$ μs. However, this value can be reduced when using a more precise hardware. Therefore, for the numerical results, we will consider $t_{SIFS} = \{2, 5, 10\}$ μs. We will compute herein the stochastic delay bounds for these different configurations and compare them to the deterministic ones.

Figures 4.11 and 4.12 illustrate the delay bounds with different values of SIFS under FIFO scheduling when considering the deterministic and stochastic arrival curves, and $\eta_f = \{1, 2\}$, respectively. We can clearly see the noticeable enhancements of the delay bounds when using stochastic arrival curves, with reference to the deterministic one when $\eta_f = 1$. Furthermore, under stochastic arrival curve, when SIFS decreases, the delay bounds decrease. However, under $\eta_f = 2$, the delay bound with deterministic curve is better than the delay bounds with stochastic arrival curves for the values of SIFS higher than 2 μs. This fact shows the impact of the SIFS on the system performances.

Figures 4.13 and 4.14 illustrate the delay bounds under FP when considering the same scenarios as FIFO with $\eta_f = \{1, 2\}$, respectively. The same conclusion concerning the delay bounds tightness when using stochastic arrival curves hold under FP. Furthermore, the system schedulability is enhanced for TC_2 when considering $\eta_f = 2$ and $t_{SIFS} = 2$ μs, with reference to $\eta_f = 1$, where the network utilization guaranteeing the system schedulability increases to 0.25, instead of 0.15. The results show the importance of the selected reliability mechanisms,

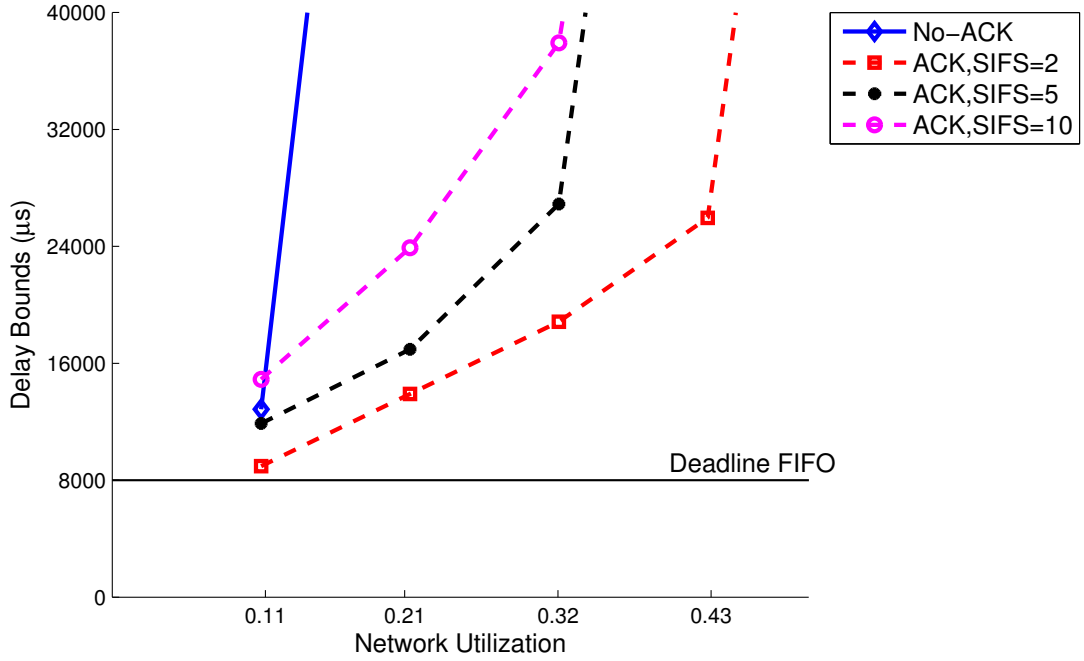

Figure 4.11: Stochastic vs deterministic delays with $\eta_f = 1$ under FIFO scheduling

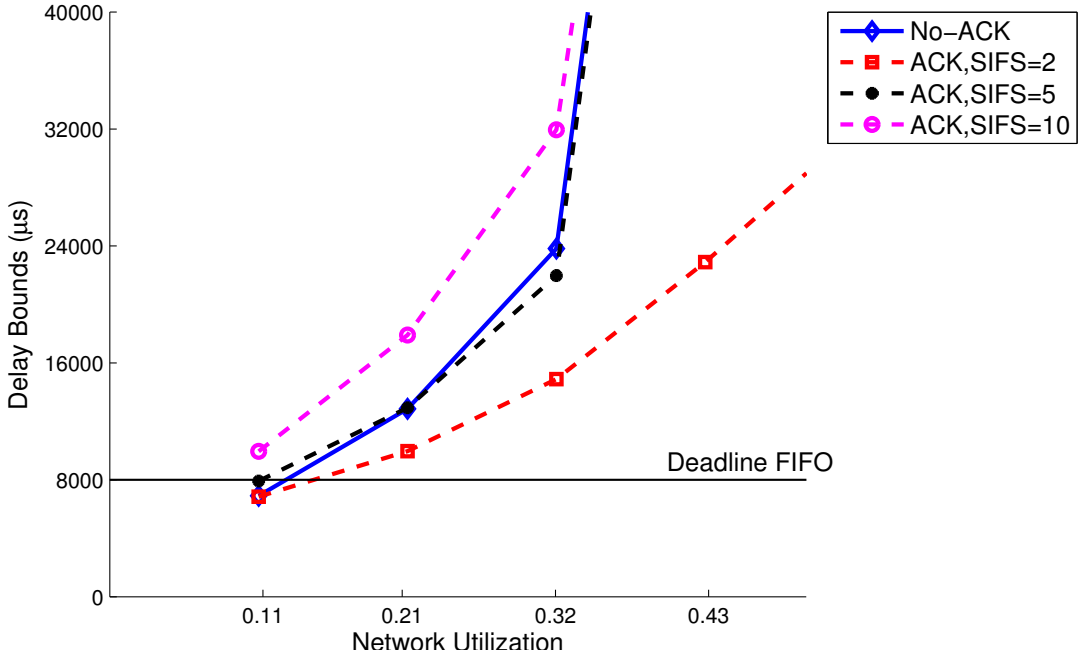

Figure 4.12: Stochastic vs deterministic delays with $\eta_f = 2$ under FIFO scheduling

i.e. time and frequency diversity or retransmssions with acknowledgment mechanism for our proposal and their impact on the system schedulability, and consequently scalability.

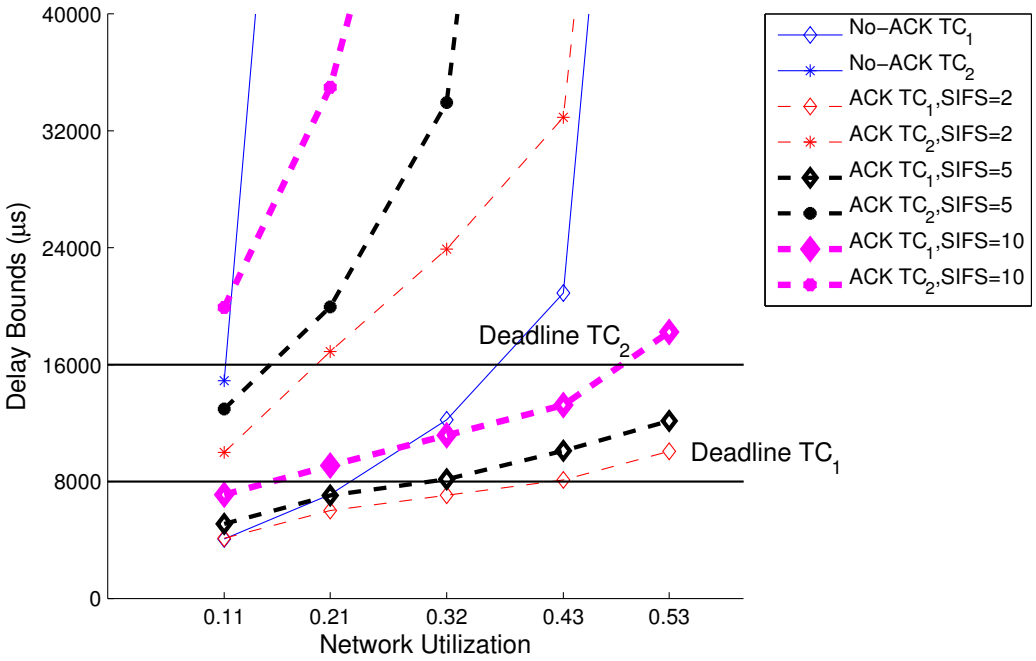

Figure 4.13: Stochastic vs deterministic delays with $\eta_f = 1$ under FP scheduling

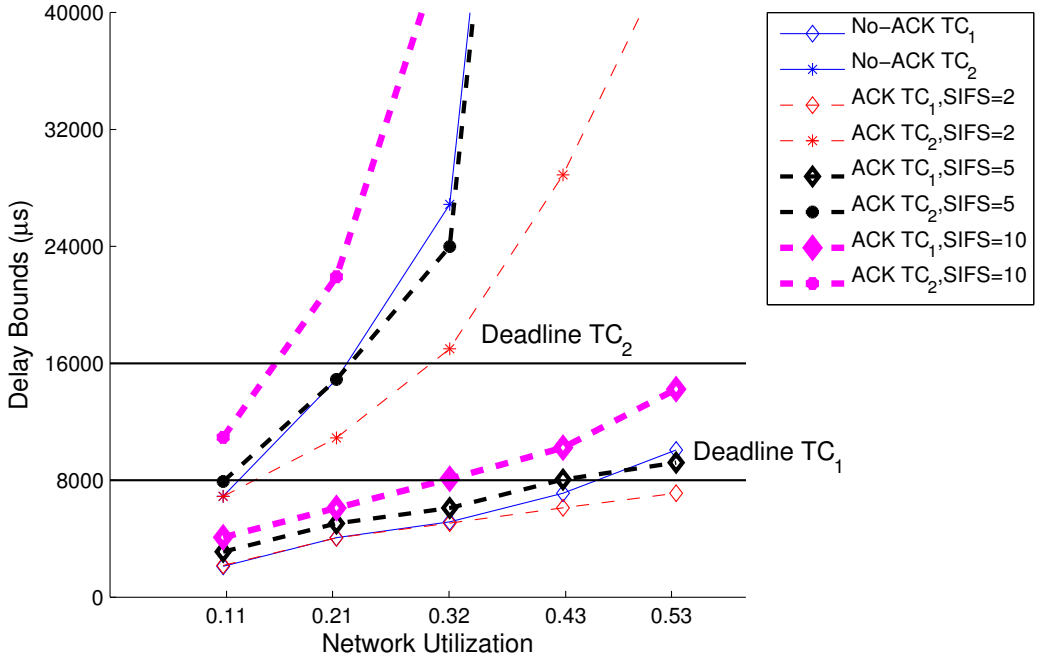

Figure 4.14: Stochastic delays vs deterministic delays with $\eta_f = 2$ under FP scheduling

4.4 Conclusion

In this chapter, the enhancements of the performance offered by the wireless safety-critical network has been conducted by tuning the different parameters of the system. First, refined system models, based on Network Calculus and ILP approach were detailed under the different scheduling policies. The impact of these models has been very beneficial to reduce the delay bounds and enhance the system schedulability and scalability. Then, the TDMA cycle duration was optimized to reduce the delay bounds while guaranteeing the system schedulability and reliability. The results show the importance of this parameter to enhance the system performances. Finally, we considered the retransmission and acknowledgment mechanism combined with the frequency diversity to enhance the delay bounds tightness. The Stochastic Network Calculus was used to model the system and the obtained results have shown significant enhancements of delay bounds, with reference to the results obtained in Chapter 3 when disabling the acknowledgment and activating time diversity.

In the next chapter, we will apply these introduced approaches to a realistic avionics case study to validate our proposal ability to enhance the system scalability and reliability, while guaranteeing the system constraints.

Chapter 5

Validation on Avionics Case study

In this chapter, the validation of our proposed WSCAN performance is conducted through a realistic avionics case study. First, the avionics case study and the considered network configurations are described. Then, the timing and reliability analysis of each network configuration is performed to show the impact of each system parameter, i.e. the scheduling policy, the TDMA cycle duration and the reliability mechanism. The obtained results are discussed to verify our first conclusions on small-scale case study within the previous chapters, and to highlight the ability of our proposal to guarantee the system performance.

5.1 Case study description

Our considered case study is a representative avionics network on-board the A380. This network consists of 44 end-systems and supports almost 200 multicast traffic flows. The architecture of our proposed WSCAN is described in Figure 5.1. This architecture consists of two clusters 1 and 2, which correspond to the main and upper avionics bays of the aircraft, described in Chapter 1. The first cluster contains 23 end-systems, whereas the second one contains 21. The end-systems within each cluster are connected through wireless links, which are based on the UWB technology at 200Mbps and guarantee one-hop intra-cluster communications. Then, the inter-cluster communications are supported due to the gateways 1 and 2 associated to clusters 1 and 2, respectively. These gateways are interconnected via a 1 Gbps Switched Ethernet.

There are three supported traffic classes, described in Table 5.1. The traffic class TC_1 represents the highest priority messages with the shortest deadline, equal to 4 ms, whereas the traffic classes TC_2 and TC_3 represent the medium and lowest priority messages, respectively. The end-systems and the clusters traffic configurations are described in Tables 5.2 and 5.3, respectively. As we can notice, there are three types of nodes, i.e. N_1, N_2 and N_3, depending on the generated traffic classes. Furthermore, only long-deadline traffic classes, i.e. TC_2 and TC_3, are transmitted from one cluster to another. To conduct the timing analysis of our proposal, we

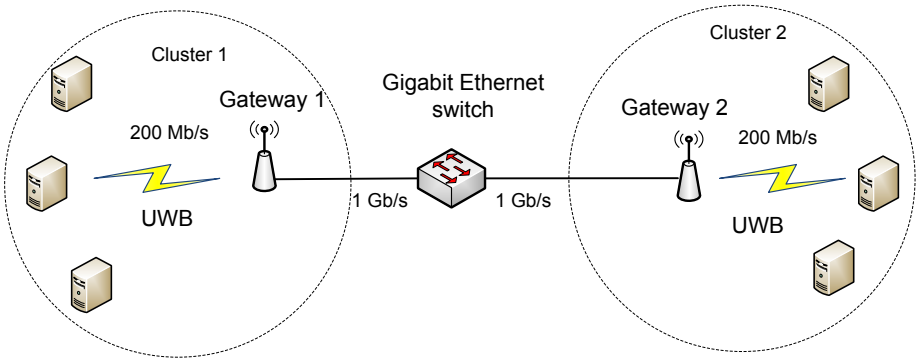

Figure 5.1: WSCAN topology

Table 5.1: Parameters of Traffic Classes

	T (μs)	Dl (μs)	Payload (Byte)
TC_1	4000	4000	412
TC_2	16000	16000	662
TC_3	32000	32000	912

Table 5.2: End-systems Traffic Configuration

Cluster 1				
Node type	Num of nodes	TC_1	TC_2	TC_3
N_1	5	1	0	1
N_2	6	1	1	0
N_3	12	0	2	3
Incoming gateway GW_1	1	0	6	8
Cluster 2				
Node type	Num of nodes	TC_1	TC_2	TC_3
N_1	5	1	0	1
N_2	6	1	1	0
N_3	10	0	2	3
Incoming gateway GW_2	1	0	8	10

consider four configurations to show the impact of each system parameter on its performance. These configurations are described in Table 5.4. The first configuration is used to show the impact of the scheduling policy and the system modeling, denoted by extended and refined in Chapter 4, on the system predictability and reliability. While the three other configurations are considered to highlight the impact of the TDMA cycle durations and the selected reliability mechanism on the system schedulability and scalability. The PER of the UWB technology is

Table 5.3: Clusters Traffic Configuration

Traffic Class	Intra-cluster			Inter-cluster	
	TC_1	TC_2	TC_3	TC_2	TC_3
Number of flows in Cluster 1	11	30	41	6	8
Number of flows in Cluster 2	11	26	35	8	10

Table 5.4: Network configurations

Configuration 1	• Scheduling policies within End-systems: FIFO or FP • TDMA cycle durations of clusters 1 and 2, equal to the shortest deadline, e.g. 4ms • Slots allocation is based on the TPSS scheme • Reliability mechanisms: time and frequency diversity while disabling the acknowledgment mechanism (No-ACK)
Configuration 2	• Scheduling policies within End-systems: FIFO or FP • Optimal TDMA cycle durations of clusters 1 and 2 obtained with the algorithm described in Section 4.2.2 of Chapter 4 • Slots allocation is based on the TPSS scheme • Reliability mechanisms: time and frequency diversity while disabling the acknowledgment mechanism (No-ACK)
Configuration 3	• Scheduling policies within End-systems: FIFO or FP • TDMA cycle durations of clusters 1 and 2, equal to the shortest deadline, e.g. 4ms • Slots allocation is based on the TPSS scheme • Reliability mechanisms: retransmission and acknowledgment mechanism (ACK), combined with the frequency diversity
Configuration 4	• Scheduling policies within End-systems: FIFO or FP • Optimal TDMA cycle durations of clusters 1 and 2 obtained with the algorithm described in Section 4.2.2 of Chapter 4 • Slots allocation is based on the TPSS scheme • Reliability mechanisms: retransmission and acknowledgment mechanism (ACK), combined with the frequency diversity

fixed and equal to $PER_{UWB} = 10^{-3}$ and the required PER level of our avionics applications is equal to $PER_L = 10^{-10}$.

5.2 Impact of the Scheduling Policy

In this section, we will show the impact of the scheduling policy on the system performance. Therefore, we compute the delay bounds for the configuration 1 of Table 5.4 under FIFO and FP scheduling policies, based on the Network Calculus models introduced in Chapter 3, denoted as extended, which integrate the non-preemptive message transmission impact. Furthermore, the number of frequencies to guarantee the system reliability is varied, η_f in $\{1, 2, 3, 4\}$, and the corresponding number of transmissions is η_t in $\{4, 2, 2, 1\}$, respectively. The obtained results in this case are described in Figure 5.2.

— For $\eta_f = 1$, the delay bounds of the three traffic classes are infinite for both scheduling policies FIFO and FP. In this case, the number of required transmissions is $\eta_t = 4$, which induces a high input traffic rate, greater than the offered network rate 200 Mbps. This fact consequently leads to infinite delay bounds and unschedulable system configuration. Hence, using only one frequency to guarantee the system schedulability and reliability is not a feasible solution for our considered case study.

— For $\eta_f = (2, 3)$, the obtained delay bounds are the same because the required transmissions is $\eta_t = 2$ for both cases. Hence, to limit the system complexity, it is better to use only two frequencies, instead of three, to guarantee the same system reliability level. However, as we can see in Figure 5.2, the delays bounds of the three traffic classes under FIFO and FP do not respect their corresponding deadlines. For instance, the delays for the traffic class TC_3 is greater than 32 ms for both cases. Hence, although implementing the proposed WSCAN with only two frequencies guarantee the system reliability, this configuration does not respect the system schedulability.

— For $\eta_f = 4$, there is a significant enhancement on the delay bounds for both scheduling policies. Indeed, in this case only one transmission $\eta_t = 1$ is enough to guarantee the system reliability, which is equivalent to a system behavior under an error-free environment. However, the FIFO policy does not guarantee the system schedulability where the delay bound for the traffic class TC_2 is greater than its deadline (16 ms). On the other hand, the FP policy leads to a schedulable configuration where the obtained delay bounds for the different traffic classes respect their deadlines. Hence, implementing our proposed WSCAN with four frequencies and FP policy within the end-systems seems the only feasible solution, which respects the timing and reliability constraints. However, this solution will clearly induce a high system complexity and integration costs.

The obtained results under the configuration 1 of our proposed WSCAN highlight the impact of the scheduling policy on the system performance and validate our first conclusions concerning

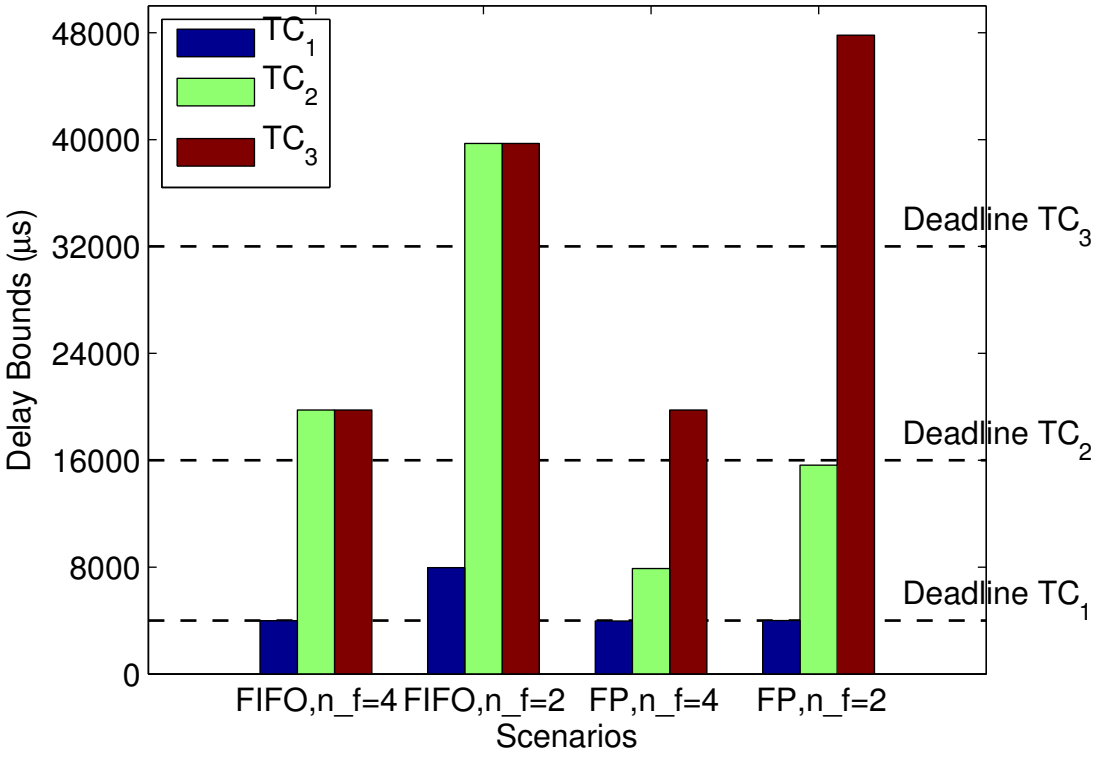

Figure 5.2: Delay bounds for configuration 1 based on the extended NC Models

the better ability of the FP policy to guarantee the system requirements, with reference to FIFO. It is worth noting in this case the trade off between guaranteeing the system performance in terms of predictability and reliability, and limiting the system complexity and integration costs.

5.3 Impact of the System Model

Our objective in this section is to show the impact of the considered system model on our proposal performance, and particularly the system schedulability and reliability. A comparative analysis of the delay bounds, obtained with the extended model of Chapter 3 and the refined model of Chapter 4 is conducted herein.

To achieve this aim, we consider the configuration 1 of Table 5.4 to compute the delay bounds under FIFO and FP scheduling policies when varying the number of frequencies, η_f in $\{1, 2, 3, 4\}$, based on the two system models. The obtained results are illustrated in Figures 5.3 and 5.4, respectively.

— Under FIFO, when $\eta_f = 1$, we still have infinite delay bounds and non-schedulable system configuration with the refined system model. For $\eta_f = 2$, we can notice a significant enhancement of the delay bounds of traffic classes TC_2 and TC_3 under the refined model,

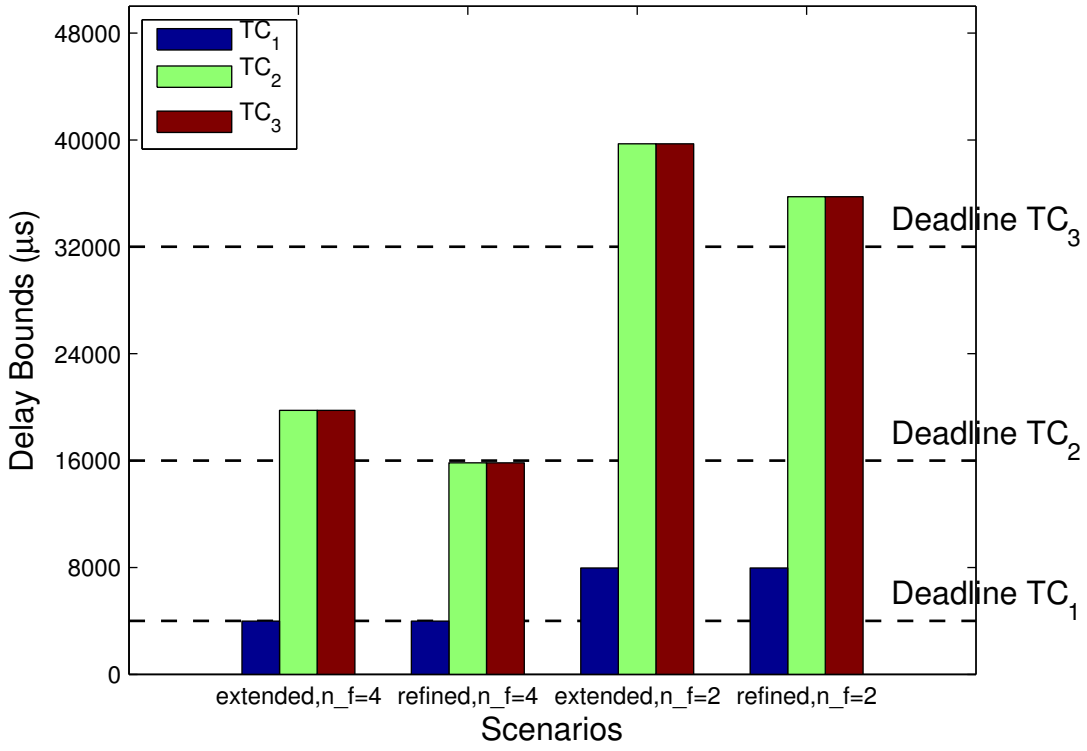

Figure 5.3: Delay bounds with extended vs refined models under FIFO

with reference to the extended one. However, the schedulability of the system still is not guaranteed for both cases. Finally, unlike the extended model, the refined one leads to a schedulable system configuration with $\eta_f = 4$, where the delay bound of the traffic class TC_2 becomes lower than its respective deadline 16 ms. Hence, implementing our proposed WSCAN with four frequencies and FIFO policy within the end-systems becomes a feasible solution, guaranteeing the timing and reliability constraints.

— Under FP, we observe the same delay bounds improvement than FIFO, when using the refined model instead of the extended one. However, for both cases, we still have the same system configuration, which guarantees the system predictability and reliability, e.g. $\eta_f = 4$.

These results confirm our first conclusions in Chapter 4 and highlight the importance of the system model to improve the performance analysis of our proposal. Furthermore, we can conclude that the refined models outperform the extended ones in terms of delay bounds tightness, and consequently the system schedulability and scalability.

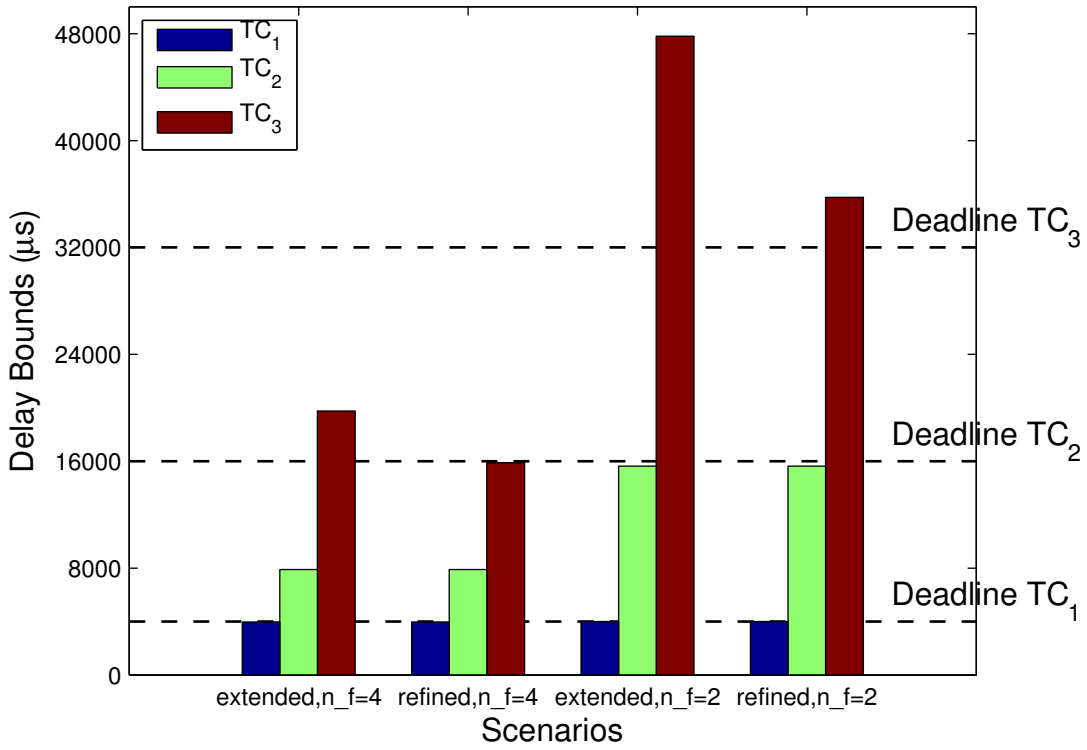

Figure 5.4: Delay bounds with extended vs refined models under FP

5.4 Impact of the Reliability Mechanism

We will show in this section the impact of the selected reliability mechanism on the system performance in terms of schedulability and scalability. We have already compared the two considered reliability mechanisms for our WSCAN, e.g. time and frequency diversity or retransmission with acknowledgment mechanism combined with frequency diversity, in Chapter 4 for a small-scale test case. The latter has shown better ability to guarantee tighter delay bounds compared to the former, and consequently improve the system schedulability and scalability. Therefore, we will verify herein these first conclusions for our avionics case study.

To achieve this aim, we compute the delay bounds for configurations 1 and 3 in Table 5.4, under FIFO and FP policies when considering the following assumptions:

— The number of frequencies is $\eta_f = 2$. In fact, the behavior of the system when $\eta_f = 4$ is equivalent to its behavior under error-free environment for which only one transmission on each frequency is sufficient to guarantee the system reliability and predictability. Therefore, there is no need for retransmission and acknowledgment mechanisms in this particular case.

— The duration SIFS is varied when considering configuration 3, where SIFS in $\{2, 5, 10\}$ μs, to show the impact of the technological overhead on the system performance.

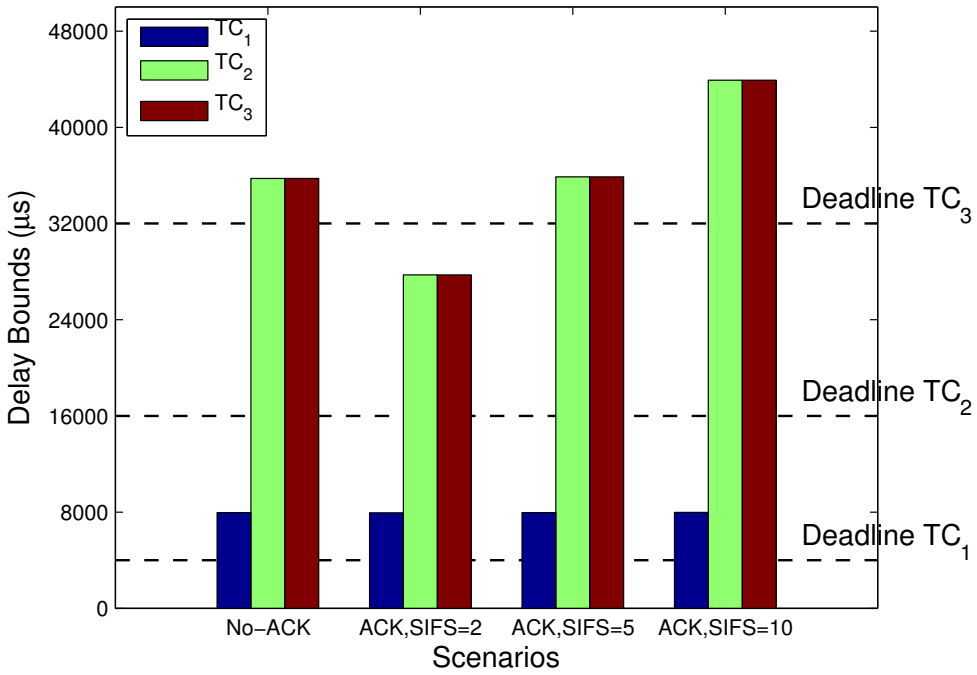

Figure 5.5: Delay bounds with No-ACK and ACK under FIFO with $\eta_f = 2$

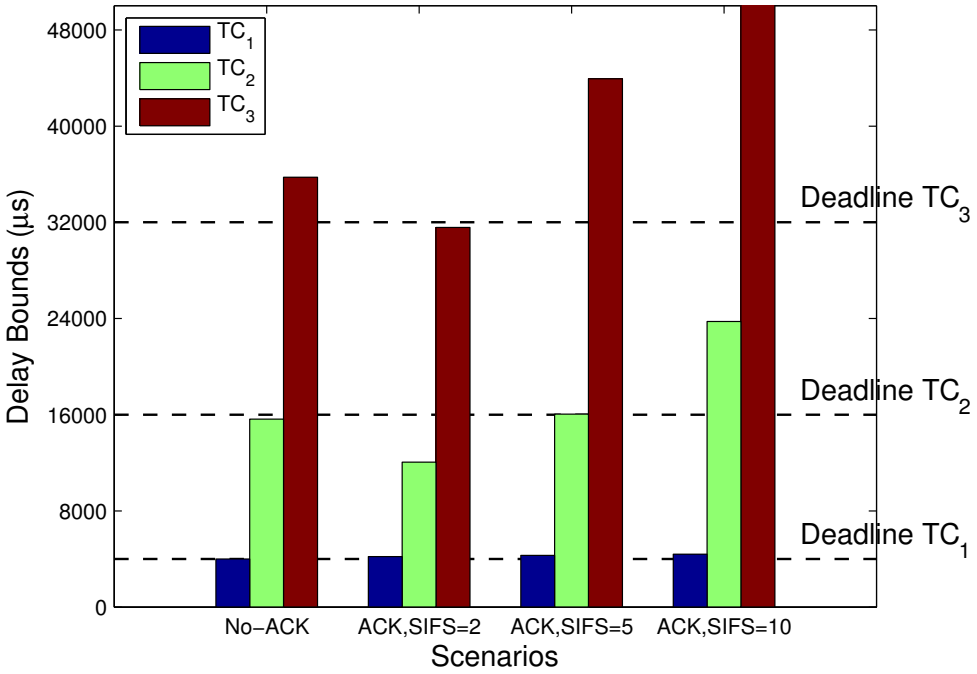

Figure 5.6: Delay bounds with No-ACK and ACK under FP with $\eta_f = 2$

The obtained results for these different system configurations under FIFO and FP policies are illustrated in Figures 5.5 and 5.6, respectively.

— Under FIFO, first we notice the impact of the SIFS duration on the delay bounds obtained with the configuration 3. In fact, when SIFS decreases, the delay bounds decrease for the different traffic classes. This is mainly due to the technological overhead impact on the acknowledgment process duration, and consequently the delay bounds. Furthermore, there is a significant enhancement in terms of delay bounds tightness under configuration 3 with SIFS duration = 2 μs, with reference to configuration 1. However, a non-accurate SIFS duration under configuration 3 may lead to worse performance than the configuration 1. For instance, for configuration 3 with SIFS =10 μs, the delay bounds of traffic classes TC_2 and TC_3 are greater than the ones obtained under configuration 1. Although, the use of retransmission with acknowledgment mechanism enhances the tightness of the delay bounds and consequently the system scalability, using only two frequencies with FIFO policy still leads to a non-feasible implementation, since the system schedulability is not guaranteed.

— Under FP, with configuration 3, we observe the same impact of the SIFS duration on the delay bounds, with reference to FIFO policy. Moreover, the delay bounds tightness is improved under configuration 3 with SIFS = 2 μs, which almost satisfies the timeliness constraints, i.e. $TC1$ does not respect its deadline. These results suggest that with the optimal TDMA configuration, the network may be schedulable with the reliability mechanism based on retransmission and ACK when using number of frequencies $\eta_f = 2$.

5.5 Impact of the TDMA Cycle Duration

The aim of this section is to highlight the impact of the TDMA cycle duration on the system performance in terms of schedulability, reliability and scalability. Therefore, we compare the delay bounds obtained with the two pairs of configurations (1, 2) and (3,4) of Table 5.4, under FIFO and FP policies when varying the number of frequencies.

First, we consider the configurations 1 and 2 with the reliability mechanism based on diversities and no-ACK and the number of frequencies $\eta_f = \{2, 4\}$. These results are illustrated in Figures 5.7 and 5.8, respectively.

To compute the optimal TDMA cycle durations of clusters 1 and 2, we apply the optimization algorithm described in Section 4.2.2 of Chapter 4 with a sampling step $q_c = 100$ μs for each scheduling policy and frequency number. The obtained cycle values under FIFO are the same for both cases $\eta_f = 2$ and $\eta_f = 4$, where $\{c_1, c_2\} = \{3900, 3700\}$ μs. However, under FP, we obtain

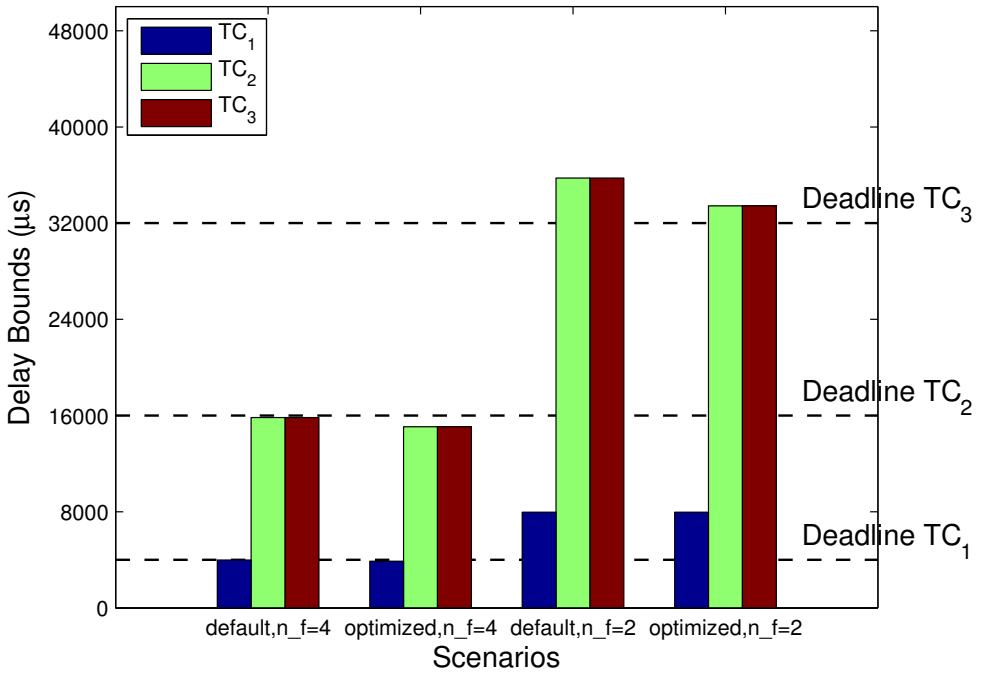

Figure 5.7: Delay bounds with default vs optimized TDMA cycles under FIFO

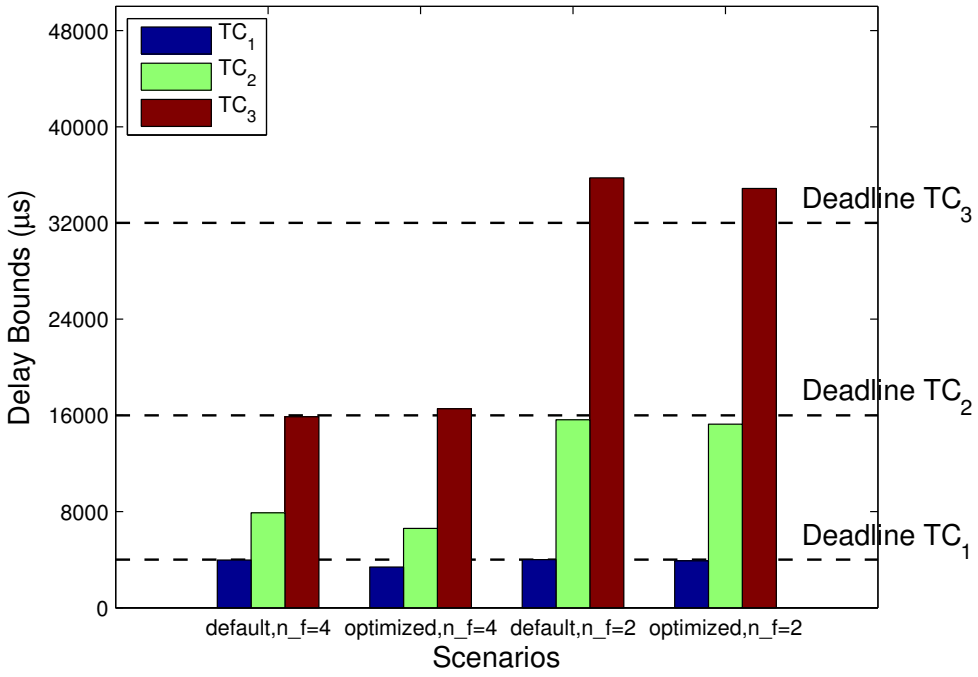

Figure 5.8: Delay bounds with default vs optimized TDMA cycles under FP

different cycle durations depending on the frequency number, where $\{c_1, c_2\} = \{3400, 3200\}$ μs and $\{c_1, c_2\} = \{4000, 3800\}$ μs with $\eta_f = 4$ and $\eta_f = 2$, respectively.

As we can see from the figures, there is a significant enhancement of the delay bounds for FIFO when considering the system configuration 2 with optimal cycle durations, compared to the system configuration 1 with default cycle durations. For the FP scheduling, the delay bound tightness is still enhanced but less obvious than FIFO scheduling. Under FP scheduling, with $\eta_f = 4$, the delay bounds of TC_1 and TC_2 are reduced while the delay bound of TC_3 is slightly increased. This is due to assigning bigger weight parameters for higher priority traffic classes. With $\eta_f = 2$, the tightness of delay bounds is enhanced slightly since the default configuration is close to the optimal configuration.

Second, we evaluate the configurations 3 and 4 with the reliability mechanism based on retransmission and ACK combined with frequency diversity with $\eta_f = 2$. We only consider SIFS $= \{2, 5\}$ μs since SIFS $= 10$ μs increases significantly the delay bounds as shown in Section 5.4. These results for FIFO and FP scheduling polices are illustrated in Figures 5.9, and 5.10, respectively.

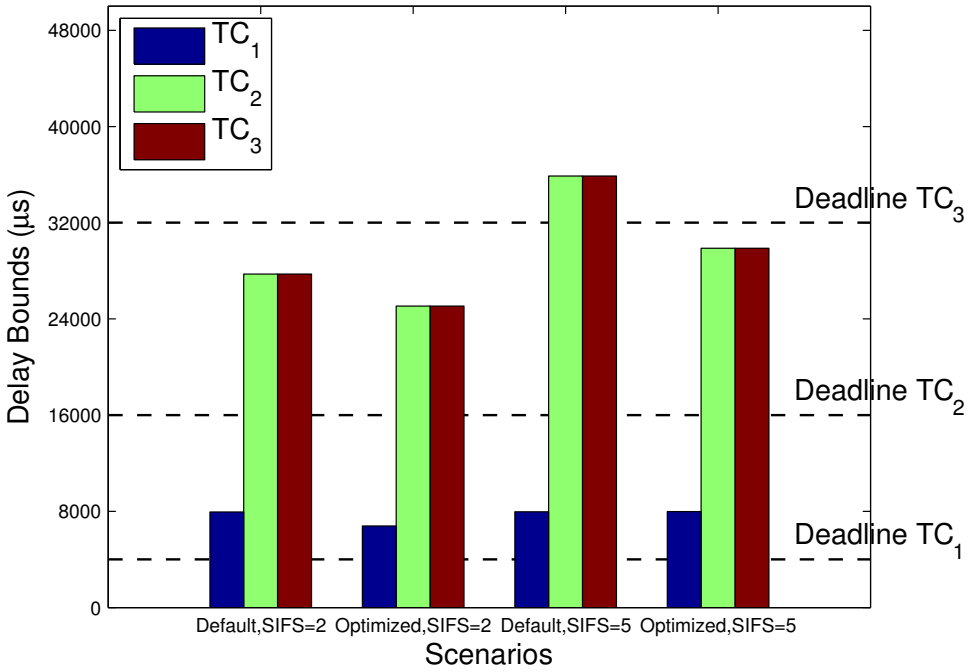

Figure 5.9: Stochastic delay bounds with default and optimized TDMA cycles under FIFO with $\eta_f = 2$

To compute the optimal TDMA cycle durations of clusters 1 and 2, we also apply the optimization algorithm described in Section 4.2.2 of Chapter 4 with a sampling step $q_c = 100\mu$s

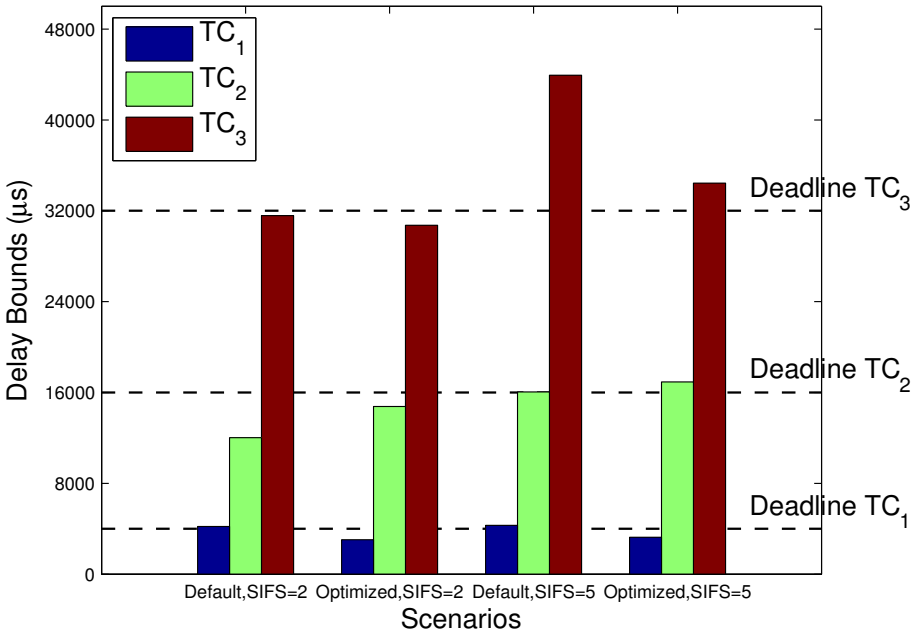

Figure 5.10: Stochastic delay bounds with default and optimized TDMA cycles under FP with $\eta_f = 2$

for each scheduling policy and frequency number. The optimal cycle values under FIFO are $\{c_1, c_2\} = (1700, 1600)$ μs and $\{c_1, c_2\} = (2000, 1800)$ μs for SIFS $= \{2, 5\}$ μs, respectively. For FP, the optimal ones are $\{c_1, c_2\} = (1500, 1400)$ μs and $\{c_1, c_2\} = (1600, 1500)$ μs for SIFS $= \{2, 5\}$ μs, respectively.

We can see clearly that there is a significant enhancement of delay bounds for both FIFO and FP when considering the configuration 4 with optimal cycle durations, with reference to the configuration 3. Moreover, the system configuration 4 under FP with SIFS $= 2$ μs leads in this case to a feasible WSCAN implementation guaranteeing the system schedulability and reliability while enhancing the system scalability, with reference to configuration 2 and 3.

Hence, due to the optimal TDMA cycle durations and the reliability mechanism based on retransmission and acknowledgment, implementing our proposed WSCAN with only two frequencies and FP policy within the end-systems becomes a feasible solution, which guarantees the system constraints. This result shows the importance of the TDMA cycle duration choice and the beneficial impact of the optimized configuration, especially on the system scalability. This result also confirms our first conclusions in Chapter 4 where this selected reliability mechanism outperforms the time and diversity frequency mechanisms, in terms of system schedulability and scalability. Moreover, the system complexity is reduced when considering the configuration 4, where two frequencies become enough to guarantee the system reliability, instead of four

frequencies with the configuration 2.

5.6 Conclusion

In this chapter, the validation of our proposed WSCAN has been conducted through a realistic avionics case study. The obtained results with the different system configurations have confirmed our first conclusions in Chapter 3 and 4 concerning the ability of our proposal to guarantee the system constraints, in terms of predictability and reliability.

To highlight the impact of each system parameter on the guaranteed performance, first, we have shown the consequences of the scheduling policy on the system schedulability, and validate the ability of FP policy to outperform the FIFO policy in terms of delay bounds tightness. Then, we have validated the importance of the system model choice to improve the system performance, and particularly the use of the refined system model defined in Chapter 4, with reference to the extended model in Chapter 3. Afterwards, the beneficial impact of the optimization process of the TDMA cycle duration on the system scalability has been confirmed, with reference to the default TDMA cycle duration. Finally, the choice of the reliability mechanism, and particularly the retransmission with the acknowledgment mechanism combined with the frequency diversity, has shown a significant enhancement of the system performance in terms of predictability, scalability and complexity, with reference to using the time and frequency diversity mechanism.

Hence, for our case study, the proposed WSCAN when considering the retransmission with the acknowledgment mechanism with only two frequencies and FP policy within end-systems has been validated as a feasible solution, which guarantees the system requirements while enhancing the system scalability and complexity.

Conclusions and Perspectives

1 Conclusions

Althoug the current avionic communication architecture fulfills the main avionics requirements, it leads at the same time to a significant quantity of wires and connectors, which increases the system weight and costs. To handle these emerging requirements, we proposed in our thesis the integration of wireless technology in the avionics context, and particularly a Wireless Safety-Critical Avionics Network (WSCAN) based on the ECMA-368 technology (High-Rate Ultra Wideband) to replace the backup network of the AFDX backbone. Although the many interesting benefits of using wireless technology in terms of reducing weight and costs, increasing flexibility and efficiency and simplifying maintenance process, there still are many challenging issues to be handled to adapt this technology to avionics, mainly due to its sensitivity to interference and jamming attacks.

First, we designed a new WSCAN with various features to guarantee avionics requirements.

— A hybrid wired/wireless architecture is proposed for WSCAN based on HR-UWB and switched Ethernet technologies where the end-systems in the same avionics bay can communicate in single hop communication. Each avionics bay defines a cluster, which is protected from interference and jamming attack by using electromagnetic shielding [52] solutions. Then, the inter-cluster communication is handled by specific gateways and all gateways are interconnected through a Gigabit Ethernet switch.

— To meet the timeliness requirements, many modifications of ECMA-368 standard have been integrated, including a more precise synchronization mechanism and off-line slots allocation with the contention-free TDMA-based MAC protocol.

— Furthermore, to guarantee the reliability requirement, two mechanisms have been proposed, i.e time, frequency diversity and retransmissions combined with enhanced acknowledgment mechanism for multicast communication.

Second, to analyze the performance of our proposed WSCAN, we proceed as follows:

— We proposed a system modeling based on Network Calculus, integrating the TDMA behavior with different scheduling policies, e.g. FIFO, FP and WRR. Therefore, we first extended the classical models by integrating the impact of non-preemptive communication for FIFO and FP policies. Furthermore, we proposed a new model for non-preemptive WRR with TDMA-based protocol. These proposed models have been defined for error-free environment, and then extended to the error-prone environment by integrating the impact of the reliability mechanism.

— Preliminary performance analysis has been conducted through a small scale test case. The obtained results have shown the significant impact of the non-preemptive transmission on delay bounds under different scheduling policies, which leads to a lower network utilization with reference to the classic models. Furthermore, the impact of diversity techniques has been investigated and the results have shown the efficiency of the FP policy combined with the time and frequency diversity to guarantee system predictability and reliability, with reference to FIFO and WRR.

Third, to enhance the delay bounds tightness, and consequently the system schedulability, various enhancement processes have been integrated, depending on many system parameters.

— We have refined the system models, based on Network Calculus and ILP approach, under different service policies. The impact of these models has been discussed and we have shown their ability to improve the system schedulability and scalability.

— An optimization process of the TDMA cycle duration has been introduced to minimize the delay bounds while guaranteeing the system constraints. The results have shown the importance of this parameter to enhance the system performance.

— The retransmission and acknowledgment mechanism, combined with frequency diversity have been introduced as an alternative reliability mechanism instead of time and diversity mechanism. Based on a stochastic modeling, we have conducted the performance analysis of this alternative, and the obtained results show its efficiency to improve the delay tightness.

Finally, to validate our proposed WSCAN, we consider a realistic avionics case study. The performance guarantees of this proposed network were analyzed to verify the system constraints and highlight the impact of each system parameter.

— First, we have shown the importance of selecting the accurate scheduling policy within end-systems. In this case, the FP policy has shown a better ability to improve the schedulability with reference to FIFO. In fact, in this case, the network is schedulable only with FP scheduling policy and $\eta_f = 4$.

— Second, we have confirmed the impact of the system model on the guaranteed performances through a comparative analysis of delay bounds, obtained using the extended and the refined models. The results have shown that the refined models enhance the delay bounds tightness, and consequently the system schedulability. Indeed, the network becomes schedulable under both FIFO and FP scheduling policies and $\eta_f = 4$ when using refined models.

— Third, the benefits of the optimized cycle duration on the system scalability have been confirmed, compared to a default choice of cycle duration. The optimal TDMA cycle for each cluster, reduced the delay bounds of each traffic class, with reference to the default TDMA cycle.

— Finally, the ability of the reliability mechanism based on retransmission and acknowledgment mechanism to improve the delay bounds tightness, and consequently the system schedulability and scalability has been validated. In this case using only two frequencies and FP policy within end-systems has been considered as a feasible solution, which guarantees the system constraints while enhancing the system scalability and complexity, with reference to using time and frequency diversity.

2 Perspectives

— **WSCAN Implementation and Testing:** the hardware implementation of our proposed WSCAN is necessary to confirm its timeliness and reliability guarantees. Many introduced features for our proposal have to be validated in practice, such as:

  — reprograming the MAC protocol to integrate: the enhanced synchronization mechanism to support multicast communication, the classic modification of the superframe to reduce the protocol overhead and finally the TDMA off-line configuration;

  — testing the proposed reliability mechanisms to validate the possibility of implementing two or more antennas to perform the frequency diversity. Moreover, the enhanced reliability with ACK and retransmission needs to be tested to verify its feasibility;

  — the isolation of each cluster has to be validated to prove the absence of interference with other devices and the security of network;

  — the channel error model needs to be investigated and characterized to validate the considered assumptions. A more realistic model than the assumed one could be considered.

— **Wireless technologies for sensor/actuator networks:** The sensor/actuator networks are a part of safety-critical avionics system. These networks based on ARINC 429

and CAN buses induce a significant quantity of cables to interconnect the sensors and actuators. We can use wireless technologies to replace these networks to reduce the cable-related weight and costs or used as backup networks to increase the reliability. However, CAN [8] and ARINC 429 [7] are low rate data buses, and the distance between two nodes in sensor/actuator networks can be very long (up to 100 m). Hence, for this kind of networks, we need to find the most suitable technology and design an adequate wireless sensor/actuator network to avoid interference and security problems, while guaranteeing the system predictability and reliability. It is worth noting that the isolation of the network for this kind of applications will be more difficult than for the backup network of the AFDX backbone because of their long range.

Appendix A

Network Calculus Overview

Consider the set of real-valued, non-negative, and wide-sense increasing functions:

$$\mathcal{F} = \{f : \mathbb{R}^+ \to \mathbb{R}^+, \forall t > s : f(t) \geq f(s), f(0) = 0\}$$

Let $f, g \in \mathcal{F}$, three operators are defined as follows:

— min-plus convolution:

$$f \otimes g(t) = \inf_{0 \leq s \leq t} \{f(s) + g(t-s)\} \tag{A.1}$$

— min-plus deconvolution:

$$f \oslash g(t) = \sup_{\forall u \geq 0} \{f(t+u) - g(u)\} \tag{A.2}$$

— positive and non-decreasing upper closure:

$$f_\uparrow = \max(\sup_{0 \leq s \leq t} f(s), 0) \tag{A.3}$$

A flow is defined in terms of an arrival process $R(t)$ and a departure process $R^*(t)$, accumulating the number of input and output bits in some queuing system. There are two performance metrics that need to be evaluated: the flow's *backlog* and *virtual delay*.

Definition 1. *The flow's backlog process at time t is defined as*

$$b(t) = R(t) - R^*(t) \tag{A.4}$$

Definition 2. *The flow's virtual delay at time t is defined as*

$$d(t) = \inf\{\tau \geq 0 : R(t) \leq R^*(t+\tau)\} \tag{A.5}$$

Network Calculus provides the method to compute the delay and backlog bounds based on the definition of *arrival curve* and *service curve* illustrated in Figure A.1.

Definition 3. *(Arrival Curve) A function α is an arrival curve for a data flow with an input cumulative function R, such that $R(t)$ is the number of bits received until time t, iff:*

$$\forall t, s \geq 0, s \leq t, R(t) - R(s) \leq \alpha(t - s) \tag{A.6}$$

Definition 4. *(Simple service curve) The function β is the simple service curve for a data flow with an input cumulative function R and output cumulative function R^* iff:*

$$\forall t \geq 0, R^*(t) \geq R \otimes \beta(t) \tag{A.7}$$

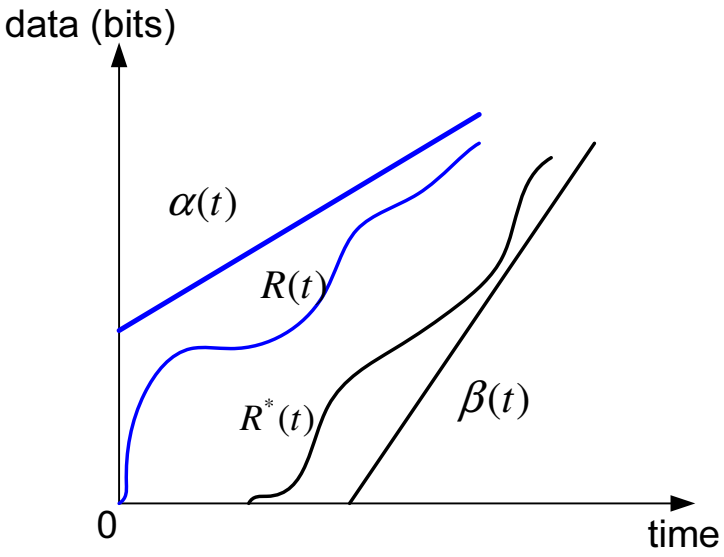

Figure A.1: Arrival Curve and Service Curve

There is a special subclass of simple service curve, called *strict service curve*. Consider a backlogged period (s, t) such that $R(\tau) - R^*(\tau) > 0, \forall \tau \in (s, t)$. The definition of strict service curve is given as follows.

Definition 5. *(Strict service curve) The function β is the strict service curve for a data flow with an input cumulative function R and output cumulative function R^*, if for any backlogged period (s, t), $R^*(t) - R^*(s) \geq \beta(t - s)$.*

Based on the arrival and service curves α and β, the delay and backlog bounds can be computed through the following theorems, and are illustrated in Figure A.2.

Theorem 5. *(Delay bound) Assume a traffic flow $R(t)$, constrained by the arrival curve $\alpha(t)$, traverses a system that provides the service curve $\beta(t)$. At any time t, virtual delay $d(t)$ satisfies,*

$$d(t) \leq \sup_{\forall t \geq 0} \{\inf\{\tau \geq 0 : \alpha(t) \leq \beta(t + \tau)\}\} = h(\alpha, \beta) \tag{A.8}$$

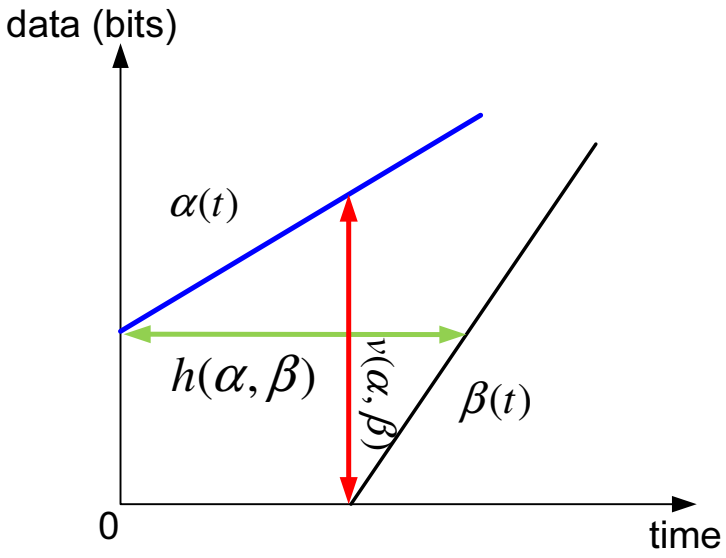

Figure A.2: Backlog and Virtual Delay

The delay bound defines the maximum delay that would be experienced by a bit arriving at time t. Graphically, the delay bound is the maximum horizontal deviation between $\alpha(t)$ and $\beta(t)$ as shown in Figure A.2.

Theorem 6. *(Backlog bound) Assume that a traffic flow $R(t)$, constrained by arrival curve $\alpha(t)$, traverses a system that provides service curve $\beta(t)$. The backlog $b(t)$ for all t satisfies,*

$$b(t) \leq \sup_{t \geq 0}\{\alpha(t) - \beta(t)\} = \alpha \oslash \beta(0) = v(\alpha, \beta) \tag{A.9}$$

Graphically, the backlog bound is the maximum vertical deviation between $\alpha(t)$ and $\beta(t)$ as shown in Figure A.2.

Then, to compute the end-to-end performances through a flow path, we need the following theorems.

Theorem 7. *(Output bound) Assume that a traffic flow R(t), constrained by arrival curve $\alpha(t)$, traverses a system that provides service curve $\beta(t)$. The output flow is constrained by the following arrival curve:*

$$\alpha^*(t) = \sup_{s \geq 0}\{\alpha(t+s) - \beta(s)\} = \alpha \oslash \beta(t) \tag{A.10}$$

Corollary 4. *(Output bound) Assume that a traffic flow R(t), constrained by arrival curve $\alpha(t)$, has delay bound D when traversing a system. The output flow is constrained by the arrival curve:*

$$\alpha^*(t) = \alpha(t + D) \tag{A.11}$$

Theorem 8. *(Residual service curve) [63] Let f_1 and f_2 be two flows crossing a system that offers a strict service curve β such that f_1 is constrained by the arrival curve α_1, then*

— *The residual service curve offered to f_2 is:*

$$\beta_2 = (\beta - \alpha_1)_{\uparrow} \tag{A.12}$$

— *If f_1 has strictly higher priority than f_2 and can preempt f_2, the service curve β_2 in Equations A.12 is a strict service curve.*

— *If f_1 has strictly higher priority than f_2 but cannot preempt f_2 (non-preemptive fixed priority), and considering $l_{2,max}$ is the maximum packet length of f_2, then the strict residual service curve offered to f_2 is:*

$$\beta_2 = (\beta - \alpha_1 - l_{2,max})_{\uparrow} \tag{A.13}$$

Corollary 5. *Consider a system with the strict service β and m flows crossing it, f_1,f_2,..,f_m. The maximum packet length of f_i is $l_{i,max}$ and is upper-constrained by the arrival curve α_i. The flows are scheduled by the non-preemptive strict priority (NPFP) policy where $f_i \succ f_j \Leftrightarrow i < j$. For each $i \in \{2, .., m\}$, the strict service curve of f_i is given by:*

$$(\beta - \sum_{j<i} \alpha_j - \max_{k \geq i} l_{i,max})_{\uparrow} \tag{A.14}$$

Theorem 9. *(Impact of packetization) Consider a system with a service curve β under fluid model. Consider l_{max} the maximum packet length of the crossing flows. Under packetized model, this server offers a service curve $[\beta - l_{max}]^+$, where $[x]^+ = \max(x, 0)$.*

Finally, we introduce the extension concepts of Network Calculus, the data scaling function and the maximum scaling curve based on the work of [56] that are used to model the gateways in our proposal in Chapters 3 and 4.

Definition 6. *(Scaling function) A scaling function $S \in \mathcal{F}$ assigns an amount of scaled data $S(a)$ to an amount of data a.*

Definition 7. *(Maximum scaling curve) Consider a scaling function S. The maximum scaling curve $\overline{S} \in \mathcal{F}$ satisfies,*

$$\overline{S(b)} \geq \sup_{a \in [0,\infty)} \{S(b+a) - S(a)\} = S \oslash S(b) \tag{A.15}$$

Theorem 10. *(Bounds for Scaling Functions) Consider $R(t)$ an input flow for a scaling function S with maximum scaling curve $\overline{S}$ and $\alpha(t)$ be the arrival curve of $R(t)$. An output arrival curve of scaled flow $S(R(t))$ is:*

$$\alpha_S(t) = \overline{S}(\alpha(t)) \tag{A.16}$$

Definition 8. *(Maximum packet curve) [62] Consider $\mathcal{P}(t)$ a cumulative function of* ***entire*** *packets at time t, then $\mathcal{P}$ has a maximum packet curve Π if for $\forall 0 \leq s \leq t$,*

$$\mathcal{P}(t) - \mathcal{P}(s) \leq \Pi(t - s) \tag{A.17}$$

Definition 9. *(Minimum packet curve) [62] Consider $\mathcal{P}(t)$ a cumulative function of* ***entire*** *packets at time t, then $\mathcal{P}$ has a minimum packet curve π if for $\forall 0 \leq s \leq t$,*

$$\mathcal{P}(t) - \mathcal{P}(s) \geq \pi(t - s) \tag{A.18}$$

Theorem 11. *(Output packet curve) Assume that an input with a cumulative function of entire packets $\mathcal{P}$, constrained by the packet curve Π, has the delay D when traversing a system. Then, the cumulative function of entire packet of the output has a maximum packet curve Π^* given by:*

$$\Pi^*(t) = \Pi(t + D) \tag{A.19}$$

Appendix B

Stochastic Network Calculus Overview

In this appendix, we present the basic concepts of Stochastic Network Calculus and introduce our proposed theorems in case of the stochastic strict service curves, with their detailed proofs.

B.1 Stochastic Arrival Curve

Definition 10. *[17] A flow with an input cumulative function R is said to have a traffic-amount-centric (t.a.c) stochastic arrival curve α^ϵ iff for all $t \geq s \geq 0$, there holds:*

$$Pr\{R(t) - R(s) > \alpha^\epsilon(t-s)\} \leq \epsilon$$

We denote that $R \sim_{ta} \alpha^\epsilon$.

Definition 11. *[17] A flow with an input cumulative function R is said to have a virtual-backlog-centric (v.b.c) stochastic arrival curve α^ϵ iff for all $t \geq s \geq 0$, there holds:*

$$Pr\{\sup_{0\leq s\leq t}[R(t) - R(s) - \alpha^\epsilon(t-s)] > 0\} \leq \epsilon$$

We denote that $R \sim_{vb} \alpha^\epsilon$.

Definition 12. *[17] A flow with an input cumulative function R is said to have a maximal-(virtual)-backlog-centric (m.b.c) stochastic arrival curve α^ϵ iff for all $t \geq s \geq 0$, there holds:*

$$Pr\{\sup_{0\leq s\leq t}\sup_{0\leq u\leq s}[R(s) - R(u) - \alpha^\epsilon(s-u)] > 0\} \leq \epsilon$$

We denote that $R \sim_{mb} \alpha^\epsilon$.

Theorem 12. *[17] (Superposition) Consider N flows with cumulative input functions R_i, $i = 1, 2, .., N$, respectively. Let R denote the aggregate input cumulative functions. If $\forall i$, $R_i \sim_{ta}$ or $\sim_{vb}$ or $\sim_{mb} \alpha_i^{\epsilon_i}$, then $R \sim_{ta}$ or $\sim_{vb}$ or $\sim_{mb} \alpha^{\epsilon}$, correspondingly, where:*

$$\alpha^{\epsilon}(t) = \sum_{i=1}^{N} \alpha_i^{\epsilon_i}(t)$$

and

$$\epsilon = \sum_{i=1}^{N} \epsilon_i$$

Figure B.1 illustrates the relations between the definitions of Stochastic Arrival Curves (SAC).

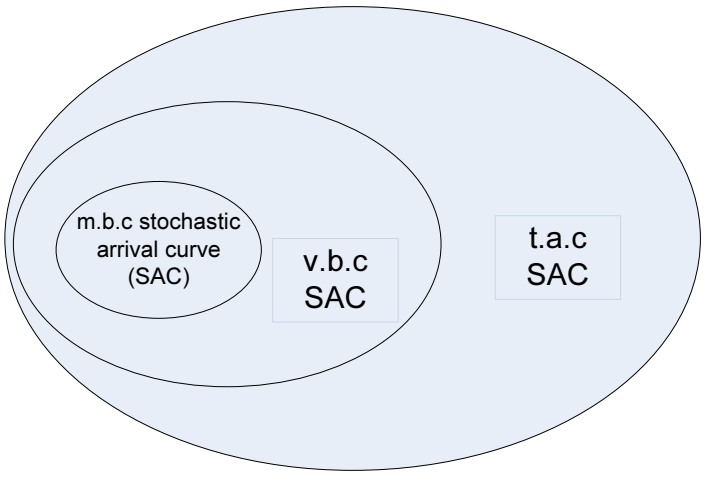

Figure B.1: Relations between the different Stochastic Arrival Curves

B.2 Stochastic Service Curve

Definition 13. *[61] (Weak stochastic service curve) A system S is said to provide the weak stochastic service curve β^{ϵ} iff for all $t \geq 0$, there holds:*

$$Pr\{R^*(t) > R \otimes \beta^{\epsilon}(t)\} \geq 1 - \epsilon$$
$$\Leftrightarrow \quad Pr\{\sup_{0 \leq s \leq t} [R^*(t) - R(s) - \beta^{\epsilon}(t-s)] < 0\} \leq \epsilon$$

Definition 14. *[61] (Stochastic service curve) A system S is said to provide the stochastic service curve β^{ϵ} iff for all $t \geq 0$, there holds:*

$$Pr\{\sup_{t \geq 0}[R^*(t) - R \otimes \beta^{\epsilon}(t)] > 0\} \geq 1 - \epsilon$$
$$\Leftrightarrow \quad Pr\{\sup_{0 \leq s \leq t < \infty} [R^*(t) - R(s) - \beta^{\epsilon}(t-s)] < 0\} \leq \epsilon$$

Definition 15. *[61] (Stochastic strict service curve) A system S is said to provide the stochastic strict service curve β^ϵ iff for any backlogged period $(s,t]$, there holds:*

$$Pr\{R^*(t) - R^*(s) > \beta^\epsilon(t-s)\} \geq 1 - \epsilon$$

Figure B.2 illustrates the relations between the three definitions of Stochastic Service Curves (SSC).

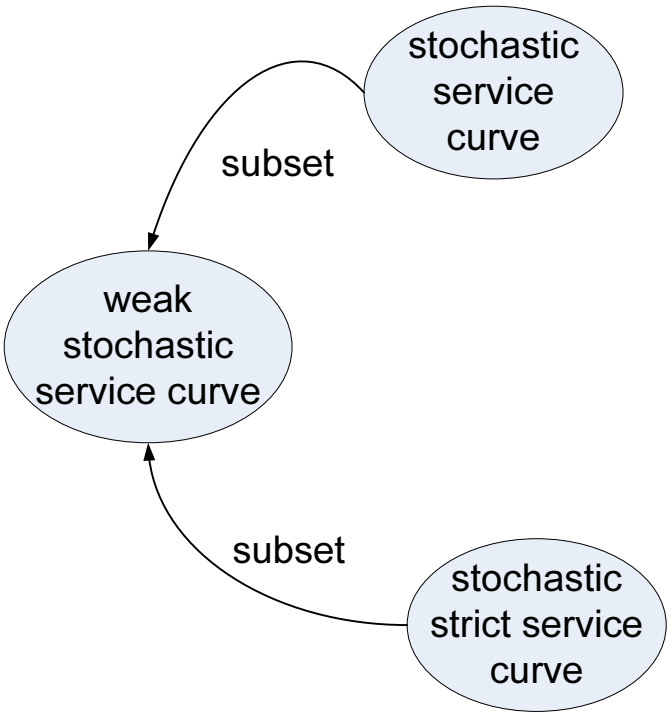

Figure B.2: Relations between the Stochastic Service Curves

B.3 Performance Evaluation

B.3.1 Why Stochastic Network Calculus is hard?

Consider the input cumulative function $R(t)$ that has the t.a.c SAC α^{ϵ_α} and the system S that has the weak SSC β^{ϵ_β}. Let $B = v(\alpha^{\epsilon_\alpha}, \beta^{\epsilon_\beta})$ be the stochastic backlog. The objective is to evaluate the upper bound of $Pr\{R(t) - R^*(t) > B\}$.

First, we remind an inequality in probability: Let X and Y be 2 random variables, there holds:

$$Pr(X + Y > 0) \leq P(X > 0) + P(Y > 0) \tag{B.1}$$

We have:

$$Pr\{R(t) - R^*(t) > B\} = Pr\{R(t) - R^*(t) - B > 0\} \tag{B.2}$$

Since $Pr\{R \otimes \beta^{\epsilon_\beta}(t) - R^*(t) > 0\} < \epsilon_\beta$, then:

$$\begin{aligned} Pr\{R(t) - R^*(t) - B > 0\} &\leq Pr\{R(t) - R \otimes \beta^{\epsilon_\beta}(t) - B > 0\} + Pr\{R \otimes \beta^{\epsilon_\beta}(t) - R^*(t) > 0\} \\ &< Pr\{R(t) - R \otimes \beta^{\epsilon_\beta}(t) - B > 0\} + \epsilon_\beta \end{aligned}$$

On the other hand, since $\forall 0 \leq s \leq t$, $\beta^{\epsilon_\beta}(t-s) + B \geq \alpha^{\epsilon_\alpha}(t-s)$, then

$$\begin{aligned} Pr\{R(t) - R \otimes \beta^{\epsilon_\beta}(t) - B > 0\} &= Pr\{\sup_{0 \leq s \leq t}\{R(t) - R(s) - \beta^{\epsilon_\beta}(t-s) - B\} > 0\} \\ &\leq Pr\{\sup_{0 \leq s \leq t}\{R(t) - R(s) - \alpha^{\epsilon_\alpha}(t-s)\} > 0\} \end{aligned}$$

We can see that with a v.b.c SAC, we can conclude that $Pr\{\sup_{0 \leq s \leq t}\{R(t) - R(s) - \alpha^{\epsilon_\alpha}(t-s)\} > 0\} \leq \epsilon_\alpha$. However, with a t.a.c SAC, the only bound we can achieve is:

$$\begin{aligned} Pr\{sup_{0 \leq s \leq t}\{R(t) - R(s) - \alpha^{\epsilon_\alpha}(t-s)\} > 0\} &\leq \sum_{s=0}^{t} Pr\{\{R(t) - R(s) - \alpha^{\epsilon_\alpha}(t-s)\} > 0\} \\ &\leq (t-s)\epsilon_\alpha, \text{ which cannot be bounded.} \end{aligned}$$

Hence, it is difficult to express $Pr\{R(t) - R^*(t) > B\}$ giving ϵ_α and ϵ_β.

B.3.2 The main theorems

Theorem 13. *(Backlog and delay bounds) Consider a system S with input R. If R has a v.b.c (or m.b.c) SAC α^{ϵ_α}, and system S has a weak SSC β^{ϵ_β}, then the backlog is bounded by:*

$$Pr\{B(t) > v(\alpha^{\epsilon_\alpha}, \beta^{\epsilon_\beta})\} < \epsilon_\alpha + \epsilon_\beta$$

The delay is bounded by:

$$Pr\{D(t) > h(\alpha^{\epsilon_\alpha}, \beta^{\epsilon_\beta})\} < \epsilon_\alpha + \epsilon_\beta$$

Theorem 14. *(Output bound) Consider a system S with input R. If R has a v.b.c SAC α^{ϵ_α}, and system S has a (weak) SSC β^{ϵ_β}, then the output is (t.a.c) v.b.c SAC and equal to $(\alpha \oslash \beta)^{\epsilon_\alpha + \epsilon_\beta}$. If R has a m.b.c SAC α^{ϵ_α}, and system S has a SSC β^{ϵ_β}, then the output is m.b.c SAC and equal to $(\alpha \oslash \beta)^{\epsilon_\alpha + \epsilon_\beta}$.*

Theorem 15. *(Residual bound) Consider a system S with two inputs R_1 and R_2. If R_1 has a v.b.c SAC $\alpha_1^{\epsilon_1}$, and system S has a weak SSC β^{ϵ_β}, then the residual service curve for R_2 is weak SSC and equal to $(\beta - \alpha_1)_\uparrow^{\epsilon_1 + \epsilon_\beta}$. If R_1 has a m.b.c SAC $\alpha_1^{\epsilon_1}$, and system S has a SSC β^{ϵ_β}, then the residual service curve for R_2 is SSC and equal to $(\beta - \alpha_1)_\uparrow^{\epsilon_1 + \epsilon_\beta}$.*

B.3.3 Extended theorems with stochastic strict service curves

In this part, we detail our proposed theorems which simplify the computation of the delay and backlog bounds, and the properties of output arrival curve and residual service curve, when the traffic has a t.a.c SAC and the system has a Stochastic Strict Service Curve (SSSC).

Theorem 16. *Consider a server offering a stochastic strict service curve β^{ϵ_β} to an input process R. Suppose that R has a t.a.c stochastic arrival curve α^{ϵ_α}. The following hold.*

1. *Delay bound: $Pr\{d(t) \leq h(\alpha^{\epsilon_\alpha}, \beta^{\epsilon_\beta})\} \geq 1 - \epsilon_\alpha - \epsilon_\beta$*
2. *Backlog bound: $Pr\{B(t) \leq v(\alpha^{\epsilon_\alpha}, \beta^{\epsilon_\beta})\} \geq 1 - \epsilon_\alpha - \epsilon_\beta$*
3. *Output (t.a.c stochastic arrival curve $\alpha^{*,\epsilon_\alpha+\epsilon_\beta}$ for R^*):*

$$\alpha^{*,\epsilon_\alpha+\epsilon_\beta} = \alpha^{\epsilon_\alpha} \oslash \beta^{\epsilon_\beta}$$

$$\Updownarrow$$

$$\forall t \geq s \geq 0 : Pr\{R^*(t) - R^*(s) \leq \alpha^{*,\epsilon_\alpha+\epsilon_\beta}(t-s)\} \geq 1 - \epsilon_\alpha - \epsilon_\beta$$

Proof. First, we prove the virtual delay bound. Let $D = h(\alpha^{\epsilon_\alpha}, \beta^{\epsilon_\beta})$. We have $\alpha^{\epsilon_\alpha}(t) \leq \beta^{\epsilon_\beta}(t + D), \forall t \geq 0$. As $R(t)$ and $R^*(t)$ are continuous, we have $R(t) = R^*(t + D(t))$.

If $D(t) = 0$, it is a trivial case.

If $D(t) > 0$, t is in the backlogged period. Let s be the starting time of this backlogged period. We have $R(s) = R^*(s)$. For any $0 < d < D(t)$, $R(t + d) \geq R(t) > R^*(t + d)$. Therefore, $(s, t + D(t))$ is a backlogged period. Then, we have:

$$Pr\{R(t) - R(s) \leq \alpha^{\epsilon_\alpha}(t-s)\} \geq 1 - \epsilon_\alpha$$

and

$$Pr\{R^*(t + D(t)) - R^*(s) \geq \beta^{\epsilon_\beta}(t + D(t) - s)\} \geq 1 - \epsilon_\beta$$

Since $R(t) - R(s) = R^*(t + D(t)) - R^*(s)$, then

$$Pr\{\alpha^{\epsilon_\alpha}(t-s) \geq \beta^{\epsilon_\beta}(t - s + D(t))\} \geq (1 - \epsilon_\alpha)(1 - \epsilon_\beta) \geq 1 - \epsilon_\alpha - \epsilon_\beta$$

$$\Rightarrow Pr\{\beta^{\epsilon_\beta}(t + D) \geq \beta^{\epsilon_\beta}(t - s + D(t))\} \geq 1 - \epsilon_\alpha - \epsilon_\beta.$$

Hence,

$$Pr\{D(t) \leq D\} \geq 1 - \epsilon_\alpha - \epsilon_\beta$$

Second, we prove the backlog bound.

If $B(t) = 0$, it is the trivial case.

If $B(t) > 0$, t is at the backlogged period. Let s be the starting time of the backlogged period. We have $R(s) = R^*(s)$ and the following:

$$Pr\{R(t) - R(s) \leq \alpha^{\epsilon_\alpha}(t-s)\} \geq 1 - \epsilon_\alpha$$

$$Pr\{R^*(t) - R^*(s) \geq \beta^{\epsilon_\beta}(t-s)\} \geq 1 - \epsilon_\beta$$

Therefore,

$$Pr\{R(t) - R^*(t) \leq \alpha^{\epsilon_\alpha}(t-s) - \beta^{\epsilon_\beta}(t-s)\} \geq 1 - \epsilon_\alpha - \epsilon_\beta$$

Hence,

$$Pr\{B(t) \leq v(\alpha^{\epsilon_\alpha}, \beta^{\epsilon_\beta})\} \geq 1 - \epsilon_\alpha - \epsilon_\beta$$

Third, we prove the output arrival curve. We have

$$\alpha^{*,\epsilon_\alpha+\epsilon_\beta}(t) = \alpha^{\epsilon_\alpha} \oslash \beta^{\epsilon_\beta}(t) = \sup_{u \geq 0}\{\alpha^{\epsilon_\alpha}(t+u) - \beta^{\epsilon_\beta}(u)\}$$

We need to prove that

$$\forall t \geq s \geq 0, Pr\{R^*(t) - R^*(s) \leq \alpha^{*,\epsilon_\alpha+\epsilon_\beta}(t-s)\} \geq 1 - \epsilon_\alpha - \epsilon_\beta$$

If s is the starting time of the backlogged period, then we have $R(s) = R^*(s)$ and

$$\begin{aligned} Pr\{R^*(t) - R^*(s) \leq \alpha^{*,\epsilon_\alpha+\epsilon_\beta}(t-s)\} &\geq Pr\{R(t) - R(s) \leq \alpha^{*,\epsilon_\alpha+\epsilon_\beta}(t-s)\} \\ &\geq 1 - \epsilon_\alpha \geq 1 - \epsilon_\alpha - \epsilon_\beta \end{aligned}$$

else let $w < s$ be the starting time of the backlogged period, then we have $R(w) = R^*(w)$ and

$$\begin{aligned} & Pr\{R^*(t) - R^*(s) \leq \alpha^{*,\epsilon_\alpha+\epsilon_\beta}(t-s)\} \\ \geq\ & Pr\{(R(t) - R(w)) - ((R^*(s) - R^*(w)) \leq \alpha^{*,\epsilon_\alpha+\epsilon_\beta}(t-s)\} \end{aligned}$$

From the definitions of SAC and SSC, we have:

$$Pr\{R(t) - R(w) \leq \alpha^{\epsilon_\alpha}(t-w)\} \geq 1 - \epsilon_\alpha$$

$$Pr\{R^*(s) - R^*(w) \geq \beta^{\epsilon_\beta}(s-w)\} \geq 1 - \epsilon_\beta$$

Hence,

$$\begin{aligned} & Pr\{(R(t) - R(w)) - ((R^*(s) - R^*(w)) \leq \alpha^{\epsilon_\alpha}(t-w) - \beta^{\epsilon_\beta}(s-w)\} \\ \geq\ & (1-\epsilon_\alpha)(1-\epsilon_\beta) \geq 1 - \epsilon_\alpha - \epsilon_\beta \end{aligned}$$

Since $\alpha^{\epsilon_\alpha}(t-w) - \beta^{\epsilon_\beta}(s-w) \leq \alpha^{*,\epsilon_\alpha+\epsilon_\beta}(t-s)$, therefore

$$Pr\{R^*(t) - R^*(s) \leq \alpha^{*,\epsilon_\alpha+\epsilon_\beta}(t-s)\} \geq 1 - \epsilon_\alpha - \epsilon_\beta$$

□

Theorem 17. *(Residual stochastic strict service curve for **fixed priority**)*

1. *(Preemptive fixed priority) Consider a system offering a strict stochastic service curve β^{ϵ_β} to the input $R_1 + R_2$ and suppose that R_1 is upper-constrained by t.a.c stochastic arrival curve $\alpha_1^{\epsilon_1}$. **If** R_1 **has strictly higher priority than** R_2 **and** R_1 **can preempt** R_2, then the residual stochastic **strict** service curve for R_2 is $\beta_2^{\epsilon_\alpha+\epsilon_\beta}$ where*

$$\beta_2^{\epsilon_\alpha+\epsilon_\beta} = (\beta^{\epsilon_\beta} - \alpha_1^{\epsilon_1})_\uparrow$$

2. *(Non-preemptive fixed priority) Consider a system offering a strict stochastic service curve β^{ϵ_β} to the input R_1+R_2 and suppose that R_1 is upper-constrained by t.a.c stochastic arrival curve $\alpha_1^{\epsilon_1}$. **If** R_1 **has higher priority than** R_2 **but** R_1 **cannot preempt** R_2, then the residual stochastic **strict** service curve offered to R_2 is $\beta_2^{\epsilon_\alpha+\epsilon_\beta}$, where*

$$\beta_2^{\epsilon_\alpha+\epsilon_\beta} = (\beta^{\epsilon_\beta} - \alpha_1^{\epsilon_1} - l_{2,max})_\uparrow$$

where $l_{2,max}$ is the maximum packet length of R_2,

Proof. First, we detail the proof for the case of preemptive fixed priority server. Consider the backlogged period (u, v) for R_2, then u and v are in the same backlogged period of the aggregate flow, and:

$$Pr\{R_1^*(t) + R_2^*(t) \geq R_1^*(u) + R_2^*(u) + \beta^{\epsilon_\beta}(t-u)\} \geq 1 - \epsilon_\beta$$

Consider the backlogged period (p, q), where p and q are the starting and ending time of the backlogged period, for R_1 such that $p \leq u$ and p is the closest to u. There are two cases:
Case 1: If $q \leq u$, then u is not in backlogged period of R_1. Hence, $R_1(u) = R_1^*(u)$ and $R_1^*(v) \leq R_1(v)$.

Since (u, v) is the backlogged period of R, then

$$Pr\{R_2^*(v) - R_2^*(u) \geq \beta^{\epsilon_\beta}(v-u) - (R_1^*(v) - R_1^*(u))\} \geq 1 - \epsilon_\beta$$

Hence,

$$Pr\{R_2^*(v) - R_2^*(u) \geq \beta^{\epsilon_\beta}(v-u) - (R_1(v) - R_1(u))\} \geq 1 - \epsilon_\beta$$

Since $Pr\{R_1(v) - R_1(u) \leq \alpha^{\epsilon_1}(v-u)\} \geq 1 - \epsilon_1$, then

$$\begin{aligned} & Pr\{R_2^*(v) - R_2^*(u) \geq \beta^{\epsilon_\beta}(v-u) - \alpha^{\epsilon_1}(v-u)\} \\ \geq \quad & (1-\epsilon_\beta)(1-\epsilon_1) \geq 1 - \epsilon_\beta - \epsilon_1 \end{aligned}$$

This formula is also correct for all $w \in [u, v]$, then

$$Pr\{R_2^*(w) - R_2^*(u) \geq \beta^{\epsilon_\beta}(w-u) - \alpha^{\epsilon_1}(w-u)\} \geq 1 - \epsilon_\beta - \epsilon_1$$

Since $R_2^*(v) \geq R_2^*(w)$,then

$$Pr\{R_2^*(v) - R_2^*(u) \geq \beta^{\epsilon_\beta}(w-u) - \alpha^{\epsilon_1}(w-u)\} \geq 1 - \epsilon_\beta - \epsilon_1$$

Therefore,

$$Pr\{R_2^*(v) - R_2^*(u) \geq \sup_{w\in[u,v]}(\beta^{\epsilon_\beta}(w-u) - \alpha^{\epsilon_1}(w-u))\} \geq 1 - \epsilon_\beta - \epsilon_1$$

From the definition of upper closure and considering the $s = w - u \in [0, v-u]$,

$$(\beta^{\epsilon_\beta} - \alpha^{\epsilon_1})_\uparrow(v-u) = \max\{\sup_{s\in[0,v-u]}(\beta^{\epsilon_\beta}(s) - \alpha^{\epsilon_1}(s)), 0\}$$

Since $R_2^*(v) - R_2^*(u) \geq 0$, then

$$Pr\{R_2^*(v) - R_2^*(u) \geq (\beta^{\epsilon_\beta} - \alpha^{\epsilon_1})_\uparrow(v-u)\} \geq 1 - \epsilon_\beta - \epsilon_1$$

Case 2: If $q > u$, during interval $[p, u]$, flow R_1 has higher priority than R_2. Therefore, we have $R_2^*(u) = R_2^*(p)$ and $R_1(p) = R_1^*(p)$. The backlogged period of the aggregate traffic happens during the period (p, v), then:

$$Pr\{R_1^*(v) + R_2^*(v) \geq R_1^*(p) + R_2^*(p) + \beta^{\epsilon_\beta}(v-p)\} \geq 1 - \epsilon_\beta$$

Since $R_1^*(v) - R_1^*(p) \leq R_1(v) - R_1(p)$, then

$$Pr\{R_1^*(v) - R_1^*(p) \leq \alpha^{\epsilon_1}(v-p)\} \geq 1 - \epsilon_1$$

Hence,

$$\begin{aligned} & Pr\{R_2^*(v) - R_2^*(p) \geq \beta^{\epsilon_\beta}(v-p) - \alpha^{\epsilon_1}(v-p)\}\} \\ \geq \quad & (1-\epsilon_\beta)(1-\epsilon_1) \geq 1 - \epsilon_\beta - \epsilon_1 \end{aligned}$$

Similar to case 1, we have

$$Pr\{R_2^*(v) - R_2^*(p) \geq \sup_{s\in[0,v-p]}(\beta^{\epsilon_\beta}(s) - \alpha^{\epsilon_1}(s))\} \geq 1 - \epsilon_\beta - \epsilon_1$$

Since $R_2^*(p) = R_2^*(u)$ and $v - p \geq v - u$, then

$$Pr\{R_2^*(v) - R_2^*(u) \geq \sup_{s\in[0,v-u]}(\beta^{\epsilon_\beta}(s) - \alpha^{\epsilon_1}(s))\} \geq 1 - \epsilon_\beta - \epsilon_1$$

Hence,

$$Pr\{R_2^*(v) - R_2^*(u) \geq (\beta^{\epsilon_\beta} - \alpha^{\epsilon_1})_\uparrow(v-u))\} \geq 1 - \epsilon_\beta - \epsilon_1$$

Second, the proof for non-preemptive fixed priority is conducted similarly to the one for preemptive fixed priority. However, we need to integrate $l_{2,max}$ which is considered as "self

competitive term". This notion of "competition versus itself" is counter-intuitive, and deserves an explanation. Consider a backlogged period of the low priority flow R_2. Before beeing served by the server, the flow R_2 must wait the end of service of the high priority flow R_1. However, due to the non-preemption, the high priority flow can be blocked by one packet of the low priority flow, and this could be a previous backlogged period of the flow R_2 and not the current one. □

Corollary 6. *Consider a non-preemptive fixed priority server with a stochastic strict service curve β^{ϵ_β} and N flows crossing it, $F_1, F_2, ..., F_N$. The maximum packet length of flow F_i is $l_{i,max}$ and F_i has a t.a.c stochastic arrival curve $\alpha_i^{\epsilon_i}$. Suppose that $F_i \succ F_j$ if $i < j$ and F_i cannot preempt F_j. For each $2 \leq i \leq N$,*

$$\left(\beta^{\epsilon_\beta} - \sum_{j<i} \alpha_j^{\epsilon_j} - \max_{k \geq i} l_{k,max}\right)_{\uparrow}^{\epsilon_\beta + \epsilon_1 + .. + \epsilon_{i-1}}$$

is the residual stochastic strict service curve offered to F_i.

Definition 16. *(Stochastic delay bound). Consider a system S with input R. The virtual delay $D(t)$ is bounded by stochastic delay bound D^ϵ if it holds for all $t \geq 0$:*

$$Pr\{D(t) \leq D^\epsilon\} \geq 1 - \epsilon$$

Theorem 18. *(Sum of stochastic delays) Consider an input R crossing n systems $S_1, ..., S_n$ in tandem. Assume that the stochastic delay bounds of R in $S_1, ..., S_n$ are $D_1^{\epsilon_1}, ..., D_n^{\epsilon_n}$, respectively. The end-to-end stochastic delay bound of R through n systems is given by:*

$$D^\epsilon = \sum_{i=1}^{n} D_i^{\epsilon_i}$$

where $\epsilon = \sum_{i=1}^{n} \epsilon_i$.

Proof. Consider $D_i(t)$ the virtual delay at system S_i. We have

$$\begin{aligned} Pr\{D(t) \leq D^\epsilon\} &\geq \Pi_{i=1}^{n} Pr\{D_i(t) \leq D_i^{\epsilon_i}\} \\ &\geq \Pi_{i=1}^{n}(1 - \epsilon_i) \geq 1 - \sum_{i=1}^{n} \epsilon_i = 1 - \epsilon \end{aligned}$$

□

Appendix C

Theorem Proofs

We present in this appendix the proofs of theorems and corollaries described in Chapters 3 and 4.

Theorem 1 of Chapter 3. *Consider an end-system having a lower bound of offered time slot* $\overline{s^k}$*, generating N traffic flows and implementing a FIFO policy, the offered strict service curve when considering non-preemptive message transmission is:*

$$\overline{\beta^k}(t) = \beta_{c,\overline{s^k}}(t - WT + (c - \overline{s^k})), \forall t \geq 0$$

where

$$WT^k = e_{max} + c - s^k$$

and

$$\overline{s^k} = \begin{cases} \lfloor \frac{s^k}{e} \rfloor e & \text{if } e_{max} = e_{min} = e \\ \max\{s^k - e_{max}, e_{min}\} & \text{Otherwise} \end{cases}$$

Proof. Let $R(t), R^*(t)$ be the input and output cumulative functions of the total flow, respectively. To prove that the obtained curve is a strict service curve, we have to prove as specified in Definition 5 of Appendix A that for all backlogged period $]\tau, t]$:

$$R^*(t) - R^*(\tau) \geq \overline{\beta}(t) = \beta^k_{c,\overline{s^k}}(t - \tau - WT^k + (c - \overline{s}))$$

We will verify Definition 5 for all the possible values of t and τ giving WT^k and $\overline{s^k}$, as follows:

— if $t - \tau \leq WT^k$, $R^*(t) - R^*(\tau) \geq 0 = \overline{\beta^k}(t - \tau)$

— If $WT^k \leq t - \tau \leq WT^k + \overline{s^k}$,
let $u = \inf_w\{w \in]\tau, t] | R^*(w) < R^*(w + \epsilon), \forall \epsilon > 0\}$, where u is the starting time to serve

flow f and $R^*(u) = R^*(\tau)$. There are two cases:

Case 1: $u > \tau$. We have $u \leq \tau + WT^k$, then

$$\begin{aligned} R^*(t) - R^*(\tau) &= R^*(t) - R^*(u) \\ &\geq R^*(t - (\tau + WT^k - u)) - R^*(u) \\ &= B(t - \tau - WT^k) = \overline{\beta^k}(t - \tau) \end{aligned}$$

Case 2: $u = \tau$. Let $v = \inf\{w \in]\tau, t] | R^*(w) = R^*(w + \epsilon), \forall \epsilon > 0\}$, where v is the ending time of a offered slot.

$\triangleright$ If $t \leq v$, then $R^*(t) - R^*(\tau) = B(t - \tau) > \overline{\beta^k}(t - \tau)$

$\triangleright$ If $v < t \leq v + c - \overline{s^k}$, then

$$\begin{aligned} &R^*(t) - R^*(\tau) \geq R^*(v) - R^*(\tau) = B(v - \tau) \\ &= \overline{\beta^k}(v + c + e_{max} - s^k - \tau) \geq \overline{\beta}(v + c - \overline{s^k} - \tau) \geq \overline{\beta^k}(t - \tau) \end{aligned}$$

$\triangleright$ If $v + c - \overline{s} < t \leq \tau + WT + \overline{s}$,
let $u' = \inf\{w \in]v, t] | R^*(w) < R^*(w + \epsilon), \forall \epsilon > 0\}$, where u' is the beginning time of a slot. We have $u' \leq v + c - \overline{s}$. If $t \leq u' + \overline{s}$,

$$\begin{aligned} R^*(t) - R^*(\tau) &= R^*(t) - R^*(u') + R^*(v) - R^*(\tau) \\ &= B(t - u') + B(v - \tau) \\ &\geq B(t - (v + c - \overline{s^k}) + v - \tau) \\ &= B(t - \tau - (c - \overline{s^k})) \geq \overline{\beta^k}(t - \tau) \end{aligned}$$

Otherwise, $R^*(t) - R^*(\tau) \geq R^*(u' + \overline{s^k}) - R^*(u') = B\overline{s^k} \geq \overline{\beta^k}(t - \tau)$.

— If $WT^k + \overline{s^k} < t - \tau$, there must exist t' such that $t = t' + mc, (m \in \mathbb{N}^+)$ and $WT^k - (c - \overline{s^k}) = e_{max} - (s^k - \overline{s^k}) \leq t' - \tau < WT^k + \overline{s^k}$. Consider an arbitrary backlogged period $]t' + ic, t' + (i + 1)c]$ where $0 \leq i \leq m$ and $i \in \mathbb{N}$. The node can serve the aggregate flow at least during $c - \overline{s^k}$, then

$$R^*(t' + (i + 1)c) - R^*(t' + ic) \geq B\overline{s^k}$$

$$\begin{aligned} \text{Hence, } R^*(t) - R^*(\tau) &= R^*(t) - R^*(t') + R^*(t') - R^*(\tau) \\ &\geq Bm\overline{s^k} + \overline{\beta^k}(t' - \tau) = \overline{\beta^k}(t - \tau) \end{aligned}$$

Definition 5 is then verified for the different values of t and τ giving WT^k and $\overline{s^k}$ which finishes the proof. □

Corollary 1 of Chapter 4. *Consider an end-system having the minimum offered TDMA time slot* $\overline{\overline{s^k}}$*, a refined strict service curve guaranteed on TDMA-based network under FIFO multiplexing is*

$$\overline{\overline{\beta^k}}(t) = \beta_{c,\overline{\overline{s^k}}}(t - WT + (c - \overline{\overline{s^k}}))$$

Proof. The proof is similar to the proof of Theorem 1. We have only to replace the parameters $\overline{s^k}$ in the first proof by the parameter $\overline{\overline{s^k}}$. □

Theorem 2 of Chapter 3. *Consider aggregate flow* $f^k_{\leq i}$ *having a lower bound of offered TDMA time slot* $\overline{s^k_{\leq i}}$*, transmitted by an end-system implementing FP policy, the strict service curve guaranteed to* $f^k_{\leq i}$ *when considering non-preemption feature is:*

$$\overline{\beta^k_{\leq i}}(t) = \beta_{c,\overline{s^k_{\leq i}}}(t - WT^k_{\leq i} + (c - \overline{s^k_{\leq i}})), \forall t \geq 0$$

where

$$WT^k_{\leq i} = \min(e^{i<j\leq N}_{max} + e^{1\leq j\leq i}_{max} + c - s^k, c),$$

and

$$\overline{s^k_{\leq i}} = \begin{cases} \lfloor \dfrac{s^k}{e} \rfloor e & \text{if } e^{1\leq j\leq i}_{max} = e^{1\leq j\leq i}_{min} = e \\ \max(e^{1\leq j\leq i}_{min}, s^k - e^{1\leq j\leq i}_{max}) & \text{Otherwise} \end{cases}$$

Proof. The proof is similar to the proof of Theorem 1. We have only to replace the parameters WT^k and $\overline{s^k}$ in the first proof by the parameter $WT^k_{\leq i}$ and $\overline{s^k_{\leq i}}$, respectively.

□

Corollary 2 of Chapter 4. *Consider aggregate flow* $f^k_{\leq i}$ *having the minimum offered TDMA time slot* $\overline{\overline{s^k_{\leq i}}}$*, a refined strict service curve guaranteed on TDMA-based network under FP multiplexing is*

$$\overline{\overline{\beta^k_{\leq i}}}(t) = \beta_{c,\overline{\overline{s^k_{\leq i}}}}(t - WT^k_{\leq i} + (c - \overline{\overline{s^k_{\leq i}}}))$$

Proof. The proof is similar to the proof of Theorem 1. We have only to replace the parameters WT^k and $\overline{s^k}$ in the first proof by the parameter $WT^k_{\leq i}$ and $\overline{\overline{s^k_{\leq i}}}$, respectively.

□

Theorem 3 of Chapter 3 *The strict service curve for flow* f^k_i*, transmitted by a node implementing a non-preemptive WRR combined with TDMA system is*

$$\overline{\beta^k_i}(t) = \beta_{\overline{c},\overline{w^k_i}}(t)$$

where $\overline{w_i^k} = \lfloor \frac{w_i^k}{e_i} \rfloor * e_i$, *and* $\overline{c} = e_{max} + (c - s^k) + \sum_{j=1}^{N} \overline{w_j^k}$.

Proof. Let $R(t)$and $R^*(t)$ be the input and output cumulative functions of flow f_i, respectively. Consider an arbitrary backlogged period $]\tau, t]$, we prove that $R^*(t) - R^*(\tau) \geq \overline{\beta_i^k}(t - \tau)$.

— If $0 \leq t - \tau \leq \overline{c} - \overline{w_i^k}$, $R^*(t) - R^*(\tau) \geq 0 = \overline{\beta_i^k}(t - \tau)$

— If $\overline{c} - \overline{w_i^k} < t - \tau \leq \overline{c}$, there are 3 cases:

1) There is a complete slot s inside $]\tau, t]$. Within this slot f_i^k can be transmitted $\lfloor \frac{w_i^k}{e_i} \rfloor$ messages because the other flows can only be served in maximum amount of time $\sum_{j=1, j\neq i}^{N} \overline{w_j^k}$.

$$R^*(t) - R^*(s) \geq B * \lfloor \frac{w_i^k}{e_i} \rfloor * e_i = B * \overline{w_i^k} \geq \overline{\beta_i^k}(t - \tau)$$

2) There is a partial slot s inside $]\tau, t]$. The maximum time where f_i^k is blocked is bounded by
$c - s^k + \sum_{j=1, j\neq i}^{N} \overline{w_j^k}$, then

$$\begin{aligned} R^*(t) - R^*(\tau) &\geq B(t - \tau - (c - s^k + \sum_{j=1, j\neq i}^{N} \overline{w_j^k})) \\ &> B(t - \tau - (\overline{c} - \overline{w_i^k})) = \overline{\beta_i^k}(t - \tau) \end{aligned}$$

3) There are 2 partial consecutive slots within $]\tau, t]$. The maximum time where f_i^k is blocked is bounded by $c - s^k + e_{max} + \sum_{j=1, j\neq i}^{N} \overline{w_j^k}$. The difference with case 2 is the impact of e_{max} which represents the worst case of idle remaining time between two consecutive slots. Hence,

$$\begin{aligned} R^*(t) - R^*(\tau) &\geq B(t - \tau - (c - s^k + e_{max} + \sum_{j=1, j\neq i}^{N} \overline{w_j^k})) \\ &= B(t - \tau - (\overline{c} - \overline{w_i^k})) = \overline{\beta_i^k}(t - \tau) \end{aligned}$$

— If $\overline{c} < t - \tau$, there must exist t' such that
$t = t' + mc, (m \in \mathbb{N}^+)$ and $0 \leq t' - \tau < c$. Hence,

$$\begin{aligned} R^*(t) - R^*(\tau) &= (R^*(t) - R^*(t - \overline{c})) \\ &\quad + (R^*(t - \overline{c}) - R^*(t - 2\overline{c})) + ... \\ &\quad + (R^*(t') - R^*(\tau)) \\ &\geq m * B * \overline{w_i^k} + \overline{\beta_i}(t' - \tau) = \overline{\beta_i^k}(t - \tau) \end{aligned}$$

□

Corollary 3 of Chapter 4. *Consider a flow f_i^k, the refined strict service curve guaranteed on TDMA-based network under non-preemptive WRR multiplexing is*

$$\overline{\overline{\beta_i^k}}(t) = \beta_{\overline{\overline{c}},\overline{\overline{w_i^k}}}(t)$$

where $\overline{\overline{w_i^k}} = x_i^* * e_i$ *and* $\overline{\overline{c}} = e_{max} + c - s + \sum_{j=1}^{N} \overline{\overline{w_j^k}}$

Proof. The proof is similar to the proof of Theorem 3. We have only to replace the parameters $\overline{w^k}$ in the first proof by the parameter $\overline{\overline{w^k}}$. □

Bibliography

[1] T. Coelho, R. Macedo, P. Carvalhal, J. Afonso, L. Silva, H. Almeida, M. Ferreira, and C. Santos, "A fly-by-wireless UAV platform based on a flexible and distributed system architecture." Industrial Technology, ICIT, 2006.

[2] C. Ossa, "Design, Construction and Control of a Quadrotor Helicopter Using a New Multirate Technique," Master's thesis, Concordia University, 2012.

[3] A. Akl, T. Gayraud, and P. Berthou, "Investigating Several Wireless Technologies to Build a Heteregeneous Network for the In-Flight Entertainment System Inside an Aircraft Cabin." Wireless and Mobile Communications (ICWMC), 2010.

[4] Dai, Xuewu and Sasloglou, Konstantinos and Atkinson, Robert and Strong, John and Panella, Isabella and Yun Cai, Lim and Mingding, Han and Chee Wei, Ang and Glover, Ian and Mitchell, John E and others, "Wireless communication networks for gas turbine engine testing," International Journal of Distributed Sensor Networks, 2012.

[5] R. Yedavalli and R. Belapurkar, "Application of wireless sensor networks to aircraft control and health management systems," Journal of Control Theory and Applications, vol. 9, no. 1, pp. 28–33, 2011.

[6] A. E. E. Committee, "Aircraft Data Network Part 7, Avionics Full Duplex Switched Ethernet (AFDX) Network, ARINC Specification 664." Aeronautical Radio, 2002.

[7] Avionic Systems Standardisation Committee, "Guide to avionics data buses," 1995.

[8] R. B. GmbH, "CAN specification Version 2,0," 1991.

[9] C. Furse and R. Haupt, "Down to the wire," Spectrum, IEEE, vol. 38, 2001.

[10] A. Willig, K. Matheus, and A. Wolisz, "Wireless Technology in Industrial Networks." Proceedings of the IEEE, 2005.

[11] P. Suriyachai, J. Brown, and U. Roedig, "Time-critical data delivery in wireless sensor networks," Distributed Computing in Sensor Systems, pp. 216–229, 2010.

[12] J. N. Yelverton, "Wireless avionics." Digital Avionics Systems Conference, DASC, 1995.

[13] O. Elgezabal Gomez, "Fly-by-wireless: Benefits, risks and technical challenges." Fly by Wireless Workshop (FBW), 2010.

[14] A. Akl, T. Gayraud, and P. Berthou, "Investigating Several Wireless Technologies to Build a Heteregeneous Network for the In-Flight Entertainment System inside an Aircraft Cabin." The 6th International Conference on Wireless and Mobile Communications, 2010.

[15] F. Leipold, D. Tassetto, and S. Bovelli, "Wireless in-cabin communication for aircraft infrastructure," Telecommunication Systems, 2011.

[16] W. Alliance, "ECMA-368 High Rate Ultra Wideband PHY and MAC Standard." ECMA Std., 2008.

[17] Y. Jiang, "A basic stochastic network calculus," ACM SIGCOMM Computer Communication Review, vol. 36, no. 4, pp. 123–134, 2006.

[18] C. B. Watkins and R. Walter, "Transitioning from federated avionics architectures to integrated modular avionics." 26th Digital Avionics Systems Conference, DASC, 2007.

[19] N. Thanthry and R. Pendse, "Aviation data networks: Security issues and network architecture." International Carnahan Conference on Security Technology, 2004.

[20] T. Coelho, R. Macedo, and et al., "A fly-by-wireless UAV platform based on a flexible and distributed system architecture." IEEE International Conference on Industrial Technology, 2006.

[21] E. Muhammad and C. Pham, "Adaptive duty-cycled MAC for low-latency mission-critical surveillance applications." Ad-hoc, Mobile, and Wireless Networks, 2014.

[22] B. Malinowsky, J. Gronbaek, and H.-P. Schwefel, "Realization of timed reliable communication over off-the-shelf wireless technologies." Wireless Communications and Networking Conference (WCNC), 2013.

[23] M. Hamdi, N. Boudriga, and M. S. Obaidat, "WHOMoVeS: An optimized broadband sensor network for military vehicle tracking," International Journal of Communication Systems, vol. 21, no. 3, pp. 277–300, 2008.

[24] S. C. Ergen and P. Varaiya, "PEDAMACS: Power efficient and delay aware medium access protocol for sensor networks," Mobile Computing, IEEE Transactions on, vol. 5, no. 7, pp. 920–930, 2006.

[25] A. Rowe, R. Mangharam, and R. Rajkumar, "RT-Link: A time-synchronized link protocol for energy-constrained multi-hop wireless networks." Sensor and Ad Hoc Communications and Networks, SECON, 2006.

[26] M. Salajegheh, H. Soroush, and A. Kalis, "HYMAC: Hybrid TDMA/FDMA medium access control protocol for wireless sensor networks." Personal, Indoor and Mobile Radio Communications (PIMRC), 2007.

[27] A. N. Kim, F. Hekland, S. Petersen, and P. Doyle, "When HART goes wireless: Understanding and implementing the WirelessHART standard." Emerging Technologies and Factory Automation (ETFA), 2008.

[28] K. Pister and L. Doherty, "TSMP: Time synchronized mesh protocol," IASTED Distributed Sensor Networks, 2008.

[29] S. Munir, S. Lin, E. Hoque, S. Nirjon, J. A. Stankovic, and K. Whitehouse, "Addressing burstiness for reliable communication and latency bound generation in wireless sensor networks." 9th ACM/IEEE International Conference on Information Processing in Sensor Networks, 2010.

[30] J. Le Boudec and P. Thiran, Network calculus: a theory of deterministic queuing systems for the internet. Springer-Verlag, 2001.

[31] T. L. Crenshaw, S. Hoke, A. Tirumala, and M. Caccamo, "Robust implicit edf: A wireless mac protocol for collaborative real-time systems," ACM Transactions on Embedded Computing Systems (TECS), vol. 6, no. 4, p. 28, 2007.

[32] A. Koubâa, M. Alves, E. Tovar, and A. Cunha, "An implicit GTS allocation mechanism in IEEE 802.15. 4 for time-sensitive wireless sensor networks: theory and practice," Real-Time Systems, vol. 39, no. 1-3, pp. 169–204, 2008.

[33] J. B. Schmitt and U. Roedig, "Sensor network calculus–a framework for worst case analysis," in Distributed Computing in Sensor Systems. Springer, 2005, pp. 141–154.

[34] P. Cappanera, L. Lenzini, A. Lori, G. Stea, and G. Vaglini, "Optimal joint routing and link scheduling for real-time traffic in TDMA wireless mesh networks," Computer Networks, vol. 57, no. 11, pp. 2301–2312, 2013.

[35] S. Bluetooth, "Bluetooth specification," 2007.

[36] Z. Alliance, "IEEE 802.15. 4, ZigBee standard," 2009.

[37] C. Quintana, V. Guerra, J. Rufo, J. Rabadan, and R. Perez-Jimenez, "Reading lamp-based visible light communication system for in-flight entertainment," Consumer Electronics, IEEE Transactions on, vol. 59, no. 1, pp. 31–37, 2013.

[38] S. Galli and O. Logvinov, "Recent developments in the standardization of power line communications within the IEEE," Communications Magazine, IEEE, vol. 46, no. 7, pp. 64–71, 2008.

[39] T. Paul and T. Ogunfunmi, "Wireless LAN comes of age: Understanding the IEEE 802.11 n amendment," Circuits and Systems Magazine, IEEE, vol. 8, no. 1, pp. 28–54, 2008.

[40] J. Blanckenstein, J. Garcia-Jimenez, J. Klaue, and H. Karl, "A Scalable Redundant TDMA Protocol for High-Density WSNs Inside an Aircraft," 2014.

[41] F. M. Leipold, "Wireless UWB Aircraft Cabin Communication System," Ph.D. dissertation, Munchen, Technische Universitat Munchen, 2011.

[42] S. K. Chilakala, "Development and Flight Testing of a Wireless Avionics Network Based on the IEEE 802.11 Protocols," Master's thesis, University of Kansas, 2008.

[43] D. Hope, "Towards a Wireless Aircraft," 2011.

[44] H. Zhong and T. Zhang, "Block-LDPC: A practical LDPC coding system design approach," Circuits and Systems I: Regular Papers, IEEE Transactions, vol. 52, no. 4, pp. 766–775, 2005.

[45] T. Baykas, C.-S. Sum, Z. Lan, J. Wang, M. A. Rahman, H. Harada, and S. Kato, "IEEE 802.15. 3c: the first IEEE wireless standard for data rates over 1 Gb/s," Communications Magazine, IEEE, vol. 49, no. 7, pp. 114–121, 2011.

[46] T. Malm, M. Kivipuro, J. Hérard, and J. Bøegh, "Validation of safety-related wireless machine control systems," 2007.

[47] R. Seifert, Gigabit Ethernet: technology and applications for high-speed LANs. Addison-Wesley Longman Publishing Co., Inc., 1998.

[48] K. Lee and J. Eidson, "IEEE-1588 Standard for a Precision Clock Synchronization Protocol for Networked Measurement and Control Systems." In 34th Annual Precise Time and Time Interval (PTTI) Meeting, 2002.

[49] H. Cho, J. Jung, and et al., "Precision time synchronization using ieee 1588 for wireless sensor networks." The International Conference on Computational Science and Engineering, 2009.

[50] R. Albu, Y. Labit, T. Gayraud, and P. Berthou, "An energy-efficient clock synchronization protocol for Wireless Sensor Networks." IFIP Wireless Days (WD), 2010.

[51] J. Kuri and S. Kasera, "Reliable multicast in multi-access wireless LANs," Wireless Networks, vol. 7, no. 4, 2001.

[52] X. C. Tong, Advanced materials and design for electromagnetic interference shielding. CRC Press, 2008.

[53] A. Koubâa, M. Alves, E. Tovar, and A. Cunha, "An implicit GTS allocation mechanism in IEEE 802.15.4 for time-sensitive wireless sensor networks: theory and practice," Real-Time Systems, vol. 39, 2008.

[54] E. Wandeler and L. Thiele, "Optimal TDMA time slot and cycle length allocation for hard real-time systems." ASP-DAC, 2006.

[55] N. Gollan and J. Schmitt, "Energy-Efficent TDMA Design Under Real-Time Constraints in Wireless Sensor Networks." MASCOTS, 2007.

[56] M. Fidler and J. B. Schmitt, "On the way to a distributed systems calculus: An end-to-end network calculus with data scaling," ACM SIGMETRICS Performance Evaluation Review, vol. 34, no. 1, 2006.

[57] H. Wang, J. Schmitt, and F. Ciucu, "Performance modelling and analysis of unreliable links with retransmissions using network calculus." Teletraffic Congress (ITC), 2013.

[58] H. Wang and J. B. Schmitt, "On the Way to a Wireless Network Calculus–The Single Node Case with Retransmissions," Tech. Rep., 2010.

[59] R. Lubben and M. Fidler, "On the delay performance of block codes for discrete memoryless channels with feedback." Sarnoff Symposium (SARNOFF), 2012.

[60] J. Xie and Y. Jiang, "An analysis on error servers for stochastic network calculus." Local Computer Networks, 2008.

[61] Y. Jiang and Y. Liu, Stochastic network calculus. Springer, 2008.

[62] A. Bouillard, N. Farhi, and B. Gaujal, "Packetization and packet curves in network calculus." Performance Evaluation Methodologies and Tools (VALUETOOLS), 2012.

[63] A. Bouillard, L. Jouhet, E. Thierry et al., "Service curves in Network Calculus: dos and don'ts," Tech. Rep., 2009.

Résumé

1. Contexte et Motivations

La complexité de l'architecture de communication avionique ne cesse de croitre à cause de l'augmentation du nombre des sous-systèmes interconnectés et l'expansion de la quantité des données échangées. Afin de répondre à ces besoins émergents, l'architecture avionique actuelle, comme celle de l'A380, l'A400M ou l'A350, est basée sur un réseau fédérateur à haut débit de type AFDX (Avionics Full Duplex Switched Ethernet) pour interconnecter les sous-systèmes critiques. Ensuite, chaque sous-système avionique pourrait être directement connecté à un réseau de capteurs/actionneurs à faible débit, de type ARINC429 ou CAN. De plus, pour augmenter le niveau de fiabilité du système, un réseau de secours, basé sur de l'Ethernet commuté, est implémenté afin de garantir un service continu en cas de pannes.

Bien que cette architecture réponde aux principales exigences avioniques, elle implique également des coûts d'intégration significatifs à cause de la quantité croissante du câblage et des connecteurs utilisés. De plus, ces interconnections avioniques sont soumises à des risques d'incendie et d'usure qui dégradent la fiabilité du système. Afin de répondre à ces besoins émergents, nous proposons dans cette thèse l'intégration des technologies sans fil dans le contexte avionique comme principale solution pour diminuer le poids et la complexité dus au câblage.

Dans ce contexte, notre objectif principal est de concevoir et de valider un nouveau réseau avionique sans fil afin de remplacer le réseau de secours, associé au réseau fédérateur AFDX.

Afin d'atteindre cet objectif, nous allons tout d'abord identifier dans le **Chapitre 2** les principaux défis lors de l'utilisation des technologies sans fil dans un contexte avionique, afin de choisir la plus pertinente vis à vis des exigences avioniques. Par conséquent, la technologie High Rate Ultra Wideband (HR-UWB) est sélectionnée parmi les technologies sans fil sur étagère, en raison de son haut débit, de son protocole d'accès déterministe et de ses divers mécanismes de sécurité. La conception d'un réseau avionique alternatif, basé sur la technologie HR-UWB est ainsi proposée. Ce dernier implémente un protocole d'arbitrage TDMA et des divers mécanismes de fiabilité pour garantir les exigences de déterminisme et de sûreté.

Par la suite, dans le **Chapitre 3,** afin d'évaluer l'impact de notre proposition sur les performances du système, nous procédons à la modélisation de l'architecture réseau proposée. Puis, nous introduisons une méthode d'analyse temporelle afin de calculer les délais de bout en bout et vérifier les contraintes temporelles et de fiabilité du système.

Afin d'améliorer les marges d'évolutivité du système, nous étudions différentes solutions pour réduire au maximum le pessimisme des délais de bout en bout dans le **Chapitre 4**. Les principales solutions proposées sont les suivantes: (i) optimiser la modélisation du système à l'aide de l'approche Integer Linear Programming (ILP), combinée à la théorie du Network Calculus; (ii) identifier la configuration optimale du protocole TDMA, c.à.d. la durée du cycle et l'allocation des slots, qui minimise les délais ; (iii) évaluer l'impact de divers mécanismes de fiabilité sur les délais en introduisant des modèles stochastiques, basés sur le Stochastic Network Calculus.

Enfin, dans le **Chapitre 5**, les performances de notre réseau proposé sont validées à travers une étude de cas avionique réaliste ; et les résultats obtenus mettent en évidence la capacité de notre proposition à garantir les exigences du système en termes de déterminisme et de fiabilité.

2. Architecture Avionique Actuelle

Dans cette section, nous présentons d'abord le réseau avionique actuel basé sur des technologies filaires et les exigences avioniques à respecter. Ensuite, nous décrivons les avantages et risques de l'utilisation des technologies sans fil dans le contexte avionique et identifions les problématiques relevées par cette alternative.

2.1 Réseaux standards

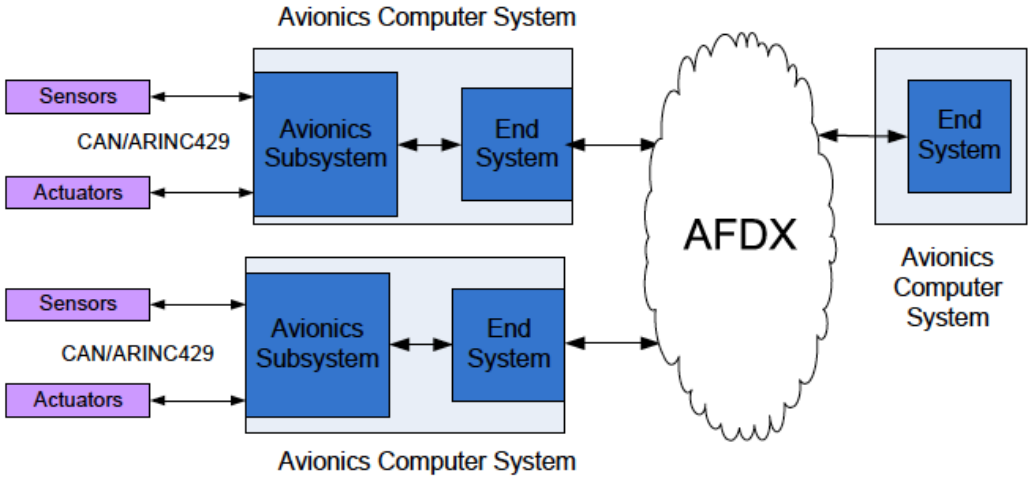

Figure 1 : Architecture Avionique Actuelle

Comme le montre la Figure 1, le réseau avionique actuel est constitué d'un réseau haut débit AFDX pour interconnecter les systèmes avioniques où certains d'entre eux admettent un réseau dédié des capteurs/actionneurs basé sur les bus CAN ou ARINC429. Les sous-systèmes critiques, interconnectés au réseau haut débit, sont géographiquement concentrés dans deux compartiments avioniques (principal et haut), comme indiqué dans la Figure 2.

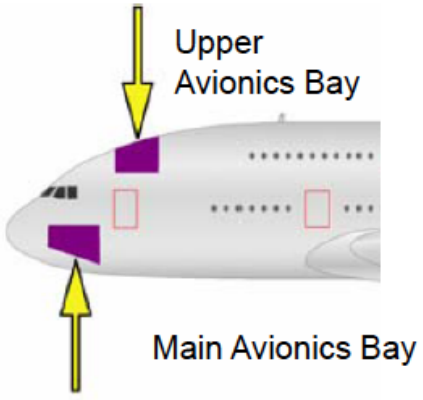

Figure 2 : Compartiments Avioniques

AFDX : Le réseau AFDX [1] est basé sur la protocole Full Duplex Switched Ethernet à 100 Mbps, intégré avec succès dans les avions de nouvelle génération comme l'Airbus A380. Cette technologie a réussi à garantir le déterminisme des communications grâce aux mécanismes ajoutés dans les commutateurs et le concept de Virtual Link (VL). Ce dernier permet de réserver une bande passante garantie . chaque flux de donn.es et représente une communication multicast d'un sous système vers un ensemble fixe d'autres sous-systèmes. Chaque VL est caractérisé par : (i) BAG (Bandwidth Allocation Gap), allant en puissances de 2, de 1 à 128 millisecondes, ce qui représente la durée d'inter-arrivée minimale entre deux trames consécutives ; (ii) MFS (Maximum Frame Size), allant de 64 . 1518 octets représentant la taille de la plus grande trame envoyée durant chaque BAG.

CAN : Le bus CAN [3] est un bus de donn.es 1 Mbps fonctionnant selon le mécanisme producteur/consommateur basé sur des priorités fixes. Les messages sont diffusés sur le bus et chaque équipement CAN filtre les données consommées en fonction de l'identifiant CAN. Les collisions sur le bus sont résolues selon le protocole CSMA/CR (Carrier Sense Multiple Access/ Collision Resolution) bas. sur la méthode d'arbitrage bit à bit. La trame CAN peut contenir des donn.es utiles d'une longueur allant jusqu'à 8 octets et un overhead de 6 octets en raison des différentes en-têtes et le mécanisme de bourrage.

ARINC429 : Le ARINC429 [2] est un bus de données à 100 Kbps garantissant des communications point à point. Il s'agit d'un bus de données mono-émetteur/multi-récepteurs avec des communications unidirectionnelles permettant ainsi une grande fiabilité de transmission au prix d'un nombre important de connections et un débit limité.

2.2 Exigences Avioniques

Afin de remplacer le réseau Avionique (AN) pour les systèmes temps réel critique, les exigences suivantes doivent être intégrées et respectées :

- ***Temps réel dur et déterminisme*** : AN doit se comporter d'une manière prévisible où les latences de transmission doivent être bornées et respectant les contraintes temporelles du système ;
- ***Fiabilité et disponibilité*** : en terme de tolérance aux pannes, AN admet un haut niveau de criticité et la probabilité requise de défaillance est inférieure à 10^{-9} par heure de vol. Par conséquent, AN a besoin d' implémenter des mécanismes de détection et de correction d'erreurs afin de satisfaire cette condition. Concernant la maintenabilité, la durée de vie d'un système avionique est environ de 20 à 30 ans ce qui impose une procédure de conception incrémentale pour ajouter facilement des fonctions tout au long de cette durée. Par conséquent, les technologies utilisées pour AN doivent être matures et disponibles à long terme ;
- ***Sécurité*** : dans [11], les auteurs soulignent les exigences de sécurité pour l'AN qui doit garantir : i) la confidentialité des données en évitant les écoutes passives des utilisateurs non autorisés ; (ii) l'intégrité des données afin de garantir que le message de l'expéditeur ne soit pas modifié lors des transmissions ; (iii) l'authentification pour éviter l'accès non autorisé au réseau ;
- ***Compatibilité électromagnétique*** : le réseau avionique doit faire face à un environnement physique hostile aux vibrations importantes, variation de la température et de l'humidité. En outre, il doit être capable de fonctionner normalement en présence de bruit radioélectrique intense et ne doit pas provoquer des interférences avec d'autres systèmes embarqués.

2.3 Identification des problématiques

Dans cette section, nous discutons les avantages et les risques de mettre en œuvre des technologies sans fil pour le réseau avionique critique. Puis, nous identifions les défis de recherche principaux.

De nos jours, l'introduction de la technologie sans fil au contexte avionique critique est devenue possible, mais également conseillée pour les raisons suivantes. ***Tout d'abord***, un réseau avionique sans fil permet une réduction de poids, une augmentation de la flexibilité et des performances du syst.me grâce à une consommation moins importante de carburant et une meilleure autonomie de vol. ***Puis,*** il permet d'éliminer les problèmes de câblage liés au vieillissement améliorant ainsi l'extensibilité et la sécurité du système grâce à une procédure plus simple de localisation des erreurs et moins de risques d'incendie. ***Enfin***, la mise en œuvre du réseau avionique sans fil réduira les coûts, non seulement lors de la procédure de conception, de production et de développement, mais aussi pour la maintenance et la révision.

Actuellement, il y a une nouvelle tendance à utiliser des technologies commercial-off-the-shelf (COTS) plutôt que de concevoir une solution dédiée pour réduire les coûts de développement. Cependant, le problème avec COTS est de concilier les exigences des applications grand public et celles des systèmes critiques. Pour les technologies sans fil, les problèmes principaux sont liées à la sensibilité du système contre les interférences électromagnétiques (EMI). Ceci est principalement dû aux phénomènes naturels ou des événements artificiels qui pourraient être internes ou externes à l'avion, par exemple, appareils électroniques portable (PED), les communications par satellite ou la radionavigation. Ceci entraine la dégradation du débit des données et de la qualité de service ou l'effondrement du réseau. De plus, il y a une question de sécurité en raison de l'accès et la manipulation des informations envoyées (Man-in-the-Middle) et les attaques du déni de service (DoS) [12]. Ainsi, nous pouvons remarquer qu' il y a un compromis à faire afin de satisfaire l'efficacité et la fiabilité lors de la mise en œuvre des technologies sans fil pour les applications critiques. Nous identifions ici les problématiques à résoudre afin de concevoir un nouveau réseau avionique sans fil.

Evaluation des technologies sans fil : Afin de dériver une spécification pour un réseau avionique sans fil, il faut commencer par analyser les caractéristiques du réseau avionique actuel. Puis, en se basant sur ces spécifications, il faudrait évaluer les technologies sans fil existantes et choisir la plus adaptée à ce contexte.

Conception de WAN : une fois que le choix de la technologie sans fil est fait, les autres aspects importants à considérer sont :

- L'architecture du réseau : remplacer les interconnexions avioniques actuelles par des connexions sans fil pose un bon nombre de questions concernant le regroupement et la topologie du réseau considérée, mais aussi les mécanismes pour éviter les interférences.
- Le protocole MAC : le choix du protocole MAC affecte directement le déterminisme des communications, important pour les systèmes avioniques critiques. Par conséquent, le protocole MAC doit être bien défini pour garantir cette exigence.
- Mécanismes de fiabilité : pour le réseau avionique critique, la probabilité de défaillance ne doit pas être supérieure à 10^{-9} par heure de vol. Par conséquent, tout système sans fil doit satisfaire cette exigence. La question soulevée concerne la faisabilité d'un réseau avionique entièrement sans fil ou la nécessité d'un réseau de

secours filaire. De plus, les communications avioniques sont principalement multicast, nécessitant l'intégration de mécanismes de notification et de retransmission adaptés pour réduire l'overhead des communications. Les mécanismes de fiabilité doivent être bien choisis pour répondre à ces exigences.

- Mécanismes de sécurité : la sécurité est l'un des critères les plus importants à atteindre pour des applications avioniques critiques. Par conséquent, le réseau avionique sans fil doit assurer l'authentification, l'encodage et l'intégration des données afin d'éviter les attaques "man-in-the-middle" ou DoS.

Evaluation des performances : pour les applications embarquées avioniques, il est essentiel que le réseau de communication réponde aux exigences de certification où les contraintes temps réel sont garanties. Cependant, l'utilisation des technologies sans fil peuvent augmenter les latences de communication en raison des erreurs de transmission. Par conséquent, des contraintes temps réel doivent être vérifiées dans un environnement erroné. Afin de mener cette analyse des performances au pire des cas du réseau, une analyse d'ordonnançabilité appropriée doit être envisagée.

3. Etat de l'art : technologies sans fil et le temps réel

La complexité de l'architecture de communication avionique va croissant en raison du nombre important des sous-systèmes interconnectés et l'expansion de la quantité des données échangées.

Certes l'architecture actuelle répond aux exigences avioniques, mais elle impose en même temps des coûts très élevés d'intégration et de maintenance dus essentiellement à la quantité importante de câblage et à la diversité des connecteurs. A titre d'exemple, les coûts liés au câblage lors de la fabrication et l'installation sont estimés à 2000$ par kilogramme, ce qui conduit à un coût total de14 millions de dollars pour un avion comme A320 et de 50 millions de dollars pour B787 [4]. Pour les avions de nouvelle génération comme l'A380, on peut compter jusqu'à 500 km de câbles, considérés comme l'une des principales raisons des retards estimé à 2 milliards de dollars. En plus des contraintes des coûts d'intégration et de maintenance, le système d'interconnexion avionique est soumis à des risques importants d'incendies qui peuvent induire une dégradation au niveau de la fiabilité et des performances du système. Il est ainsi nécessaire de réduire le câblage au niveau des avions de nouvelle génération afin d'améliorer les coûts d'intégration et d'utilisation du système, notamment en terme de consommation de carburant, mais aussi en terme de fiabilité et de performances. Par conséquent, notre proposition est basée sur l'intégration des technologies sans fil pour les systèmes avioniques critiques. De nos jours, la technologie sans fil est devenue l'une des solutions les plus rentables grâce à son omniprésence, sa simplicité et sa maturité. Elle a été récemment mise en œuvre dans de nombreuses applications temps réel critiques telles que les réseaux de capteurs [5] et les réseaux industriels [6], mais aussi les applications avioniques. Dans ce domaine spécifique, il y a quelques travaux récents pour les véhicules aérien sans pilote (UAV) [7] et des solutions propos.es pour l'avionique civil qui peuvent être classées en fonction du niveau de criticité du système visé et de l'ensemble des exigences à remplir.

Comme le montre la Figure 3, le réseau des données et de communication avionique (ADCN) est principalement constitué de trois types de systèmes : les systèmes critiques de haute priorité et puis les systèmes de haute performance et monde ouvert correspondant aux priorités moyennes et basses. Pour ces deux dernières catégories, l'une des contraintes principales est d'augmenter la consommation de bande passante, tandis que le comportement

déterministe et la garantie des délais sont secondaires. Dans le domaine des systèmes monde ouvert, dans [8], les auteurs ont mené des simulations et des expériences sur l'utilisation de technologies standard sans fil pour le réseau In Flight Entertainment (IFE). Les résultats obtenus pour une architecture hétérogène basée sur Ethernet et technologies sans fil USB (Wireless USB) sont prometteurs en terme de qualité de service en considérant le comportement moyen du syst.me. Pour les systèmes de haute performance, [9] a étudié la technologie Ultra Wide Bande (UWB) pour les communications cabine avec l'allocation optimisée des ressources et la validation de la solution s'est basée sur les simulations. Les réseaux sans fil ont été aussi étudiés pour la surveillance et la maintenance de l'avion comme dans [10].

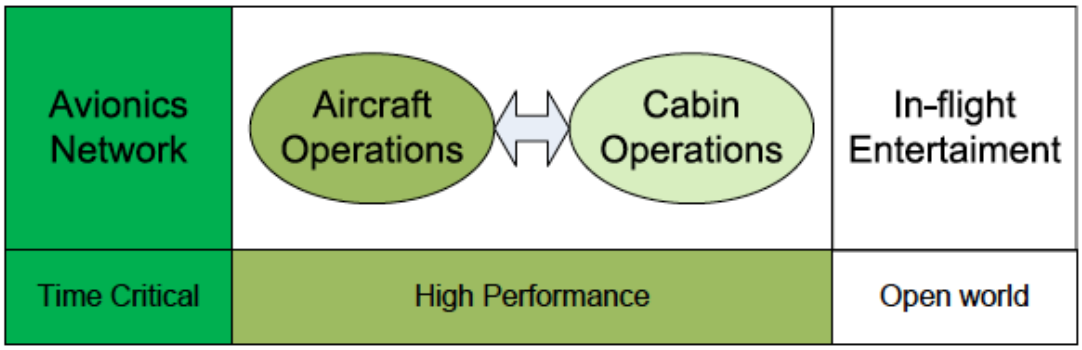

Figure 3 : le réseau ADCN

Pour les systèmes critiques, une des exigences principales à remplir est le déterminisme des communications. Dans ce domaine, il n'y a pas eu à notre connaissance des propositions d'intégration des technologies sans fil. Nos principales contributions sont ainsi: (i) spécification des besoins du syst.me avionique critique; (ii) évaluation des technologies sans fil existantes versus les exigences avioniques afin de choisir la plus adaptée à ce contexte; (iii) conception d'un réseau avionique sans fil prenant en compte les exigences avioniques; (iv) évaluation de performances et optimisation des ressources du système; (v) la validation de notre proposition sur une étude de cas réaliste d'un réseau avionique critique.

4. Spécification et Analyse qualitative

Dans cette section, nous présentons les spécifications principales du réseau sans fil avionique. Puis, nous détaillons les technologies sans fil existantes répondant aux spécifications identifiées et nous discutions les avantages et les inconvénients de chacune versus les exigences avioniques.

4.1 Spécifications

Afin de remplacer le réseau avionique actuel avec un réseau sans fil, les exigences décrites précédemment doivent être garanties et les conditions spécifiques du contexte avionique doivent être intégrées. Les caractéristiques principales identifiées sont les suivantes :

- Le débit de transmission offert par le réseau actuel est de 100 Mbps. La nouvelle technologie doit ainsi fournir la plus grande capacité pour répondre aux besoins de passage. l'échelle durant la vie d'un avion (20-30 ans). Par conséquent, la technologie sans fil considérée doit au moins offrir ce débit requis de données de 100 Mbps ;
- La distance entre 2 compartiment avioniques différents est de 6 mètres, mais peut être extensible. La technologie sans fil doit ainsi avoir une portée supérieure ou égale à 6 mètres ;

- Actuellement, il y a 50 à 80 systèmes connectés au réseau avionique. Par conséquent, la technologie choisie pour ce type de communication doit supporter au moins ce nombre de nœuds ;
- Les systèmes avioniques actuels sont considérés comme des équipements complexes implémentant de nombreuses fonctions avioniques. Ils doivent ainsi être en continu alimentés électriquement et leurs positions sont fixes. Par conséquent, les problèmes liés à la consommation d'énergie et à la mobilité ne sont pas considérés comme des objectifs importants dans le contexte avionique ;
- L'AFDX est basé sur le concept Virtual Link (VL) représentant des communications multicast. Par conséquent, la configuration de communication doit être "any et multi-cast" pour le réseau avionique sans fil avec une topologie peer-to-peer ;
- Les données avioniques ont des contraintes temporelles strictes et un haut niveau de sécurité. Par conséquent, le déterminisme et la fiabilité des communications sont très importantes. Ces exigences impliquent des méthodes d'accès déterministes avec mécanismes de fiabilité précis.

Les caractéristiques principales identifiées des couches physiques et MAC pour le réseau avionique sans fil sont résumées dans le tableau 1.

TABLE 1 – Caractéristiques des couches physiques et MAC

		Réseau haut debit
Couche physique	Débit	$\geq$ 100Mbps
	Taille	50 – 80 noeuds
	Portée (mètre)	4 – 6 m
	Topologie	peer-to-peer
	Type de communication	any, multicast
Couche MAC	Mécanisme	déterministe
	Délai	Garantie de bout-en-bout
	Fiabilité	Garantie de bout-en-bout
	Energie	Pas de limitations spécifiques sur la consommation d'énergie

4.2 Les technologies sans Fil vs exigences avioniques

Les technologies sans fil les plus courantes qui répondent à la contrainte du débit requis sont décrites dans cette section.

4.2.1. IEEE 802.11

Parmi les nombreuses variantes de la norme IEEE 802.11, seule la norme IEEE 802.11n [13] peut fournir le débit de donn.es suffisant pour remplacer le réseau avionique actuel. La norme IEEE 802.11n fonctionne à 2,4 et 5 GHz avec deux options de bande passante de 20 MHz ou 40 MHz. Cette norme est basée sur des antennes multi-émission-multi-réception (MIMO) pour atteindre le débit de données maximum de 600 Mbps pour une distance de 30 mètres pour les environnements intérieurs. Le protocole MAC de IEEE 802.11n est bas. sur le mécanisme de CSMA/CA; et il intègre un protocole basé sur la compétition DCF (Distributed Coordination Function) pour le mode ad-hoc et puis un protocole sans compétition PCF (Point Coordination Function) pour le mode infrastructure.

Au niveau de la couche PHY, IEEE 802.11n met en œuvre le code correcteur d'erreurs (FEC) et de vérification de parité (LDPC) pour contrôler les erreurs et améliorer la fiabilité. Au niveau de la couche MAC, IEEE 802.11n utilise la retransmission automatique (ARQ) avec différents types d' acquittements. En terme de sécurité, la norme IEEE 802.11n adopte les mêmes mécanismes que IEEE 802.11i bas. sur trois protocoles de confidentialité des données:

Wired Equivalent Privacy (WEP), Temporal Key Integrity Protocol (TKIP) et Counter-Mode/CBC-MAC Protocol (CCMP). Puis, l'authentification est améliorée en utilisant le protocole EAP (Extensible Authentication).

Certes la norme IEEE 802.11n peut fournir le débit de données suffisant, la fiabilité requise et les bons mécanismes de sécurité pour les applications avioniques, mais il y a encore très peu de résultats concernant l'utilisation de la technique MIMO en multicast. De plus, cette norme serait naturellement plus sensible aux interférences provoquées par des systèmes IFE et des dispositifs communs comme un ordinateur portable ou un PDA qui opèrent dans les mêmes bandes de fréquences. Ces aspects constituent une limitation sérieuse pour utiliser la norme IEEE 802.11n pour le réseau avionique.

4.2.2 ECMA-368

ECMA-368 est une norme pour la technologie de High Rate Ultra Wide-Band (HR-UWB) [14]. Cette norme fonctionne à large bande de fréquence de 3,1 GHz . 10,6 GHz, divisée en 14 bandes de 528 MHz chacune. Aujourd'hui, il reste encore trois bandes libres, communes dans le monde entier(bandes 9, 10 et 11). Ce fait est très intéressant pour les applications avioniques qui ont besoin de bandes de fréquences universelles pour éviter la reconfiguration en cours de vol. Mais aussi, ça permet de réduire les risques d'interférences avec les dispositifs commun. ECMA-368 peut supporter un débit de données à 110 Mbps, 200 Mbps et 480 Mbps pour des distances respectives de 10 m, 6 m et 2 m.

ECMA-368 supporte la topologie peer-to-peer et deux protocoles MAC : l'accès prioritaire de contention (PCA) et le protocole de réservation distribué (DRP). Le premier est un protocole basé sur la compétition, tandis que le second est un protocole bas. sur le TDMA pour garantir un accès exclusif. En terme de fiabilité, ECMA-368 intègre les codes FEC avec différents taux de codage au niveau de la couche PHY et des mécanismes de retransmission avec acquittement immédiat (Imm-ACK) et acquittement de bloc(ACK-B) au niveau de la couche MAC. Cette norme intègre des mécanismes de sécurite solides. Pour le chiffrement des données, elle utilise l'algorithme AES avec Pairwise Transient Key (PTK) pour les communications unicast, et Group Transient Key (GTK) pour les communications multicast et broadcast. En outre, comme IEEE 802.11n, l'intégrité est garantie avec MIC et l'authentification est basée sur le 4-way handshake.

Cette technologie répond ainsi à la plupart des spécifications du réseau avionique mais il reste tout de m.me la vérification des performances offertes en pratique.

4.2.3 IEEE 802.15.3c

Cette technologie est considérée comme l'une des technologies sans fil les plus récentes. Cette dernière vise à garantir des communications sans fil avec haut débit (jusqu'à 3 Gbps) sur la bande de fréquence 60 GHz. En raison d'une très forte atténuation par absorption d'oxygène, 60 GHz doit être basée sur des antennes directionnelles avec la condition nécessaire Lightof- Sight (LOS) pour atteindre une distance de 10m et un débit de 3 Gbps.

Cette technologie est encore en cours de développement avec plusieurs options pour les techniques de modulation et le protocole MAC. En terme de fiabilité, cette technologie intègre les données d'agrégation et d'acquittement comme IEEE 802.11n et elle introduit quelques améliorations aux retransmissions de MSDU individuels et différents taux de codage pour MSDU agrégées.

En raison de ses exigences de LoS et de son immaturité, cette technologie est considérée comme inadaptée pour remplacer le réseau avionique actuel.

4.3 Sélection de la technologie sans fil adaptée

Les caractéristiques principales des technologies sans fil décrites ci-dessus sont résumées dans le tableau 2. La comparaison de ces trois technologies en termes d'exigences avioniques est indiquée dans le tableau 3. A partir de cette analyse, ECMA-368 est considérée comme la technologie la plus adaptée pour remplacer le réseau avionique actuel grâce à son haut débit de données, son protocole MAC déterministe et ses mécanismes de sécurité. Cependant, il y a encore des problématiques à résoudre afin d'intégrer cette technologie dans le contexte avionique.

TABLE 2 – Paramètres des technologies sans fil

Norme	802.11n	HR-UWB	60 GHz
Portée (m)	30	10	10
Bandes de fréquence	2.4, 5GHz	3.1-10.6 GHz	60GHz
Bande passante	20/40Mhz	500MHz-7.5GHz	7GHz
Canaux	3	14	1
Technique de modulation	64QAM	QPSK	QPSK, 64QAM
Spectre étalé	OFDM	MB-OFDM	OFDM or SC-FDE
Exigence LoS	No	No	Yes
Débit (Mbps)	600	110 (10m)/ 200(6m)/480(2m)	3000
Encodage	RC4, AES	AES	NA
Topologie	ad-hoc, infrastructure	peer-to-peer	NA
Protocole MAC	CSMA/CA DCF, PCF	TDMA or CSMA/CA HCF	TDMA

TABLE 3 – Technologies san fil vs exigences avioniques

	802.11n	ECMA-368	IEEE 802.15.3c
Déterminisme	PCF (Yes), DCF (No)	TDMA (Yes), PCA (No)	TDMA (Yes)
Fiabilité	Moyenne	Moyenne	Moyenne
Sécurité	Haute	Haute	N.A
Sensibilité EMC	Haute	Bas	Bas

5. Conception

Dans cette section, nous présentons tout d'abord l'architecture considérée pour le réseau avionique sans fil. Ensuite, nous détaillons le protocole MAC sélectionné pour améliorer la prévisibilité des communications et garantir le déterminisme. Enfin, les mécanismes de fiabilité sélectionnés pour répondre aux exigences avioniques sont décrits.

5.1 Architecture

Comme il est décrit dans le tableau 1, le réseau avionique critique actuel se compose de 80 systèmes au maximum. Ils sont concentrés dans deux compartiments avioniques (principal et en haut) à la tête de l'avion, comme le montre la figure 2. En outre, la distance maximale entre deux systèmes au niveau de chaque compartiment est inférieure à 6 m.

Nous considérons les deux groupes de sous-systèmes dans les compartiment principal et en haut de l'avion où on attribue à chaque groupe une bande fréquence réservée pour éviter les interférences avec les deux autres. Ainsi, le débit atteint à l'intérieur de chaque groupe dans un périmètre de 6 mètres est d'environ 200 Mbps. De plus, chaque groupe a une topologie peer-to-peer qui garantit des communications mono-saut au sein du même groupe.

La communication inter-groupes est gérée par des passerelles spécifiques et les modes de communication entre les passerelles peuvent être unicast, multicast ou broadcast. Comme la distance entre les deux compartiments avioniques peut être supérieure à 6 mètres (voir figure 2), deux solutions principales sont envisageables dans ce cas pour l'interconnexion des passerelles: l'interconnexion sans fil ou filaire.

Avec des interconnexions sans fil entre les passerelles, les délais de bout en bout peuvent augmenter en raison du mécanisme d'accès TDMA requise et la communication de type half duplex. De plus, cette architecture devrait être plus sensible aux interférences et réduire l'extensibilité du système. En effet, l'ajout de nouveaux compartiments avioniques au milieu ou à l'arrière de l'avion induira beaucoup plus de nœuds de relais entre les passerelles. Le taux offert dans ce cas est d'environ 200 Mbps entre deux nœuds relais consécutifs, mais beaucoup plus petit entre les passerelles. Par conséquent, cette solution est considérée comme inadéquate pour les communications intergroupes du réseau avionique sans fil.

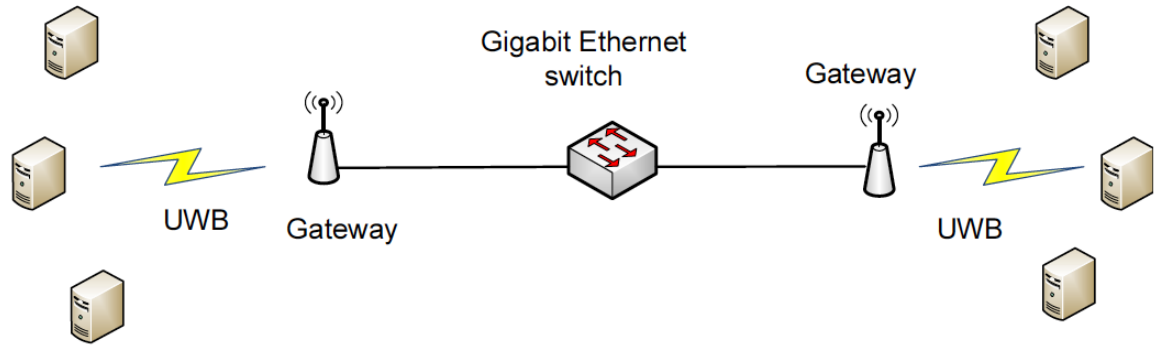

Figure 4 : Architecture hybride du réseau proposé

Afin de faire face aux contraintes d'une architecture complétement sans fil, une architecture hybride basée sur un Ethernet Commuté Full Duplex à 1Gbps pour interconnecter les trois passerelles est considérée comme une solution intéressante. Comme le montre la figure 4, un commutateur central est utilisé pour connecter les trois passerelles. Contrairement à l'interconnexion sans fil où les passerelles sont tenues de transmettre leurs messages seulement pendant leurs intervalles de temps exclusifs, avec le Full Duplex Switched Ethernet, chaque passerelle peut transmettre immédiatement ses messages au commutateur, pour être ensuite transmis à la(es) destination(s) finale(s). Par conséquent, cette caractéristique permet les communications haut débit, déterministes et fiables. De plus, cette architecture hybride est plus extensible car d'autres compartiments avioniques au milieu ou . l'arrière de l'avion peuvent être facilement interconnectés. Compte tenu de tous ces avantages, nous considérons l'architecture hybride pour la conception du réseau avionique sans fil.

Il est intéressant de noter que les passerelles et le commutateur dans cette architecture hybride ont des fonctions clés. Chaque passerelle doit convertir les trames ECMA-368 reçues de tout système avionique de son groupe associé en trames Ethernet pour être transmises au commutateur Ethernet. Par conséquent, pour maintenir la transparence des communications de bout en bout, chaque passerelle proc.de comme suit : chaque trame ECMA-368 reçue est encapsulée dans une trame Ethernet (qui respecte les tailles minimales et maximales) et puis transmise au commutateur Ethernet ; et chaque trame Ethernet reçue à partir du commutateur

Ethernet est décapsulée afin d' extraire la trame de ECMA-368 pour être ensuite transmise à la destination finale. Les trames ECMA-368 et Ethernet à 1Gbps sont décrites dans les figures 5 et 6.

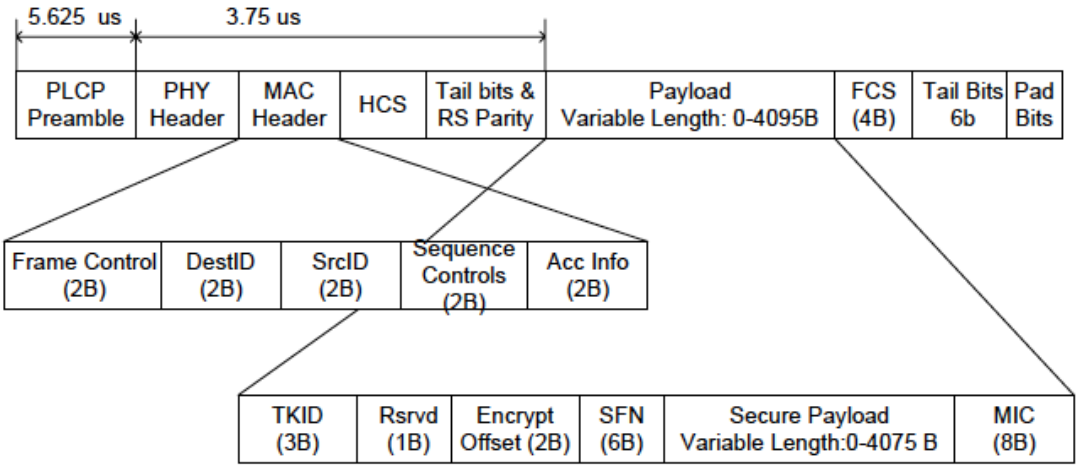

Figure 5 : la structure de trame de ECMA-368

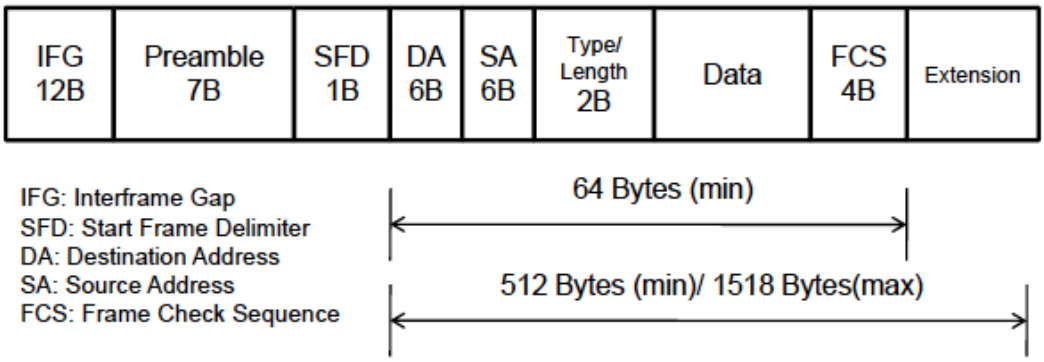

Figure 6 : structure de la trame Ethernet

Le commutateur Ethernet est un dispositif actif qui identifie le port de destination d'un paquet entrant et le transmet au port spécifique. Si plusieurs paquets ont le m.me port de destination, les files d'attente sont utilisées pour résoudre le problème de collision. Les commutateurs Ethernet peuvent être identifiés par leur technique de commutation et leur politique d'ordonnancement. Deux types de techniques de commutation sont actuellement mises en œuvre dans les commutateurs Ethernet: Cut Through and Store and Forward. Avec la première, uniquement l'en-tête de chaque paquet est décodée afin de déterminer le port de destination et le reste est transmis sans vérification des erreurs. Avec la deuxi.me, le commutateur attend jusqu'à la réception complète du paquet et le transmet au port de destination en cas d'absence d'erreurs. Dans notre cas, nous choisissons la deuxi.me technique de commutation pour améliorer la sécurité des communications puisque aucun paquet corrompu ne sera transmis. Ensuite, la politique d'ordonnancement est utilisée pour transmettre des paquets au niveau du port de sortie du commutateur. Nous considérons la politique simple la plus répandue, First Come First Served (FCFS), où les paquets sont servis dans leurs ordres d'arrivée, sans tenir compte de leurs caractéristiques temporelles.

5.2 Protocole MAC

Comme décrit dans la section 4.2.2, ECMA-368 supporte deux protocoles MAC : PCA et PRA. Le premier est un protocole de compétition basé sur des classes de qualité de service (QoS), tandis que le second est un protocole basé sur TDMA pour garantir un accès exclusif au médium. Or pour des applications avioniques, il est essentiel de garantir un comportement prévisible respectant les contraintes temps réel dur. Le protocole DRP semble ainsi plus adapté que le PCA pour ce contexte. Cependant, l'attribution de intervalles d'accès et la durée du cycle doivent être soigneusement configurées afin de gérer efficacement les différents types de trafic et garantir leurs contraintes temporelles associées.

Les hypothèses suivantes sont considérées pour notre proposition :

- Configuration hors ligne : Etant donné que tous les messages générés sont connus a priori, le mécanisme d'allocation d'intervalles d'accès est configuré hors ligne et il sera suivi de manière statique par tous les systèmes lors du déploiement du réseau ;
- Les intervalles d'accès et les durées des cycles : au cours de chaque cycle mineur, l'intervalle de temps alloué pour chaque système avionique est fixé et admet une durée définie dépendant de son trafic généré. Par conséquent, les intervalles d'accès n'ont pas forcément la même durée pour tous les systèmes et la durée du cycle peut varier d'un groupe à l'autre ;
- Le mécanisme de synchronisation pour mettre en œuvre un protocole TDMA précis pour le réseau avionique critique, le degré de précision du mécanisme de synchronisation utilisé est d'une grande importance.

Pour les réseaux filaires, de nombreux mécanismes de synchronisation ont été mis en œuvre avec succès avec un degré de précision de quelques nanosecondes, et le plus connu est le protocole IEEE1588 [15]. Cependant, pour les réseaux sans fil, atteindre ce degré de précision semble plus compliqué en raison de nombreux facteurs variables lors de la communication. Un travail récent [16] a étudié les performances du IEEE1558 pour les réseaux de capteurs sans fil et la précision obtenue est inférieure à 200 nanosecondes. Cependant, les travaux de [16] ne peuvent pas être directement appliqués à notre contexte en raison du grand nombre de messages échangés pour la synchronisation. Il est ainsi nécessaire d'optimiser l'overhead de la phase de synchronisation.

Les auteurs dans [17] ont proposé une version améliorée de [16] pour les communications en diffusion en mono-saut, appel. IEEE 1588-PBS (synchronisation de diffusion par paire). L'objectif principal de ce protocole consiste à réduire l'overhead de la phase de synchronisation et de minimiser la consommation d'énergie tout en assurant un degré de précision d'environ 200 nanosecondes. IEEE 1588-PBS est basé sur un maître du temps pour réaliser le mécanisme de synchronisation, et un esclave actif pour recevoir le message de synchronisation et pour envoyer la demande au maître. Les autres nœuds sont des nœuds passifs qui écoutent les données échangées entre le maître et l'esclave actif pour estimer le temps actuel. La figure 7 illustre le mécanisme de IEEE 1588-PBS. Il est intéressant de noter la grande disponibilité de ce mécanisme où si le nœud actif échoue, un des nœuds passifs peut être élu pour effectuer la synchronisation.

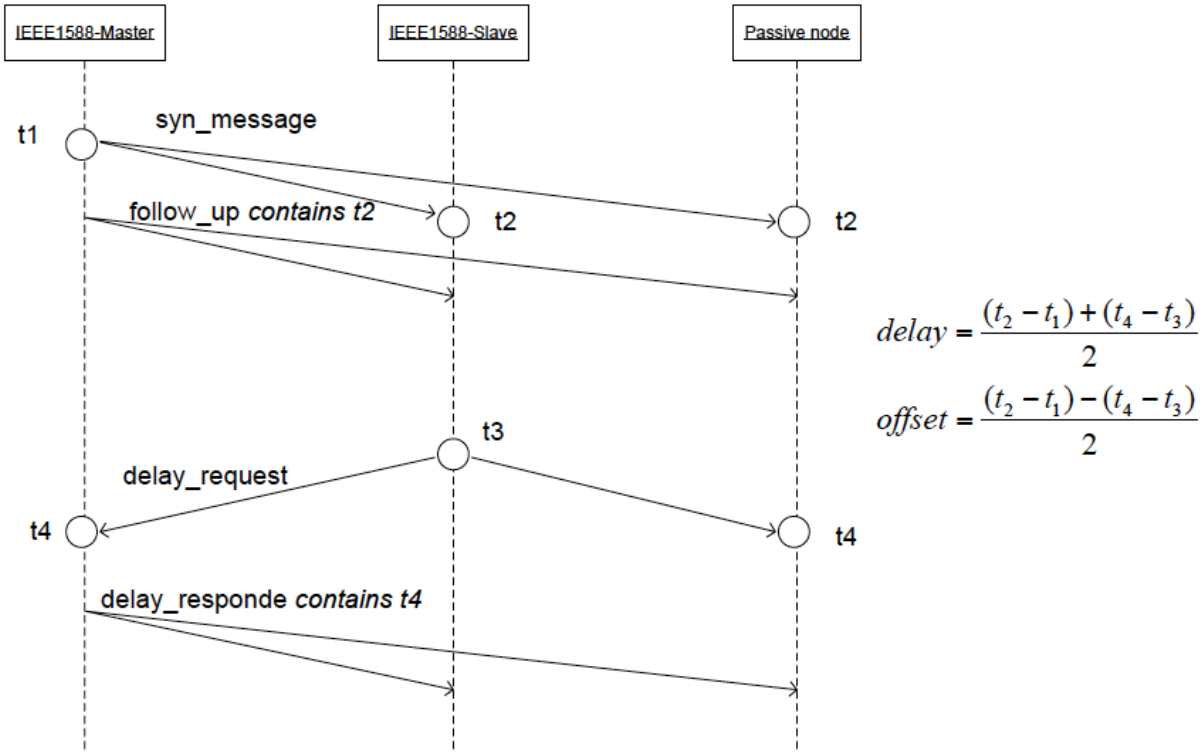

Figure 7 : protocole de synchronisation

Par conséquent, en raison de sa précision, de sa haute disponibilité et de son optimalité en terme d'overhead, l'IEEE1588-PBS est considéré comme un candidat intéressant pour les applications avioniques critiques pour garantir la précision de la mise en œuvre du protocole TDMA.

5.3 Les mécanismes de fiabilité

Pour le réseau avionique critique, la probabilité de défaillance doit être inférieure à 10^{-9} par heure de vol. Cette condition peut être facilement assurée avec le réseau avionique actuel. Cependant, avec la technologie sans fil, la tâche semble plus compliquée en raison de l'environnement de propagation erronée et les interférences. Afin de faire face à cette limitation, nous proposons deux solutions possibles pour réduire la probabilité d'erreurs afin de remplacer le réseau avionique actuel.

La première méthode consiste à désactiver l'acquittement et l'utilisation de mécanismes de diversité au niveau des fréquences et du temps. Pour la diversité des fréquences, chaque paquet est transmis sur différentes fréquences en même temps, ce qui diminue la probabilité de perte. Pour la diversité au niveau temporel, chaque paquet est transmis plusieurs fois sur la même fréquence. La figure 8 illustre un exemple de la diversité au niveau temporel et de fréquences dans le cas de deux fréquences et deux transmissions par paquet au niveau temporel.

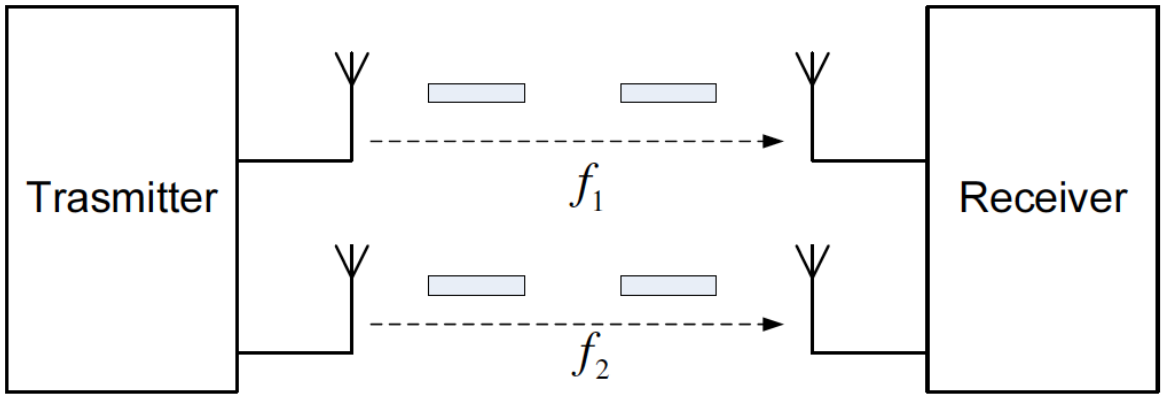

Figure 8 : mécanismes de diversité au niveau temporel et fréquences

Bien que la désactivation du mécanisme d'acquittement aide à réduire l'overhead de communication, il peut induire en même temps une mauvaise utilisation de la capacité du réseau, étant donné que chaque paquet est retransmis un nombre fixe de fois, même si il est entièrement reçu avec succès. Par conséquent, l'activation de l'acquittement associé à la diversité au niveau des fréquences est considérée comme une deuxième alternative. Etant donné que le modèle de communication pour les applications avioniques est multicast, un mécanisme d'acquittement amélioré est ainsi nécessaire pour éviter les collisions entre les messages d'acquittement envoyés par différents récepteurs et réduire les overheads.

Dans ce domaine spécifique, dans [18], les auteurs proposent un mécanisme d'acquittement amélioré pour les communications multicast. Cette approche consiste à sélectionner l'un des récepteurs comme un "leader" pour renvoyer un message à l'expéditeur. Si le paquet est correctement reçu, alors le leader enverra un acquittement positif (ACK) à l'expéditeur, sinon il n'y a pas de retour du leader. Cependant, en cas de transmission erronée pour les autres récepteurs, ils répondront avec ACKs négatifs. Par conséquent, ces NACKs peuvent entrer en collision avec le message ACK envoyé par le leader, qui indique un besoin de retransmission de la part de l'expéditeur. Enfin, lorsque l'expéditeur reçoit NACK ou le Time Out se produit, le paquet est retransmis immédiatement à tous les récepteurs. Cette approche est illustrée dans la figure 9.

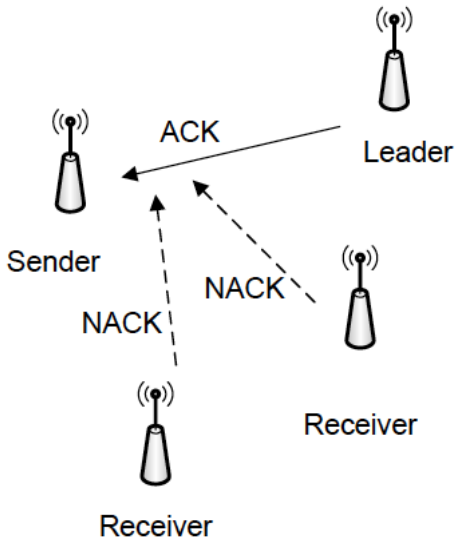

Figure 9 : communication multicast fiable

5.4 Isolation du réseau

Pour protéger le réseau sans fil critique de toute ingérence extérieure et les attaques de brouillage, nous introduisons des méthodes d'isolation du réseau, basées sur des solutions de blindage. En effet, la concentration géographiques des sous systèmes avioniques et les courtes distances de 6 mètres entre les différents nœuds facilitent l'isolation du réseau à l'aide de différentes méthodes décrites dans [20], comme par exemple, une peinture spéciale ou chambre anéchoïque légère. Ces méthodes peuvent bloquer les signaux de fréquence radio dans la plage de 100 KHz à 10 GHz, voire 100 GHz. Par conséquent, les attaquants extérieurs ou les équipements passagers ne peuvent pas accéder, modifier ou interférer avec le réseau sans fil.

6. Analyse et Optimisation des performances

Dans le chapitre 3, afin de vérifier les performances temporelles de notre réseau sans fil proposé, nous avons introduit une modélisation des différentes parties du système de communication en se basant sur la théorie du Network Calculus. Ensuite, une analyse des bornes des délais de bout en bout est détaillée en considérant différentes politiques de service au niveau des sous-systèmes tels que: First In First Out (FIFO), Fixed Priority (FP), et Weighted Round Robin (WRR), et divers mécanismes de fiabilité. Enfin, l'évaluation préliminaire des performances à travers un réseau de petite échelle est fournie.

Les résultats obtenus dans ce cas ont montré que les contraintes temporelles du système est garantie uniquement sous une faible utilisation du réseau. Ce fait est principalement dû au pessimisme des bornes des délais de bout en bout, qui dépendent de nombreux paramètres du système, tels que la durée du cycle de TDMA et sa configuration, mais aussi le mécanisme de fiabilité sélectionné. Par conséquent, un défi majeur consiste à améliorer les performances du système pour augmenter l'utilisation du réseau et garantir les contraintes temporelles et de fiabilité du système. Ce problème a ainsi été abordé dans le chapitre 4 en explorant diverses solutions.

Dans le chapitre 4, quelques approches d'optimisation des performances du système sont conduites pour obtenir des bornes moins pessimistes sur les délais de bout en bout, et permettre ainsi d'améliorer l'évolutivité et la fiabilité du système. Premièrement, nous avons proposé une modélisation plus fine des sous systèmes, basée sur le formalisme du Network Calculus et Integer linear Programming, pour minimiser le pessimisme des délais de bout en bout. Ensuite, une approche d'optimisation adéquate de la durée du cycle TDMA est introduite pour améliorer l'évolutivité du système. Par la suite, nous avons considéré les mécanismes de fiabilité basés sur les retransmissions et l'acquittement afin d'évaluer leur impact sur la fiabilité du système, en comparaison avec la désactivation du mécanisme d'acquittement. Enfin, une évaluation préliminaire des performances de ces améliorations introduites est réalisée sur une étude de cas à petite échelle.

Les résultats obtenus montrent la capacité de notre proposition à améliorer l'ordonnançabilité et la fiabilité du système, tout en garantissant ses exigences.

7. Validation

La validation des performances du réseau sans fil proposé est réalisée à travers une étude de cas avionique réaliste. L'étude de cas de l'avionique et les configurations de réseau considérés sont décrits au début du Chapitre 5 et un résumé est donné dans la table 5. Puis, l'analyse temporelle et de fiabilité de chaque configuration du réseau est effectuée pour démontrer l'impact de chaque paramètre du système sur les performances obtenues.

Nous avons considéré en particulier la politique d'ordonnancement, la durée du cycle TDMA et le mécanisme de fiabilité. Les résultats obtenus sont discutés pour mettre en évidence la capacité de notre proposition à garantir les exigences du système.

Configuration 1	• Politique de service: FIFO or FP • Durée des cycles TDMA des clusters 1 et 2, est égale à la plus courte deadline (4ms) • L'allocation des slots est basée sur le schéma TPSS (Time Proportionnal Slot Size) • Mécanismes de fiabilité: les mécanismes de diversité au niveau temporel et fréquences, en désactivant l'acquittement (No-ACK)
Configuration 2	• Politique de service: FIFO or FP • Durée optimale des cycles TDMA des clusters 1 et 2, obtenue via l'algorithme d'optimisation décrit dans le Chapitre 4 • L'allocation des slots est basée sur le schéma TPSS (Time Proportionnal Slot Size) • Mécanismes de fiabilité: les mécanismes de diversité au niveau temporel et fréquences, en désactivant l'acquittement (No-ACK)
Configuration 3	• Politique de service: FIFO or FP • Durée optimale des cycles TDMA des clusters 1 et 2, obtenue via l'algorithme d'optimisation décrit dans le Chapitre 4 • L'allocation des slots est basée sur le schéma TPSS (Time Proportionnal Slot Size) • Mécanismes de fiabilité: retransmission et acquittement avec un mécanisme de diversité au niveau des fréquences (ACK)

Table 4 : les différentes configurations du système

- **Impact de la politique de service au niveau des sous systèmes :** nous calculons les bornes sur les délais de bout en bout pour la configuration 1 de la table 4 en considérant les politiques de service FIFO et FP, en se basant sur les modèles Network Calculus du système introduits dans le chapitre 3, et en variant le nombre de fréquences et de transmission pour les mécanismes de fiabilité. Par conséquent, la mise en œuvre de notre proposition avec quatre fréquences et la politique de service FP au niveau des sous-systèmes semble être la seule solution possible, qui respecte les contraintes temporelles et de fiabilité du système. Cependant, cette solution va induire clairement une complexité et des coûts d'intégration système importants. Ces résultats montrent l'impact de la politique de service sur les performances du système. Il est intéressant de noter dans ce cas, le compromis entre garantir les performances du système en termes de prévisibilité et de fiabilité, et limiter sa complexité et ses coûts d'intégration.

- **Impact de la durée du cycle TDMA :** nous comparons les bornes sur les délais de bout en bout, obtenus avec les deux configurations 1 et 2 de la table 4, en considérant les politiques de service FIFO et FP et variant le nombre de fréquences. Bien que la configuration basée sur la durée du cycle TDMA optimale améliore les délais obtenus, et par conséquent l'évolutivité du système, la seule implémentation admissible de

notre réseau sans fil respectant les contraintes du système reste toujours celle basée sur l'utilisation de quatre fréquences et la politique de service FP au sein des sous-systèmes. Ce résultat montre l'importance du choix de la durée du cycle TDMA et l'impact bénéfique de la configuration optimisée, en particulier sur l'évolutivité du système.

- **Impact des mécanismes de fiabilité :** nous comparons les bornes sur les délais obtenus pour les configurations 2 et 3. Les résultats obtenus montrent que grâce au mécanisme de retransmission et d'acquittement, l'implémentation de notre réseau sans fil proposé avec seulement deux fréquences et la politique de service FP dans les sous-systèmes devient une solution réalisable, garantissant les contraintes du système. Ce résultat confirme nos premières conclusions du chapitre 4, où ce mécanisme de fiabilité choisi surpasse en termes de performances les mécanismes de diversité au niveau temporel et des fréquence. En outre, la complexité du système est réduite avec la configuration 3, où l'utilisation de deux fréquences seulement devient suffisante pour garantir la fiabilité du système, au lieu de quatre fréquences avec la configuration 2.

8. Conclusion

Les architectures de communication avionique actuelles impliquent un poids et des coûts d'intégration importants à cause de la quantité croissante du câblage et des connecteurs utilisés. Afin de répondre à ces besoins émergents, nous avons proposé dans cette thèse l'intégration des technologies sans fil dans le contexte avionique comme principale solution pour diminuer le poids et la complexité dus au câblage.

Tout d'abord, nous avons conçu un réseau avionique de secours basé sur la technologie HR-UWB, implémentant un protocole d'arbitrage TDMA et des divers mécanismes de fiabilité pour garantir les exigences de déterminisme et de sûreté.

Par la suite, nous avons procédé à l'évaluation des performances de notre proposition en termes de délais en se basant sur des méthodes analytiques. Par ailleurs, nous avons étudié différentes solutions afin d'améliorer les marges d'évolutivité et de fiabilité du système.

Enfin, nous avons validé notre réseau proposé à travers une étude de cas avionique réaliste; et les résultats obtenus ont mis en évidence la capacité de notre proposition à garantir les exigences du système en termes de déterminisme et de fiabilité.